CEREBROSPINAL FLUID MECHANICS DURING AND AFTER EXPERIMENTAL SPINAL CORD INJURY

by

Claire Frances Jones

BSc, The University of Western Australia, 2003

BEng, The University of Western Australia, 2003

MSc, The University of Leeds, 2005

A THESIS SUBMITTED IN PARTIAL FULFILLMENT OF

THE REQUIREMENTS FOR THE DEGREE OF

DOCTOR OF PHILOSOPHY

in

The Faculty of Graduate Studies

(Mechanical Engineering)

THE UNIVERSITY OF BRITISH COLUMBIA

(Vancouver)

June 2011

Abstract

Despite concentrated research efforts there is currently no treatment for spinal cord injury (SCI). Several researchers have identified that cerebrospinal fluid (CSF) may have a role in the biomechanics of the injury event and in the secondary physiologic response, but this has not been closely examined. The aim of this thesis was to develop a large animal model and a benchtop model of human SCI, and to use these to characterise (1) the pressure response of the CSF during the SCI event, (2) the effect of CSF thickness on mechanical indicators of injury severity, and (3) the pressure differentials and cord morphology associated with thecal occlusion and decompression.

Study 1 presented the large animal model and provided preliminary CSF pressure transient data that indicated further investigation was warranted. In Study 2, the CSF pressure transients from medium and high severity human-like SCIs were characterised. The peak pressures at 30 mm from the impact were within the range associated with experimental traumatic brain injury, but the wave was damped to peak pressures associated with noninjurious everyday fluctuations by 100 mm. In Study 3, results from the bench-top model demonstrated that the thickness of the CSF layer is directly proportional to the resultant peak CSF pressure, cord compression and impact load.

In Study 4, the cranial-caudal CSF pressure differential increased gradually over eight hours of thecal occlusion. Decompression eliminated or reduced the differential, after which it did not change significantly. These results indicate that lumbar CSF pressure measured prior to decompression may not be representative of CSF pressure cranial to an injury. In Study 5, the change in spinal cord and thecal sac morphology after surgical decompression was assessed with ultrasound. Moderate SCI was associated with a residual cord deformation and then gradual swelling, while high severity SCIs exhibited immediate swelling which occluded the thecal sac within five hours.

The different aspects of CSF response to SCI demonstrated in this thesis can potentially be used to assess and validate current and future models of SCI, and to guide future studies of clinical management strategies such as CSF drainage and early decompression.

Preface

A version of Chapter 2 has been submitted for publication. Jones CF, Lee JHT, Kwon BK and Cripton PA. *Development of a large animal model to measure dynamic cerebrospinal fluid pressure during spinal cord injury*. This study was performed in conjunction with two other studies designed by BK Kwon; I wrote part of the ethics applications. I was responsible for designing the injury model and pressure measurement methods for the study. I constructed the injury device, assisted with the animal surgeries, collected and analysed the data, carried out the statistical analysis and was the primary author of the manuscript. Ethical approval was provided by the University of British Columbia Animal Care Committee under certificates A08-0934 and A08-0935.

A version of Chapter 3 has been submitted for publication. Jones CF, Lee JHT, Burstyn U, Okon E, Kwon BK and Cripton PA. *Cerebrospinal fluid pressures during dynamic contusion-type spinal cord injury in a pig model*. I was responsible for designing the study and associated apparatus, and writing the ethics application. I assisted and/or supervised the surgeries, collected and analysed the data, carried out the statistical analysis and was the primary author of the manuscript. I received some assistance with histology preparation. Ethical approval was provided by the University of British Columbia Animal Care Committee under certificate A09-0366.

A version of Chapter 4 is being prepared for submission. Jones CF, Kwon BK and Cripton PA. *CSF pressure transients, cord deformation and load transmission are affected by CSF thickness and impact velocity in a bench-top model of contusion type SCI*. I was responsible for designing the study, designing and constructing the experimental apparatus, performing the experiments and collecting the data. I received assistance with processing the high speed x-ray images. I analysed the data and was the primary author of the manuscript.

A version of Chapter 5 is being prepared for submission. Jones CF, Newell RS, Lee JHT, Cripton PA and Kwon BK. *The pressure distribution of cerebrospinal fluid responds to residual compression and decompression in an animal model of acute spinal cord injury*. I was responsible for designing the study and associated apparatus, and writing the ethics application. I assisted and/or supervised the surgeries, collected and analysed the data, and was the primary author of the manuscript. I received some assistance with statistical analysis. Ethical approval was provided by the University of British Columbia Animal Care Committee under certificate A09-0366.

A version of Chapter 6 is being prepared for submission. Jones CF, Kwon BK and Cripton PA. *Gross morphological changes of the spinal cord immediately after surgical decompression in a large animal model of traumatic spinal cord injury*. I was responsible for designing the study and associated apparatus, and writing the ethics application. I assisted and/or supervised the surgeries, collected and

analysed the data, and was the primary author of the manuscript. Ethical approval was provided by the University of British Columbia Animal Care Committee under certificate A09-0366.

Table of Contents

List of Tables

List of Figures

List of Abbreviations

ASIA	American Spinal Injury Association
BBB	Blood brain barrier
BSCB	Blood spinal cord barrier
CAP	Central arterial pressure
CCI	Controlled cortical impactor
CNS	Central nervous system
CPP	Cerebral perfusion pressure
CSF	Cerebrospinal fluid
CSFP	Cerebrospinal fluid pressure
CSFPPA	Cerebrospinal fluid pulse pressure amplitude
CT	Computed tomography
CVP	Central venous pressure
ECG	Echocardiogram
EMG	Electromyography
EP	Evoked potential
FE	Finite element
FIR	Finite impulse response (filter)
FP	Fluid percussion
HR	Heart rate
ICP	Intracranial pressure
IH	Infinite Horizon (impactor)
IM	Intramuscular
IV	Intravenous
LMM	Linear mixed model
MAP	Mean arterial pressure
MASCIS	Multicenter Animal Spinal Cord Injury Study
MR	Magnetic resonance
NHP	Non human primate
NYU	New York University (impactor)
OSU	Ohio State University (impactor)
PLL	Posterior longitudinal ligament
PMHS	Post mortem human subject
RMSSD	Root mean squared of standard deviation
SCI	Spinal cord injury
SCIWORA	Spinal cord injury without radiographic abnormality
SCIWORET	Spinal cord injury without radiographic evidence of trauma
SCPP	Spinal cord perfusion pressure
SD	Standard deviation
TAAA	Thoracoabdominal aortic aneurysm
TBI	Traumatic brain injury

List of Symbols

F	Force [N]
g	Acceleration due to gravity [m/s^2]
g-cm	The product of grams and centimeters, employed as a "unit" of injury severity in weight-drop SCI models.
h	Height [m]
I	Impulse [Ns]
m	Mass [kg]
ms	Milliseconds
t	Time [s]
v	Velocity [m/s]

Acknowledgements

Many individuals have contributed to the successful completion of this thesis and my broader academic experience at UBC. I would like to express sincere gratitude to the following people without whom this journey would have been vastly different and not nearly as enjoyable.

The mentorship of my supervisory committee has extended far beyond this thesis and provided unique insights into different academic philosophies. My Ph.D. supervisor, Dr Peter Cripton, provided academic, intellectual and emotional support over many years. Thank you for the many opportunities you have given me to grow as a researcher and teacher. I will always treasure your eternal optimism and your friendship. My unofficial co-supervisor Dr Brian Kwon - from hands-on surgery to sage advice, it always felt like my work was just as important to you as it was to me. It has been a pleasure and a privilege to work with you and your staff. Dr Tom Oxland, thank you for your calm and thoughtful direction and support.

A small army of people contributed to the animal experiments and tolerated considerable disruption to their lives during that time: the veterinarians and staff at UBC Animal Care, Gordon Gray, Tamara Godbey, Bev Chua, Rhonda Hildebrandt and Kari Jones - thank you for looking after my girls so well and for welcoming me into your workplace; and my animal surgeons, Jae Lee and Uri Burstyn.

Past and present members of the Cripton, Oxland, Wilson, Kwon, Hodgson and McKay labs who have contributed, in one way or another, to my academic growth. Special mention to Robyn Newell, Emily McWalter, Jennifer Douglas, Angela Melnyk, Lindsay Nettlefold, Hannah Gustafson, Laura Greaves, Shannon Kroeker, JD Johnson, Tim Bhatnagar, Carolyn van Toen, Tim Nelson, Chee Leung, Tim Schwab, Qingan Zhu, Chad Larson, Anthea Stammers, Elena Okon, Jessica Hillyer, Melonie Burrows and Danmei Liu.

Glenn Jolly and Marcus Fengler, for their timely support and advice at times of electronic and mechanical crisis.

Robyn Newell, Peter Cripton, Pete Ostafichuk and Frank Ko, for your various contributions to my teaching, TAing and supervising experience at UBC.

Sincere and heartfelt thanks to Robyn Newell and Emily McWalter for their friendship, patience and care, and for providing perspective when it was needed most. I could not have asked for a better Canadian family - thank you for sharing this journey with me.

My friends in Perth, and around the world, who have tolerated long silences and always welcome me back as though no time has passed. Special thanks to Steve, Danielle, Monique, Deb, Esther and Murray.

My family, who continue to provide me all things necessary for grounding and success, and the motivation to get back to Australia. To my parents, Eleanor and Trevor, for believing in me, encouraging me and loving me during this long journey. My sisters, Christine, Nicole and Michelle, their partners, and little John, Adele and Luke, for their understanding of my absence from their lives. Special thanks to Christine for her care in Vancouver.

Chapter 1   Introduction

1.1 Overview

The cerebrospinal fluid is an important, but little studied, component of the central nervous system. There is a presumption that it provides mechanical protection for the neural tissue but there is little experimental data to confirm this for the spinal cord. In contrast, some clinical and experimental evidence suggests that cerebrospinal fluid (CSF) may contribute to the transmission of energy away from the spinal cord injury (SCI) site, leading to remote diffuse injury. There has also been recent interest in manipulating CSF pressure to control spinal cord perfusion after SCI, but the effects of subarachnoid occlusion caused by SCI and of subsequent surgical decompression on pressure differentials along the spine are not well understood. This thesis examines the transient response of the CSF pressure during the primary injury event and the trends in CSF pressure and layer thickness in the hours following SCI, using novel large animal and physical bench-top models.

The transient CSF pressure response during experimental SCI in animals has been reported by two groups [1-3]. However, these studies reported limited data and used fluid-filled catheters and external transducers which can lead to damping and lengthening of the signal. Measuring CSF pressure in the spinal region is technically difficult because the fluid layer is very thin, even in humans and large animals. Spinal catheters generally have a diameter similar to the CSF layer thickness in the cervical and thoracic region and are therefore likely to alter the mechanical response of the tissues and the fluid flow. Some physical models have also measured pressure inside a surrogate cord material during simulations of SCI, but due to the complex geometry and mechanical properties of the central nervous system (CNS) tissues these may not provide a biofidelic response; in addition, none have incorporated the CSF layer. Miniature transducers that permit the sensing element to be implanted in the subarachnoid space have been developed relatively recently. Combined with a large animal model and a human-like experimental SCI, reasonable measurements of subarachnoid pressure transients at multiple locations along the spinal cord are feasible.

SCI often results in residual compression of the spinal cord and occlusion of the CSF pathways (subarachnoid space) due to bony malalignment or fragments and spinal cord swelling. Early decompression is advocated and CSF drainage has been proposed as treatment options to increase tissue perfusion and reduce secondary ischaemic damage. Because it is not possible to measure CSF pressure cranial to the injury site in SCI patients, it is not known whether a pressure differential develops over the lesion site in the hours after injury, and if so, if it is then resolved by decompression. The complexity of the physiological processes that regulate CSF and vascular pressures makes this difficult to predict. In

addition, the time course of spinal cord swelling and hence the patency of the subarachnoid space after decompression has not been studied.

The introductory chapter aims to provide an overview of SCI biomechanics, the current state of knowledge regarding the contribution of CSF pressure at the time of SCI, and its behaviour in the hours following SCI with an occluded and decompressed subarachnoid space. This chapter is presented in seven sections. First, a basic anatomical review of the spine, spinal cord and associated tissues is given, followed by the functions, physiology and pressure characteristics of the cerebrospinal fluid system. Then the etiology, mechanisms, risk factors and pathophysiology of SCI are outlined, along with two treatment options that are associated with the current work. Next, a framework for the mechanical aspects of SCI is provided: the properties of the soft tissues and fluid, mechanical parameters influencing SCI severity, CSF pressure transients measured in previous models of SCI and injury thresholds of the neural tissue are outlined. This is followed by a critical appraisal of past and present methods used to replicate human trauma in experimental SCI models, and the transducers that have previously been used to measure CSF pressure in the CNS. The chapter concludes with a statement of the thesis objectives and hypotheses which are addressed in the studies presented in Chapters 2 through 6. Chapter 7 discusses the contribution this thesis makes to understanding of the role of CSF in the injury and hyperacute phase, with recommendations for future research.

1.2 The spine and spinal cord

This section provides an introduction to the location and structure of the spinal anatomy associated with SCI, including the spinal column, the spinal cord and its cellular components, the meninges and the cerebrospinal fluid system. A more detailed introduction to CSF physiology, function and mechanics are provided in the following sections.

1.2.1 Anatomical orientations

The three major anatomical planes are the coronal, sagittal, and transverse (or axial) planes (Figure 1-1). The relative locations of structures are described by five pairs of terms, as defined in Table 1-1. Throughout this thesis, the terms associated with quadrupedal animals are generally used, except the term cranial is substituted for rostral.

Table 1-1 Anatomical orientations and locations

Human	Quadruped	Description
Anterior / Posterior	Ventral / Dorsal	Structures relative to the front/back of the body
Cranial / Caudal Superior/Inferior	Rostral / Caudal	Relative location along vertical axis, towards the head / towards the feet
Medial / Lateral	Medial / Lateral	Proximity to the median sagittal plane / sides of the body
Proximal / Distal	Proximal / Distal	Proximal (closer to a structure's origin), distal (further from a structure's origin)
Superficial / deep	Superficial / deep	Relative position with respect to surface of body
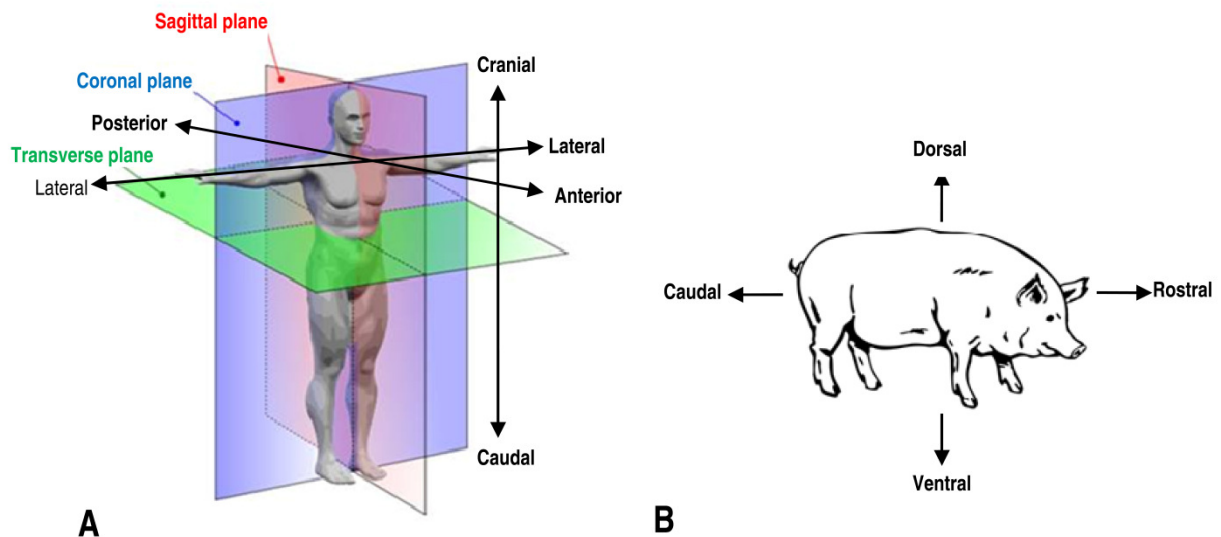
Figure 1-1 Planes and directions used to describe anatomical positions in the (A) human and (B) quadruped. Image (A) adapted from Wikimedia Commons.

1.2.2 Spinal column

The spinal column houses the spinal cord, giving it structure, suspending it, and protecting it from traumatic loading. The human spinal column consists of 33 vertebra, which are divided (from cranial to caudal) into the cervical (7), thoracic (12), lumbar (5), sacral (5 fused) and coccygeal (3-4 fused) regions, by virtue of specific anatomical features and function. The spine has a natural lordotic (anterior convex) curve in the cervical and lumbar regions, and kyphotic (anterior concave) curve in the thoracic region (Figure 1-2).

Each vertebra is comprised of the vertebral body, which is the main axial load bearing element, and a series of posterior elements which are attached to the vertebral body via the pedicles. The posterior

3

vertebral body and posterior elements form the vertebral foramen, which, when stacked together, form the spinal canal in which the spinal cord resides. Adjacent vertebrae are separated by intervertebral discs, relatively flexible elements which allow intervertebral motion and some compliance for damping loads. The posterior elements comprise the laminae, a number of processes for the attachment of the spinal muscles, and the facet joints which limit intersegmental motion.
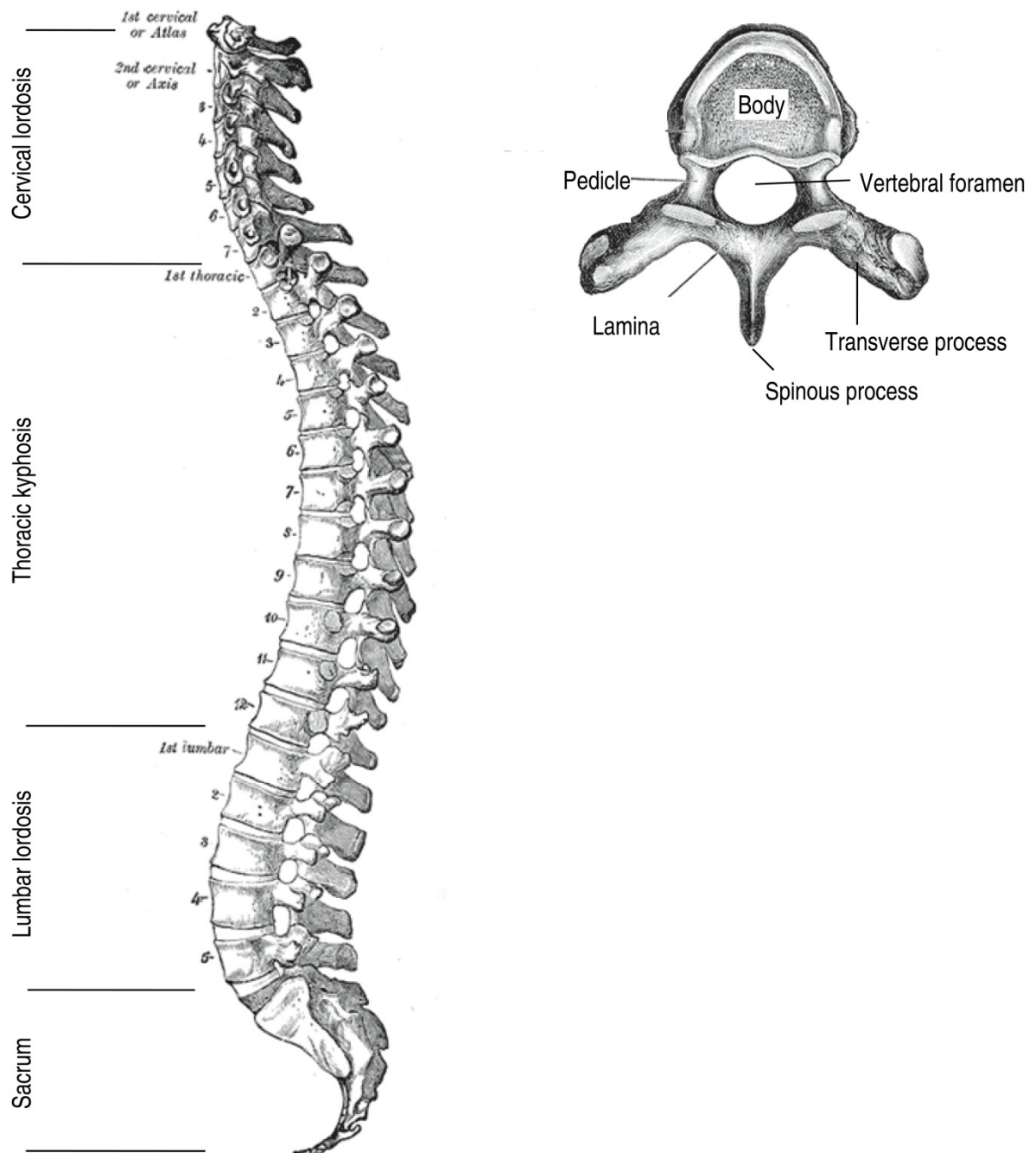
Figure 1-2 Sagittal view of the human spinal column (left), superior view of a typical thoracic vertebra (right) Graphics adapted from Gray's Anatomy 1918 (copyright expired).

1.2.3   Spinal cord

The spinal cord is categorised into regions and levels corresponding to those of the spinal vertebrae. Each level controls the functions of a particular region of the body via a defined set of spinal

nerves (see below). The spinal cord is continuous with the brainstem and extends approximately two-thirds of the spinal column from the foramen magnum to approximately the second lumbar vertebra (L2). The inferior end of the spinal cord tapers to the *conus medullaris*, at the end of which a filament of pial tissue continues to attach to the coccyx. The spinal cord is roughly oval in cross-section, with the major axis in the coronal plane, and has an increased cross-section at the cervical and lumbosacral enlargements which are situated at the lower cervical and thoracic regions, respectively. These enlargements correspond to the increased nerve supply to the upper limb (C3–T1) and the lower limb (L1–S3) plexuses (Figure 1-3, right).

In axial cross-section, the spinal cord consists of two primary tissue types – the inner gray matter with a distinct butterfly or 'H' shape, and the surrounding periphery of white matter (Figure 1-3, left). The grey matter contains neuronal cell bodies which make motor and sensory signals and decisions relating primarily to the functions served by the spinal segment that they reside in, as well as glial cells that support these neuronal functions. The white matter contains myelinated ascending and descending axons that transmit signals between neurons of the brain/brainstem and those of the spinal cord grey matter, or between spinal levels. The grey matter is highly vascularised, while the white matter is less so.

Communication between the central and peripheral nervous system occurs via 31 pairs of spinal nerves. Each pair enter and exit the spinal canal laterally at each vertebral level, via the intervertebral foramina (Figure 1-3, left). Each spinal nerve comprises two bundles of nerve roots, one containing motor fibres that exit the anterior (ventral) cord and the other containing sensory fibres that enter on the posterior (dorsal) cord. Because the spinal cord is shorter than the vertebral column, the nerve roots become progressively longer and travel further before reaching their intervertebral entry/exit point in the more caudal regions. The cluster of roots inferior to the tapered end of the spinal cord, are called the *cauda equina* (Figure 1-3, right).

As previously mentioned, each level of the spinal cord controls a particular body region. Due to the localised functions of the grey matter, damage to a particular level of the spinal cord results in neurological deficits in the body regions associated with that level. In contrast, damage to the white matter tracts interrupts the passage of signals between the brain and the segments caudal to the level of injury, thus affecting the functions maintained below that level that are controlled by the brain.
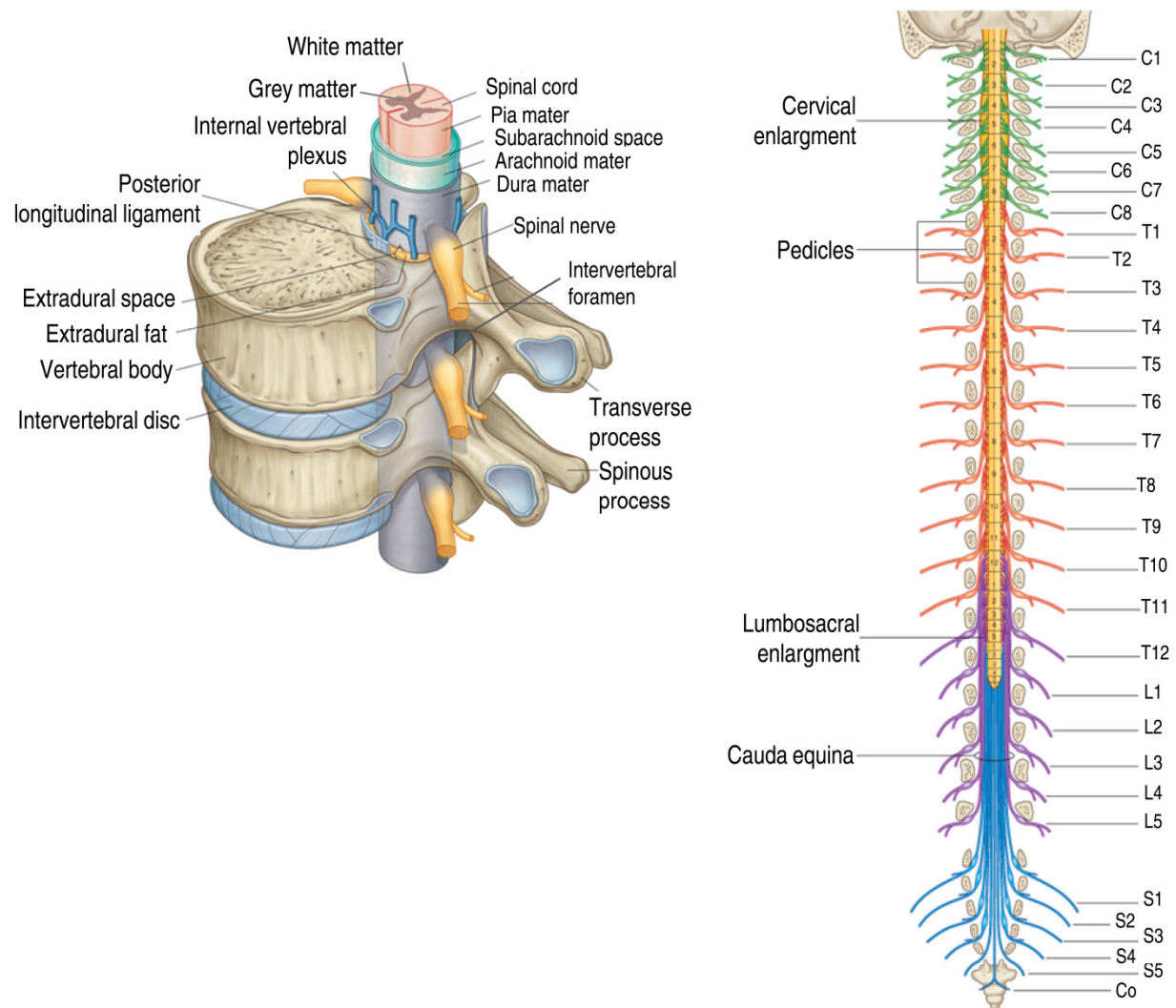
Figure 1-3 Anatomy of the spinal vertebra and spinal cord. Two vertebrae, each with the inferior intervertebral disc. The spinal cord, meninges, venous plexus are situated in the spinal canal, between the vertebral body and posterior elements of the vertebrae (left). The segmental arrangement of the spinal nerves, showing the cervical and lumbar enlargement and the cauda equina in the lumbar region (right). Adapted from Drake et al., Gray's Anatomy for Students, 2005, with permission from Elsevier:Churchill Livingston [4].

1.2.4   Functional divisions and cellular components of the spinal cord

The grey matter can be divided into three functional regions: the dorsal (posterior), ventral (anterior) and intermediate horns; these columns of grey matter extend various lengths along the spinal cord. The dorsal grey matter contains sensory neurons, while the ventral grey matter contains motor neurons. The intermediate horn contains sympathetic neurons. The white matter also has three functional divisions: the dorsal, ventral and lateral columns. The dorsal column contains axon fibre tracts that carry ascending sensory information from the spinal cord to the brain. The ventral columns contain axon fibre

7

tracts that carry descending motor information from the brain to the spinal cord. Subdivisions of the lateral columns have both sensory and motor tracts.

In addition to the neurons and axons described above, the glial cells of the spinal cord perform support functions for the neurons and axons. These include: microglia, which are specialised macrophages that remove damaged neurons and infectious agents; astrocytes, that regulate the extracellular chemical environment; and oligodendrocytes, which form myelin for coating the axons.

1.2.5 Meninges

The spinal cord is covered by three membranous layers, collectively referred to as the meninges. The inner most is the pia mater, a thin transparent membrane that is closely adhered to the spinal cord and covers the spinal blood vessels. The middle layer is the arachnoid mater. Both the pia and arachnoid membranes are thin, transparent and avascular. They are connected by extremely thin strands of connective tissue called the arachnoid trabeculae. The arachnoid is closely adhered to the outermost layer, the dura mater, and these two membranes are commonly referred to collectively as the dura. The dura mater is a thicker, stronger membrane comprised of an elastic matrix with collagen fibres. All three membranes extend over the spinal nerves and the brain. The "space" between the arachnoid and pia, referred to as the subarachnoid space or the intrathecal sac, contains the cerebrospinal fluid, and is continuous with the cerebral ventricles and cerebral subarachnoid space. It also contains the spinal arteries and veins. The spinal cord and pia are tethered within the dura/arachnoid by the denticulate ligaments which extend between the interior borders of the subarachnoid space, midway between the dorsal and ventral nerve roots (Figure 1-4). The spinal dura is located in the spinal canal by attachments to the foramen magnum and to the coccyx via the *filum terminale*. The epidural or extradural "space" separates the dura mater from the surface of the spinal canal. It contains variable amounts of epidural fat, the subdural venous plexus, spinal arteries and lymphatic vessels, as well as the ligamentum flavum and posterior longitudinal ligament (PLL) at the posterior and anterior border of the canal, respectively (Figure 1-3, left).
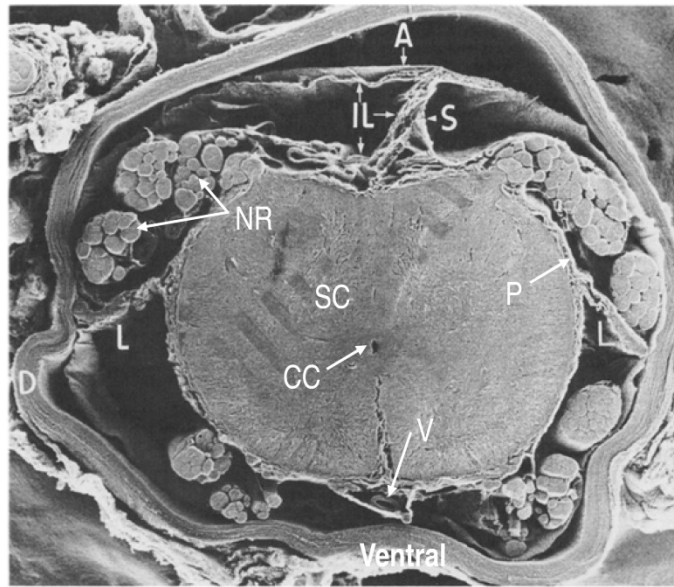
Figure 1-4 Scanning electron micrograph of the lumbar spinal cord of a 15-month-old child. The spinal cord (SC) contains the central canal (CC) and is closely surrounded by the pia mater (P). The dentate ligaments (L) are seen on each side of the cord, and the dorsal septum (S) at the top of the cord; both are continuous with the pia and merge into the arachnoid mater (A). The individual layers of the dura (D) can be seen. The subarachnoid space contains nerve roots (NR) and blood vessels (V). Note that the arachnoid mater is more closely associated with the dura mater and the dural circumference is more oval in shape *in vivo*. Adapted from Journal of Neurosurgery, 69(2), Nicholas and Weller, The fine anatomy of the human spinal meninges. A light and scanning electron microscopy study, 276-82, 1988, with permission from the American Association of Neurological Surgeons (AANS) [5].

1.2.6   Ventricular system

There are four cerebrospinal fluid filled ventricles in the brain, connected by a series of channels (Figure 1-5). The two lateral ventricles are within the cerebral hemispheres, and each connect to the more caudal and midline third ventricle via the interventricular foramen of Monro. The fourth ventricle is located in the midline between the brain stem and cerebellum, and is connected to the third by the cerebral aqueduct of Sylvius. The ventricles contain choroid plexuses which are capillary rich cellular masses that form CSF, as described in Section 1.3.2. Cerebrospinal fluid enters the cranial and spinal subarachnoid spaces via several apertures in the roof of the fourth ventricle (foramen of Magendie and two foramina of Luschka), and this ventricle is continuous with the central canal of the spinal cord inferiorly.
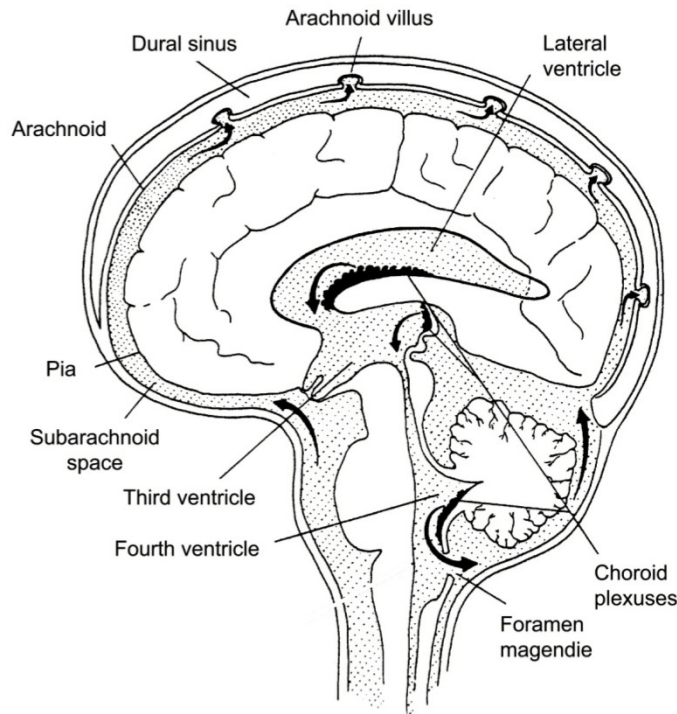
Figure 1-5 The ventricular system within the human brain. The locations of the choroid plexuses (solid black structures) and the distribution of CSF (dotted area). Adapted from Neuroscience, 129(4), Brown et al., Molecular mechanisms of cerebrospinal fluid production, 957-70, Copyright (2004), with permission from Elsevier [6].

1.3   Function, physiology and pressure characteristics of the CSF system

CSF is a transparent, colourless, water-based fluid that is formed, circulated and reabsorbed in the ventricles and the subarachnoid space surrounding the brain and spinal cord. It has a similar composition to blood plasma but contains less protein. The adult human ventricles and subarachnoid space (cranial and spinal) contain around 25 and 115 mL of CSF respectively, for a collective volume of approximately 140 mL [7]. CSF is formed at a rate of around 0.35 mL per minute [8,9], and thus has a complete volume turnover every 6-8 hours [10]. The functions, physiology and mechanics of CSF are complex but a basic understanding of each is necessary to appreciate how CSF may attenuate or amplify the severity of a SCI, at the time of injury and in the subsequent hours. This is an area of ongoing research and so this section highlights the current understanding as it pertains to this thesis.

1.3.1   Functions of CSF

CSF is commonly ascribed five main physiologic and mechanical functions: (1) providing a chemical environment conducive to the efficient transmission of neural signaling; (2) carrying nutrients and waste to and from the CNS; (3) providing neutral buoyancy for the brain and spinal cord; (4)

protecting the neural tissue from contact with the cranium or spinal canal during external body loading; and (5) protecting the CNS from acute blood pressure changes which would alter tissue perfusion, by volume adjustment.

This thesis addresses aspects of the latter two items, and an appreciation of the physiology and mechanical characteristics of the CSF pathways and flow is necessary to appreciate the interpretation of the results of the studies herein.

1.3.2   CSF formation, circulation and reabsorption

The normal mechanisms, regulators and locations of CSF production and absorption are not well understood. There is considerably less known about the system's response to spinal pathology, particularly that resulting from traumatic injury. A detailed account of current knowledge is given by Johanson et al. [11], and a brief description is given here.

1.3.2.1   Formation locations, mechanisms and rates

It is generally agreed that the CSF is formed in the ventricular system in the cranial vault, more specifically originating in the choroid plexus, ependyma and parenchyma. Quantifying the relative contribution of the sources to total CSF production is technically challenging [12], because considerable operative manipulation is required and unknown compensatory mechanisms may arise [13]. Current agreement is that around 60-90% of formation is choroidal, although estimates have ranged from around 30 to 70% [14,15]. The diffusion of interstitial fluid across the ependyma or pia mater in the brain, may contribute 20-30% of fluid production [13]. Importantly, both of these sources are in the cranial vault. No *spinal* CSF production has been found in cats [16,17], monkeys [18] or dogs [19].

The choroid plexuses are branched structures made up of villi projecting into the ventricles, where each villus is a single layer of epithelial cells overlying a cluster of connective tissues and blood capillaries. The CSF is generated by these epithelial cells via a two step process. The first step is the passive filtration of plasma (ions and water) across the choroidal capillary endothelium, driven by the pressure-gradient between the capillary blood and choroid interstitial fluid. The second step is active secretion across a single-layered epithelium, which is regulated by a complex array of epithelial transporters and ion channels. Further details are given by Brown and colleagues [6,20].

The normal CSF formation rate has been determined for several species and appears proportional to species size and therefore probably total CSF volume (Table 1-2). Formation rate varies with age and this may reflect changes in brain CSF volume [21,22]; it also varies throughout the circadian rhythm [23].

Table 1-2 CSF formation rates and weight range of various mammals. Weights are as stated by authors unless otherwise indicated. To the author's knowledge, there is currently no published data for the pig.

Species	Weight (kg)	CSF formation rate (mL/hr) [reference]
Mouse	0.02-0.04*	0.02±0.004 [24]
Rat	0.2-0.4*	0.12 [25]
Monkey	2-4 2.1-4.1	1.70±0.15 [18] 1.80-2.65 [26]
Cat	2-6*	0.9±0.6 [27]
Dog	12-17	2.76±0.12 - 2.82±0.36 [28]
Sheep	60-90‡ [29] 25-30 35-40 NR†	2.46±0.42 (young) 1.86±0.44 (middle aged) 1.17±0.16 (old) [22] 3.37±0.38 [30] 4.94±0.10 [31] 6.67±1.06 [32]
Goat	30-60‡ [33]	9.6 [34]
Human	25-40* 60-80 60-100* 60-100*	21±1.2 (children) [9] 20.4±7.8 (young adults) [35] 11.4±4.2 (elderly, ~77yrs) 24.6±14.4 (young, ~29yrs) [21] 22.2 [8]

*estimated

†NR=not reported

‡from alternate paper from same group

Response of the CSF formation rate to CSF pressure is considered negligible under normal physiological conditions. In short-term experimental elevation of intracranial pressure (ICP) in animals, this effect has been seen in some [36,37] but not all animals [28,34,38] and humans [9,35]. The rate is decreased with significantly elevated intracranial pressure; presumably the initial passive filtration step is diminished due to the decreased choroidal blood flow [13] (see Section 1.3.3.2). The rate of formation is also thought to be modified by metabolic and other physiological processes, such as osmotic pressure of the blood [12,34] but little is known about these. The presence of autonomic nerve terminals in the choroid plexus has led some researchers to suggest that there is neurogenic control of CSF secretion [12,39]; however, the functional role of the innervations in normal and pathological conditions is largely unknown.

1.3.2.2 Absorption locations and mechanisms

CSF is cleared into the lymph and venous systems at several locations via several physiological mechanisms; recent reviews have been given by Kapoor et al. and Johnston et al. [40,41]. Initially, the cranial and spinal [42] arachnoid granulations and villi were thought to be the sole site for CSF reabsorption into the superior sagittal sinus and epidural veins. Arachnoid villi are herniations of arachnoid membrane into either the lumen of the superior sagittal sinus in the brain or the small spinal veins adjacent to spinal nerve roots. More recently, both cranial and spinal lymphatic drainage pathways

have been acknowledged [43]. The cranial pathway is primarily through the cribriform plate into the cervical lymph, and the spinal pathway is via lymphatic channels in the dura [41]. Lymphatic absorption accounts for 40-48% of CSF clearance in sheep [30], and there is morphological evidence for similar lymphatic absorption in humans and non-human primates [44].

CSF reabsorption is a passive process driven by a pressure differential between the subarachnoid and venous systems and the rate has a relatively linear relationship to CSF pressure over a wide range of pressures [13,45]. In normal individuals, absorptive capacity is thought to be much greater than that needed to maintain mass balance [38]. Human data have shown that absorption begins at a CSF pressure of 5 mmHg (no venous pressure reported) [9], and in animals reabsorption occurred at a CSF-to-venous pressure differential of 1.5-7 mmHg [46,47]. The pressure differential is crucial to the operation of the arachnoid villi, which act as a one-way valve and allow the passage of CSF into the blood when CSF pressure is higher than venous, but collapse when this gradient is reversed so that blood cannot pass the other way. Recent evidence suggests that the lymphatic mechanism predominates at lower pressure gradients while the arachnoid villi are secondarily recruited at higher CSF pressures [48].

Spinal absorption has been demonstrated to account for 25% of total absorption in sheep [49] and 50% in cats [27]. In humans, spinal absorption is estimated to occur at around 10 mL/hr [35], which probably accounts for around 50% of total absorption given the formation rates stated above. Increased spinal absorption is associated with activity compared to resting, in humans [35]. The number of observed arachnoid villi increases from the cervical to the lumbar spine in humans [50], which may imply a caudally increasing absorption rate.

1.3.3   CSF pressure and flow

Similar to other physiological pressures, the CSF pressure is pulsatile. It is described with a mean value and an amplitude value. The mean value is termed the mean CSF pressure, or simply the CSF pressure, and its characteristics are described in Section 1.3.3.2, below. The amplitude is most commonly called the pulse pressure amplitude and is described in Section 1.3.3.3, below.

1.3.3.1   *Tissue perfusion pressure and pressure-volume compensation*

The spinal cord perfusion pressure (SCPP) is a measure of the pressure gradient across the capillary bed of the tissue, and relates directly to tissue blood flow and therefore to the supply of oxygen to the tissue's cells. It cannot be measured directly and is therefore defined as the difference between the mean arterial pressure (MAP) and the CSF pressure (CSFP), i.e., SCPP=MAP-CSFP. This relationship shows that, for a given MAP, there is a CSF pressure threshold above which the perfusion pressure is inadequate

to prevent tissue ischaemia. Further, it implies that the perfusion of the tissue can be controlled by manipulating the mean arterial pressure and/or the CSF pressure.

The largely incompressible components of the CNS (the brain, spinal cord, CSF and blood) are contained within the rigid bony confines of the cranium and spinal canal, thus an increase in the volume of one component requires an equivalent decrease in the volume of another in order to maintain constant pressure. This reciprocal compensation is finite and is termed the intracranial compliance. The phenomenon is most commonly described for the compensation of cytotoxic (extracellular) and/or vasogenic brain swelling. The cranial venous sinuses are compressed, the CSF is displaced from the cranium to the spinal subarachnoid space and the compliant epidural venous plexus is compressed [51-53]. The compliance curve, which plots intracranial pressure (ICP against intracranial volume as shown in Figure 1-6, has three phases: (A) adequate compensatory reserves, (B) increasing volume but ICP maintained, and (C) compensatory reserve exhausted. In the latter phase a small change in volume leads to a significant change in ICP.

Although the compensatory systems are described for the cranial space, it is important to note that under non-pathological conditions, the cranial and spinal CSF spaces are communicating, and therefore compensation for increased spinal cord volume could conceivably occur in the opposite direction; i.e. fluid volume may be directed from the spine towards the cranium, or flow into the spinal compartment may be decreased, to maintain constant pressure. This does not appear to have been discussed in the published literature.
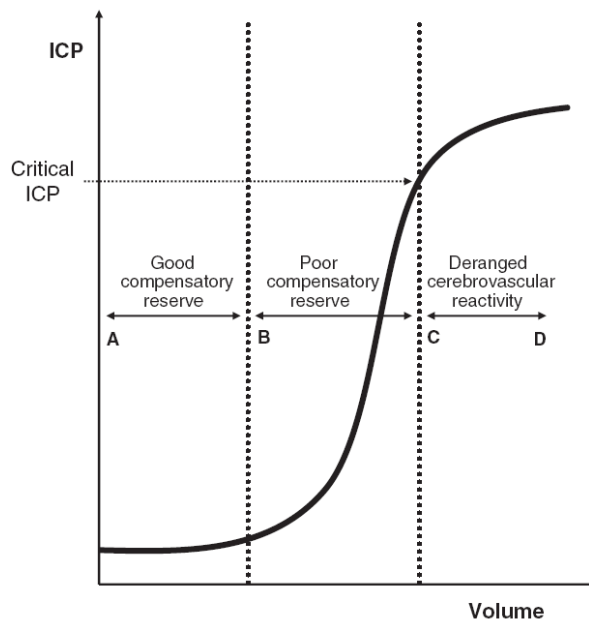
Figure 1-6 Intracranial pressure volume curve. (A-B) good compensatory reserve, fairly constant ICP maintained despite changes in volume; (B-C) poor compensatory reserve, small changes in volume produce large changes in ICP; (C-D) terminal dysfunction of cerebrovascular responses. Reproduced from Anesthesia and Analgesia, 106(1), Smith et al., Monitoring intracranial pressure in traumatic brain injury, 240-8, 2008, with permission from Wolters Kluwer Health [54].

1.3.3.2   *CSF pressure*

Physiological pressures are usually stated in millimeters of mercury (mmHg), or centimeters of water (cmH$_2$O), where 1 mmHg = 1.34 cmH$_2$O = 0.13 kPa = 0.019 psi. Clinically, CSF pressure measured by lumbar puncture can form part of the diagnosis of subarachnoid haemorrhage, meningitis, cerebral venous sinus thrombosis, idiopathic intracranial hypertension, and intracranial hypovolaemia [55]. It is measured with the patient horizontal in the lateral decubitus position, and the reference level, or "zero", is the pressure in the right atrium of the heart. CSF pressure can also be measured in the ventricles, where it is termed intracranial pressure (ICP); this can also refer to intraparenchymal pressure, but this is not necessarily equivalent to the former [54]. When measured in the supine position, lumbar CSF pressure is the same as ICP in patients with a communicating subarachnoid space [56]. Normal CSF pressure ranges between 5-15 mmHg for the adult [54,57-60], and is lower for children (3-7 mmHg) and infants (1.5-6 mmHg) [54]. The acceptable, non-pathologic, upper limit varies between sources, with the highest being around 18.5 mmHg [58,61].

Considerable transient changes in spinal CSF pressure can be elicited by various everyday activities and clinical tests which temporarily alter the intra-abdominal or venous plexus pressures. For example, spinal CSF pressure can be altered by nose blowing (18.2 mmHg), breath holding (12.1 mmHg), sniffing (-3.8 mmHg) [62] and coughing (40 mmHg) [63]. The Valsalva manoeuvre, in which the

individual exhales forcibly against a closed airway, can elevate CSF pressures to 35 mmHg in normotensive patients [59,64] (Figure 1-7, left). The Queckenstedt test, which involves acute occlusion of the jugular veins, can induce increases of up to 10.7 mmHg [63] (Figure 1-7, right). Changes in the diameter of the lumbar intrathecal sac have been visualised radiographically for these two maneouvres [65]. Although these changes can be up to three times the normal pressure, they do not invoke injury during the short period of application.
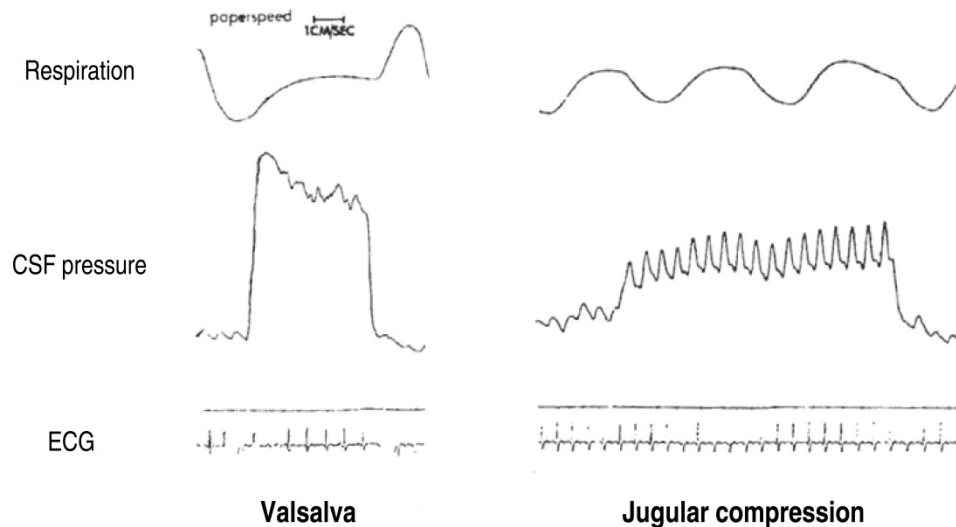
Figure 1-7 CSF pressure response (central trace) to Valsalva manoeuvre (left) and jugular compression (Queckenstedt test, right), with reference respiration trace (top) and echocardiogram (ECG) trace (bottom). Note that ordinate scales were not provided in the original publication. Adapted with permission from Lakke, Queckenstedt's test; electromanometric examination of CSF pressure on jugular compression and its clinical value, 1969, © Excerpta Medica [66].

Lumbar CSF pressure can differ from ICP when the subarachnoid space is occluded at, or caudal to, the foramen magnum. This has been observed in patients with a mass lesion or brain swelling that displaces the brain toward the foramen magnum [67], and with transtentorial or tonsillar herniation [68]. Pressure differentials associated with subarachnoid occlusion are the basis of the "spinal block infusion test" [69] and the Queckenstedt test [70], although these appear to have largely been superseded by imaging studies which can visually demonstrate occlusion of the subarachnoid space. Lumbar puncture in the presence of a complete spinal block due to a spinal tumour can cause "downward spinal coning", which indicates the presence of a low pressure compartment below the tumour [71]. Further, in a patient with severe cervical spondylosis, a low lumbar pressure measurement returned a false-negative result for hydrocephalus [72], and intracranial hypertension has been noted in several cases of spinal tumours [73-77]. In cats with a cervical obstruction induced by subarachnoid kaolin injection, CSF pressure was on

16

average 1.5 mmHg higher on the cranial side than the caudal side after four months [78]. Jugular occlusion caused a mean increase in lumbar CSF pressure of 29.7 mmHg in six patients with incomplete spinal block, compared to only 4.2 mmHg in five patients with a complete block [79]. Another implication of obstructed CSF flow is that the volume compensation capacity of each compartment would be restricted to the venous compensation available in that compartment. Therefore, relatively small changes in tissue volume would likely have a substantial effect on compartment pressure.

The pressure-volume relationships of the intracranial and spinal spaces, described in Section 1.3.3.1 above, indicate that CSF pressure is strongly influenced by vascular pressures and volumes, which are in turn influenced by changes in the rates of CSF formation and absorption, osmotic pressure and equilibrium, rates of diffusion and secretion of metabolites, sympathetic nervous system activity and dural elasticity, among other factors. In short, there are very complex interactions between these fluid systems, which make it difficult to predict the reaction of the system to trauma and the secondary sequelae.

1.3.3.3 *CSF pulsations*

CSF pressure has three predominant pulsatile components: respiratory, vascular and slow wave [54], of which only the first two are applicable to this work (Figure 1-8). The respiratory pulsation is due to changes in the pressure differential between the subarachnoid space and the pleural or intra-abdominal cavities that occur over the respiratory cycle [80]. These fluctuations occur at a rate of 8-20 cycles/min (0.15-0.35 Hz), with an amplitude of around 0.75-3.75 mmHg for regular breathing and 3.75-7.5 mmHg for deep breathing [81]. This effect is also common to central arterial and venous pressure measurements [82]. The accepted "true" CSF pressure is during the phase of ventilation when the pleural pressure is closest to zero, i.e. at end-expiration [80]. The value may be derived by manual observation of the pressure trace, or by applying digital filtering algorithms to the signal [83].

The vascular pulsation is coincident with the heart beat and therefore has a frequency of 1-1.6 Hz (60-100 beats/min). Several intertwined mechanisms for transmission of the pulsation from the blood to the CSF have been proposed, and it is likely that a combination of these contribute. They include: brain and spinal cord motion due to expansion of, and intramural transmission from, the cranial and spinal arteries [84-86], variation in the size of the lateral ventricles [87,88] and choroid plexus expansion [89].

The predominantly cranial location of the aforementioned pulsation sources is consistent with differences observed between the cranial and caudal CSF pulsations measured in both healthy and pathological subjects. The peak amplitude of the high frequency CSF pulsation is known as the pulse pressure amplitude (Figure 1-8). In normal patients it is greatest in the ventricles and decreases with caudal distance from the cisterna magna (Figure 1-9) [89,90]. It also has delayed phase in the lumbar

region compared to the ventricles and cisterna magna (Figure 1-9) [89]. It is absent in the lumbar region in patients with non-communicating hydrocephalus and spinal subarachnoid blocks [89], and in some SCI patients before decompression [91].
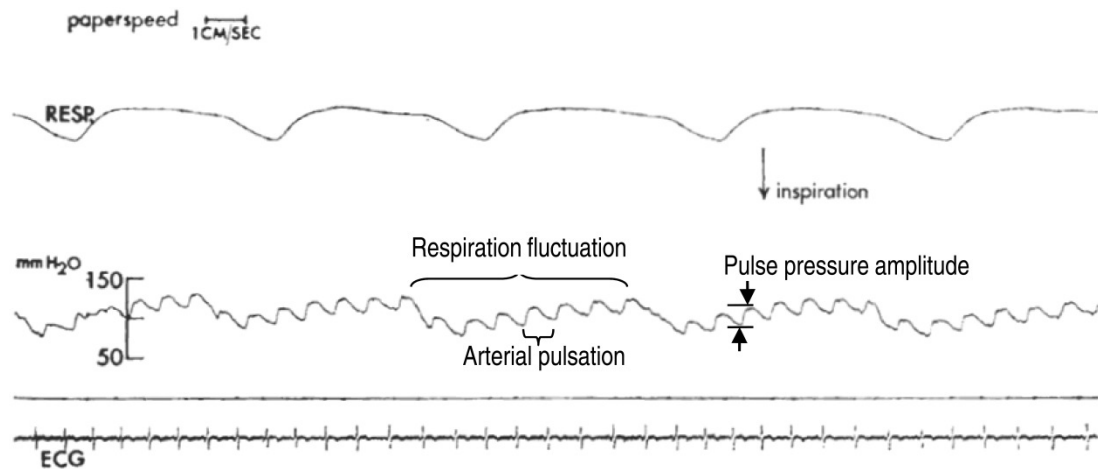
Figure 1-8 Graph of normal CSF pressure signal with arterial pulsations and respiratory fluctuations (centre), with reference respiration trace (top) and echocardiogram trace (bottom). Adapted with permission from Lakke, Queckenstedt's test; electromanometric examination of CSF pressure on jugular compression and its clinical value, 1969, © Excerpta Medica [66].

Figure 1.9 has been removed because of copyright restrictions. The figure was adapted from Figure 3, Archives of Neurology and Psychiatry, 73(2), Bering et al., Choroid plexus and arterial pulsation of cerebrospinal fluid; demonstration of the choroid plexuses as a cerebrospinal fluid pump, 165-72, 1955, American Association of Neurological Surgeons (AANS) [89].

Figure 1-9 Simultaneous recordings of a single cycle of ECG and CSF pressure pulse in the cerebral ventricle (V), cisterna magna (C), and lumbar subarachnoid space (L), in millimeters of water. The CSF waveform exhibits respiratory and vascular pulsations; note the reduced respiratory and arterial pulsations in the more caudal recordings.

The clinical meaning of the pulse pressure amplitude is not fully understood. Pulse pressure amplitude is influenced by a complex myriad of physiological variables including heart rate, arterial blood pulse amplitude, venous outflow, compliance of the arterial bed and the venous and subarachnoid spaces, and arterial carbon dioxide concentration [92, see comment by Czosnyka]. These variables act in parallel and have interacting regulating mechanisms, so they are difficult to manipulate and test independently. It is generally accepted that pulse pressure amplitude is proportional to the mean CSF pressure (Figure 1-10), the change in cerebral blood volume over the cardiac cycle and the mean arterial pressure [93-96].
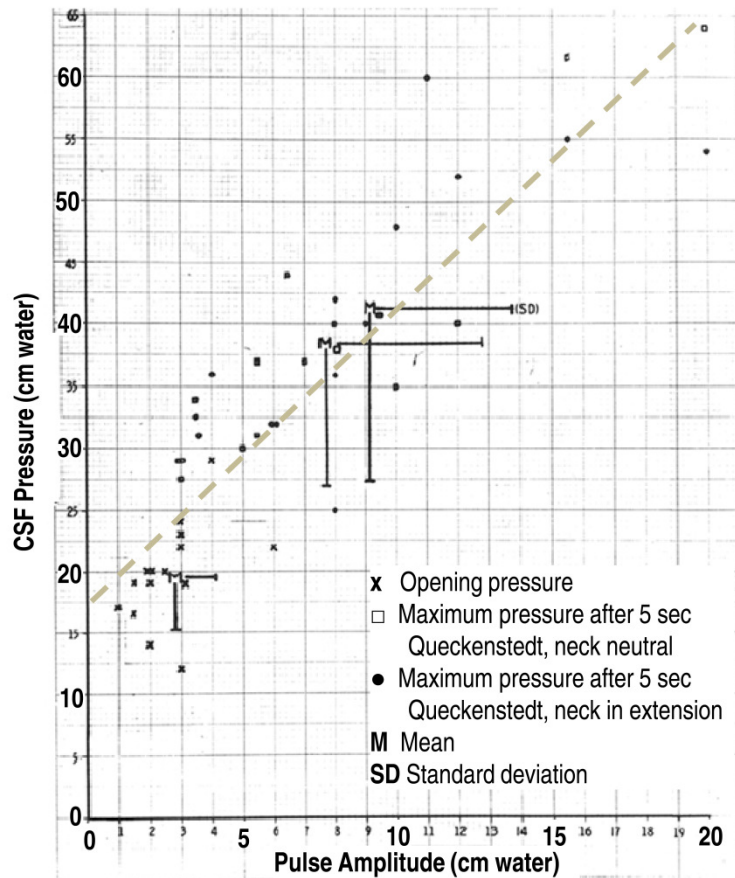
Figure 1-10 CSF pressure vs. pulse pressure amplitude in 14 healthy volunteers. Data are shown for opening pressures and peak pressures during Queckenstedt's test (jugular compression). M is for mean, and large bars are standard deviations. Grey dashed line is an estimated line of best fit added by the author. Adapted from Journal of Neurosurgery, 40(5), Gilland et al., Normal cerebrospinal fluid pressure, 587-93, 1974, with permission from the American Association of Neurological Surgeons (AANS) [58].

It has been suggested that the return of lumbar pulse pressure amplitude may be indicative of successful spinal decompression in traumatic SCI patients [91] (Figure 1-11). In the cranial space it has been investigated as a prognostic tool for normal pressure hydrocephalus [97] and paediatric hydrocephalus [98], traumatic brain injury (TBI) [99] and subarachnoid haemorrhage [92].
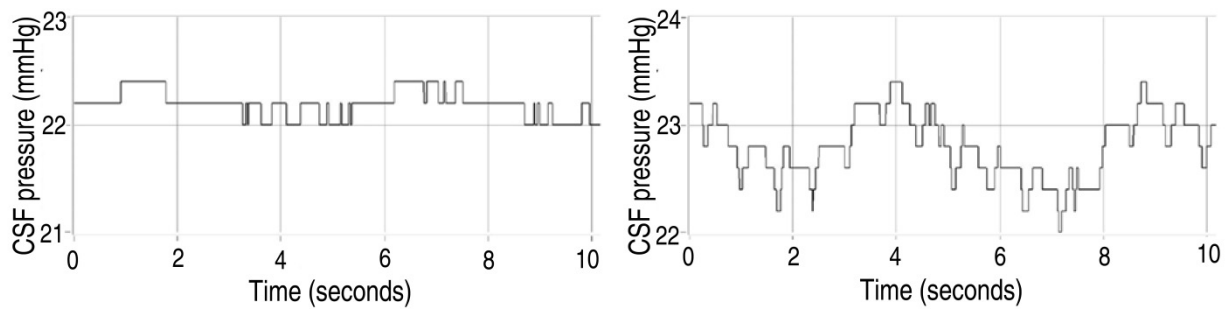
Figure 1-11 Lumbar CSF pressure waveforms in a SCI patient before and after decompression.
Note that the respiratory waveform amplitude and pulse pressure amplitude are increased after decompression. Adapted from Journal of Neurosurgery: Spine, 10(3), Kwon et al., Intrathecal pressure monitoring and cerebrospinal fluid drainage in acute spinal cord injury: a prospective randomised trial, 181-93, 2009, with permission from the American Association of Neurological Surgeons (AANS) [91].

CSF pressure in mammals has similar characteristics to humans, but the mean CSF pressure tends to be lower in magnitude. For dogs in the prone position it was 7.5±1.1 mmHg at C3, and 6.5±0.9 mmHg at L4 [100]; lumbar pressure in the cat was 8.7±0.5 mmHg [101]; primate, 7 mmHg [102]; cranially in the pig, 15±3 mmHg [103]; and in the rat lumbar pressure was 4.2±2.5 mmHg [104]. In the rat cisterna magna, the mean pressure was 4.1 mmHg and rose to approximately 15 mmHg with Valsalva [105]. Several authors have noted that spinal pressure is responsive to changing the angle of the animal's body [100] and raising the animal's head [101], both results are a logical consequence of altering the hydrostatic pressure acting on the lumbar measurement location. Intracranial CSF pressures of up to 100 mmHg in primates [102] and 152 mmHg in pigs [103] have been experimentally induced for short periods without ischaemia or death.

1.3.3.4   *CSF flow pathways and velocity*

Like all fluids within the body, the cerebrospinal fluid is undergoing constant motion to maintain homeostasis. At any one time, only a small proportion of the total CSF resides in the spinal subarachnoid space; the majority circulates around the brain. Magnetic resonance (MR) imaging illustrates that the flow of cerebrospinal fluid is pulsatile; at the foramen magnum, during each cardiac cycle there is a short period of cranially directed flow followed by a longer period of caudally directed flow into the spinal subarachnoid space. While the cranio-cervical junction stroke volume is around 0.8-2 mL per cardiac cycle, the bulk flow volume is estimated to be only 0.032 mL per cardiac cycle [86,88,106].

Various MR protocols and computational fluid dynamics models have been used to estimate CSF flow velocities. Flow velocity estimated by MR images in healthy adults was 2.0-3.35 cm/s at the cervical spine [107], 0.8-3.0 cm/s at C2 [86] and 0.6-1.1 cm/s at L3/4 [108]. A computational fluid dynamics model estimated peak velocities of 1.25 and 0.19 cm/s at the brain stem and at L1, respectively

[106]. The fluid dynamics model of Loth et al. [88] indicated that flow remains laminar throughout the flow cycle (Reynolds number 150-450) and that inertial effects dominate the flow field for physiological flow rates and fluid properties, particularly in the cervical and lumbar regions where the subarachnoid annulus is largest.

The velocity with which the normal physiologic CSF pressure wave travels down the spinal canal is generally estimated to lie within the range of 3-5 m/s [106,109,110]; two other estimates have been on the order of 12 m/s but are thought erroneous due to inaccurate material property assignments [111] and errors in assumption of the wave initiation site [110,112].

1.3.4 Summary

CSF formation occurs at various sites in the brain and is regulated by passive and active mechanisms that are not well understood. There is a bulk flow of CSF from the cranial to the spinal compartment and no CSF formation sites have been detected in the spine of animals that have been tested. CSF absorption back into the lymph and venous systems occurs at both cranial and spinal sites in approximately equal proportions, and is thought to be passively mediated by the pressure gradient between the subarachnoid and venous systems.

CSF pressure is determined by many complex interactions that govern the CSF formation and absorption rates, as well as the distribution of pressure and volume within the cranial and spinal vascular systems. The balance of mean arterial pressure and CSF pressure is critical for adequate perfusion of the neural tissue. Current knowledge indicates that the CSF pressure cranial to a subarachnoid occlusion could rise to pathological levels if the mechanisms of pressure-volume compensation and formation-absorption regulation are insufficient.

CSF pressure has pulsatile components that are respiratory and vascular in origin. The vascular pulsation, or pulse pressure amplitude, has shown promise as a prognostic indicator for various CNS conditions. One study has shown that an increase in lumbar pulse pressure amplitude may indicate successful decompression in SCI patients.

1.4 Human traumatic spinal cord injury

Although it is a relatively rare occurrence, SCI causes profound and permanent physical disability, most often in young, otherwise healthy individuals. It has enormous personal, social and economic costs. A thorough understanding of the etiology, primary injury mechanisms and risk factors for SCI is essential to developing successful prevention and treatment strategies. Studies in animals and humans have generated a substantial body of knowledge regarding the pathophysiology of SCI, however some phenomena remain unexplained. No pharmacological treatment has yet proven to be efficacious in

clinical trials; clinical management strategies such as decompression and perfusion maintenance aim to reduce secondary spinal cord damage, but their effects are not well understood.

1.4.1 Epidemiology

The incidence, etiology and trends in SCI are similar across developed countries such as Australia, Canada, European Union, and the USA [reviewed by 113,114]. In general the statistics exclude individuals who die before admission. Two studies have reported pre-admission death rate of 16% [115,116], while estimates of pre- and post-admission deaths range 15-30% and 4-17%, respectively [117]. In the developed world, the annual incidence of *non-fatal* traumatic SCI with persistent neurological deficit is estimated at 12.1 to 57.8 per million population [114], which translates to approximately 11,000 new injuries every year in the United States. Survival after SCI is approximately 95% of the general population for age and gender at 1 year, and 92% at 10 years. Survivorship is better for the young, females, those with paraplegia and incomplete injuries [118], and those without concomitant TBI [119]. Complications after injury are mostly due to pneumonia, pulmonary emboli, septicemia related to pressure sores and urinary tract infections.

SCI overwhelmingly affects males more than females at a ratio of around 4:1 [113,114,120]. Age-specific incidence generally displays a bimodal distribution [114]: approximately half of all SCIs occur between the ages of 16 and 30, and around 10% percent occur at age 60 or older (NSCISC, 2009). The main causes of SCI are motor vehicle accidents (43%), falls (20%), violence (18%) and sports (10%) [120] (Figure 1-12). While transport-related SCI remains the highest group, several authors have highlighted an increased incidence of fall-induced injuries, particularly in the elderly population [121,122].

1.4.2 SCI classification

Neurological deficit associated with SCI is classified by (1) the most caudal level with *normal* sensory and motor function, (2) the completeness of the injury, which refers to the detection of *any* neurological function caudal to the injury site, particularly in the lower sacral region, (3) the American Spinal Injury Association (ASIA) impairment scale (AIS), and (4) for complete injuries, the zone of partial preservation, which refers to an area between the injury and S5 that retains some motor or sensory function. The AIS scale is a graded categorisation where AIS A injuries are complete, AIS B through D injuries are incomplete, and AIS E means no neurological deficit (Table 1-3). Nearly half (45%) of all individuals with SCI are classified as AIS A; AIS B and C account for around 10% each and 30% are AIS D (Figure 1-12, right) [120].

Table 1-3 ASIA Impairment Scale

AIS Grade	Level of Impairment
A	No motor or sensory function preserved in the lower sacral segments (S4 and S5)
B	Sensory but no motor function preserved, including the lower sacral segments (S4 and S5)
C	Motor function present below the injury, and strengths of more than half of the key muscles are graded < 3 of 5
D	Motor function present below the injury, and strengths of more than half of the key muscles are graded ≥ 3 of 5
E	Motor and sensory functions in key muscles and dermatomes are normal

Adapted from the ASIA 2006 Standard Neurological Classification of Spinal Cord Injury Worksheet [123].
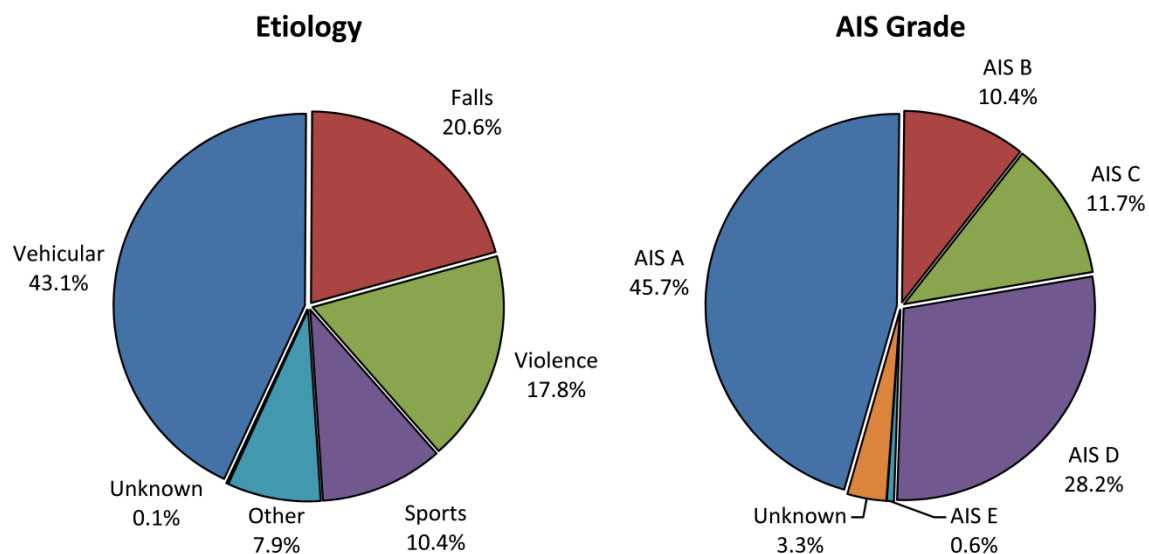
Figure 1-12 SCI etiology (left) and AIS grade at time of discharge (right). Compiled from NSCISC 2009, Table 27 and Table 60 [120].

1.4.3   Spinal fracture and SCI mechanisms

The majority of traumatic SCIs occur as a result of dynamic contact between the vertebral column and the spinal cord, usually with failure or loss of integrity of the bone and/or discs. Insight into the mechanism of the injury, for example the principal loading direction and magnitude, is gained by analysing the injury patterns seen in imaging studies such as radiographs and MR images. A number of classification systems have been proposed, for example those of Denis [124,125], Magerl [126] and the Spine Trauma Study Group [127,128]. These systems categorise column injuries by the degree of disruption of the anterior and posterior vertebral elements, spinal ligaments and intervertebral discs, and assist the clinician in defining the resultant spinal stability, likelihood of neurological involvement and appropriate treatment paths.

Burst fractures and fracture-dislocations each comprise around 30-40% of vertebral fractures, making them the most common type associated with SCI [117] (Figure 1-13). A smaller proportion of SCIs occur without observable column disruption and are termed SCI without radiographic abnormality (SCIWORA) *or* obvious radiographic evidence of trauma (SCIWORET). Other modalities of SCI include laceration injuries which are common to knife and gunshot injuries, chronic myelopathy resulting from canal stenosis or a mass lesion, and ischaemia related to blockage of the vertebral arteries. The model used in this thesis is thought to mimic most closely the burst fracture and fracture-dislocation injury mechanism which results from an obvious dynamic interaction between the spinal cord and column.

Cervical spinal cord injuries are the most common (55%), while thoracic and lumbar injuries account for 35% and 10%, respectively [117,129]. SCIs occur predominantly in the cervical region in older patients, but only 50% have an associated fracture, while SCI in thoracic and lumbar regions are almost exclusively with bony injury [130]. The most common spinal levels of injury are C5 and C6 for tetraplegic individuals, and T12 and L1 for paraplegic individuals [120,131]. Upper cervical region injuries, specifically atlanto-occipital and atlanto-axial dislocations, are often immediately fatal.
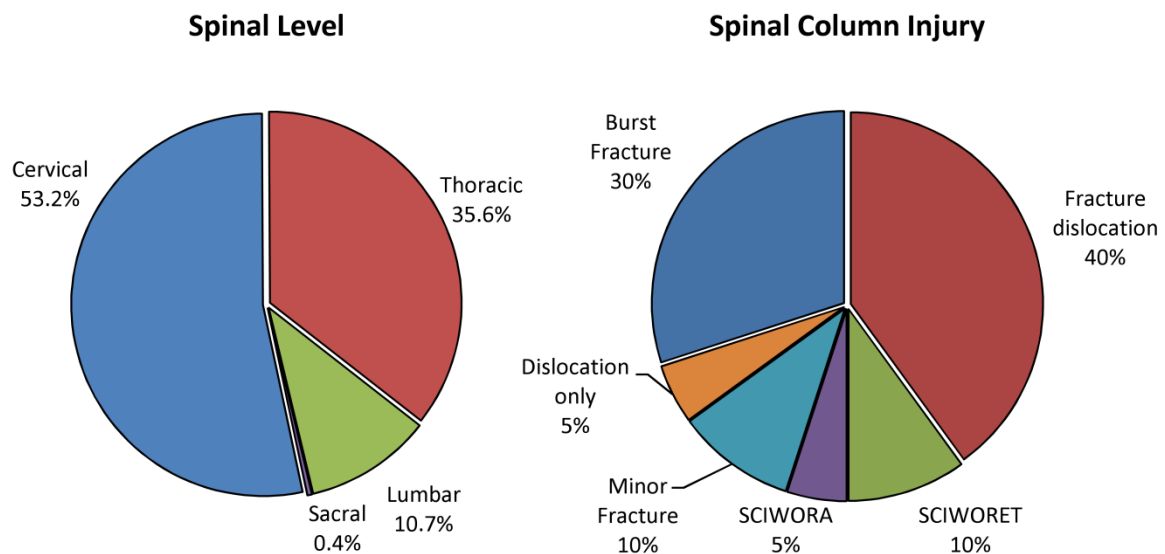
Figure 1-13 SCI spinal level (left) and spinal column injury (right). Compiled from NSCISC 2009, Table 52-55 [120] and Sekhon & Fehlings 2001, Table 5 [117].

1.4.3.1   Burst fracture

A burst fracture is characterised by failure of the vertebral body in compression, as a result of axial compression loading such as a head-first impact. This results in a loss of height of the posterior vertebral body wall, and commonly some degree of retropulsion of bone into the spinal canal, the radiographic

hallmark of a burst fracture (Figure 1-14). Biomechanical studies have shown that the final location of the bone fragment(s) does not reflect the maximum transient canal occlusion and cord compression that occurs during the dynamic event [132-134]. The post-injury sagittal-to-transverse diameter ratio of the canal [135], but not the individual diameters [135,136], of patients with thoracolumbar burst fractures are predictive of neurological impairment. Burst fractures are most common in the thoracolumbar region [137,138] (Figure 1-15).
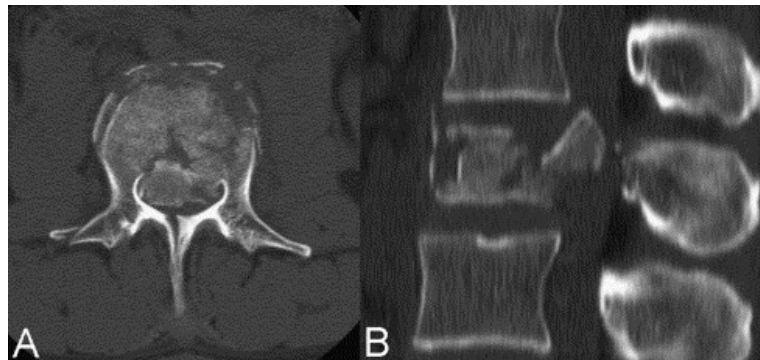
Figure 1-14 Medical images of a burst fracture at L2. Axial computed tomography (CT) image showing a lumbar burst fracture with retropulsion of bony fragments into the spinal canal causing spinal cord impingement (A). Sagittal reformatted image in the same patient, showing large amount of bone fragment in the canal (B). Adapted from European Journal of Radiology, 59(3), Valentini et al., The role of imaging in the choice of correct treatment of unstable thoraco-lumbar fractures, 331-335, 2006, with permission from Elsevier [139].
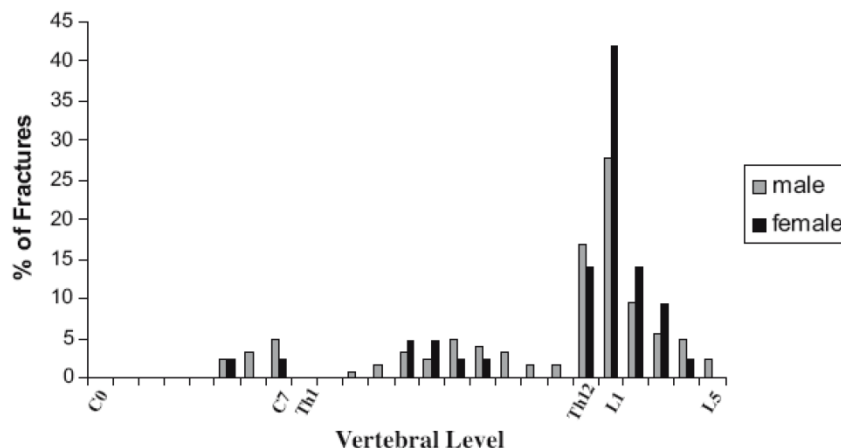
Figure 1-15 Distribution of burst fractures in the male and female population by vertebral level. Data is from 34 months at a European level-one trauma centre serving a population of 1.4 million. For clarity, only the vertebrae at the spinal region junctions are labeled. Adapted from Emergency Radiology, The incidence and distribution of burst fractures, 12(3), 2006, 124-9, Bensch et al., Figure 1, with permission from Springer Science + Business Media [138].

1.4.3.2   Dislocation and fracture-dislocation

Dislocations and fracture-dislocations involve the anterior-posterior or lateral subluxation of one vertebral body relative to the adjacent one, and are due to a variety of external loading conditions. They are inherently unstable fractures and commonly include (1) fracture of the facets where the loading is predominantly in the transverse plane, or "jumped" facets where there is a combined flexion and distraction loading that causes failure of the posterior ligaments, (2) fracture of the vertebral arches, lamina and spinous processes due to extension-compression loading, (3) displacement of the superior vertebrae posteriorly and vertebral distraction due to extension-distraction loading. Dislocation can also occur under torsional and translational loading. Medical images of a bilateral dislocation with anterior translation of the superior vertebral body and facet joint are shown in Figure 1-16.
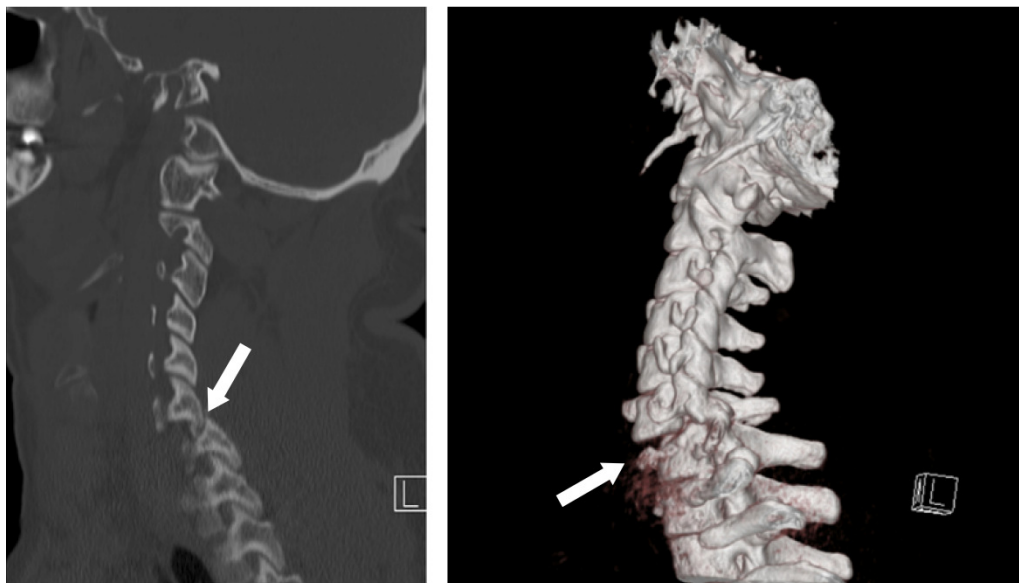
Figure 1-16 Medical images of a bilateral facet dislocation at C6-7 in a 29 year-old male. (left) Sagittal CT demonstrates bilateral facet dislocation (white arrow). (right) Three-dimensional reconstruction of CT demonstrates anterior translation of C6 vertebral body relative to C7 (white arrow). Adapted from Western Journal of Emergency Medicine, 10(1), Gomes et al., Bilateral cervical spine facet fracture-dislocation, 19, 2009 [140], Open access journal, no permission required.

1.4.3.3   Distraction

Purely distractive traumatic loads, i.e. in the axial direction only, are extremely uncommon. Cord distraction is thought to occur in concert with dislocation associated with flexion-distraction, extension-distraction and extension-compression loading. Distraction-type SCIs do not typically occlude the spinal canal and so are thought to occur as a stretching of the cord between points where it is tethered, such as the brain, filum terminalus and nerve roots. A radiograph of cervical distraction that resulted in a rare complete cord transection is shown in Figure 1-17 [141].

Figure 1-17 Lateral radiograph of distraction injury in a 41 year-old male at C5-6. Demonstrates a 3 cm distraction between the C5 and C6 vertebral bodies (white bracket). Adapted from The Journal of Emergency Medicine, 25(4), Schauer and Sokolove, Severe cervical spine distraction, 445-7, 2003, with permission from Elsevier [141].

1.4.4 SCI mechanisms

Human traumatic SCI mechanisms are generally grouped into three categories: blunt or contusive injuries that result from burst fractures and fracture dislocations, stretch or distractive injuries that are assumed to arise from SCIWORA/SCIWORET, and laceration type injuries. However, this categorisation currently has limited clinical application or benefit because treatment pathways do not differ according to the status of the spinal cord. Because the spinal cord has microstructure that is directionally dependent, biomechanics researchers have hypothesised that the primary injury is specific to the direction of the deformation and that this may one day lead to targeted treatments. Choo et al. have reported that localised patterns of primary injury [142] and secondary pathology [143] were specific to the injury mode in rats subjected to contusion, distraction and dislocation injuries.

Bunge et al. classified the pathology of 22 spinal cords obtained from persons who died between 3 hours and 22 years after suffering a SCI [144]. Such pathology probably reflects the energy associated with the injury to some degree, although for the more chronic specimens the late secondary pathophysiological processes might dominate the observed pathology. In that series, contusion injuries featuring intact surface anatomy but with areas of internal haemorrhage, necrosis and cysts comprised around 50% of cases. Solid cord injuries, those in which the cord appeared normal externally but diffuse

damage was seen on histology cross-sections, comprised 10%, and massive compression injuries (20%) exhibited highly disrupted surface and parenchymal tissue with the lesion epicentre often replaced by scar tissue. Laceration injuries (20%) were identified by a clean disruption of surface anatomy [144].

1.4.5   Anatomical risk factors for SCI

Individuals with congenitally small spinal canals are thought to be at higher risk of SCI. The Torg (or Pavlov) ratio was developed as a radiographic measure of spinal stenosis and a tool for predicting an individual's risk of cervical SCI or neuropraxia, particularly while participating in contact sports. It is commonly used in the context of play and return-to-play for contact sports with a relatively high risk of cervical SCI. The Torg ratio is defined as the ratio of the sagittal spinal canal diameter (measured from the middle of the posterior surface of the vertebral body to the nearest point of the corresponding spinal laminar line) to the sagittal diameter of the corresponding vertebral body (measured at its midpoint) [145]. Normalising to vertebral body size is an attempt to account for magnification errors in the radiographs. It has recently been shown that the measure has high sensitivity but poor predictive value for SCI [146]. This may be because it is based on bony dimensions rather than the dimension of the spinal cord and the spinal meninges. Advances in CT and MR now enable visualisation of the spinal cord and CSF; Tierney et al. [147] have suggested that an improved metric of SCI risk would quantify the "space available" for the cord as the difference between the mid-sagittal diameters of the canal and spinal cord.

The elderly population is generally thought to be at higher risk of spinal fracture and SCI from low energy trauma due to degenerative changes of the spinal column [148]. Spondylotic changes in the geriatric spinal column include disc height collapse, osteophyte growth and hypertrophy of the ligamentum flavum and facet joints [149]. In addition to reduced intersegmental flexibility, spondylotic changes can also lead to canal stenosis and associated chronic myelopathy [149]. The reduction in canal space available for the spinal cord, and potentially a reduced CSF layer around the spinal cord, are thought to predispose the geriatric population to SCI from a relatively low energy trauma, even that which does not cause fracture or ligamentous injury [150].

The notion that congenital or acquired canal stenosis increases the risk of traumatic SCI is logical but difficult to prove. Further, the emphasis on canal size or canal-to-spinal cord ratio does not consider the role of the CSF layer during the SCI event. The thickness of the CSF layer varies along the length of the spinal cord, and between different individuals. Incorporating the CSF thickness relative to the spinal cord and canal size may improve the predictive value of SCI risk metrics. Because estimating pre-injury tissue dimensions is challenging in SCI patients, biomechanics studies may provide information on the role of the CSF in SCI risk.

1.4.6   Pathophysiology of SCI

The discussion so far has concentrated on the injury that occurs at the instant of the mechanical insult. However, SCI is not a single event, but a series of complicated physiologic processes. The disruption of axons, vessels and cell membranes that occurs during the primary injury initiates a cascade of secondary cellular events which progress and change in a predictable fashion through the immediate (0-2 hours), acute (2 hours - 2 weeks), intermediate (2 weeks - 6 months) and chronic phases (more than 6 months) [151,152]. These secondary processes include vascular dysfunction, edema, ischaemia, cell necrosis, excitotoxicity, electrolyte shifts, free radical production, inflammation and delayed apoptosis [152]. This cascade is thought to be predominantly degenerative, although some responses have been found to be neuroprotective or restorative [152], and the significance of others is unclear. Experimental pharmacotherapies and other treatments attempt to attenuate, amplify or modify these responses: neuroprotective strategies aim to shield the tissue that escaped injury during the primary trauma but is vulnerable to spreading secondary damage, while neuroregenerative strategies aim to restore tissue that is damaged by the secondary cascade. Although there has been relatively little research on the primary injury, recent work has shown that the primary cellular injury characteristics vary according to the dominant mode of the spinal cord deformation [143].

The secondary processes are complex and beyond the scope of this work. This section concentrates on a brief account of local and systemic vascular changes which provide the motivation for the treatments outlined below in Section 1.4.7. It then discusses some unexplained clinical observations that may be related to the primary injury mechanism that is of interest in this work, i.e. injury mediated by a fluid pressure wave. These observations are post-traumatic ascending myelopathy and diffuse axonal injury remote to the injury site.

1.4.6.1   Vascular changes

Local vascular changes and ischaemia are thought to be among the most important contributors to the secondary injury process [153]. Although the larger vessels such as the spinal arteries are generally spared [152], the primary mechanical insult causes disruption of the microvasculature, which leads to capillary haemorrhage and small vessel thrombosis. The injury response also generates vasoconstrictors that affect nearby intact blood vessels and promote fluid accumulation (edema) at the injury site. The combined effect is a profound local hypoperfusion and ischaemia which deprive the neurons and other cells of oxygen and other nutrients. For contusion injuries, the majority of the vascular changes occur in the grey matter and lead to central necrosis and eventual cyst formation [151].

The local injury response is further compounded by systemic vascular changes. Spinal cord blood flow is normally regulated by the autonomic nervous system in response to arterial pressure changes,

local metabolic requirements, and blood carbon dioxide and oxygen levels [154]. After SCI there is a transient blood pressure increase associated with sympathetic stimulation, but this is quickly followed by a loss of sympathetic nervous system autoregulation, decreased systemic vascular resistance and increased venous capacitance and pooling, with a resultant systemic hypotension and persistent bradycardia [155].

Since local and systemic vascular changes contribute significantly to the secondary biochemical cascade, it is logical that clinical treatments should target haemodynamic support and increase local perfusion. Currently, haemodynamic support consists of maintaining blood pressure, while local perfusion is increased by decompression surgery or traction. However, the spinal CSF pressure may interact with these treatments in ways that are not presently understood. This is discussed in Section 1.4.7.

1.4.6.2   *Remote diffuse axonal injury in SCI*

As previously mentioned, the primary injury mechanisms and some aspects of the secondary injury process of SCI are not well understood. One area that has not been explored well is the existence of primary injury at some distance from the injury site. There are several clinically observed phenomena that may provide evidence of primary remote or diffuse damage. These include cervical SCIs associated with head trauma (without cervical spine injury), remote diffuse axonal injury observed at autopsy, SCIWORA and post-traumatic ascending myelopathy.

There have been several clinical observations of SCI associated with TBIs caused by acceleration of the head. Hadley et al. report cervical spinal cord contusions at autopsy of infants who sustained non-accidental whiplash-type shake injuries, or so-called shaken baby syndrome [156]. Shannon et al. report histological evidence of diffuse axonal injury in the cervical spinal cord of infants who died from shaken baby syndrome [157]. The latter hypothesised that such injury was due to a stretching of the spinal cord due to hyper-extension and flexion of the neck; however, it is possible that such injuries could be contributed to by pressure transients created by the head and brain motion. Axial strain of the cord has also been suggested to result in non-contiguous SCI [158] and diffuse axonal injury observed with spondylotic myelopathy [159]. The relevance of SCIWORA as an injury classification is currently debated in the clinical community, given the more subtle injuries that can be detected with MR imaging [160]. However, at least one study reports cases of paediatric SCIWORA with no overt evidence of spinal cord abnormality on MR imaging [161]; a fluid loading mechanism may contribute to such types of injury. Czeiter et al. showed that impact acceleration TBI in rats evoked traumatic axonal injury in the spinal cord as far away as the thoracolumbar junction [162]. They observed that the majority of the affected axons were close to the surface of the cord and proposed that a shock wave travelling through the CSF at the moment of injury could contribute to an axonal stretch damage mechanism. The authors

report that this was further supported by their unpublished observation of similar damage from fluid percussion induced injuries.

In a histological analysis of the spinal cords of 17 patients who died between 30 minutes and 6 weeks after injury, diffuse axonal injury remote from the focal injury site and at up to 24 vertebral levels from the lesion epicentre was observed in all cases [163]. The study does not hypothesise the origin of this damage. Zwimpfer et al. [164] reported a series of patients with a so-called "spinal cord concussion" in which neurological deficit was associated with a traumatic event resulting in spinal instability, but resolved completely within 72 hours after injury. The authors likened these transient deficits to brain concussion and postulated that they result from a force transmitted to the cord without direct cord compression.

In many individuals, the level and extent of a SCI can improve over the days and weeks after injury, an effect largely attributed to resolution of spinal shock and plasticity of the neural pathways. However, in up to 6% of patients neurological deficit progresses to a higher level, compared to the initial presentation, in the days and weeks after injury [165-167]. Despite being described by Frankel as early as 1969 [168], subacute post-traumatic ascending myelopathy remains a poorly understood condition, likely due to its rarity and difficulty in establishing causation [169]. To be classified as an ascending myelopathy, the neurological deficit must extend at least two levels higher than the initial assessment [169], but can be over entire spinal regions [170]. Changes in MR signal intensity generally occur up to four vertebral levels above the primary lesion [170]. Secondary deterioration has also been noted in patients that presented with cervical spine fractures but were neurologically intact at initial assessment [171]. The condition is associated with increased mortality particularly if the ascension reaches the brainstem [169,172]. Risk factors for delayed or secondary increased neurological deficit related to clinical management have been identified, including: further mechanical insult due to ongoing spinal instability, traction, halo application and Stryker frame rotation, as well as early surgical decompression and failure of haemodynamic support [165-167]. In many cases, however, there is no association with an adverse post-traumatic event, and the exact cause of deterioration cannot be determined [173].

There have been several recent case studies reporting patients with a low level spinal injury having a rapid ascending myelopathy of an unknown origin [170,173-175]. A number of hypotheses for the cause of injury ascension have been proposed, including: decreased perfusion pressure and subsequent ischaemia caused by increased venous pressure [175] or intra-abdominal pressure [174,175]; reperfusion injury after surgical decompression [176]; thrombosis in a major spinal artery leading to arterial hypotension [174,175]; infection [166,169]; and, secondary injury processes such as inflammatory or autoimmune response including apoptosis [170,172,177]. Descending lesions are not commonly reported, probably because they are undetected since they do not increase the level of neurological deficit.

Descending myelopathy has been reported for two patients, but was attributed to venous thrombosis and spinal artery occlusion [178].

These delayed ascending, remote, diffuse and non-fracture associated SCIs are not well understood, and it is possible that they are initiated during the primary injury event. The neurons, axons and glia of the spinal cord could be affected by deformation or over-pressurisation caused by a CSF pressure transient from an event that rapidly deforms the dura but does not impinge on the spinal cord. Biomechanical evidence for this mechanism is discussed in Section 1.5.4.2 below.

1.4.7 Clinical treatment options and relevant treatments in research

A considerable number of neuroprotective and neuroregenerative pharmacological strategies have shown promise in pre-clinical studies, but none have proven efficacious in clinical trials. A detailed discussion of prospective drug and cell therapies is beyond the scope of this work; a number of current reviews are available [152,153,179-181]. However, considerable advances have been made in the critical care, clinical management and rehabilitation of SCI patients and these have led to decreased immediate mortality and morbidity and increased post-injury longevity [118], as well as increased functional recovery and quality of life.

Two of the clinical treatment options that have gained support recently are early spinal cord decompression and maintenance of spinal cord perfusion via haemodynamic support. Both aim to minimise ischaemic damage to the spinal cord by increasing perfusion and oxygen delivery to the affected area and are practiced clinically to various degrees. Current acute SCI treatment guidelines present these as treatment *options* rather than treatment *standards* due to the lack of sufficient scientific evidence to convincingly prove their efficacy [182-184]. The following section discusses the current state of knowledge of each, placing them in the context of this work.

1.4.7.1 *Perfusion maintenance*

Spinal cord perfusion support is currently provided by maintaining adequate arterial oxygenation and blood pressure. The positive effect of early haemodynamic support, including cardiac inotropes to increase blood pressure, and intravenous fluid volume augmentation/resuscitation, has been recognised in a number of clinical studies [184-186]. Current guidelines recommend maintaining systolic blood pressure >90 mmHg and mean arterial blood pressure between 85-90 mmHg for one week after injury [187]. However, this regime does not consider the contribution of CSF pressure to the perfusion pressure. This is in contrast to clinical management of severe TBI patients, for whom standard care includes monitoring and controlling both ICP and blood pressure [54] to achieve perfusion targets: ICP < 20-25 mmHg, and cerebral perfusion pressure >60-70 mmHg [188].

For TBI patients, ventricular and lumbar drainage has been shown to reduce ICP and increase perfusion, if only transiently [189,190], and patient outcome with prolonged periods of ICP>20 mmHg appears to be impaired [191,192]. CSF drainage is also a recognised strategy for reducing the risk of ischaemic iatrogenic paralysis during thoracoabdominal aortic aneurysm (TAAA) repair in which the spinal cord blood supply is reduced by aortic clamping. A number of clinical trials and animal studies have demonstrated a reduced risk of neurological deficit or paralysis after TAAA surgery when controlled CSF drainage to maintain a CSFP of 10 mmHg was mandated [reviewed by 193,194,195]. A similar protocol for traumatic SCI has been proposed, and to date has been studied in one animal protocol [196] and one clinical trial [91].

Horn et al. [196] assessed the effect of CSF drainage on spinal cord tissue perfusion, injury severity and functional recovery in a rabbit contusion model. Following a displacement controlled contusion injury, they drained 0.5-1 mL of CSF from the lumbar subarachnoid space at 1, 2 and 3 hours post-injury to reduce the CSF pressure by 10 mmHg. While the drainage appeared to reduce the area of tissue damage at the injury site, it did not result in improved electrophysiological or motor outcomes. Contrary to expectations, they found that spinal cord tissue perfusion (measured by laser Doppler) decreased during intrathecal hypotension.

Kwon et al. [91] have recently reported on a prospective randomised trial of lumbar CSF drainage on 22 SCI patients. CSF was drained to 10 mmHg for 72 hours after surgical decompression, but only when neurological examination was possible and to a maximum of 10 mL per hour. Lumbar CSF pressure was recorded during the decompression surgery and periodically thereafter. No adverse events were associated with the drainage, but they did not observe a significant lowering of CSF pressure in the drainage group relative to the non-drainage group.

1.4.7.2   *Stabilisation and decompression*

Stabilisation of the spine and decompression of the spinal cord are recognised as important steps in SCI treatment. Stabilisation is required to eliminate pathological motion at the injury site and to prevent further neural tissue injury and long-term deformity. Decompression aims to alleviate residual compression of the cord caused by a malaligned canal or bony fragment. Decompression can be achieved *indirectly* by traction, which realigns the spinal canal, or *directly* by surgical intervention to remove mechanical impingement of the cord. Despite strong advocacy for early decompression, little work has been done to understand the immediate effects of decompression with regard to the morphological (swelling) response of the cord and the distribution of CSF. Intraoperative ultrasound is commonly used to assess the adequacy of decompression [197-199], but postsurgical imaging is usually not performed until 24-48 hours later, so it is not known how long the restored epidural and intrathecal spaces remain patent. A better understanding of spinal cord and CSF response to decompression would likely help to

elucidate the benefits of early decompression and perhaps to stratify prognosis by patient response to decompression.

While the need for stabilisation and decompression is acknowledged, the role of the *timing* of surgical intervention is currently uncertain. To some degree this is because of the difficulty in agreeing on what constitutes "early" and also the considerable disparity between the duration of applied compression in animal studies and reasonably achievable decompression times in the clinical setting. In *pre-clinical* animal studies, compression duration has ranged from 1 minute to 6 hr; in around half of these studies decompression occurred at 1 hour or less. In *clinical* decompression studies the most common definition of early operation is 24 or 72 hours after SCI [200] and only two studies with 8 hr limits are reported [201,202]; reported injury-to-surgery times are mostly longer than eight hours [e.g. 91,203,204], although <8 hr delay times have been reported or are thought to be achievable in some trauma centres [202,205].

Pre-clinical studies using highly diverse animal models have shown mixed benefits in histopathological, electrophysiological, blood flow and behavioural recovery measures. The following summarises those with more clinically relevant time points; a complete review is given by Furlan et al. [200]. In cats with no spinal cord signal conduction at 6 hrs after a contusion SCI, there was no difference in behavioural outcome for those that were then treated by laminectomy and those that were not decompressed [206]. In rats subjected to a contusion injury and decompressed at 0, 2, 6, 24 or 72 hours, later decompression was associated with worse histopathology, reduced electrophysiological recovery and reduced behavioural recovery at six weeks [207]. Delamarter et al. applied a 60% circumferential compression of the spinal cord at L4/5 in dogs and reported degraded functional recovery and histological findings with compression of 6 hr or longer [208]. Using the same model, Rabinowitz et al. treated dogs with decompression at 6 hr, with or without methylprednisolone, or methylprednisolone while maintaining compression until the two week experimental endpoint. Surgical decompression at 6 hrs, with or without methylprednisolone, was better than methylprednisolone alone as assessed by electrophysiology, histology and functional neurological improvement [209].

Despite discrepancies in pre-clinical results it is generally accepted that there is "evidence for a biological rationale to support early decompression" [200]. The clinical studies with an 8-hr cutoff showed shorter length of acute care and hospitalisation, less frequent complications, and better neurological outcomes [201,202], but no difference in mortality [201]. Those with later cutoffs have in general provided evidence that early surgical decompression is safe and feasible, can lead to improved neurological recovery and clinical outcome, and reduce the duration of hospitalisation [200].

Current decompression literature lacks an explicit distinction between extradural decompression and subdural decompression. Edema and haemorrhage can result in a considerable local increase in

spinal cord volume, and it is possible that epidural decompression is not sufficient in some cases to reduce parenchymal pressures and improve tissue perfusion. Increased parenchymal pressure (~20 mmHg) associated with increased water content has been recorded at the injury site two days after a compression SCI in mice [210], and adjacent to the injury site within 30 minutes of injury in cats [211]. Dural decompression (i.e. cutting open the dura) for SCI has been investigated to a limited extent both clinically [212-214], and in animal models [215-217] in the past, but does not appear in SCI treatment algorithms; it is, however, an adjunct procedure in TBI patients with ICP unresponsive to craniectomy [188]. In rats with a mild contusion SCI, durotomy 4 hours after injury was effective in reducing lesion size only when combined with a dural graft [217]. The procedure neither improved or impaired recovery in monkeys with contusion SCI [216]. In humans, the procedure included immediate suturing of the dural incision [214] and debridement of necrotic neural tissue [212,213]; all report positive outcomes but have low patient numbers, limited outcome measures and no control group. Due to the known variability in spontaneous recovery, these case reports do not permit conclusions to be drawn on the effectiveness of the durotomy procedure.

Spinal cord occlusion is due to both bony malalignment and cord edema. The former is reduced by decompression but little is known about the time course of cord swelling after SCI. Yeo et al. reported that in three of four sheep receiving a severe T10 injury (50g-20cm), contrast myelography indicated there was no flow past the injury site within one hour of injury, and in two animals this swelling remained for more than 100 hours after injury [218]. Isotope myelography results on one animal were more conservative, with full occlusion at 24 hours reverting to partial occlusion at 44 hours. Saadoun et al. report complete subarachnoid occlusion due to swelling in forceps compression injured mice at 2 days post injury, as assessed by dye myelography [210].

One animal study has measured pressures cranial and caudal to an experimental SCI, providing information about both the time course of intrathecal occlusion and the effect of SCI on pressure distribution. Shapiro et al. [211] measured parenchymal and spinal CSF pressures caudal and cranial to the SCI site in cats for at least 4 hours after injury (with no residual compression). Prior to injury the pressures at each location were equal and the CSF and tissue pressures were not different. After injury, the pressures cranial to the injury site steadily increased, peaking at around 6 mmHg above baseline 3.5 hours after injury. The pressures caudal to the injury site decreased steadily until 3.5 hours after injury (Figure 1-18). The dissociation between the caudal and cranial pressures was interpreted as a loss of communication between the compartments. In animals that were re-anaesthetised 18 to 24 hrs after injury, the cranial-caudal pressure differentials were resolved and values were similar to baseline, indicating that the subarachnoid occlusion was at least partially resolved in this time frame.
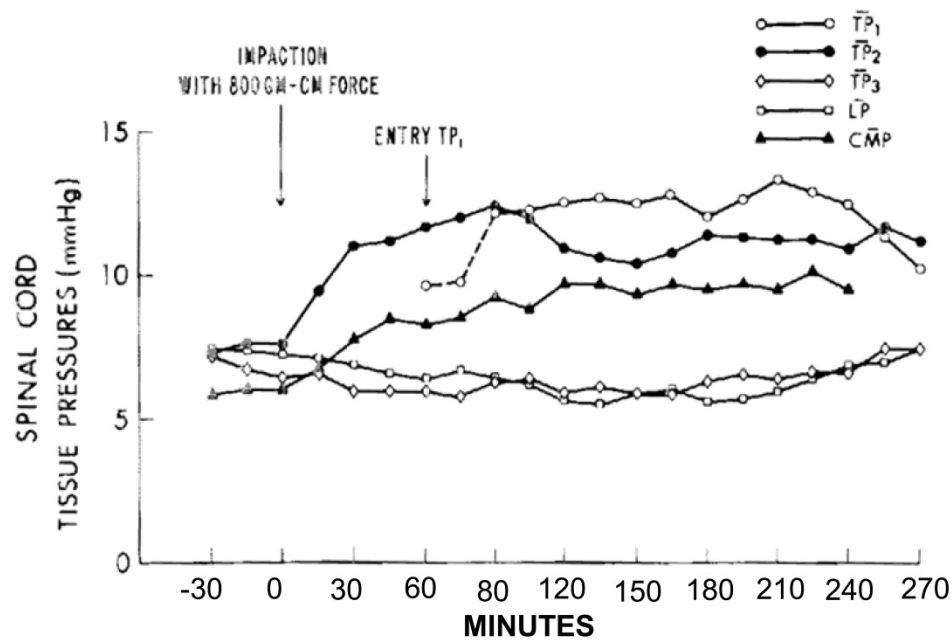
Figure 1-18 Spinal cord tissue pressure and CSF pressure versus time, after experimental SCI.
Cats were injured by 40g-20cm weight drop. Data points represent the mean pressure for each catheter obtained at 15 minute intervals for 10 animals. Differences between cranial transducers (TP1, TP2) and caudal transducers (TP3, LP) is significant (p<0.001) at 30 minutes after injury. CMP=cisterna magna pressure, LP=lumbar pressure, TP=tissue pressure. Reproduced from Surgical Neurology, 7(5), Shapiro et al., Tissue pressure gradients in spinal cord injury, 275-9, 1977, with permission from Elsevier [211].

The study of Kwon et al. [91] introduced in Section 1.4.7.1 made an interesting observation regarding CSF pressure before and after surgical decompression in their cohort with 17 cervical and 5 thoracic injuries. The lumbar CSF pressure increased on average by 7.9 mmHg at the time of decompression, with a mean injury-to-surgery time of 21.6 hrs. This implies that prior to decompression the CSF pressure cranial to the injury was higher than that caudal to the injury, which in turn indicates that lumbar pressure measurement may not be an accurate measure from which to calculate worst-case perfusion. At present, cranial CSF pressure monitoring is *not* indicated in SCI patients without concomitant brain injury and this means that cranial-to-caudal pressure gradients cannot be measured directly in humans. A better understanding of the spinal cord and CSF response to residual compression and decompression may help to identify a subset of patients which would most benefit from early decompression, or allow more definite prognoses to be made.

1.4.8   Summary

Although traumatic SCI is relatively rare, it has devastating and permanent consequences for the individual afflicted. The primary injury typically occurs from a high energy interaction between spinal canal or bone fragments, and the spinal cord via the dura and CSF. Burst fractures and fracture-

dislocations are the most common injury mechanisms resulting in SCI. Conditions that increase the stiffness of the spine or reduce the canal-to-spinal cord ratio are thought to increase SCI risk.

The primary mechanical injury is rapidly followed by secondary biological processes that further damage the spinal cord, and treatments aim to reduce or eliminate the effects of these mechanisms. Decompression and perfusion maintenance are two clinical treatment options that aim to reduce secondary ischaemic processes. It is thought that early decompression has a strong biological reasoning and is currently thought to be advantageous in patients who are otherwise stable. However, the clinical evidence does not equivocally prove efficacy. Perfusion control is currently based on maintaining a high systemic blood pressure; however, CSF pressure also contributes to the balance of tissue perfusion. Reducing CSF pressure via lumbar drainage has been proposed, but little is known about the distribution of CSF pressure in the cranial and caudal compartments following a SCI. A better understanding of how the CSF pressure and spinal cord morphology respond to traumatic SCI and subsequent decompression may inform future clinical trials and treatment pathways.

1.5   Mechanics of traumatic spinal cord injury

In SCI, the primary damage is caused by the transfer of energy from a moving bone fragment or the canal, through the epidural contents, meningeal membranes and CSF, to the spinal cord. This causes local tissue deformation and displacement, disrupting neurons and axons, and rupturing blood vessels. Injury or tissue damage is exhibited in a variety of forms, ranging from obvious gross interruption of physical structure to dysfunction or death of individual cells. The mechanical response of the spinal cord is dictated by the mechanical and rheological properties of spinal cord, dura and CSF. Therefore, a comprehensive description of these is pivotal to our understanding of the mechanics of SCI and our ability to simulate SCI with computational and physical models.

This section also discusses the impact parameters that are known to affect the severity of a SCI and the current knowledge regarding the influence of CSF during the mechanical impact. Prescribing tissue tolerances is one of the main goals of injury biomechanics; however, it is extremely challenging given the complex mechanical response of biological tissues. In the remainder of the section, the tolerance of the spinal cord tissue to strain, stress and pressure impulse are described in terms of both mechanical failure and physiologic failure. This information is largely obtained from the animal models that are described in Section 1.6.3.

1.5.1   Mechanical properties of the spinal cord

As described in Section 1.2.3, the spinal cord consists of peripheral white matter surrounding a central core of grey matter. The spinal cord exhibits the typical soft-tissue nonlinear "J" shaped stress-

strain response to uniaxial tension, with stiffness increasing with applied strain (Figure 1-19). Elastic and tangent moduli have been used to describe the stiffness from 0 to around 10% strain. In a series of tests using anaesthetised cats and dogs, Hung and colleagues determined an *in vivo* elastic modulus of around 0.26 MPa up to 5% strain in axial tension with a stretch rate of 0.02 mm/s over one or two spinal levels [219,220]. They also noted increased stiffness due to lack of hydration, lower temperature and increased time after death [221,222]. The effect of perfusion has not been tested in the spinal cord, and studies on the brain have been inconclusive; Gefen and Margulies [223] reported that perfusion did not affect stiffness of *in vivo* brain tissue, while Weaver et al. [224] found that it affected shear modulus. Estimates of moduli determined with quasi-static strain rates range from 1.02 to 1.4 MPa for *ex vivo* human and bovine cord [225-227]. A two-fold increase in elastic modulus at 72 hrs postmortem was reported for *ex vivo* bovine tissue [227].
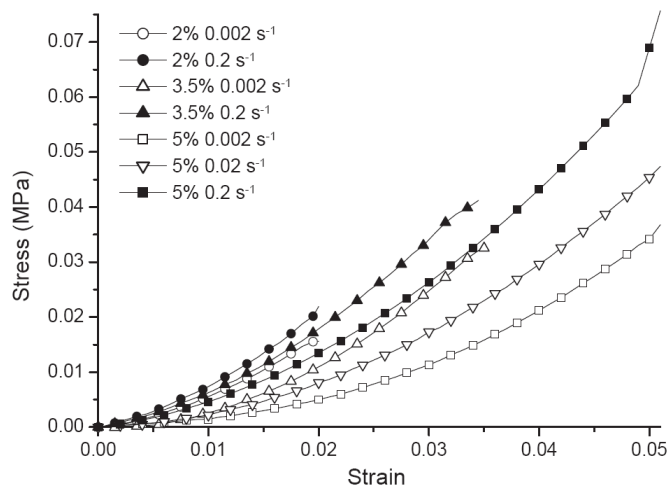
Figure 1-19 Mean stress-strain curves for uniaxial tensile tests of rat spinal cord. Specimens were preconditioned at the strain indicated in the legend. The curves exhibit a toe-region followed by stiffening at higher strains. Note the increased stiffness at the higher strain rates (filled symbols). Reproduced from Journal of Biomechanics, 38(7), Fiford et al., The mechanical properties of rat spinal cord *in vitro*, 1509-15, 2005, with permission from Elsevier [228].

Similar to other soft tissues, the hyperelastic stress-strain behaviour *in axial tension* is thought to originate from the crimped or undulating fibrous microstructure of the longitudinally oriented axons [229] and the collagen and elastin of the associated vascular tissue and connective membranes. In addition, this preferential alignment of axons is thought to contribute to anisotropic material properties [225,226], but this has not been verified experimentally [230]. The elastic moduli of white and grey matter were independent of direction when assessed by the pipette aspiration method [231]; however, this method tests a highly localised section of tissue and therefore has limited contribution from non-cellular components. The elastic moduli stated above were for spinal cords tested with intact pia mater (the pia is closely associated with the cord and is difficult to remove), and this may contribute to directional material

properties. The pia mater increased the stiffness of human cervical spinal cords tested less than 48 hours after death by fifteen-fold [225]. Tests using tissue cores have recorded tangent moduli for white and grey matter ranging from 0.03 to 0.112 MPa [232,233], which is substantially lower than for intact cords with pia mater. Since the neurons and cell bodies within the grey matter are randomly oriented, the grey matter may be less stiff than white matter in axial tension. When tested in axial tension, core specimens of grey matter had higher moduli (0.1 MPa at 15% strain) than white matter (0.038 MPa at 15% strain) [233], but this difference was not detected in a study that used the pipette aspiration method on a small section of tissue [231]. At the cellular level, spinal cords with demyelinated axons and/or loss of glial cells were less stiff and had lower tensile strength than controls, indicating that myelin and the glial matrix contribute to the tensile response [234].

Transverse tensile loading and axial and transverse compression loading have not been extensively investigated. The elastic modulus for rabbit spinal cord in transverse tension was estimated at 0.016 MPa with the pia, and 0.005 MPa without pia. Ozawa reported greater stiffness in cords with pia, compared to those without, when transverse compression exceeded 1 mm or around 30% of the anterior-posterior diameter [235]. Porcine white matter exhibits nonlinear [236] and rate dependent stress-strain behaviour in axial compression [237]. Considerably more work has been done on the compression and shear properties of the brain, which has a similar cellular makeup but lacks anisotropy [reviewed by 230]. The majority of SCI animal models apply either quasi-static or dynamic transverse compression loads, but in general they are not appropriate for determining material properties since the geometry of the tissue undergoing compression cannot be well defined. For example, Hung et al. [238] demonstrated the variation in "overall moduli" from zero to 40% transverse compression for a single *in vivo* cat spinal cord without dura. However, the modulus was defined as the ratio of stress to compressive strain, as per the tensile definition, which does not directly translate to transverse compression of a cylinder. The combination of inverse finite element model analysis and materials testing for prescription of material properties of very soft biological tissues has been advocated [239], and a recent study has implemented such a scheme to derive constitutive models of spinal cord white matter [240]. The inverse finite element approach may prove helpful for deriving mechanical properties from transverse compression tests in the future.

Due to its high water content, the spinal cord displays highly viscoelastic properties. The loading and unloading profiles in uniaxial tension exhibit hysteresis, indicating strain history dependence of the stress-strain response [219-222,238,241]. *Ex vivo* uniaxial tensile tests have shown that stiffness increases with strain rate for intact pia-covered human [226], adult and neonatal rat [242,243] spinal cords, and biopsy specimens of bovine white and grey matter [232]. One study did not detect a difference with strain rate for human specimens with and without pia mater [225]. Several studies have reported stress relaxation properties; higher initial strain and strain rate produced higher stresses at the end of

relaxation [226,232,242,243]. The relaxation period tracked in these experimental protocols has varied markedly from 25 sec [226] to 30 min [228]. Several groups have derived constitutive equation constants for various viscoelastic material models [226,242,243].

Few studies have tested intact spinal cords to failure to obtain ultimate tensile stress and strain. Biopsy specimens of bovine white matter failed at 0.061 MPa and 126% strain, compared to grey matter at 0.043 MPa and 50% strain [233]. The lower ultimate tensile stress and strain of grey matter compared to white matter may be consistent with the pattern of central grey matter damage and peripheral white matter sparing that is observed in human and experimental SCI [152]. Rat spinal cords (with pia) failed at 12% strain and 0.08 MPa [228], and chick embryo cords failed at 42% strain and a stress of 0.085 MPa [234]. *In vivo* cat and dog cords attained a (quasi-static) strain of 40-50% before the grips slipped, without tissue failure [219-221,241].

The variability in results due to viscoelasticity, postmortem degradation and sensitivity to hydration, temperature and perfusion are compounded by difficulty in defining cross-sectional area and in gripping the specimen. Most tensile tests use the intact cord rather than cutting test coupons and therefore approximate the cross-sectional area as that of an ellipse with major and minor axes corresponding to the lateral and anteroposterior diameters. It is difficult to provide end conditions that grip the sample without slippage and that do not affect the tissue behavior and introduce end effects. Differences in preloading and preconditioning protocols also contribute to variation within and between studies [244]. There may also be natural variation by species and age.

1.5.2   Mechanical properties of the spinal meninges

Like other connective tissues, the spinal meninges are a composite of collagen and elastin fibres in extracellular matrix material and have non-linear elastic properties. The elastic and viscoelastic tensile mechanical properties have been studied for human dura [245-253], and that of several mammals including bovine [249,254,255], non-human primate [256], canine [257-259] and rat [260]. In all cases the dura was indistinct from the arachnoid mater for testing and the majority of studies have concentrated on lumbar dura only. Only one study has tested the spinal pia mater [235].

There is considerable variability in mechanical properties among species and studies. This can be partly attributed to differences in experimental protocol, such as strain rate, preconditioning, environmental conditions, storage conditions, and end fixation. In general the dura is one or two orders of magnitude stiffer than the spinal cord, with elastic modulus ranging from around 1 to 150 MPa across the species listed above. The failure stress ranges approximately 1.4 to 28.5 MPa, and failure strain is between 33 and 100%. The elastic modulus of rabbit *pia mater*, calculated from the difference in elastic

modulus obtained in tensile tests of spinal cord with and without pia, was 2.3 MPa, approximately 460 times spinal cord parenchyma with the same test protocol [235].

The spinal dura is frequently assumed to be transversely isotropic [257] due to longitudinal orientation of the collagen fibres which should, according to the remodeling patterns of other connective tissues, result from being predominantly loaded in the axial direction during flexion, extension and lateral bending of the spine. Longitudinal collagen alignment has been found in some microstructural studies [248,249,260] but has not been detected in others [261,262]. One study has reported a tendency for preferential longitudinal and transverse alignment of elastin, rather than collagen, fibres [261]. The ultimate tensile stress and elastic modulus were higher in the longitudinal than the transverse direction for human [248,249,253] (Figure 1-20) and porcine dura [263], but the ultimate strain did not depend on loading direction [248,249] (Figure 1-20).
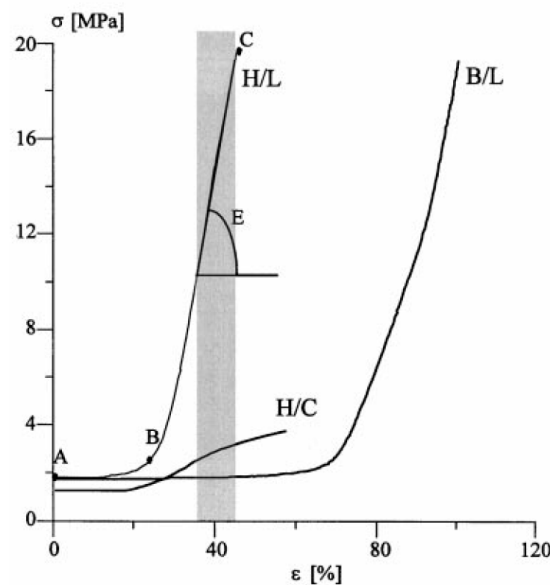
Figure 1-20 Stress-strain curve of human and bovine lumbar dura. Strain was applied in the longitudinal direction for human (H/L) and bovine (B/L) dura, and in the circumferential direction for human dura (H/C). The grey shaded region was used to calculate the elastic modulus (E). Region A-B denotes the toe-region in which little stress is applied to obtain a large strain. Reproduced from Anesthesia and Analgesia, 88(6), Runza et al., Lumbar dura mater biomechanics: experimental characterisation and scanning electron microscopy observations, 1317-21, 1999, with permission from Wolters Kluwer Health [249].

Studies on the dependence of tensile mechanical properties on dorsoventral side and spinal region have had mixed results. No difference in failure stress and strain, and elastic modulus, was found for rat dura [260], the same was found for human except that elastic modulus increased slightly with caudal progression [250]. Reduced failure stress and strain with caudal progression was observed for dorsal, but not ventral, human dura [246]. For porcine dura, transition and failure strains decreased towards the

42

lumbar region, while elastic modulus and failure stress increased with caudal progression [263]. Dorsal failure stress was lower than ventral, and the opposite relation applied for failure strain, for all spinal regions for human and porcine dura [246,263]. Elastic modulus was lower for ventral specimens than for dorsal specimens of porcine dura [263].

1.5.3   Rheological properties of the cerebrospinal fluid

CSF is a transparent, colourless fluid, derived from blood plasma. It is mostly water, and in the nonpathological individual contains small amounts of lipids, electrolytes, enzymes, vitamins, amines, sugar proteins, and blood cells. The composition may be altered by disease or injury that affects the blood-brain or blood-spinal cord barrier (BBB, BSCB).

CSF is a Newtonian fluid with a constant viscosity of 0.71 – 0.76 mPa.s at 37 °C [264]. Protein content has a slight but insignificant effect on viscosity [264,265]. Bloomfield [265] compared distilled water with CSF obtained from the ventricular shunts of 23 adult patients with hydrocephalus, pseudotumour cerebri and subarachnoid haemorrhage. Using identical protocols and on the same rheometer, the absolute viscosity ranged 0.66-0.98 mPa.s and 0.65-1.09 mPa.s, for the water and CSF samples respectively (Figure 1-21), and there was no dependence on protein, glucose or red blood cell concentration. The average specific gravity (i.e. density relative to water) of CSF from the same patients was 1.007 (range 1.0062 – 1.0082) [265]. Both Bloomfield et al. [265] and Brydon et al. [264] used CSF obtained from patients undergoing procedures for CNS pathology. Bloomfield et al. confirmed that there were higher than normal levels of protein, glucose and red blood cells in some patients, and normal levels of albumin, immunoglobulin-G and white blood cells in all patients [265]; Brydon et al. only reported protein content [264]. To the author's knowledge there is no study of CSF rheology using samples from a healthy normal population. The above properties imply that for the purpose of a mechanical model which does not attempt to replicate biochemical environment, distilled water is suitable to simulate CSF.
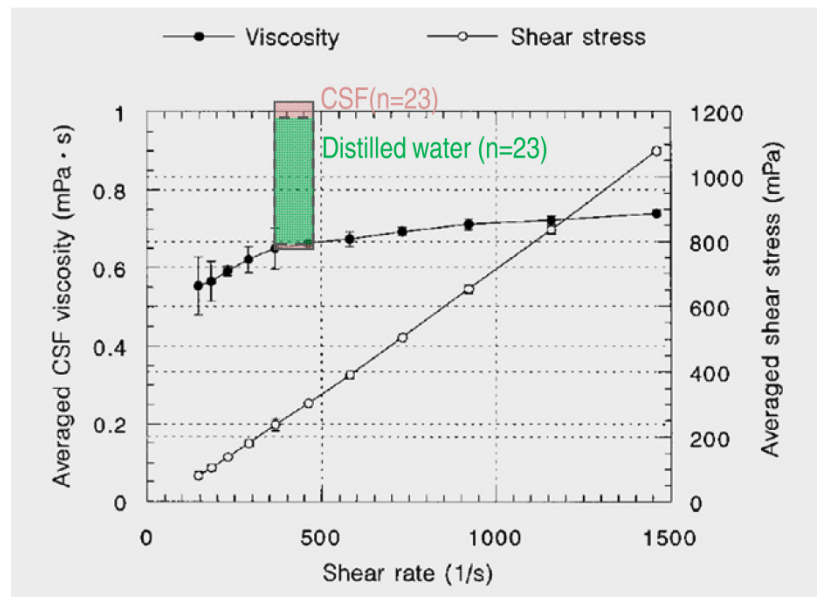
Figure 1-21 Average CSF viscosity and shear stress versus shear rate for one subject. Data points represent the mean and standard deviation of 3 replicate tests at each shear rate, for one CSF sample from a single subject. The rectangles represent the range of viscosities obtained for distilled water (dashed line, filled in green) and CSF (solid line, filled in pink) in the same study (n=23), using the same viscometer for shear rate 360-460 s^{-1}. Tests were done at 37 °C. Adapted from Paediatric Neurosurgery, 28(5), Bloomfield et al., Effects of proteins, blood cells and glucose on the viscosity of cerebrospinal fluid, 246-51, 1998, with permission from S.Karger AG, Basel [265].

1.5.4   Mechanics of traumatic tissue injury

The mechanical response of biological tissue is normally tested under controlled conditions which restrict the applied loading to one mode (tension, compression or shear) and the loading vector to one of the anatomical planes. This ideal loading is quite different from the loads applied to the spinal cord during a SCI. The models introduced in Section 1.6.3 have been used to determine the parameters of the mechanical insult that affect the extent of tissue damage. For the most part these studies assess injury severity by qualitative or quantitative assessment of neurophysiology, patterns and extent of cellular damage as seen on histology, immunohistochemistry and medical imaging, and the functional recovery of surviving animals according to animal-specific scales that rate the performance of various motor skills [266]. Such assessments are generally not of the primary injury, probably because in the immediate post-injury phase histopathology is less developed, MR imaging abnormalities can be absent and functional assessments are dominated by spinal shock [152]. However, the severity and evolution of the secondary processes are likely proportional to the severity of the primary insult and damage.

1.5.4.1 Mechanical parameters that affect SCI severity

It is well established that the severity of a SCI is dependent on the magnitude of the mechanical parameters which describe the impact. These parameters include peak force and displacement, impact and deformation velocity, impact energy and load impulse. For example, slow compression or stretching of short duration may not injure the cord, but prolonged or rapid deformations do [267]. Since the extent of the primary injury dictates the severity of secondary processes, the relative importance of different mechanical parameters has been tested. This has been done predominantly in the mode of rapid transverse compression. For these contusion-type impacts, the force-displacement profiles are dictated by the mechanical impact parameters as well as the material and structural properties of the system. It is therefore impossible to evaluate the absolute independent contribution of each to the injury outcome. Table 1-4 highlights some of the findings relating mechanical parameter to injury outcome; these have been determined using the animal models discussed below in Section 1.6.3.

Table 1-4 Summary of relationships between mechanical parameters and observed effect in experimental contusion SCI in various animals.

Mechanical parameter	Observed effect
Peak force	• Inversely proportional to locomotor recovery scores and spared tissue (but also associated with increased displacement) [268]
Peak displacement (compression)	• At high peak forces, displacement is proportional to myelin loss, macrophage response and ventral motor neuron loss and inversely proportional to motor recovery [268] • Inversely proportional to amplitude of evoked potentials [269,270] • Inversely proportional to white matter sparing and motor recovery [271] • At low velocities, tissue damage is more dependent on degree of compression than rate of application [272] • Correlates best with later locomotor scores in mice [273]
Velocity	• Impact velocity and rate of compression are proportional to haemorrhagic necrosis [269] • Proportional to behavioural recovery and tissue damage [267] • Proportional to blood-spinal cord barrier disruption [274] • In rats, contusion at 300 mm/s gave haemorrhage extending into the peripheral white matter, but at 3 mm/s vascular damage was limited to grey matter [275] • Smaller weights falling from greater heights (higher impact velocity) were associated with less haemorrhage, edema, axonal disruption and myelin fragmentation, compared to larger weights from lesser heights [276]
Impact energy	• NOT proportional to injury severity (see Section 1.6.3.1)
Impulse ($\int Fdt$)	• Proportional to lesion volume [277] • Proportional to intramedullary haemorrhage [278] • Correlates best with early (day 1) locomotor scores in mice [273]
VC (velocity x %compression)	• At higher impact velocities, damage to neural tissue is proportional to the time-varying viscous response [272] • VC_{max} =0.91, corresponds to 50% probability of full recovery [279] • VC_{max} =1.41, corresponds to 50% probability of partial recovery [279]

1.5.4.2   The mechanical role of CSF in SCI – evidence from animal models

The ability of the CSF to protect the spinal cord from contact with the spinal canal during large external loads is commonly stated in general reference texts. However, quantitative and qualitative analysis or theory of the mechanisms by which this occurs are somewhat lacking in the literature. Hung et al. [1] showed that when CSF was drained from the subarachnoid space, although the overall deformation of the dura-cord-system was similar to that with the CSF, its deformation relative to the initial diameter was greater. A similar response was shown with *ex vivo* and synthetic models of SCI [280,281]. However, none of these studies were able to visualise the spinal cord deformation through the natural or synthetic dura. On observing that altering the hydrostatic pressure of the CSF by draining some or all of it did not change the force-time or energy-time trajectories of the impact, Hung et al. further hypothesised that there was some threshold for the impact parameters above which the "shock-absorbing mechanism of the dural sac and spinal fluid" was ineffective [1]. TBI studies have shown that removing modest amounts of CSF increases brain rotation relative to the skull [282] and decreases the head impact energy required to produce cerebral concussion [283]. Ommaya suggested that the CSF might reduce shear stresses in the brain and spinal cord by damping their movement [284]. However, the brain and spinal cord differ considerably in their geometry, mass, tethering and physical response to external loading mechanisms, so observations about the brain may not be directly transferable to the spinal cord.

In contrast to the protective role, several authors have hypothesised that CSF may contribute to focal and diffuse injury when the external forces are larger than those experienced in everyday life. They propose that a pressure wave travelling away from the point of mechanical insult may transmit injurious loads to the spinal cord [1,3,162,285]. In Section 1.5.4.4 below, it is shown that the neural tissue can be damaged by fluid pressure impulses acting directly on the dura or transmitted through the skull. Further, as described in Section 1.4.6.2, the causes of post-traumatic ascending myelopathy and diffuse axonal injury remote to the primary lesion site are not known. In addition, although SCIWORA and SCIWORET injuries are commonly attributed to hyper-flexion, -extension or -distraction of the spine, this has not been confirmed. It is possible that transmission of the CSF pressure wave during the SCI event may contribute to these primary and secondary injury phenomena.

Only two groups have measured *spinal* CSF pressure during an experimental SCI (experimental SCI models are discussed in Section 1.6.3, below). Hung and colleagues [1] reported a peak positive pressure of 50 mmHg approximately 2.5 cm cephalad to the injury site in a single cat using the classic open weight-drop model with a 15 g, 5 mm diameter cylindrical weight dropped from 25 cm. The pressure trace provided indicates that the positive pressure pulse was followed by a smaller negative pressure pulse to approximately -16 mmHg (Figure 1-22). In a separate publication, using a similar

weight-drop cat model, they reported a 150 mmHg peak pressure at 1.5 cm caudal and cranial to the injury site, in response to a 20g-15cm injury [2].
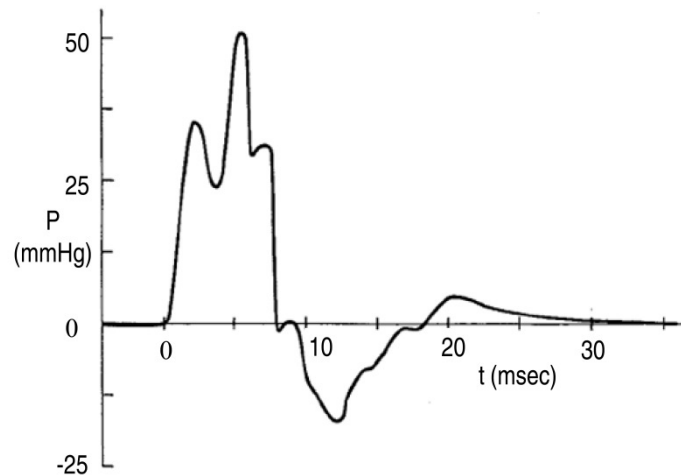
Figure 1-22 Pressure wave in spinal CSF caused by experimental SCI in a cat. Adapted from Surgical Neurology, 4(2), Hung et al., Biomechanical responses to open experimental spinal cord injury, 271-6, 1975, with permission from Elsevier and The World Federation of Neurogurgical Societies [1].

Using the closed weight-drop dog model described below in Section 1.6.3.3, Wennerstrand et al. [3] report a positive and negative pressure peak of up to 1960 mmHg and 630 mmHg, respectively, at 6 cm from the injury site for a single animal (see curve 3, Figure 1-23, left). They also noted that the peak positive and negative pressures decreased with distance from the impact site (Figure 1-23, right). At 15 cm distance these pressures had mean values of 399±89.7 mmHg and 288.2±224 mmHg (N=5), respectively, and at 44 cm, 27.5±6.6 mmHg and 19.0±6.5 mmHg (N=4). In a fluid percussion brain injury model (see Section 1.5.4.4) using rabbits, a similarly rapid damping of fluid pressure was observed [286]. The peak amplitude and duration of the pressure pulse decreased with distance from the impact site, and while cranial pressures of up to 3000 mmHg were measured, no pressure changes occurred caudal to the fifth cervical vertebra.
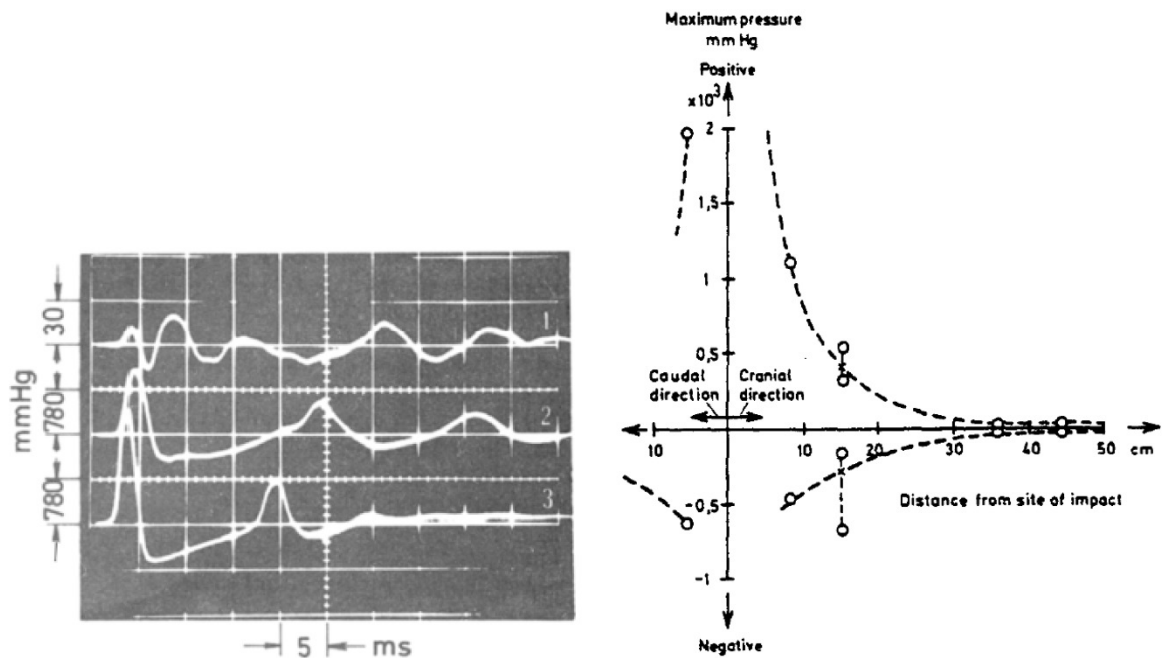
Figure 1-23 Pressure transients measured in the spinal CSF during a closed column experimental SCI. Pressure wave patterns recorded in the spinal canal on transverse impact at the L2-L3 region. Distance between the impact site and gauge points: Curve 1: 36 cm cranial; Curve 2: 8 cm cranial; Curve 3: 6 cm cranial (left). Relationship between the maximum CSF pressure and the distance between impact site and the position of the pressure transducer (right). Reproduced from Journal of Biomechanics, 11(6-7), Wennerstrand et al., Mechanical and histological effects of transverse impact on the canine spinal cord, 315-31, 1978, with permission from Elsevier [3].

Two studies have measured spinal pressures during experimental whiplash simulations. In pigs subjected to whiplash-type neck flexion-extensions, pressures recorded in the cervical spinal canal ranged from -100 to 150 mmHg [287,288]. The authors observed that higher pressures were associated with the location of nerve roots in which the neuron cell body membrane was damaged. The same group placed catheter-tip pressure sensors subdurally in the cervical spine of post-mortem human subjects undergoing whiplash sled tests and recorded pressure amplitudes between 0 and 220 mmHg [289]. Since the vascular and CSF systems were not pressurised in these tests it is unclear how these pressures relate to the *in vivo* situation.

All of these studies observed both positive peaks and negative troughs in the pressure measured at a single location. Wennerstrand et al. hypothesised that the negative pressure indicated a tensile loading in the spinal cord and dura [3]. Krave et al. observed similar characteristics in pressure traces in the brain and speculated that negative pressures causing tensile loading on the tissue are more likely to cause injury through a stretch mechanism [290]. A study on the sensitivity of brain tissue to the application of suction during neurosurgery found that negative pressures of 75-110 mmHg were sufficient to cause blood brain

barrier dysfunction and tissue injury [291]. Negative pressures applied with various vacuum techniques have been shown to induce neural tissue damage and are described in Section 1.5.4.4 below.

Several physical models have also been used to estimate the pressure in the spinal cord, but not the CSF, at the time of simulated SCIs. The construction of these models and pressure results obtained from them are discussed in Section 1.6.5.

In summary, there is limited data available on the CSF pressure transients produced during SCI. The data from experimental contusion SCIs was obtained over four decades ago and utilised transducers that were external rather than situated in the subarachnoid space (Table 1-5).

Table 1-5 Summary of spinal CSF pressure measurements at time of experimental spinal injury

	Injury model type	Animal	Measurement location	Pressure (mmHg)
Hung 1975 [1]	Open contusion (weight-drop 15 g, 25 cm)	Cat	Spinal CSF (2.5 cm caudal of epicentre)	-16 to 50
Albin 1975 [2]	Open contusion (weight-drop 20 g, 15 cm)	Cat	Spinal CSF (1.5 cm cranial/caudal of epicentre)	150
Wennerstrand 1978 [3]	Closed fracture-dislocation	Dog	Spinal CSF ~0 cm from impact 10-15 cm 15-45 cm	> 2000 1000 – 400* 400 – 30*
Bostrom 1996 [287] Svensson 1993 [288]	Whiplash (rapid head flexion/extension)	Pig	Spinal canal (cervical)	-100 to 150
Eichberger 2000 [289]	Whiplash (rapid head flexion/extension)	PMHS†	Spinal CSF (cervical)	0 – 220

*Order indicates decreasing peak pressure with distance from the impact site.
†Post mortem human subject. Note that the CSF and vascular systems were not pressurised.

1.5.4.3   Strain and stress tolerance of the spinal cord

In addition to the gross mechanical tissue failure thresholds discussed in Section 1.5.1, "failure" of neural tissue can be defined by permanent functional and behavioural deficit, permanent or transient reduced signal conduction, mechanical failure at the cellular level and cellular dysfunction. Since these mechanisms are common to all neural tissue, many experiments have been carried out with relation to TBI; however, the review below is predominantly limited to spinal cord specific experiments.

Functional recovery, the rate at which the experimental animal regains motor and sensory ability and the level which is achieved prior to the experimental endpoint, is assessed with a variety of animal-specific instruments such as the Tarlov [292] and Basso-Beattie-Bresnahan [293] scales. Despite the extensive use of contusion type injury models (predominantly weight-drop, see Section 1.6.3.1) and

functional recovery scales in large animals, surprisingly few studies have done extensive exploration to determine the thresholds for permanent injury. Macaque monkeys recovered full function within 72 hours with a 20g-10cm weight-drop injury but had irreversible paraplegia with a 20g-15cm injury [294]; in a common marmoset model with a drop height of 5 cm, full recovery occurred with a 15 g weight, residual upper limb paralysis occurred with 17 g, and almost complete loss of motor function occurred with 20 g [295]. Ford et al. present one of the most comprehensive examinations of the injury threshold for functional recovery in their cat model, and found that 20g-10cm was the threshold for zero recovery at 6 weeks post-injury (Figure 1-24) [296]. A similar analysis by Wrathall et al. showed permanent loss of hind limb weight bearing and locomotion in rats with the OSU weight-drop device (see 1.6.3.1) with a 10g-17.5 cm injury at T8 (Figure 1-24) [297].
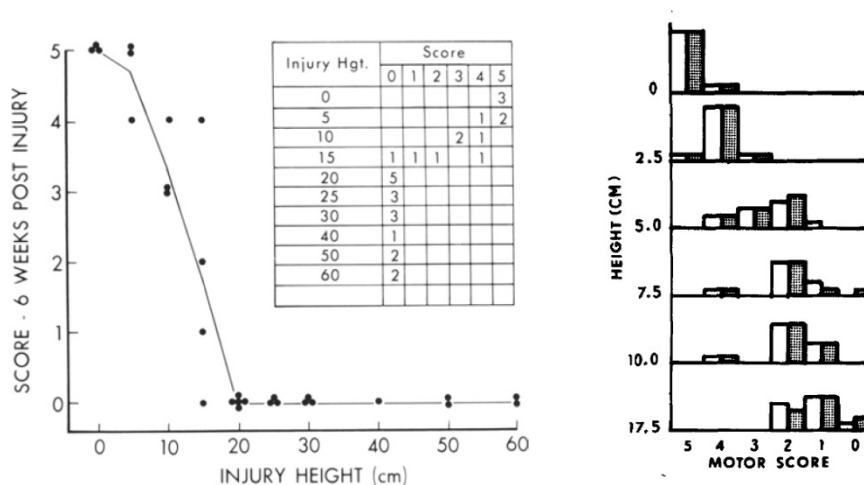
Figure 1-24 Functional recovery threshold determinations for two weight-drop SCI models. (left) Plot and tabulation of final recovery score versus injury height for cats, all with a 10 g weight. Control animals are shown at 0 cm height. Reproduced from Journal of Neurosurgery, 59(2), Ford, A reproducible spinal cord injury model in the cat, 268-75, 1983, with permission from the American Association of Neurological Surgeons (AANS) [296]. (right) Frequency distribution of final (4 week) motor score for each injury height using the OSU weight-drop device for rats, N=9 or 10 for each height. Reproduced from Experimental Neurology, 88(1), Wrathall et al., Spinal cord contusion in the rat: production of graded, reproducible, injury groups, 108-22, 1985, with permission from Elsevier [297].

Although only a small number of human SCIs occur in "pure" axial tension via the vertebral distraction mechanism, tensile loading is most likely a component of all SCI mechanisms. The effect of tensile loading on functional recovery derives from the tensile tests of Hung and colleagues that were used to determine *in vivo* mechanical properties discussed in Section 1.5.1. In dogs subjected to quasi-static strain of 10-50% strain over L1-L2, those subjected to 10% could stand within 12 hrs and had full recovery at 3 days, while 50% strain had full motor and sensory recovery at 5 days [221,241]. Similar tests on cats showed improvement within one day for strain <20%, within two days for 30-50% strain, and full recovery within 5 days for all of these animals [219]. It is not known how these strain

magnitudes compare to the strains experienced in traumatic SCI; further, the quasi-static loading rate is likely to influence the tissue damage and functional recovery in tension, as it has been shown to do in transverse compression (see Section 1.5.4.1).

Failure of *the in vivo* spinal cord to conduct action potentials occurs prior to gross mechanical failure and is due to either axon deformation or lack of tissue perfusion. Action potential conduction is assessed by measuring the amplitude of evoked potentials (EP). Nacimiento et al. applied rapid transverse compression to cat spinal cords and noted a marked decline in EP (to 74% of the uncompressed EP level) at 60% compression; compression to 80% further reduced EP to 36% and compression to 100% abolished EP completely and irreversibly [270]. During quasi-static distraction of the cervical spine in monkeys to a column strain of 8.2% and estimated cord strain of 3.7±1.7%, no evoked potential fell below 37% of control value [298]; 95% reduction is considered necessary for unrecoverable SCI in the cat and monkey [299,300]. The strain threshold for electrophysiologic impairment of the guinea pig optic nerve (strain rate 30-60/s) was 18% [301]. The membrane potential of single squid giant axons was disrupted transiently by low-rate strains up to 19%, increased strain rates caused greater and longer lasting membrane potential changes, and axons elongated past 20% strain did not recover resting potentials [302]. Action potential conduction was abolished in excised strips of guinea pig spinal cord white matter at around 100% strain, and signal recovery was dependent on degree of initial stretch [303]. In quasi-static stretching of the spinal column of dogs, spinal cord blood flow dropped to 27% of control and evoked potentials were eliminated, at an interstitial cord pressure around 46.5 mmHg (the corresponding strain was not reported) [304].

Isolated cell or cell bundle preparations have been used to determine the mechanical response of axons independent of connective tissue and vasculature. Excised unmyelinated squid giant axons fail structurally at around 25% strain when stretched at a rate of around 10/s [302]. A higher strain tolerance was reached in a cell culture preparation of axons bridged between two rows of neurons; there was no severing of axons observed at <65% strain with a strain rate of 25-35/s [305]. Axonal stretch tolerance of the guinea pig optic nerve, which is essentially a bundle of long parallel axons, at 30-60/s, was similar to the squid axon; the reported strain threshold for morphologic damage was 21% [301].

Although beyond the scope of this review, it is important to note that mechanical insult can also lead to non-catastrophic damage to the plasma membrane of cells. This "mechanoporation" does not cause cell death but transiently or permanently affects cell integrity and function, disturbing ion homeostasis, electrical activity and signalling [306]. It is thought that this may have implications for secondary damage processes [306]. Experiments in this area typically apply stretch, pressure and shear loads to *in vitro* cell preparations; several reviews are available [306-308].

The discussion above has largely been limited to measures of strain; *stress* tolerance in compression is more difficult to ascertain because the internal stress fields are likely to be different from the stress at the interface between the tissue and the compressing platen. The stress tolerance of spinal cord tissue has been estimated using an approach that combines finite element and animal models. Ouyang et al. [309] measured electrophysiology during quasi-static compression of *ex vivo* guinea pig spinal cords and determined the patterns of cellular damage with histology. These patterns were then correlated with the tissue stress derived from a finite element model subjected to the same mechanical deformations, and it was estimated that acute mechanical axon damage occurred at a von Mises stress of around 2 kPa.

1.5.4.4   *Pressure impulse tolerance of spinal cord*

As described in Section 1.5.4.2, pressure transients have been measured in the spinal CSF of animals during experimental SCI. These pressure transients may damage the spinal cord via gross deformation of the tissue or via microscopic deformation of the cellular membranes. To the author's knowledge, there is no established pressure tolerance value for the bulk spinal cord or its cellular constituents. However, several techniques that are used to study TBI induce the injury using fluid pressures that are transmitted through the CSF, without direct contact with the brain. These studies provide evidence of the fluid pressure magnitudes and durations that are sufficient to elicit an injury response in neural tissue. It is recognised, however, that tissue tolerance can be specific to the conditions of the external loading, geometry of the anatomy and local tissue differences such as vasculature, metabolic processes and cellular distribution. The three TBI models described in this section are the *in vivo* (animal) and *in vitro* (cell culture) fluid percussion methods and the *in vivo* (animal) blast injury method.

The fluid-percussion model is one of the most frequently used TBI models [310,311]. It produces brain damage or dysfunction by applying a transient pressure impulse to the intact dura via a fluid-filled chamber attached to the animal's skull. Rapid acceleration of a piston at the opposite end of the chamber produces an impulse in the fluid, which introduces a small volume of fluid into the epidural space and produces local elastic deformation of the brain [312]. The impulse is applied either centrally or lateral to the midline via a craniotomy. The resultant pathology is a mixture of focal and diffuse injury [311]. Percussive impacts are graded in terms of the peak applied pressure, and so this may provide evidence for pressure thresholds of neural tissue. However, the incident pressure is usually measured immediately upstream of the cranial attachment, and because the dura is stiffer than the neural tissue, extradural pressures are likely to be higher than the subdural pressures incident on the brain. As summarised in Table 1-6, three studies have shown that intracranial pressure transients measured adjacent to the injury are similar but smaller than those measured extracranially; only one of these placed the intracranial

transducers subdurally [313-315]. At measurement sites remote from the injury, peak pressure and impulse are attenuated, but still proportional to, the incident pressure [313].

Table 1-6 Summary of fluid percussion experimental TBI which measured intracranial pressure.
Studies are presented in chronological order. Pressures have been converted to mmHg regardless of units used in the study. All pressures are relative.

Author	Animal	Impulse location	Extradural (incident) pressure (mmHg)	Transducer location	Peak pressure (mmHg)
Sullivan 1976 [315]	Cat	Central	304-3800	Extradural, Supratentorial (adjacent to impulse)	304-3800
Stalhammar 1987 [313]	Cat	Central	990† 2200† 3800†	Extradural, Supratentorial (adjacent to impulse) / Infratentorial‡	990 / 800† 2280 / 2130† 4180 / 3800†
Clausen 2005 [314]	Rat	Lateral	1440 ± 76 1275 ± 76	Ipsilateral ventricle Contralateral ventricle	1328 ± 228 1380 ± 228

* NR=no reported, but publication from same group found that incident pressure similar to extradural pressure [286]

† Selected data, estimated from plots

‡ Transducers placed against unopened dura

§ NR=not reported. Authors report device can deliver 0-25 bar but do not report the incident pressure for the selected data shown.

Despite the difficulties in defining the actual pressure incident on the brain, the incident pressures that have been applied give an estimate of pressures required to produce neurological injuries of different severities. Some examples in different animals are shown in Table 1-7 below. The pressures resulting in a moderate to severe TBI typically range from 1000 to 3000 mmHg, with an impulse duration of around 20 ms. Mild injuries are reported for pressures as low as 300 mmHg [312,316,317]. Considerably higher pressures were tolerated in sheep than the other animals [318], but the reason for this is not clear.

Table 1-7 Selection of animal models reporting incident pressure and outcome with the fluid percussion injury method. Studies are presented in order of ascending animal size.

Author	Animal	Impulse location	Pressure (mmHg)	Outcome/severity rating
			Intracranial (parenchymal)	
Walter 1999 [319]	Swine	Lateral	3040-3420§ (anterior) 2050-2200§ (middle) (10-15 ms duration)	NR*
			Extracranial (incident)	
McIntosh 1989 [316]	Rat	Central	75-760 1140-1520 2280-2660 w/o ventilation 2280-2660 w/ ventilation (21-23 ms duration)	Slight neurological deficit at 4 weeks Moderate neurological deficit at 4 weeks Severe neurological deficit at 4 weeks Severe neurological deficit at 4 weeks but less than w/o ventilation
Delahunty 1995 [320]	Rat	Central	1520 ± 38	Moderate; transient neurological suppression and persistent motor and memory deficit
Rinder 1969 [317]	Rabbit	Central	140-690ǁ 310-960 600-1850	no concussion slight concussion severe concussion
Hartl 1997 [321]	Rabbit	Lateral	2625 (20-25 ms duration)	Increased ICP, white blood cell activation
Sullivan 1976 [315]	Cat	Central	1140 1672 1976 2432 3040	No EEG‡ changes; physiological response but no pathology Physiological response but no pathology EEG‡ recovery severely impaired. Macroscopic lesions Extensive basal subarachnoid haemorrhage Haemorrhagic contusion at impact site
Hayes 1987 [312]	Cat	Central	0-680† 760-2960† 3040-3800†	Mild (microscopic SAH‡ and petechial IPH‡) Moderate Severe, irreversible
Marmarou 1990 [322]	Cat	Central Lateral	2165 2165	4 of 7 survived at 24 hr 5 of 11 survived at 24 hr
Hilton 1993 [323]	Cat	Central	1350 ± 152 2075 ± 53	No midbrain or brainstem haemorrhage Lesion area 33.8±7.3 mm²
Millen 1985 [318]	Dog	Central	2400 2225 2235	<6 min physiologic change <25 min profound electrical activity depression Increased plasma catecholamine concentration
Pfenninger 1989 [324]	Piglet	Central	mean 2700, peak 12000 (18 ms duration)	Increased ICP, decreased CPP and cerebral blood flow up to 2 hr
Armstead 1994 [325]	Piglet	Lateral	1397-1691 (12-23 ms duration)	Decreased cerebral blood flow and oxygenation
Fritz 2005 [326]	Piglet	Lateral	 2354 ± 441 3016 ± 736	Immediate increased ICP (both groups) Focal pathological damage Diffuse axonal injury; second ICP peak @ 5 hr post-injury w/ reduced cerebral blood flow
Millen 1985 [318]	Sheep	Central	3085, 4940,5700,6460,7600	No physiological change

* NR=not reported, w/=with, w/o=without

As noted in Section 1.5.4.2, negative pressures have been observed during experimental SCI in animals. Several studies have applied negative pressures to the intact dura or directly on the pia to induce focal brain lesions but not diffuse injury associated with significant long-term deficits [310]. Fluid vacuum pulses of 1520-6080 mmHg and less than 100 ms duration applied to the exposed cortical surface of rats caused focal hemorrhagic lesions without overt damage to other regions [327,328]. There was blood-brain barrier breakdown at 10 min [328], and neuronal cell loss, hypertrophy of astrocytes and axonal damage immediately adjacent to the lesion at 3 days [327]. Vacuum pressures of -700 mmHg applied dynamically to the intact dura of rats and held for 5 seconds caused subarachnoid haemorrhage, neuronal damage, astrocyte response, BBB breakdown and changes in cerebral blood flow of various levels at 5 minutes to 7 days [329,330].

Transient fluid pressure impulses have been used to produce injury in *in vitro* cell cultures mounted on a rigid substrate, as summarised in Table 1-8; the techniques are reviewed by [307]. Cell cultures of neuronal and glial cells exposed to fluid pressure impulses of 1550 mmHg [331] and 362-3050 mmHg (duration 20-30 ms) [332], respectively, show cell damage and reduced viability. Single or double pressure impulses of 3800 mmHg were used to induce damage in cultured rat neurons, astrocytes and microglia [333,334].

Table 1-8 Summary of pressures used to induce injury in *in vitro* neural cell preparations. Studies are presented in chronological order.

Author	Cell culture	Incident pressure /duration (mmHg / ms)	Pathology
Suneson 1989 [331]	Neuronal (rat)	1550	Cell damage, reduced viability
Shepard 1991* [332]	Glial (human)	362 / 20-30 3050 / 20-30	Cell damage, reduced viability
Wallis 1995	Hippocampal slices (rat)	Weight-drop 1kg-61cm	Severe neuronal dysfunction
Panickar 2002* [334]	Neurons, Astrocytes, microglia (rat)	3800	Free radical production
Jayakumar 2008* [333]	Astrocytes (rat)	3800 / 25 twice	Cell swelling, mediating chemicals identified

* Same apparatus used.

Non-impact blast wave induced neurotrauma can occur from exposure to a high pressure air wave resulting from an explosion. The exact mechanism of energy transmission to the brain is unknown, but

one pathway is through the skull, dura and CSF [335]. The pathological response to blast includes many features of SCI, including diffuse edema, metabolic disturbance and vasospasm, neuronal swelling, axonal pathology and white matter degeneration. Models of blast injury expose the animal to a blast wave produced by detonation of an explosive charge, or release of compressed air in a shock tube [336]. Two studies have measured the pressure at various locations in a rat [337] and swine [338] brain during an experimental blast event (Table 1-9). In these animals the peak pressure reached inside the brain tissue was similar to the exposure pressure outside the skull. While it should be recognised that energy transmission probably differs by species head size and skull thickness [335], this implies that the incident pressures are a reasonable estimate of the peak pressures occurring in the CSF and brain and that are causing injury.

Table 1-9 Summary of models reporting incident blast pressure and resultant internal pressure.

Author	Animal	Incident pressure / duration (mmHg/ms)	Transducer location	Resultant peak pressure (mmHg)	Pathology/ Physiology/ Behaviour
Chavko 2007 [337]	rat	315 / 4.5	3rd ventricle	300 / 4.5 -50 / NR*	No injury
Bauman 2009 [338]	swine	NR*	Ipsilateral: Fore- and hind-brain, thalamus; Contralateral: thalamus	NR**. Approximately half the peak magnitude of the incident extracranial pressure	White matter degeneration, astrocytosis; vasospasm

* NR=not reported. **Due to USA Department of Defense restrictions pressure values were not reported and graphs were provided without scales in the paper [339].

Moochhala et al. [340] found that rats exposed to 21 mmHg blast pressures showed no behavioural or histological response, but those exposed to 150 mmHg (2.5 msec duration) had a significant decrement in physical tests and degenerating neurons in the cerebral cortex of the brain. Rats exposed to low level blast overpressures of 75-450 mmHg had impaired cognitive function [341] and pigs exposed to 338 mmHg pressure had small haemorrhages and signs of edema in the brain [342]. However, in contrast no injury was detected in the visual neural pathways of rats exposed to a 625 mmHg blast [343]. Exposure to pressure levels of 750-2250 mmHg caused injury to neuronal and glial cells, as well as brain edema in rats [343-349], and 1500-2250 mmHg caused transient apnoea in pigs [350]. Kato et al. [351] applied blast overpressures of 7500 mmHg to rats with craniotomies. Despite the considerably larger incident pressure than the aforementioned studies, they observed no significant haemorrhage in cortical or subcortical regions, but did note mild morphological changes such as spindle-shaped changes of neurons and elongation of nuclei toward the shock wave source at 24-hrs post shock. They suggested that the threshold for blast induced brain injury may be lower than for other organs due to an "intrinsic vulnerability of neurons" and the delicate neural vasculature. From this synopsis it is clear that the

severity of the injury incurred is dependent on the configuration of the experimental blast apparatus and the location of the animal within it. However, these values do provide an indication of the magnitudes of pressures that might be expected to cause damage to the neural tissues. A summary is provided in Table 1-10.

Table 1-10 Summary of blast injury models reporting incident blast pressure and pathology and/or behavioural outcome.

Author	Animal	Incident pressure (mmHg) / duration (ms)	Pathology, physiology and/or behavioural outcome
Kaur 1995 [344]	rat	NR / NR	Increased microglial activity
Petras 1997 [343]	rat	625 / NR 780-825 / NR 970-1300/ NR	No injury No injury (2) / injury (2) Injury
Axelsson 2000 [350]	pig	1500-2250 / 2.5-3.5	Transient apnoea and flattening of EEG (n=4) No significant change in cardiac physiology
Saljo 2000 [345]	rat	1155 / NR 1800 / NR	changes in the neuronal cytoskeleton
Saljo 2001, 2002a,b [346-348]	rat	225 / NR 450 / NR	Activate microglial cells and astrocytes; elevated immunoreactivity; neuronal apoptosis; change ICP and cognitive function
Saljo 2003 [352]	rat	139 / 2.5 197 / 2	Diffuse neuronal and glial cell damage
Moochhala 2004 [340] ‡	rat	21 / NR 150 / 2.5	No injury Neuron degeneration and physical test decrement
Kato 2007 [351]	rat*	7500 / NR 75000 / NR	Mild cell morphology changes Contusional haemorrhage, neuronal apoptosis
Saljo 2008 [342]	pig	340 / NR	Small brain haemorrhages; signs of brain edema
Saljo 2009 [341]	rat	75-450 / NR	Impaired cognition
Svetlov 2010 [349]	rat	825 / 2 1275 / 4 2685 / 1 1290 / 4 2685 / 10	Transient agitation† Lethal† Lethal† NR Focal massive haemorrhage; diffuse and focal mild neuron damage; BBB disruption

* With craniotomy

† Body not armoured

‡ Specifically concentrated on central visual pathway and terminal targets in midbrain and diencephalon

EEG=electroencephalogram, NR=not reported

1.5.5 Summary

The anisotropic and viscoelastic mechanical properties of central nervous system tissues, as well as the complex geometric structures of the individual components, make accurate prediction and modeling of mechanical response to external loading difficult. Traumatic injury to the spinal cord occurs when physical deformation resulting from direct contact with misaligned or fractured parts of the spinal canal exceeds the structural or functional tolerance of the tissue. The mechanical impact parameters influencing SCI severity include the impact velocity, the peak displacement and load, the rate of deformation, impulse and the velocity-compression product.

Since SCI arises from a transmission of kinetic energy to the spinal cord via the CSF, fluid pressure may contribute to cellular and vascular damage in SCI. Two groups have measured CSF pressure transients during experimental SCI, but it is unclear how well the SCI replicated human injury. A limited number of animals were tested and fluid-filled catheters, which potentially damp the pressure signal, were used. A fluid pressure tolerance for the spinal cord and brain likely exists but the tolerance limit is as yet unknown (or unpublished). *In vivo* and *in vitro* fluid percussion and blast injury models of TBI have shown that fluid impulses can interfere with CNS function. The incident pressures used to create mild and moderate brain injuries are within the range of those that have been measured in the spinal CSF during experimental SCI. Therefore, investigation of CSF pressure transients generated during human-like experimental SCI and measured with indwelling pressure transducers is warranted.

1.6 Modeling human traumatic spinal cord injury

Spinal cord injury researchers depend heavily on animal, cadaveric, surrogate and computational models of cord injury. The selection of model type and its specific design depend largely on the question to be answered. Both animal and surrogate models were developed in the current work and are the primary focus of this review. Although small animals (rats, mice, guinea pigs and rabbits) are currently favoured due to economy and availability, this section will predominantly be limited to a discussion of large animal models. Large animals are considered greater than around 4 kg and include dogs, sheep, pigs, cats and non-human primates (NHPs). The latter two are frequently low in weight, but cats have relatively large spinal cords for their weight and NHPs are similar to humans in that they are bipedal. The discussion is also limited to models that achieve SCI via "blunt" mechanical loading and excludes transection models, ischaemic injuries mediated by obstruction of spinal arteries, and administration of chemicals and radiation (reviewed in [353]).

1.6.1 Large animal models for experimental SCI

Animal models have been developed in a number of animal species and using several injury mechanisms [354,355] each with their own advantages and disadvantages, and therefore suited to address different questions [16,356]. The main motivation for developing *in vivo* animal models has been to study secondary pathophysiology and assess potential therapies. For these types of tests, obtaining human-like pathophysiology and measurable recovery from neurological deficit is sufficient, regardless of the mechanical parameters used to produce the injury. When studying the mechanical phenomena associated with an injury, emphasis should be placed on using mechanical parameters, such as velocity, displacement and loading direction, that replicate human SCI. If the animal selected has a spine and spinal cord that are similar in size and geometry to human and the research question concerns the mechanics rather than the neurophysiology of the injury, the parameters derived from biomechanical tests on cadavers may be applied directly to the model without need for scaling.

SCI research began in large animals; the first report of experimental SCI was in 1911, when Allen devised a method to apply a contusion injury in dogs [357] (see Section 1.6.3.1). When SCI research intensified in the late 1960s non-human primates were used and remained popular until 1981 [e.g. 294,358,359]; they are now used only sparingly [295,360,361]. Regarding contusion-type models, dogs were used little in the early 1970s, and then consistently from 1975-1982 [e.g. 362,363,364], followed by a single study in 2000 [365]. Cats were used between 1969-1989 and were used almost exclusively in the 1980s [e.g. 1,277,366,367-369]; a sheep contusion model was used by a single group in 1975-1984 [e.g. 218], and by another in 1989 [370,371]. Smaller animals (rats, rabbits, guinea pigs, ferrets and mice) were used sporadically from the 1970s, and rats have been used almost exclusively for the last 20 years. The change to rodent models was largely motivated by societal pressure, financial considerations, and the need for large scale screening of therapies [372]. The studies are too numerous to recount and only selected references have been offered; more detailed histories have been given by Dohrmann [373], Fernandez et al. [354] and Young [267].

In general, the SCI research community is supportive of the development of a large animal model as a pre-clinical testing tool [374]. The pig has wide acceptance as a laboratory animal for medical research [375] including for modeling TBI [376] and iatrogenic spinal cord ischaemia [e.g. 377,378-380]. However, the first report of experimental traumatic SCI in a pig was not until 1990 [380,381], followed by studies by three separate groups in the last five years [382-385]. As detailed in Table 1-11, each has used a different method to impart the injury. These methods have been used in various large animals previously and are critiqued in Section 1.6.3.

Pigs offer several advantages over other large animals and rodents. They usually present fewer ethical concerns than do domestic pets (such as cats and dogs) and non human primates, and some

lineages can be purchased free of common diseases. There are several miniature breeds available which are beneficial for chronic studies requiring care and handling of the paralysed animal. Of particular interest to this study is that pigs have similar spinal structure [386,387] and spinal cord vascular supply [388] to humans. With appropriate selection of breed and age, they can also have similar spinal cord dimensions to humans. The main disadvantages of pigs relate to lack of knowledge of the spinal cord tract organisation and differences in central pattern generator motor control from humans, although the latter is common to all quadrupeds.

Table 1-11 Summary of pig models of traumatic SCI

Author	Study objective	Animal characteristics	Model and experimental protocol
Owen 1990(A) [380]	Effect of distraction duration on neurological deficit measured by evoked potentials, wake-up test and histology.	Domestic, M/F* 30-45 kg Injury level: T5/6 Acute	**Quasi-static distraction.** Applied via Kostuik screws (w/ disc osteotomy and PLL transection) until evoked potential lost. Maintained for 3 to 30 minutes.
Owen 1990(B) [381]	Effect of distraction level and duration on neurological deficit measured by evoked potentials, blood flow, wake-up test and histology.	Domestic, M/F 30-45 kg Injury level: T5/6, T12/L1 or L3/4 Acute	**Quasi-static distraction.** Applied via Kostuik screws (w/ disc osteotomy and PLL transection) until evoked potential lost. Maintained for at least 20 minutes.
Bernards 2006 [383]	Effect of methylprednisolone on intravenous and intrathecal biochemical markers assessed by microdialysis.	Farm bred, M/F 18-22 kg Injury level: T13 Acute (to 250 minutes)	**Weight-drop.** 1 cm diameter steel cylinder impounder, aluminum tube guide, 25 g steel weight dropped from 45 cm. Removed immediately.
Zurita 2008 [389]	Functional recovery after autologous transplantation of bone marrow stromal cells.	Minipigs, F 20 kg Injury level: T12-13 Chronic (to 6 months)	**Clip compression.** Open dura mater, apply two surgical Heifetz's aneurysm clips for 20 min. Suture dura and cover w/ PTFE* sheet.
Skinner 2009 [384]	Feasibility of EMG* to detect motor tract injury.	Young adult pigs Injury level: high thoracic Acute	**Clip compression (lateral).** Slow or rapid compression to 50% by metal calliper. Rapid compression held for 14 sec.
Zahra 2010 [385]	Haemodynamics after complete cervical SCI.	Yorkshire domestic, F 5-9 kg, age: 3-5 wks Injury level: C3-4 Acute (to 4 hr)	**Controlled cortical impactor.** (adapted from TBI). 8 mm diameter flat tip. Complete injury: depth 5 mm, dwell 300 ms, 80 psi. Open dura, drained CSF.
Kuluz 2010 [382]	Paediatric model development.	Yorkshire domestic, F 5-7 kg, age: 3-5 wks Injury level: T7 Chronic (to 28 days)	**Controlled cortical impactor.** (adapted from TBI). 6 mm diameter flat tip. Complete injury: 5mm-60psi, 8mm-80psi; Incomplete injury: 3mm-30psi.

*M=male, F=female, EMG=electromyography, PTFE=polytetrafluoroethlyene

1.6.2 Relative size of animals for SCI models

Selecting an animal with spinal cord dimensions similar to human has the potential to improve the biofidelity of the model's mechanical response. Three dimensions are of primary importance to the current work: diameter of the spinal cord, diameter of the dural sac (or the thickness of the CSF layer), and the length of the spinal cord. Physical measurements of the CNS of animal species are sparsely reported in the published literature.

The majority of experimental SCIs are performed in the thoracic region, typically between T6 and T12. This produces hind limb paralysis but with fewer autonomic nervous system complications than higher level injuries, thus reducing the complexity of post-injury animal care [390]. The sagittal and coronal diameters of the human spinal cord are around 4-8 and 7-9 mm, respectively, in the thoracic region [391-394]. In comparison, the thoracic rat spinal cord diameter is around 1.5-2 and 2-3 mm diameter in the sagittal and coronal planes [395], in 3 kg cats the coronal diameter is around 4.5-5 mm and sagittal diameter is around 4.5 mm [396], the medium size dog has a 7 mm coronal diameter [397] and in 22 kg pigs the coronal diameter is around 6 mm [384,398]. Although it can be difficult to obtain a pre-injury measure of cord size, depending on the extent of cord exposure during surgery, surprisingly few studies have reported the size of the spinal cord for the animals they were using. This makes the comparison of injury severity difficult across different studies that have used different impounder contact areas, different sizes of animals within a species, and different species. The diameter of the cord is important for biomechanical studies so that the injury parameters can be directly translated from biomechanical cadaver studies of the burst fracture and fracture-dislocation process without requiring relatively uninformed scaling assumptions (see Section 1.6.4). Also, the importance of uniform spinal cord size within a given study has been highlighted; in a study of experimental SCI in cats, the number of surviving axons, and hence the extent of injury produced by a given impact, varied directly and significantly with the dimensions of the spinal cord [396].

Dural size (or CSF layer thickness) is documented to a limited extent for humans, and is not documented for animals. Accurate measurement of dura diameter is challenging. The dural sac changes shape when it contains no CSF (i.e. *ex vivo*), and *in vivo* measurements using CT myelography and MR imaging may contain systematic bias due to contrast media concentration, selection of the pulse sequence and window level, partial volume effects, motion artifact and resolution limitations. From observation, the dural sac of rats is insignificantly larger that the spinal cord, and the dura appears to be separated from the cord by only a thin film of intervening fluid. In contrast, when the dorsal dural sac of pigs and humans is visualised after surgical exposure, it is clearly separated from the dorsal surface of the spinal cord by a layer of CSF several millimetres thick. A human-like CSF space is important in biomechanical studies because fluid flow and pressure distribution can be dependent on the dimension of the fluid layer.

Further, the fluid layer must be large enough to accommodate the implanted transducer with limited interruption of the natural fluid flow.

The adult human spinal cord is around 41-45 cm long [399]. In comparison, the rat's spinal cord is around 9 cm long [395], adult cats weighing about 2.5 kg have spinal cord lengths of 33.9±1.6 cm (N=12) [400], adult *macaca rhesus* and *macaca irus* monkeys have spinal cord lengths of 23.2±3.7 cm and 20.1±1.6 cm, respectively (N=6 each) [401], and in farm-bred pigs weighing 20±1.4 kg the spinal cord length averages 45-55 cm [398]. The length of the spinal cord could be important in the transmission of the energy away from the injury site through the spinal cord, CSF and dura. It may also contribute to the damping and reflection of such a stress or pressure wave.

1.6.3   Methods of producing injury

Since the first documented SCI model by Allen in 1911 [357], a variety of experimental injury methods have emerged. These can be broadly categorised into dynamic and static models; the former is suitable for modeling traumatic injury, and the latter can simulate either a chronic myelopathy or residual compression resulting from traumatic SCI. Models are also designated as open: loads are applied directly to the spinal cord and dura after surgical exposure; and, closed: loads are applied to the vertebra and transmitted to the spinal cord via the anatomy. The following discussion is largely limited to methods that have been applied to large animals, with only a short reference to rodent models. However, it is noted that rodent models dominate current research, and the SCI devices for rodents are more sophisticated in terms of mechanical control and measurement. As previously mentioned, animal models need to be assessed in terms of relevant biomechanics, as well as the creation of relevant physiological response. All blunt injury models exploit the intuitive relation between injury severity and the magnitude and rate of tissue deformation. The following discussion primarily concerns the biomechanics of the injury methodology.

1.6.3.1   *Weight-drop*

Contusion SCI models in large animals have been based almost exclusively on the so-called "weight-drop" method of Allen [357,402]. Allen is credited with developing the first quantitative and standardised experimental SCI model; this consisted of locally exposing the thoracic spinal cord (dura intact) of the anesthetised dog, placing a tube oriented perpendicularly to the spinal cord, and dropping a weight through the tube. The severity of the contusion, described in "gram-centimetres", was modified by adjusting the weight or the height from which it was dropped. There was little focus on SCI in the following decades and the weight-drop method was only used by Amako in 1935 [403] and Freeman in 1953 and 1963 [404,405]. When SCI research resumed in the late 1960s, the weight-drop model was used profusely with various modifications in dogs, cats and monkeys until around 1985 when it was

adapted for the rat [297,406]. There is no generalised or commercially available large animal weight-drop device.

Unfortunately in the early use of the weight-drop method, the indeterminacy of the "g-cm" unit was not appreciated. As described above in Section 1.5.4.1, the impact velocity, force, displacement and impulse have an approximately linear relationship with injury severity (e.g. structural and cellular tissue damage, functional recovery) and mechanical indicators of severity (e.g. deformation and peak force), while impact energy does not. From elementary mechanics, the potential energy (mgh) of a dropped mass is converted to kinetic energy ($\frac{1}{2}mv^2$) at impact so that for a plastic collision the energy transferred during the impact is linearly related to both height and mass. However, the impact velocity is proportional to the square root of the height (since mgh=$\frac{1}{2}mv^2$; v=$\sqrt{2gh}$), and so is the impulse (I=mΔv). The impulse defines the peak force and the duration of the impact (I=∫Fdt). Several authors have shown at length that different weight-height combinations with the same g-cm product do not produce the same mechanical insult or resultant injury severity [276-278,366,367]. Because of the persistent use of the g-cm unit, the impact velocity and mass used in many previous studies cannot be determined, and it is difficult to judge relative injury severity.

The specifications of the interface between the device and the animal have a significant bearing on the resultant injury severity and repeatability. Such specifications include use of an impounder (and its material and mass), and the area, shape and conformity of the impacting tip relative to cord size and shape. Most devices have used an impounder resting on the dura, either balanced freely, supported by a frame or saddle placed on the vertebra, or residing in the guide tube. Impounder materials have included Teflon, aluminum, lucite, brass and plexiglass, and masses have varied from 0.1 g up to 14.7 g [367] and 26 g [366] when instrumented with load cells. The mass of the impounder, particularly relative to the dropped mass, changes the energy transfer between the falling weight, the static impounder and the spinal cord, thereby changing the cord deformation [369,407]; a heavier impounder requires more energy to be accelerated [368] and causes greater overall cord compression during the injury [364]. Loss of energy will also occur due to deformation of the impounder and mass, depending on their relative stiffness. Furthermore, impounders can cause substantial pre-impact dura and cord static deformation. With an impounder of only 0.1 g the dura deflection was 0.2 mm and with a 10 g impounder it exceeded 2 mm and likely compressed the spinal cord [369]. These results indicate that impounders should be avoided when studying the biomechanical function of the CSF and dura.

The contour and area of the impacting tip, whether an impounder or falling weight, has been shown to affect the injury. Some previous studies used concave contoured impounders [294,358], although flat circular faces were typical. The diameter of the impacting tip for cat, dog and monkey injuries was generally 5 mm. A one-fold increase or decrease in cross-sectional area led to a 20-30% inversely

proportional change in maximum deformation and peak stress [369]. Molt et al. [277] state that although using a 4, 5 and 6 mm diameter impounder changes the area by around ±50%, no changes in impulse and lesion size were detectable; however, it is not clear that the mass of the impounder was kept constant. A larger impounder area created by contouring of the tip into an arch which straddled the cord, rather than by increasing the diameter, was found to create a more severe injury and one that better simulated clinical injury [363]. Few weight-drop devices included a mechanism to eliminate "bounce" of the impactor after the initial impact [296]; bounce may lead to secondary impacts which may increase the variability of the induced injury.

A variety of materials have been used for the guide tube (e.g. Teflon, glass, plexiglass, brass, stainless steel) and the falling weight (brass, lead, steel, mercury-filled glass tube). The selection of weight-guide pairs would affect the friction characteristics, as would the configuration of holes in the guide tube and the size of the opening at the spinal cord end. High friction and air resistance would reduce the impact velocity; however, none of the early models report impact velocity. The original design by Allen used an open frame rather than tube [357], one device used a central shaft [358] and one relied on accurate alignment of the weight above the impounder and omitted a guiding device [1]. The guide tube mount is not described in most studies; for some it was attached to the surgical table [368] or a stereotactic frame [408], while others rested on saddle which sat directly on the vertebra [294]. One author reports inducing unilateral pneumothorax to reduce body movement due to chest expansion during respiration [369], but others do not report how thorax motion was compensated for in determining drop height for table-mounted devices. In contemporary rat models chest excursion is generally eliminated by partial suspension of the body weight on vertebral clamps attached to a stereotaxic frame.

The vertebral clamps also serve to stabilise the vertebral column. The need to eliminate motion and flexibility of the spinal column and ribcage under the point of injury was identified by some early researchers. In the rat, this is usually achieved by restricting the laminectomy to a single level and clamping the spinous processes of the adjacent vertebra to the stereotaxic frame [407]. However, vertebral clamping and weight suspension are more difficult to achieve in larger animals, and there are few reports that it was considered. In one device a metal saddle rigidly fixed to the injury apparatus was inserted under the cat's spinal cord [296], and in another, rigid supports were placed under the transverse processes and in turn attached to the surgical table [396].

Measurement of the mechanical input and output parameters, such as velocity, displacement and force, was largely limited to studies which focused on the biomechanics of the model and were not reported by studies of SCI pathophysiology. Two groups incorporated a load cell into the impounder [358,366] for exploring mechanics, but this device was not used to describe injuries for actual pathology or therapeutics studies. To account for the chest and spine deflection noted above, deformation of the

spinal cord must be measured independently of chest excursion [366], although not many early models collected these data.

In most experimental models the rebound of the dropped weight was assumed insignificant; the rebound elimination mechanism for one apparatus was a string attached to the weight which was pulled manually after impact [409] and another using an automatically triggered electromagnet to stop the weight in its upward flight [296].

In addition to the device-related differences described thus far, variation in biomechanics and pathophysiological response can also be due to animal selection and surgical technique. Some authors reported wide ranges of animal weights or used different breeds within one study. Spinal cord dimensions were rarely stated, but variation in size would have altered the load distribution and the relative cord compression, thus contributing to inconsistent injury severity [410]. Some studies opened the dura prior to injury [411,412], which would remove the mechanical contribution of CSF and dura, but the majority did not. Other factors which may cause variation include the tension in the dura and cord, tissue and fluid pressure, blood pressure, relative diameter of cord, subarachnoid space and canal, and proximity of the injury site to nerve roots and dentate ligaments [407].

The only standard weight-drop device is for rats: the New York University (NYU) impactor [413] also referred to as the MASCIS (Multicenter Animal Spinal Cord Injury Study) impactor as it was adopted for that large study [355]. Biomechanical standardisations put in place to increase repeatability across the MASCIS institutions included: impactor mass and tip size and shape, height settings for graded injuries at a specified spinal level, and support of the vertebral column [355]. Non-mechanical standardisations included rat strain and age, anaesthetic protocol, and timing of the injury after anaesthesia induction [267]. The device can measure impact velocity, compression and rate, and force.

1.6.3.2 *Controlled displacement and controlled force contusions*

A number of machines have been designed that produce injury while controlling either peak force or rate/peak displacement. These machines have been critical in determining the injury response to mechanical parameters that cannot be independently manipulated using a weight-drop device. These devices control the impactor's trajectory for both the loading and unloading path, thereby eliminating secondary impacts due to bounce that can occur with weight-drop devices. Although these machines have distinct advantages in the standardisation of injuries, none have been implemented for animals larger than a rat or ferret. There are currently two standard methods for delivering a controlled contusion injury to rats: the Ohio State University (OSU) impactor and the Infinite Horizons (IH) device [356].

The OSU impactor is a displacement-controlled electromechanical actuator [414-418]. Although capable of delivering speeds of 0.3 m/s, it is typically operated in the range of 0.08-0.1 m/s, to a depth of

0.8-1.1 mm (around 30-50% of cord diameter), with a dwell of 4-5 ms at maximum displacement and total event duration of about 10 ms [355]. Because it is displacement controlled, the surface of the dura must be touched to obtain the "zero" displacement before the test is started; some researchers believe that this has the potential to damage the spinal cord. Displacement and force trajectories are measured, as well as the vertebral column deflection [267]. Displacement control is a very stable and repeatable control mode. The IH impactor is a force-feedback stepper motor device, typically operated to obtain a peak load of 1-2.5 N (100-250 kdyn) and has a peak speed of 0.13 m/s [419]. No pre-injury displacement "zeroing" is required. Force-feedback is a challenging control mode, particularly at high rates and when compressing non-linear viscoelastic materials, so the repeatability can be less than displacement control. For both the OSU and IH impactors, active control of the impactor tip eliminates the impactor rebound that can occur for weight-drop devices.

Of note is the device of Anderson and colleagues [420] in which contusion was applied to the ferret spinal cord through the intervertebral foramen, without a laminectomy. This was a pneumatic device in which the maximum stroke was controlled by mechanical stopper. It was capable of velocities ranging 0.5 to 10 m/s, far greater than the above electromagnetic actuator devices [266], but it lacked a force transducer. The controlled cortical impactor (CCI) is a similar device; originally designed to impart focal brain injury, versions of this device have recently been employed to induce thoracic [382] and cervical [385] SCI in piglets, as mentioned in Section 1.6.1, and thoracic SCI in rabbits [196].

1.6.3.3   *Vertebral distraction and fracture-dislocation*

Few models of closed-column (i.e. no laminectomy) dislocation have been reported in the literature, despite fracture-dislocation being one of the most common causes of SCI. The first was described only briefly but appears to have achieved a dorsoventral dislocation via weight-drop onto, or between, the T9-T11 spinous processes of the cat [421]. As discussed in Section 1.5.4.2, a closed column dog model was used to study the CSF pressure response to lateral impact. A preset displacement was applied to the intact lumbar spine using a 4 cm diameter captive piston driven by a large free-falling weight. This method achieved spinal fractures in two, and neural damage in five, of six animals [3]. A pneumatic device to dislocate the L1/2 vertebrae of the dog is described by Fialho [362]; after dissection of the spinous processes and facet joint of L1, the L1 vertebra is held stationary and L2 is displaced laterally. Both of the contemporary dislocation models were designed for rats: the first holds T12 stationary, leaves T13 unconstrained and displaces L1 laterally to a set displacement at up to 0.15 m/s [422]; the second imparts a dorso-ventral dislocation of specified displacement at C4/5, at speeds of up to 1 m/s [423].

Vertebral distraction models have provided low-rate loading of the spinal column by fixing one of the pelvis/torso and head, and applying a tensile load to the other, in non-human primates [300] and cats

[299,424]. In the monkey [425], cat [426] and pig [380,381], distraction was achieved by resecting an intervertebral disc and loading the adjacent vertebra in tension via screws or clamps attached to the spinous processes or vertebral bodies. Early computer controlled distraction models used a materials testing machine, attaching adhesive clamps directly to the spinal cord (dura removed, pia intact) *in vivo* in cats [219] and dogs [221,241], and measured motor and sensory function for up to three weeks post-injury. Most recently, computer controlled vertebral distraction has been achieved in the rat at speeds of up to 0.9 m/s via laminar hooks at T9 and T11 [427], and at 1 m/s via dual-vertebra clamps placed across C3/4 and C5/6 [423].

1.6.3.4   *Residual compression models*

Although the aforementioned models all have the potential to provide a prolonged compression after the dynamic injury, they are generally used in a purely acute manner. Dwell times for the electromechanical devices are generally 4-5 ms [355], while weight-drop and other non-computer controlled methods have dwell times on the order of seconds because the compression is manually removed or released. A number of models have been designed to emulate the residual compression commonly present after traumatic SCI. The duration of static compression has ranged from 1 minute to days or weeks. Some of these devices are applied to the spinal cord dynamically but without rate control. Furlan et al. [200] provide a comprehensive review of residual compression models that have been used to study surgical decompression.

The clip compression model uses an aneurysm clip to apply a constant, dorsoventral and extradural force to the spinal cord for a specified length of time [428]. The closing force of the spring-loaded clip is calibrated in grams, and values corresponding to mild, moderate and severe injuries in the cervical and thoracic spinal cord have been established for the rat [429]. Although the jaws of the clip are released quickly, the dynamic parameters of the compression are not measured, and the calibrated force applies to the static condition only.

Other residual compression methods have used pistons fixed to the vertebrae (0.17 m/min then static) [430,431], ligature-type cables [208,209], and screws protruding through the vertebral body [432-434] in dogs and cats [435], and spacers hooked under laminae adjacent to a laminectomy in rats [207,436]. Modified forceps have also been used to create a predetermined static compression [410]. Weights have been "rested" on the exposed thoracic dura of cats for different durations including: 18-58 g for up to 20 min [437,438], 200g/5min, 600g/15min [439], 170g/5min [440,441]. Similar tests have been done in ferrets [442], dogs (6-60 g for 30-60 min) [443], monkeys (50g for 2 hours) [360] and rats (20/35/50 g for 1/5/10 min) [444].

The epidural balloon catheter, first used in the dog by Tarlov [292,445], has the advantage of not exposing the spinal cord at the injury level. A balloon-tipped catheter is introduced via a laminectomy at an adjacent vertebral level, and advanced to the injury level in the dorsal epidural space. The balloon is then inflated to a specified pressure and is assumed to result in a specified spinal cord compression; however, few authors have verified this and it is a potential source of variation in the method. One study modified this approach by using an inflatable cuff that was placed around the circumference of the cord after a laminectomy at the injury level [216]. Some authors report a "rapid" inflation and immediate (within 30 sec) deflation of the balloon [446,447], while others use it to compress the cord for periods greater than one minute and up to several weeks [447-450]. Regardless, the balloon catheter is not considered a "dynamic" device, compared to the other contusion models where the impact has a duration of 5 to 20 ms. The balloon catheter method has been used in the dog [365,447,451-454], cat [446,455], monkey [448-450,456-459] and lamb [370,371].

1.6.3.5 Comparison of the injury strategies

Each injury model has strengths and limitations which makes it suited to studying particular aspects of the biomechanics of the injury. Large animal models present some unique challenges in device design. The requirements for sterility are more stringent than for rodents, particularly for chronic protocols or those that require long periods of anaesthesia. This can influence the type of device selected and aspects of its design such as materials and transducer selection.

For studying the physical behaviour of the spinal cord-dura-CSF during the injury, the weight-drop method is probably the most representative of the typical non-penetrating human injury. No control or limit is placed on the peak displacement or load so that the dura, CSF and spinal cord are compressed until the applied energy is absorbed by the tissues, in much the same way that it can be imagined a bone fragment comes to rest in the spinal canal. Open contusion injuries are intended to replicate the anterior-posterior compression seen in the burst fracture and fracture-dislocation mechanisms of injury. However, the contusion is applied to the dorsal surface while the ventral surface is more likely contacted in a human burst fracture SCI. Closed column dislocation and distraction models could conceivably better replicate the bone-cord interaction, but in practice they lack repeatability, do not directly measure spinal cord loading and deformation, and for large animals the externally applied forces must be very large to disrupt the spinal column. They can also produce an unstable column, which may cause complications in a chronic protocol.

Models that measure load and displacement have the advantage that animals can be eliminated from the study if the biomechanical parameters of their injury lie outside pre-defined acceptable corridors [268,271]. Stabilisation of the spinal column has been identified as a challenge to all open models and is

probably more challenging to address for large animals due to their higher weight and greater respiratory motion.

A summary of advantages and disadvantages of the SCI models is presented in Table 1-12.

Table 1-12 Summary of types of experimental SCI models, the animals used, and the advantages and disadvantages of each.

Injury Model	Animals	Advantages	Disadvantages
Contusion			
Weight-drop (open)	Dog, Cat, NHP, Rabbit, Rat, Mouse, Sheep, Pig	• Similar to real injury • Unrestricted velocity	• Dorsal injury • Laminectomy required • Uncontrolled unloading (bounce of weight) • Force, velocity, displacement not usually measured
EM or pneumatic actuator (displacement control)	Rat, Ferret, Piglet	• Controlled unloading • Measure force and displacement	• Dorsal injury • Laminectomy required • Relatively low velocity • Establish zero position
EM actuator (force control)	Rat	• Controlled unloading • Measure force and displacement	• Dorsal • Laminectomy required • Relatively low velocity
Distraction			
Directly coupled to spinal cord or dura	Dog, Cat	• Real injury mechanism • May replicate canal-cord contact	• Difficult to prevent grip slippage
Via bony anatomy	NHP, Cat, Pig, Rat	• Real injury mechanism • May replicate canal-cord contact	• Lacks repeatability • More complex machine
Dislocation/Fracture (closed)			
Vertebral weight drop	Dog, Cat	• Potentially more biofidelic • Canal intact at injury site • Reduced pre-injury surgery	• Very large weight/height required • Lacks repeatability • Force, deformation of spinal cord not measured
Controlled vertebral displacement	Dog, Rat	• Potentially more biofidelic • Canal intact at injury site	• More complex machine required • Vertebral clamping is critical • Unstable spine post-injury
Quasi-static compression			
Clip compression	Rat, Guinea pig	• Simple equipment • Dorsal-ventral	• Rate of application uncontrolled • Uninstrumented for force, compression rate • Force calibration may change over time
Resting weight	Dog, Cat, NHP	• Simple	• Rate of application uncontrolled • Uninstrumented for force compression rate
Spacer/bead/ligature	Dog, Cat, NHP, Sheep	• Canal intact at injury site	• Rate of application uncontrolled • Deformation not measured
Epidural balloon	Dog, Rat	• Canal intact at injury site	• Rate of application uncontrolled • Deformation not measured, full expansion assumed

1.6.4 Selection of mechanical input parameters

A SCI model that seeks to ellicit a biofidelic mechanical response and obtain a human-like SCI must faithfully simulate the mechanical inputs to the injury event. These mechanical inputs may include load magnitude and rate, displacement and velocity. Closed models seek to simulate the impact between the impacting object and the external anatomy. This loading regime can be estimated from accident reconstruction methods. Open models seek to simulate the impact between two or more parts of the internal anatomy, for example a bone fragment contacting the spinal cord during a burst fracture. The appropriate mechanical inputs for this scenario are more difficult to estimate.

Depending on the selected method of load application (see Section 1.6.3), an experimental contusion SCI could be specified with mechanical parameters such as impact velocity, maximum displacement or load, rate of application of the displacement or load, or applied energy. To model a burst fracture injury mechanism, the ideal open weight-drop model would use an object with the same mass and cross-sectional area as a typical bone fragment, and an impact velocity matching that with which the bone fragment is retropulsed into the spinal canal. However, determining these parameters is not trivial.

Two *in vitro* biomechanical studies have measured the rate of canal occlusion while inducing burst fractures by applying a dynamic axial load to thoracolumbar spinal segments with the spinal cords removed. Panjabi et al. [132] produced 13 burst fractures in 9 human specimens with an incremental trauma method, and provided example occlusion-time data for T12 and L1 for one specimen (Figure 1-25). From this data, it is seen that after an initial 1 mm of relatively low-rate occlusion, the velocity was approximately linear until the peak occlusion, and this occurred over 2.25-2.5 ms. The occlusion velocities for this specimen were determined to be 2.4 and 1.6 m/s for T12 and L1 respectively.
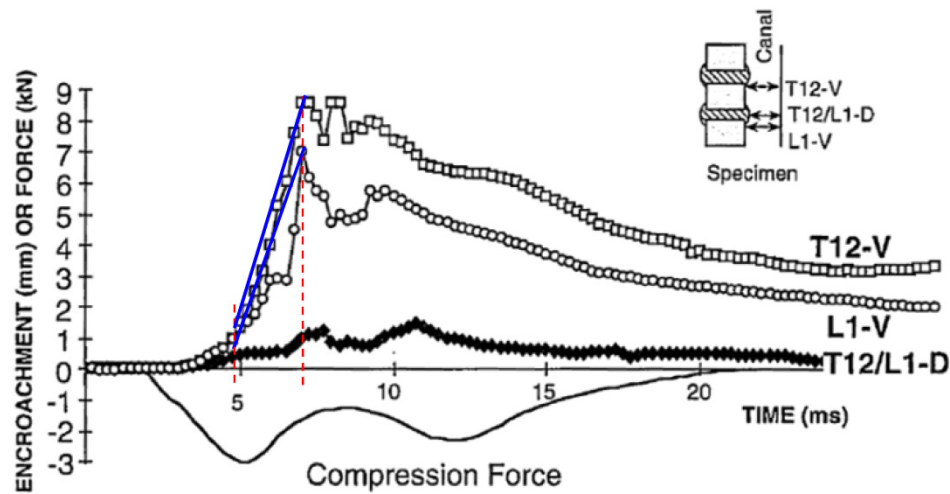
Figure 1-25 Canal occlusion (mm) and compression force (kN) during an experimental burst fracture in the thoracolumbar spine. Example data of canal occlusion versus time at the T12 and L1 vertebral levels for specimen SP7. The red dashed lines indicate the start and end points used for calculation of the velocity. The velocities of the occlusions were approximated by the slope of the blue lines. Adapted from Journal of Spinal Disorders, 8(1), Panjabi et al., Dynamic canal encroachment during thoracolumbar burst fractures, 39-48, 1995, with permission from Lippincott Williams and Wilkins [132].

The authors provided the maximum occlusion for all the other burst fractures in the series, and the mean velocities were derived for these, between 0.75 mm and peak occlusion and assuming a duration of 2.25 ms, as per Table 1-13 below. The mean occlusion velocity was 2.1±0.8 m/s.

Table 1-13 Canal occlusion velocities for burst fractures at T12 and L1. Derived from data of Panjabi et al., 1995 [132].

Level T12			Level L1		
Specimen #	Occlusion (mm)	Velocity (m/s)	Specimen #	Occlusion (mm)	Velocity (m/s)
SP1	5.1	1.9	SP3	5.4	2.1
SP2	3.4	1.2	SP4	5.3	2.0
SP3	7.4	3.0	SP5	5.7	2.2
SP7	8.6	3.5	SP6	4.7	1.8
SP8	4.6	1.7	SP7	7.0	2.8
SP9	2.6	0.8			

By applying high velocity axial loads in a drop-tower apparatus, Wilcox and colleagues [134,460] produced burst fractures in three-level thoracolumbar bovine specimens (spinal cord and dura removed) and visualised the transient canal occlusion with an arrangement of high speed cameras and mirrors. Although bone fragment velocities are not reported directly, they can be estimated from the representative data presented graphically as percent canal occlusion versus time (e.g. Figure 1-26, left). This, in

combination with scaled photographs of representative specimens from which the estimated anterior-posterior canal dimension ranged from 11 to 15.7 mm (Figure 1-26, right), results in bone fragment velocity estimates of 0.95 – 3.52 m/s. Finite element simulations [133,461] and *in vitro* simulations [462] derived from this work have used bone fragment velocities ranging 1 – 10 m/s and 2.5 – 7.5 m/s, respectively.
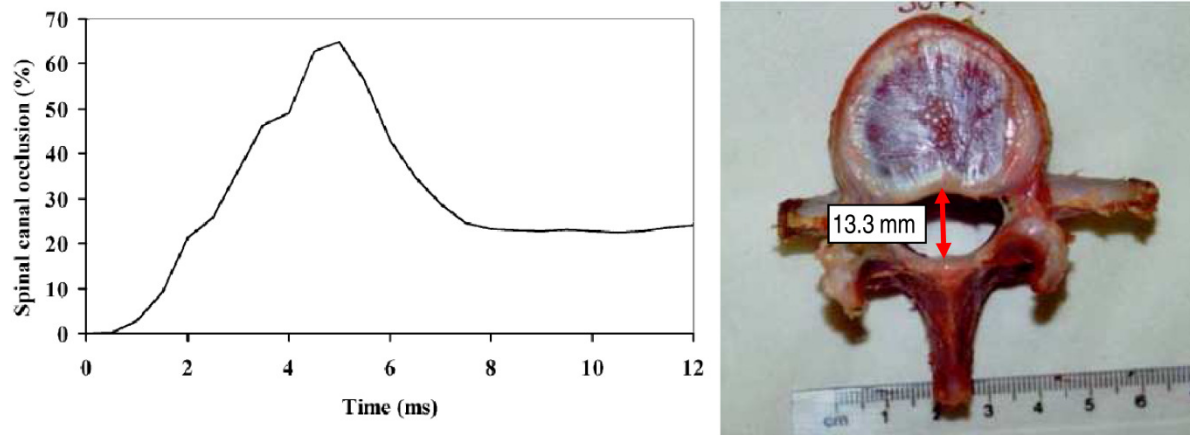
Figure 1-26 Percent spinal canal occlusion versus time for a representative *in vitro* experimental burst fracture (left)[134][134][134][134][134]; Photograph of representative bovine vertebra for estimating anterior-posterior canal diameter (right). (left) Reproduced from Journal of Biomechanics, 35(3), Wilcox et al., Measurement of canal occlusion during the thoracolumbar burst fracture process, 381-84, 2002, with permission from Elsevier [134]. (right) Adapted with permission from Wilcox, A biomechanical investigation of the burst fracture process, 2002, PhD Thesis, University of Leeds, ©Ruth Wilcox [460].

Ivancic et al. [463] simulated bilateral facet dislocation in cervical functional spinal units using an impact sled and measured the dynamic canal diameter. The mean peak canal narrowing velocity was 0.23 ± 0.06 m/s for 10 specimens, which is substantially lower than the values obtained in the burst fracture studies.

The mass and cross-sectional area of bone fragments arising from the aforementioned *in vitro* burst fracture investigations were not reported in these biomechanical studies. However, subsequent work from Wilcox and colleagues [462] reports a design criterion for synthetic bone fragments in the range of 5.8 ± 1.7 g based on fragments collected from the bovine specimens aged 14-21 days [460]. These vertebral bodies had a lateral width and anterior-posterior depth (e.g. Figure 1-26, right) comparable to human thoracolumbar vertebrae (35-50 mm and 30-35 mm, respectively [464]). As shown below, this is lower than the impactor weights used for large animal weight-drop models. In comparison, the wet weight of human thoracolumbar vertebrae ranges from 250-550 g [465].

To the author's knowledge, none of the previously used large animal models of SCI have utilised mechanical parameters derived from an analysis of human injury. In fact there is little justification given for the various combinations of height (velocity) and mass that have been used in the various weight drop apparatus. Graded models typically utilised empirically determined parameters to produce the desired injury severities based on survivability, short- or long-term functional recovery and lesion distribution and shape. These are arguably satisfactory metrics for the study of injury physiology, but probably not ideal for biomechanical studies. Figure 1-27 illustrates the drop heights and weights that have been used in previous large animal models, and the corridor for human burst fracture parameters as indicated above (dotted black rectangle). This shows that the majority of large animal models have used higher masses and lower velocities than have been measured for burst fracture type mechanisms in *in vitro* spine specimens.
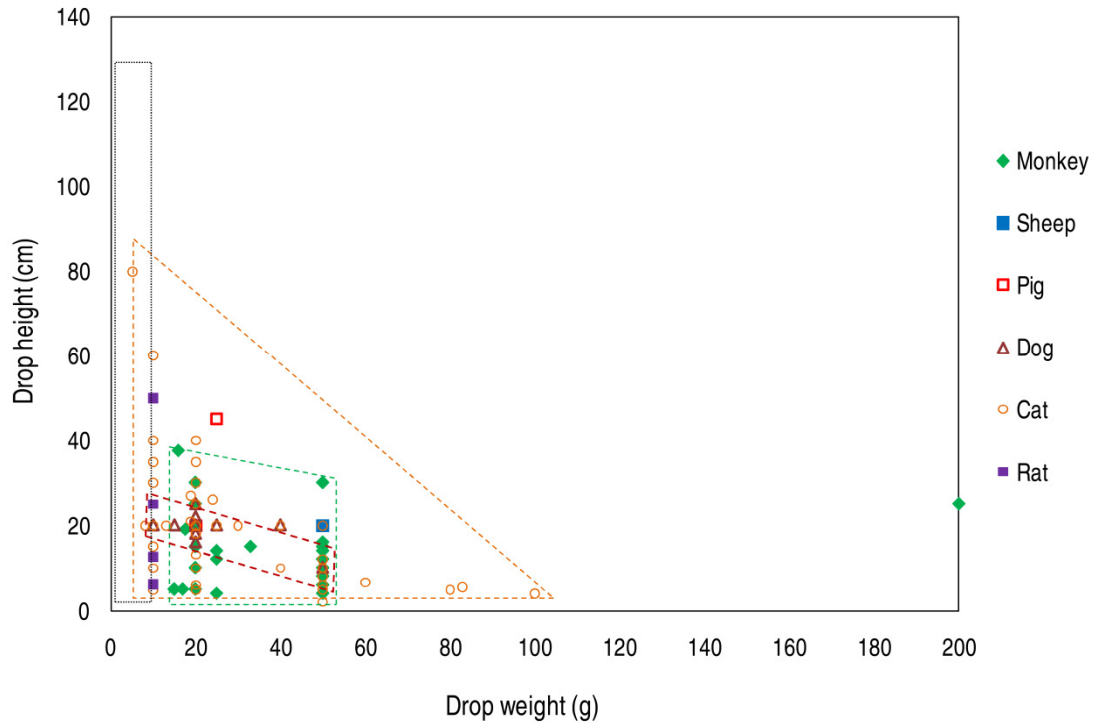
Figure 1-27 Injury parameters reported to induce transient or permanent paresis in various large animal weight-drop models. The data was collated from all available large animal studies that used an open weight-drop model and reported separate drop weight and height information, from 1968 to present. The weight-height combinations used in the studies presented in Chapter 2 and 3 are also shown (filled red markers). Dashed areas indicate nominal "injury corridors" for cat (orange), dog (dark red) and monkey (green) models. Dotted black rectangle indicates the range of heights that would theoretically produce occlusion velocities measured for burst fracture and dislocation events observed in the biomechanical experiments described in the text above.

1.6.5   Synthetic models of SCI

Several synthetic models have been devised to study the mechanics of blunt spinal cord trauma. Some have included separate elements for spinal cord, CSF and dura, with varying effort to accurately replicate the mechanical and structural properties of the synthetic "tissues". Synthetic spinal cords are advantageous due to the rapid changes in mechanical properties of the natural spinal cord after death [227]. Synthetic spinal cords have been fabricated from Tygon tubing [466,467], gelatine [468,469], silicone elastomer [280,470], and silicone gel with Dacron fibres [471,472]. Dura does not degrade rapidly if adequately hydrated and may be stored frozen, however few studies have incorporated natural dura or a surrogate material. One study fitted excised bovine dura over synthetic cords [280], and one study used a vinyl rubber glove material [281] to simulate dura in a bench-top model.

Hall and colleagues [280,281,462] simulated burst fracture spinal cord impingement by projecting a simulated bone fragment at bovine and/or synthetic spinal cords suspended in a materials testing machine and recorded the resultant deformation. These models showed that decreased bone fragment velocity, presence of and increased tension in the posterior longitudinal ligament (PLL) [462], presence of CSF [280,281] and increased bone fragment cross-sectional area [281] reduced the peak deformation of the spinal cord, but dura alone did not [280,462]. However, in these studies the cord was not directly visualised, and an assumption of full collapse of the subarachnoid space was made in order to derive maximum spinal cord compression.

Hall et al. [462] reported peak pressures in the spinal cord of around 300-560, 600-2250 and 1425-2700 mmHg at the injury site, with impact velocities of 2.5, 5 and 7 m/s, respectively, with different PLL tensions and posterior element configurations. In a similar model that used a weight-drop rather than projectile impact, Pintar [468] and Yoganandon [469] placed a synthetic spinal cord instrumented with squares of pressure sensitive film into cadaveric cervical spines with a C4 laminectomy, and subjected them to weight-drops of 100 to 600 g-cm. Peak pressures ranged approximately 1425-3075 mmHg at the impact site, and 225-450 mmHg at the adjacent spinal level.

Some studies have simulated loads to the spinal column to induce fracture and measured the response of the spinal cord to canal contact. The aforementioned instrumented synthetic cord was placed in two cadaveric cervical spines, with heads, that were subjected to axial loading at 3.1 and 6.1 m/s [469]. The first recorded a peak pressure of 1507 and 188 mmHg corresponding to a C5 burst fracture and C4 wedge fracture, respectively. The second recorded peaks of 83 and 675 mmHg, adjacent to a mild C5 compression fracture and a C3 compression fracture, respectively.

Xie et al. [473] removed the spinal cord of eight thoracolumbar cadaver specimens, placed a pressure transducer against the posterior canal wall at L1 and filled the dura with water, sealing the intervertebral foramen. The specimens were potted to leave L2-4 free, and subjected to a 5.4 m/s axial impact by weight-drop. They observed positive pressure waves of 217-2415 mmHg associated with burst fractures. When no burst fracture occurred, there were both positive and negative pressure waves, with a range of 488-607 mmHg, which they attributed to intervertebral disc deformation.

Chang [466] and Tran [467] utilised an occlusion transducer that measured changes in pressure in a fluid filled tube placed in the canal of spines subjected to axial loading. They do not report pressures except for one example trace which shows a clipped signal at 250 mmHg during a C3 compression fracture.

Bilston et al. [472] subjected a physical head-spine model to rapid hyperflexion/extension and measured strains in a surrogate spinal cord with an internal ink grid. In flexion, strains were highest in

the cranial cord, at 20-35%, with strain rates 7-19 s^{-1}. In extension the cord tended to shorten locally, tensile strains were not above 12%, and strain rates ranged 1-12 s^{-1}. The same model was used in simulations of head-first impact, where flexion-compression loading caused C2 dislocation and extension-compression loading caused C4/5 dislocation [474]. Adjacent to the injury location, cord strains were up to 40%, and strain rates were up to 6.5 s^{-1}.

Only some of these studies report considering the application of an appropriate spinal cord and/or dura pre-strain. These are likely to contribute substantially to the mechanical response of the model during the impact.

1.6.6   Summary

The complex mechanical and physiologic aspects of SCI necessitate the use of animal, synthetic and computational models that attempt to replicate various aspects of the injury event. Contemporary large animal models of SCI are sparse, despite offering unique features of human-like scale and physiologic similarity, both of which are advantageous for pre-clinical and biomechanical studies.

A variety of contusion, dislocation, distraction and static compression models of SCI have been used over the last five decades. Devices that provide a controlled displacement or load profile are useful for producing consistently graded injuries and studying the independent effects of mechanical variables. However, the weight-drop method produces a time-varying rate of compression, and has the potential to best mimic the biomechanics of a contusion SCI such as that resulting from a burst fracture or fracture-dislocation. When applied to an animal with a spinal cord of similar dimensions to humans, appropriate injury parameters (impact velocity and mass) may be estimated from *in vitro* biomechanical tests which have induced common spinal fracture types and measured the velocity and mass of the bone fragments and/or canal occlusion produced. *In vivo* large animal models currently provide the most biofidelic simulation of the human spinal cord/dura/CSF response to mechanical insult.

Several synthetic and cadaver models have also been used to study the effect of various anatomical features, such as the dura, PLL, canal width and spinal degeneration, on spinal cord deformation and pressure. The advantages of such models include control of physical dimensions and ease of test repetition and elimination of physiologic effects; disadvantages include the simplification of the anatomical structure and material properties of the system. These studies have shown to some extent that tissue and fluid pressure pulses occur during impacts that simulate SCI. However, few have incorporated dura and CSF into the model.

1.7   Measuring CSF pressure in the brain and spine

The salient characteristics of normal CSF pressure were introduced in Section 1.3.3, and pressure transients in the CSF and parenchyma during experimental CNS trauma were discussed in Sections 1.5.4.2 and 1.5.4.4. This section reviews and critiques the measurement locations and transducer types that are, or have been, used for quasi-static measurement in clinical settings and for dynamic measurements during experimental CNS trauma.

1.7.1   Quasi-static clinical and experimental pressure measurement

CSF pressure is routinely measured in the brain and to a lesser extent in the lumbar spine. It is used for the clinical diagnosis and monitoring of pathologies such as hydrocephalus and traumatic brain injury. Spinal CSF pressure is measured in the lumbar cisterna where the existence of the cauda equina provides an ideal location to advance a needle and catheter into the subarachnoid space with minimal risk of neural damage. Cranial CSF pressure, or intracranial pressure (ICP), is measured in the ventricles or parenchyma and less commonly in the subarachnoid and epidural spaces. Although early experimental studies used water or mercury manometers, clinical and experimental transducers are now largely based on strain gauge and fibre optic technology.

The gold standard for ICP and lumbar CSFP monitoring is an intraventricular or lumbar catheter and rigid-walled tubing connected to an external pressure sensor, usually with a semiconductor strain gauge transducer [54,475]. The catheter may also function as a drain to remove fluid. The external transducer must be levelled to a standard anatomical reference position, most commonly the midpoint of the right atrium [80]; it is periodically exposed to atmosphere, via a stopcock, for zeroing.

Both fluid and parenchymal measurements are performed with indwelling "microtip" transducers. Those currently available are based on semiconductor strain gauges (e.g. Codman, Johnson and Johnson, Raynham, MA; Neurovent-P, Raumedic AG, Munchberg, Germany) and fibre-optic cavities (e.g. Camino, Integra Neuroscience, Plainsboro, NJ). The primary concerns with indwelling transducers are zero drift and temperature sensitivity, because they cannot be zeroed *in situ*. Drift has been evaluated for a number of clinical ICP transducers using bench testing [476-480] and in clinical practice [481-483], although the latter is challenging given that minor atmospheric changes are significant in physiologic pressure terms.

Clinical transducers are typically unsuitable for dynamic measurements because they have a low frequency response. Further, the diameters of the catheters or indwelling transducers used for clinical applications are around 1 to 3 mm, which is relatively large compared to the spinal CSF thickness. These limitations are addressed by some of the transducers introduced below.

1.7.2   Dynamic experimental CNS injury pressure measurement

Transient CSF pressure has been measured in the spine in only three studies (see Section 1.5.4.2). This discussion is therefore broadened to include transducers used for cranial CSF and parenchymal pressure measurements, some of which were introduced in Section 1.5.4.4. Most researchers have recognised the importance of using transducers with a sufficiently high frequency response. These transducers can be grouped into three categories: piezoelectric, piezoresistive and fibre optic.

Piezoelectric transducers utilise a piezoelectric crystal which responds to mechanical strain by generating a voltage. They have inherently high natural frequency and exhibit linearity over a wide range, but can only be used to measure dynamic events. They typically have a relatively large metal casing, which means they need to be surface-mounted to a rigid interface, such as the skull. Due to this casing they are considered a robust device. Early studies of the pressure transmitted to the brain from explosive detonation used piezoelectric transducers mounted in the orbits of deceased rabbits [484] and monkeys [485]. Others have mounted similar types of transducers through trephined holes in the skull of cats undergoing fluid percussion TBI [313] and swine adjacent to firearm noise [342]. These authors report puncturing the dura but not sealing it around the transducer. The spinal CSF pressures measured in the closed weight drop dog model described earlier were made with a piezoelectric transducer coupled to a fluid-filled catheter [3].

Piezoresistive transducers consist of semiconductor or metal strain gauges bonded to a flexible membrane. The strain gauge changes resistance in proportion to the deformation of the membrane which is caused by the incident fluid pressure. These transducers have a reasonably high frequency response and can be used for both static and dynamic measurements. Piezoresistive transducers have been skull mounted in post mortem human subjects (PMHS) during frontal head impact experiments [486] and in swine subjected to whiplash motions [288,487]. Miniaturised piezoresistive transducers have been mounted at the end of flexible catheters to allow implantation into the brain parenchyma of swine [319,488] to measure the response to fluid percussion and blast TBI, and into the spinal subarachnoid space of PMHS [289] and swine [287] in whiplash simulations. The piezotransistor or "Pitran" transducer was coupled to a fluid-filled catheter to measure the spinal CSF pressures adjacent to a weight drop SCI in cats [1,2].

All three of the studies that have measured spinal CSF pressure during experimental SCI used transducers that were coupled to the subarachnoid space via some length of fluid-filled catheter and tubing [1-3]. This method is not ideal because, depending on the length of the tubing, it can lead to considerable damping of the signal magnitude and stretching of the signal duration. This effect was explored by Wennerstrand et al. [3] using a bench-top model in which the signal from a reference

transducer placed in direct contact with the fluid was compared with the fluid-filled catheter transducer placed the same distance from the impact (Figure 1-28).
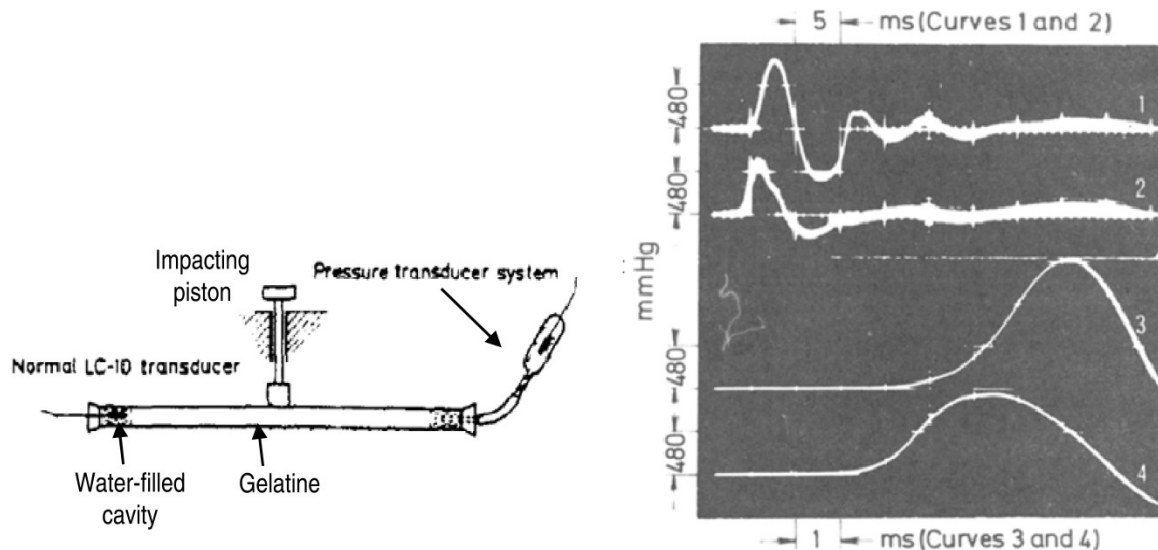
Figure 1-28 Comparing a fluid-filled catheter transducer and indwelling transducer: apparatus schematic and results. (left) Schematic of a physical model used to test a fluid-filled catheter pressure transducer (as used in animal experiments) against a reference transducer in direct contact with the fluid. (right) Simultaneous responses of the two pressure transducer systems. Curve 1: fluid-filled catheter system, Curve 2: reference transducer, Curve 3: magnification of curve 1, Curve 4: magnification of curve 2. Adapted and reproduced from Journal of Biomechanics, 11(6-7), Wennerstrand et al., Mechanical and histological effects of transverse impact on the canine spinal cord, 315-31, 1978, with permission from Elsevier [3].

Fibre optic transducers are a contemporary technology that utilise the Fabry-Perot optical interferometry principle. The sensor tip contains a very small optical cavity between two partially reflective parallel surfaces. The outer surface is a diaphragm that deflects under pressure, thus causing a change in the optical cavity depth, and a subsequent change in the cavity reflectance. When a light signal is transmitted down the fibre to the sensor, the intensity of the reflected light is proportional to the pressure acting on the diaphragm. These transducers have the advantage of being extremely small and flexible, which is advantageous for implanting in small fluid spaces to enable direct and highly localised contact with the fluid or tissue. They do not need to be mounted rigidly to bone; rather they can be attached to soft tissues using adhesive or suture. Their low mass and flexibility reduces the extent to which they alter the mechanics of the system. However, they are delicate and therefore prone to breakage, and can be cost prohibitive. Miniature fibre optic transducers have been used in a rat to measure ventricular CSF pressure response to blast overpressure [337], and in rabbit brain parenchyma to measure response to fluid percussion, controlled cortical impact and weight-drop experimental TBI [314].

Pressure changes in the brain parenchyma of rabbits due to rotational acceleration impulses have also been measured with fibre optic transducers [290].

The characteristics of the transducers that have been used for dynamic measurements of pressure associated with CNS trauma are detailed in Table 1-14.

Table 1-14 Comparison of pressure transducers used to characterise dynamic experimental CNS injuries, grouped by type. Note that where specifications were not stated in the paper, attempts were made to find details from the manufacturer.

Author	Location [animal]	Model / Manufacturer	Size (mm)	Range / Linearity (mmHg relative)	Frequency characteristics
Piezotransistor					
Albin 1975 [2] Hung 1975 [1]	Thoracic spine CSF, via fluid filled catheter [cat]	Pitran P-10 / Stow Laboratories	NR	NR / 0.5%	Natural frequency 150 kHz
Piezoelectric					
Clemedson 1956 [484] Romba 1961 [485]	Cranial CSF, orbit mounted [rabbit, monkey]	BC-10 / Atlantic Research	NR	0 – 15515 / to 517150 / ±1% acc.	Frequency range 3 Hz-75 kHz
Wennerstrand 1978 [3]	Thoracic spine CSF, via fluid-filled catheter [dog]	LC-10 / Celescon Industries Inc.	NR	75 – 75000 / NR	Frequency range 0.2 Hz-100 kHz
Rinder 1968 [489] Stalhammar 1987 [313]	Brain, flush with dura through trephined hole [rabbit, cat]	Type 6-01 / Vibrometer	NR	NR	Natural frequency 150 kHz; dynamic rise time <0.1ms
Saljo 2008 [342]	Brain parenchyma, skull mounted, dura punctured [swine]	Model 8103 (hydrophone) / Bruel & Kjaer	9.5 mm dia.	NR	Frequency range 0.1 Hz-20 kHz
Piezoresistive (semiconductor or metal foil strain gauge)					
Sullivan 1976 [315]	Brain, flush with dura through trephined hole [cat]	PA 85-100 / Statham Laboratories	NR	NR	Natural frequency 10 kHz
Nahum 1977 [486] Ortengren 1996 [487] Svensson 1993 [288]	Surface flush with internal skull, opened dura at PT site [PMHS, swine]	8510-100 / Endevco	5 mm dia.; (3.8 mm) face diameter	-750 – 5250 / NR	Natural frequency 180 kHz Frequency range 0-10 kHz
Suneson 1990b [490]	Brain parenchyma, skull mounted, dura punctured [swine]	8514-100 / Endevco mounted in thin polyethylene catheter	NR	0 – 5171 / NR	NR
Walter 1999 [319]	Brain parenchyma [swine]	MikroTip / Millar	1.5 mm dia.	± 300 / NR	100 kHz freq. response (-3dB)

Author	Location [animal]	Model / Manufacturer	Size (mm)	Range / Linearity (mmHg relative)	Frequency characteristics
Eichberger 2000 [289] Boström 1996 [287]	Cranial and cervical spine subarachnoid space [PMHS] Cervical spine, subarachnoid space [swine]	Catheter tip / NR	NR	NR	NR
Fibre optic (Fabry-Perot optical interferometry)					
Chavko 2007 [337]	Ventricle via skull trephine hole [rat]	FOP-MIV / Fiso Technologies	Dia. 0.55 mm sensor, 0.25 mm fibre w/ 0.9 mm coating	0 – 400 / NR	Sampling rate 100 kHz
Bauman 2009 [338]	Brain parenchyma and ventricle [swine]	FOP-MIV / Fiso Technologies	NR	NR	NR
Clausen 2005 [314]	Ventricle via skull trephine hole [rat]	NR / Samba	0.34 mm dia.	684 – 3800 / NR	Sampling rate 500 Hz
Krave 2005 [290]	Brain parenchyma [rabbit]	Samba 3000 / Samba Sensors AB	0.42 mm sensor, radiopaque coated fibre 0.45 mm dia. Enclose fibre in 0.9mm OD PTFE tube	-535 – 3740 / NR	Sampling rate 15 kHz

*PMHS = post mortem human subject

NR=not reported

1.7.3   Summary

Cranial and spinal CSF pressure measurement is practiced clinically as a diagnostic, prognostic and monitoring tool. Quasi-static measurements are usually done with fluid-filled catheters connected to external piezoresistive pressure transducers, or miniature indwelling piezoresistive or fibre-optic devices. A primary concern for long-term CSF pressure measurements is transducer zero drift, and for external transducers strict attention must be paid to the zeroing protocol to achieve accurate physiologic values.

The response of CSF pressure to an experimental external impulse has been measured in a limited number of studies. In the past, the accuracy of pressure transients measured in the thin spinal CSF layer was limited by the pressure transducers available; the fluid-filled catheters used were likely to dampen and lengthen the dynamic fluid impulse signal. Contemporary miniature transducers offer the potential for indwelling measurements in large animals during injury. Miniature and flexible transducers can be implanted through soft tissues and into thin fluid-filled spaces, with minimal alteration of the biomechanics of the system.

1.8   Research objectives and rationale

The general objective of this research is to develop an understanding of how the CSF influences the extent of damage induced during the instant of a SCI, and how it responds to both the initial mechanical insult and the physiological processes that occur in the hours after such an injury. The results of these studies will improve understanding of the biomechanics of SCI, and provide data which will enable SCI researchers to better understand the limitations of current models and to develop more biofidelic physical, animal and computational models. Furthermore, it will provide an insight into several aspects of the injury sequelae that cannot be studied in the clinical population and that may have implications for the clinical and surgical management of SCI patients. The objectives will be addressed in three phases comprising a total of five studies.

Phase 1: Characterising CSF pressure transients during the spinal cord injury event

Objectives of Study 1: Develop a large animal model, and associated instrumentation, of SCI capable of delivering an injury with human-like mechanical parameters to a system of human-like scale. Specify a CSF pressure measurement and data acquisition system useful for both high-speed injury measurements, and measurements over extended periods.

Rationale: Biomechanical phenomena – and arguably biological phenomena as well – are best studied in models that are similar in scale to their human counterpart. The need for a contemporary large animal

model of SCI to be used in pre-clinical testing is generally agreed upon in the SCI research community. Previous large animal injury devices have not been able to measure load or displacement. Only two groups have measured CSF pressure transients during SCI, and the data reported were limited. In Chapter 2, the first version of a new injury model is presented along with preliminary pressure results.

Objectives of Study 2: Characterise the transient CSF pressure distribution associated with injuries created with human-like mechanical injury parameters, and compare these to previously reported pressure tolerances of neural tissue.

Rationale: There is experimental and clinical evidence that central nervous system tissue is susceptible to damage by fluid pressure impulses. At present, no studies have measured the transient CSF pressures created during a human-like SCI event. The pressure transients associated with two injury severities created with human-like mechanical parameters, and a comparison to known pressure tolerances of neural tissue, are described in Chapter 3. This chapter also presents the final version of the injury model.

Phase 2: Exploring the effect of CSF thickness and impact velocity on CSF pressure transients during the injury event

Objectives of Study 3: Design and construct a synthetic model which is anatomically and mechanically similar to the spinal cord – CSF – dura system, and investigate the influence of CSF thickness and impact velocity on transient pressure distribution, cord compression, and load transmission.

Rationale: While *in vivo* animal models are an invaluable model of the human condition, they offer limited opportunity to finely control independent variables and thereby study their effect on the dependent variables. By employing a synthetic model, the thickness of the CSF and the impact velocity could be adjusted, and the effect of these adjustments on the pressure transients, cord compression and load transmission could be measured. The results of this bench-top model are presented in Chapter 4.

Phase 3: Post-injury CSFP differentials before and after decompression, and the effect of decompression on spinal cord and thecal sac dimensions

Objective of Study 4: Profile the CSF pressure distribution in the 14 hours after injury, under conditions of sustained compression (eight hours) and decompression (six hours).

Rationale: The immediate post-injury phase is recognised as a critical phase in instituting neuroprotective strategies, yet little is known about the physical response of the cord and CSF in this time period. CSF drainage has been proposed as a clinical management strategy to increase spinal cord perfusion. This treatment would involve draining CSF from the lumbar region when some lumbar CSF pressure threshold is exceeded. However, pressure differentials may exist across the injury site if there is residual cord compression and subarachnoid occlusion. It is not possible to study these effects in the patient population

because (1) introducing catheters cranial to the injury creates risk of higher injury, and ventricular shunting is not indicated unless there is concomitant brain injury, and (2) the time lapse between injury, hospitalisation and stabilisation precludes study in the hyperacute phase. Chapter 5 presents the profile of the CSF pressure cranial and caudal to an experimental SCI in a large animal over eight hours of residual compression followed by six hours of decompression.

Objective of Study 5: Profile the patency of the subarachnoid space (with respect to spinal cord deformation and swelling) in the hours after decompression.

Rationale: Early decompression is currently a treatment option for SCI patients with residual canal stenosis and spinal cord compression. However, little is known about the immediate effects of decompression on the spinal cord morphology or the patency of the subarachnoid space. In many patients, post-surgical magnetic resonance images show that the spinal cord has swollen and the thecal sac appears to be occluded within 24 to 48 hours after decompression. It is not possible carry out serial imaging studies on patients during this time period due to their significant care requirements. Spinal cord and dura morphology was evaluated, using ultrasound imaging, at the injury site for six hours after decompression of an experimental SCI in a large animal. This study is presented in Chapter 6.

Chapter 2   A Large Animal Model of SCI to Measure CSF Pressure[1]

2.1 Introduction

Spinal cord injury (SCI) often results in considerable permanent neurological impairment. The handful of promising experimental treatments that have been tested in human clinical trials have failed to demonstrate convincing efficacy, prompting numerous researchers to identify areas where the process of translation from pre-clinical animal models to clinical application could be improved [491-494]. One issue of concern is the potentially important distinctions between the human spinal cord and the rodent or mouse spinal cord with which the vast majority of SCI research is conducted. Not only may there exist unique anatomic and physiologic characteristics, but the sheer size and scale differences between rodent and human may be important. By providing a more human-like anatomic scale and physiology, a large animal model may help to bridge the gap between basic science and clinical practice [374].

One potentially important shortfall of the rat and mouse species that are currently in prominent use is the lack of a cerebrospinal fluid (CSF) filled intrathecal space commensurate in size to its spinal cord [495], as well as the small size of the central nervous system (CNS) as a whole [395]. The CSF is commonly thought to protect the spinal cord during activities of daily living. However, several researchers have posited that tissue injury may occur remote from the site of mechanical insult as the result of a pressure or stress wave transmitted in the CSF and spinal cord tissue during SCI [1,3,162]. A pressure transient mediated injury mechanism could help to explain observations such as post-traumatic ascending myelopathies that can occur via an unknown etiology [170,173,174] and diffuse axonal injury remote to the primary mechanical insult observed in SCI patients [163] and in the spinal cord of infants with shaken baby syndrome [156,157]. Determining if the CSF has the potential to transmit injurious loads away from the primary injury site, and if so, under what conditions this can occur, could improve the selection of SCI models, increase understanding of primary and secondary cellular response, and allow interventions to be tested in a more clinically applicable experimental setting.

The established rodent models of SCI are inappropriate for the study of CSF pressures associated with injury because the intrathecal space is extremely small and therefore transducers can only be placed in the cisterna magna and lumbar cistern [104,105,496]. Further, even transducers less than 1 mm in diameter would constitute a large fraction of the rodent CSF system total volume and are therefore likely to lead to changes to the mechanical behaviour of the cord, dura and fluid during impact. In most cases

---

[1] A version of Chapter 2 has been submitted for publication. Jones CF, Lee JHT, Kwon BK and Cripton PA. Development of a large animal model to measure dynamic cerebrospinal fluid pressure during spinal cord injury.

the medium-to-large species that were previously used for weight-drop SCI models, such as cats [e.g. 277,366,367,369], dogs [e.g. 362,363,364], sheep [e.g. 218,370], and small non-human primates [e.g. 294,295,358,359], had spinal cord dimensions considerably smaller than humans. Contemporary models using these species are largely limited to hemisection [e.g. 497,498] rather than contusion injuries, but contusion injuries are more clinically relevant as they represent the majority of human non-penetrating injuries [355].

Pigs have been used extensively for the study of TBI and have a number of characteristics that make them useful for studying SCI, including a more human-like diameter of both the cord and intrathecal space [376]. Pigs have also been frequently used for models of SCI induced by ischaemia [377-379,381]. There are several reports of contusion [382,383] and clip compression [384,389] SCI models in pigs, although most do not provide a biomechanical analysis of the impact (i.e. impactor shape, energy, velocity, force). The pig has spinal cord [384,398] and CSF dimensions that are similar to an adult human [391-394] and is therefore suitable for characterisation of various aspects of the biomechanics of SCI, and in particular of the role of CSF during and immediately after the injury.

Despite both historical and contemporary recognition of the potential for a mechanical role of CSF in SCI [1,3,280,281], there have been very few attempts to determine intrathecal fluid pressures either during experimental SCI in animals, or by using computational or physical models. To the authors' knowledge, only two groups have measured spinal fluid pressure in an animal model during experimental SCI. Peak pressures of 50 mmHg and 150 mmHg were measured close to the injury site in single cats subjected to 15g-25cm and 20g-15cm weight-drop injuries [1,2]. In dogs subjected to closed-spine lateral impacts, peak CSF pressure ranged from positive peak 1960 mmHg to a negative peak of -630 mmHg, at 6 cm from the injury site for a single animal. Both positive and negative pressure magnitudes decreased with distance from the impact site, reaching 27.5 mmHg and -19 mmHg at 44 cm from the impact [3]. Spinal CSF pressures have also been measured with limited success in cadavers [289] and pigs [288,487] during simulated whiplash events using rigid needle-mounted transducers. Computational (finite element) models of SCI typically have not included fluid elements [e.g. 461,495,499], due in part to a lack of data for validation.

Recent availability of sub-1 mm diameter, flexible, low-range pressure transducers with high frequency response, based on fibre optic and strain gauge technology, has made transducer placement in the spinal intrathecal space a realistic, although still challenging, prospect. Such transducers have been applied to intracranial fluid pressure measurement in various TBI models such as fluid percussion, cortical impact, contusion and acceleration and blast wave models [290,314,337]. However, they have not been used in the spinal intrathecal space or for studying SCI. This may be partly attributed to the lack of an appropriate contemporary large animal SCI model with proportionately large intrathecal sac

dimension. The objectives of this study were to establish an *in vivo* porcine model of SCI suitable for studying the mechanics of CSF pressure during injury, and to determine changes in pressure magnitude at several locations cranial and caudal to the injury site during the SCI event using implanted miniature intrathecal pressure transducers.

2.2 Methods

The experimental protocol was approved by the Animal Care Committee of the University of British Columbia and complied with the guidelines and policies of the Canadian Council on Animal Care.

2.2.1 Animals

Seventeen female Yucatan miniature pigs (Memorial University of Newfoundland, Canada; Sinclair Bio-Resources, Windham, ME, USA) were group housed and acclimatised at our facility for at least one week before surgery. At surgery the animals' mean age was 20.9 (SD 2.2) weeks, and mean weight was 22.5 (SD 2.0) kg. Anaesthesia was induced with intramuscular (IM) injection of Telazol 4-6 mg/kg; animals were endotracheally intubated and maintained on isoflurane (2-2.5% in O_2 or as required) during the procedure. Mechanical ventilation was maintained at 10-12 breaths/min with a tidal volume of 10-12 mL/kg. Analgesics (hydromorphone 0.15 mg/kg IM and morphine 1mg/kg IM) were administered before the surgery and as needed during the procedure. Antibiotic (cefazolin, 20 mg/kg) was given intravenously (IV) immediately before surgery and again at four hours. Hydration was maintained with IV lactated Ringer's solution. Core temperature was monitored with a rectal temperature probe and maintained at 38.5-39.5 °C with a circulating-water heating pad. A catheter was placed in the femoral artery to monitor arterial pressure. A urinary catheter was placed either urethrally or suprapubically, and allowed to flow freely. Anaesthetic level was monitored and adjusted to maintain heart rate, blood oxygen and blood pressure within normal physiological limits. All animals were subsequently used for separate studies where the SCI applied in this study was a required step in the protocol.

2.2.2 Injury device

A custom modified weight-drop device (Figure 2-1 and Figure 2-2) was designed to impart the SCI at T10 using either a 50 g (Group A, n=5; Group B, n=6) or 100 g (Group C, n=6) weight released from 50 cm. Because Group A animals were used for model development, we did not collect complete velocity, force and CSF pressure data for all animals (see Table 2-1); in all other respects Group A was identical to Group B. The weights used were higher than would be expected for a bone fragment associated with a burst fracture, but corresponded to the upper range previously used for large animal experimental SCI [e.g. 218,276,358,360,366,500] and were lower than the estimated wet weight of human thoracolumbar vertebra (250-550 g) [465]. The height was selected to produce impact velocities

within the range estimated for bone fragments during thoracolumbar vertebral burst fractures, 1-7.5 m/s (Section 1.6.4) [132,462].

The injury device was attached to the spine unilaterally at T9 and T12 with pedicle screws (4.5 x 35 mm, CD Horizon, Medtronic, Minneapolis, MN). A titanium rod (5.5 mm diameter, 70 mm length, CD Horizon, Medtronic, Minneapolis, MN) bridging these screws was then rigidly fixed to the base of an articulating arm with three ball joints (Model 660 (modified), L.S. Starett, Athol, MA, USA). This allowed the aluminum guide cylinder (12.7 mm internal diameter, 60 mm length) to be held perpendicular to the spinal cord, with its lowest end approximately 2 mm from the dura surface. The weight consisted of a 12.6 mm diameter stainless steel cylinder instrumented with a load cell (range ±222 N, nonlinearity and hysteresis ±0.5% of full scale, nonrepeatability ±0.1% of full scale, LLB215, Futek Advanced Sensor Technology, Irvine, CA, USA). A 9.53 mm diameter spherical stainless steel impact tip was fixed to the load cell. This diameter closely matched the maximum lateral diameter of the thoracic dura, as measured by *in vivo* magnetic resonance imaging in three animals (unpublished data). The load cell cable was guided in a channel running the length of the guide cylinder. The weight drop was triggered by removing a pin that bridged the centre of the guide cylinder and held the tip of the weight at 50 cm from the dural surface.

A high speed camera (Phantom V9, Vision Research Inc., Wayne, NJ, USA) with a low distortion lens (AF Zoom-Nikkor, Nikon, Tokyo, Japan) was used to track quadrant markers (12.7 mm diameter) that were rigidly attached to the top of the weight and the side of the guide cylinder. Images with a field of view of approximately 50×275 mm were obtained at 5000 frames per second and 240×1344 resolution, for 1.1 seconds. The high speed images were used to determine the velocity of the falling weight. Force data and high speed video were acquired for Groups B and C, but not for Group A.
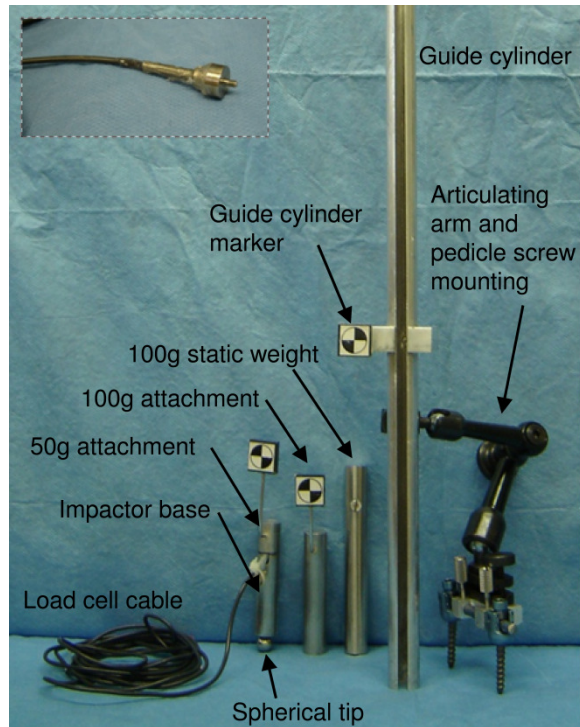
Figure 2-1 Photo of the components of the modified weight-drop injury device. Inset: close-up of the load cell installed within the weight base, above the spherical impactor tip.
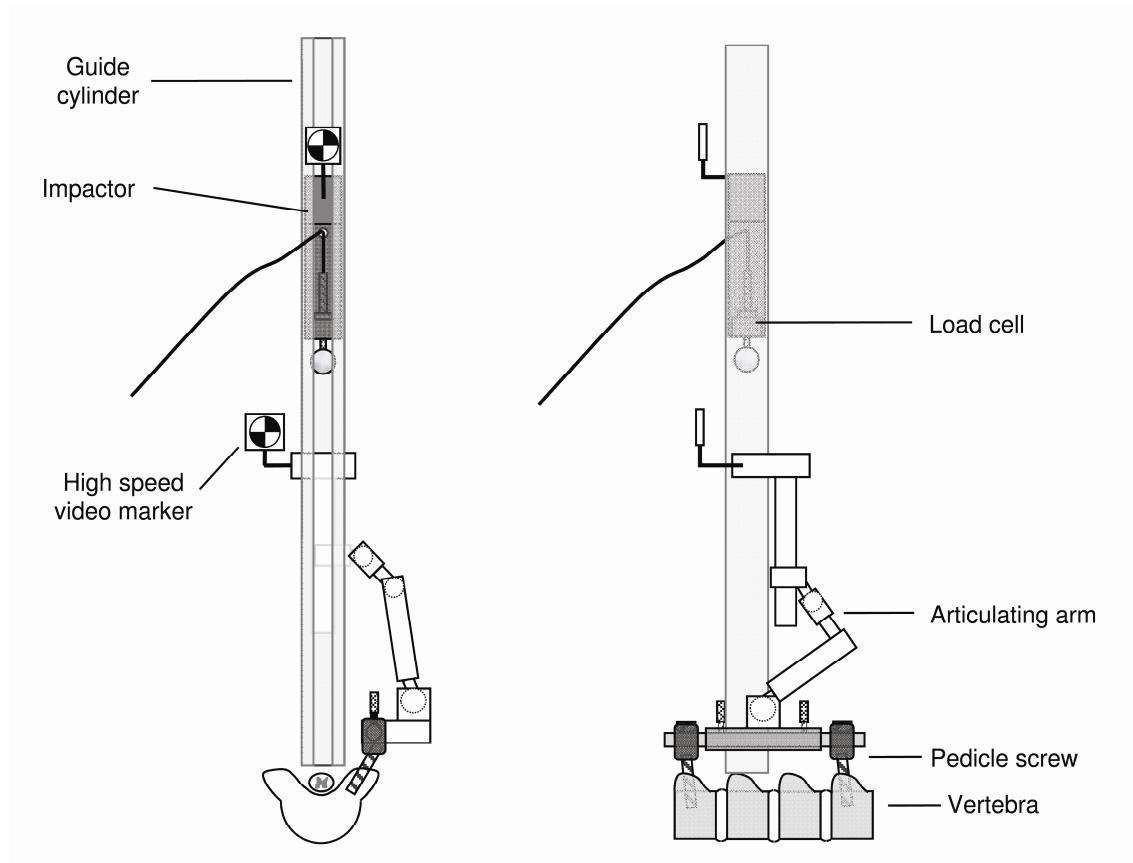
Figure 2-2 Schematic of front view (left) and side view (right) of the weight-drop device installed over four vertebrae.

2.2.3   Pressure transducers

CSF pressures were measured with miniature fibre optic pressure transducers (Preclin 420LP and Samba202 Control Unit, Samba Sensors, Sweden) with a sensor tip of 0.36 mm diameter, and a bare fibre diameter and length of 0.25 mm and 50 mm, respectively. The sensors had a measurement range of -37.5 (vacuum) to 262.5 mmHg, and an accuracy of ±0.38 mmHg +2.5% (of reading) up to 188 mmHg and +4% (of reading) above 188 mmHg. The frequency response of this transducer is not published, but it has been used previously to measure *in vivo* response to blast overpressures [341,342] and experimental TBI [290,314].

In this model development study the number of pressure transducers inserted in each animal increased as our technique improved and obtaining a seal between the transducer and the dura became reliable. In Group A we placed one (n=3) or two (n=2) transducers at a nominal 100 mm from the injury site. In Groups B and C we inserted two transducers in every animal (n=12) at a nominal 100 mm from

the injury site. These transducer sites are referred to as "cranial-far" and "caudal-far". In two Group C animals we placed an additional two transducers at a nominal 20 mm from the injury site. These transducer sites are referred to as "cranial-near" and "caudal-near" (Figure 2-3).

2.2.4   Surgical protocol

The animal was anaesthetised and the dura-enclosed spinal cord was exposed via a laminectomy from approximately T7 to T14. The laminectomy was widened at T10 to facilitate passage of the weight. Pedicle screws were inserted unilaterally into T9 and T12, and the articulating arm fixed in place. The animal was tilted, head down, and the pressure sensors were inserted in the locations described previously. The dorsal dura was pinched with forceps and gently lifted, a small hole was made in the raised portion with a 20 Ga needle tip, and the sensor advanced 50 mm into the intrathecal space along the dorsal aspect of the cord. A small cone-shaped bone wax plug was moulded around the fibre to plug the hole in the dura, and this assembly was sealed with cyanoacrylate adhesive gel. The distance from the injury epicentre to the pressure transducer tip was measured with callipers. The cranial-far and caudal-far transducer faced away from the injury site, while the cranial-near and caudal-near faced towards the injury site (Figure 2-3). The animal's head was raised to bring the thoracic spinal cord into a horizontal position and the guide cylinder was attached and aligned vertically using spirit levels. Immediately prior to the injury, the animal's ventilation was stopped to cease respiration motion and the trigger pin was removed to induce the injury, after which ventilation was resumed. The weight was removed from the spinal cord five minutes after impact. For the subsequent studies, five animals remained under anaesthetic for a further 11 hours and were then euthanised with an overdose of sodium pentobarbital (120 mg/kg IV) without waking, and 12 animals were woken from anaesthetic immediately after injury and then enrolled in a separate functional recovery study for three months, after which time they were euthanised. This heterogeneity did not influence the present study, which focused on the pressure behaviour during injury only.
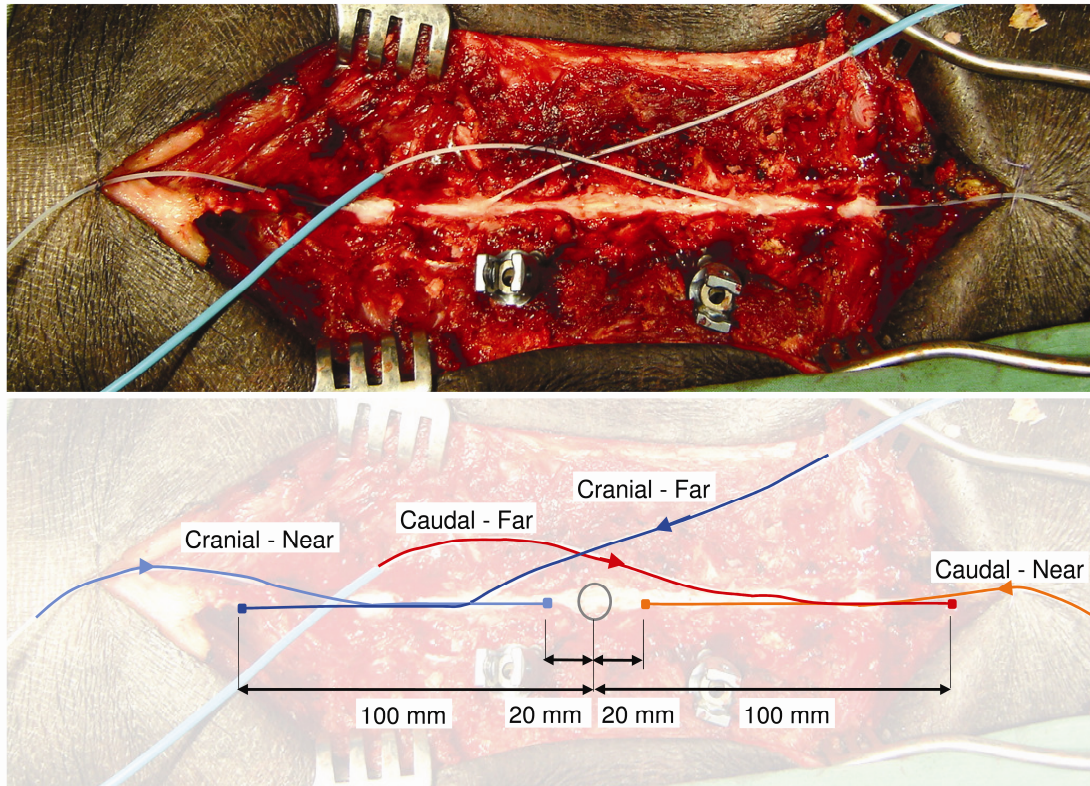
Figure 2-3 Photo showing the surgical site, with 4 pressure transducers implanted intrathecally, a widened laminectomy at the injury site (T10), and pedicle screws in T9 and T12 (top); same photo with overlay indicating locations of pressure transducer tips relative to the injury site (shown as a circle) (bottom). The two near transducers were only implanted for two of the Group C animals.

2.2.5   Data acquisition, analysis and statistics

Pressure and load data were acquired at a sampling rate of 50 kHz with custom LabVIEW programs (V8.6, National Instruments, Austin, TX, USA) and post-filtered with a two-way low-pass 4th-order Butterworth filter with a 5 kHz cut-off frequency using custom Matlab code (V2008a, The Mathworks, Matick, MA, USA). High speed video was captured using the camera software (Phantom V9.0.640, Vision Research Inc., Wayne, NJ, USA). Data were synchronised via the video trigger pulse. The markers in the high speed images were semi-automatically tracked using TEMA software (V3.2-024, Image Systems AB, Linköping, Sweden) using the quadrant marker setting. The location of each marker in the first video frame was manually identified by the operator. The software algorithm searched within a defined area on each subsequent image to locate each marker based on dark and light areas forming a quadrant pattern. The centre of symmetry of each marker was then identified using Gaussian derivative filters. The software algorithm is independent of rotation and the scale of the marker.

For each animal in Group A the peak positive and negative pressures were determined for each implanted transducer. In Groups B and C the following parameters were determined for each animal: impact velocity, peak load, and peak positive and negative pressures for each transducer. All pressures are reported relative to the pressure value immediately prior to the injury event because the average CSF pressure at any point along the length of the spine is dependent on the vertical height relative to the highest point in the fluid system (i.e. the hydrostatic pressure) [100] as well as the effect of pressure fluctuations from the respiratory and arterial pulse cycles. The injury input and output parameters and the pressure transducer locations for each experimental group are detailed in Table 2-1.

Table 2-1 Input injury parameters, numbers of successfully recorded model assessment (output) parameters, and pressure transducer sites by experimental group.

	Group A (n=5)	Group B (n=6)	Group C (n=6)
Input parameters			
Drop weight (g)	50	50	100
Drop height (cm)	50	50	50
Model assessment measures			
Velocity	-	n=6	n=5
Displacement	-	n=6	n=5
Force	-	n=5	n=4
Pressure assessment measures			
Peak positive and negative pressure	Cranial-far (n=4) Caudal-far (n=3)	Cranial-far (n=6) Caudal-far (n=6)	Cranial-far (n=6) Caudal-far (n=6) Cranial-near (n=2) Caudal-near (n=2)

To assess the general characteristics of the model, non-parametric descriptive statistics (median, 25th and 75th percentile) were determined for each parameter for Group A, B and C separately. Differences in injury parameters (impact velocity, peak load and peak CSF pressures) between Group B and C were assessed with Mann-Whitney U Tests. Group A was omitted from this analysis because only CSF pressure was measured in these animals. For animals in Groups B and C, Wilcoxon matched pairs tests were used to assess differences in peak positive pressure, peak negative pressure and the distance of the sensor face from the injury epicentre, for the cranial and caudal sites. A p-value less than 0.05 was considered statistically significant.

2.3 Results

All animals remained stable past the experimental endpoint of this study. Two animals in the recovery study died within three days of surgery, one from aspiration pneumonia and the other from an unknown cause. Both were from Group C. The CSF loss during transducer insertion was visually estimated to be around 1-3 mL per animal. Areas of haemorrhage were observed on the dorsal aspect of

the cord in all animals when the weight was removed. This haemorrhage typically extended approximately 1 cm both cranial and caudal of the epicentre. The haemorrhage pattern was often discontinuous, with the central area corresponding to the contact area of the impactor tip devoid of visible blood. We considered the injuries for all groups to be "severe" due to the haemorrhage observed immediately after injury, the limited hind-limb motor function in pigs that were monitored for three months post-injury, and subsequent histology which showed little white matter sparing at the injury site [501].

The impact parameters and peak negative and positive pressures at the "far" location for each test are shown in Table 2-2. As noted in Table 2-1 above, due to technical difficulties load data were not collected for one test in Group B and two in Group C, and displacement data were not available for one in Group B. The pressure data for the "near" location are provided in Figure 2-6.

Table 2-2 Injury parameters and peak positive and negative CSF pressures (relative) at the "far" location for instrumented SCIs with 50 g and 100 g weight-drop.

Animal ID	Weight	Pre-impact Velocity	Peak Load	Distance cranial-far	Distance caudal-far	Peak –ve cranial-far	Peak +ve cranial-far	Peak –ve caudal-far	Peak +ve caudal-far
	(kg)	(m/s)	(N)	(mm)	(mm)	(mmHg)	(mmHg)	(mmHg)	(mmHg)
Group A (50 g weight)									
P406	21.0	-	-	nom. 100	nom. 100	-	-	-2.4	95.3
P403	20.5	-	-	nom. 100	nom. 100	-2.7	57.3	-	-
P412	22.0	-	-	nom. 100	nom. 100	-2.5	201.4	-	-
P408	25.5	-	-	nom. 100	nom. 100	-9.6	34.3	-16.3	61.2
P1202	24.0	-	-	nom. 100	nom. 100	-52.6*	86.7	-22.2	131.1
Group B (50 g weight)									
P1219	23.5	2.25	50.2	112	-117	-3.2	80.7	-4.9	55.4
P1241	24.0	2.63	58.0	111	-99	-4.1	134.6	-3.2	201.9
P1216	23.5	2.72	82.1	112	-105	-17.9	115.4	-18.7	72.3
P1205	24.0	2.76	54.0	109	-110	-36.0	136.0	-9.6	81.8
P407	22.5	2.58	46.8	98	-118	-4.1	105.5	-5.5	130.4
P1080	25.5	2.26	-	138	-150	-5.0	40.5	-6.1	24.2
Valid N	6	6	5	6	6	6	6	6	6
Median	23.8	2.6	54.0	112	-114	-4.6	110.5	-5.8	77.1
25th%ile	23.5	2.3	50.2	109	-118	-17.9	80.7	-9.6	55.4
75th%ile	24.0	2.7	58.0	112	-105	-4.1	134.6	-4.9	130.4
Group C (100 g weight)									
P1242	20.5	2.70	139.5	94	-104	-51.9*	11.0	-28.6	18.4
P1262	17.5	2.77	165.2	83	-94	-27.5	71.2	-21.3	101.5
P1264	22.0	2.52	125.2	98	-100	-7.5	272.9*	-28.0	208.5
P410	21.5	2.73	101.1	65	-88	-34.7	20.7	-31.2	48.2
P416	23.5	2.78	-	100	-100	-27.7	105.6	-17.6	69.4
P411	22.0	-	-	91	-112	-9.4	187.2	-26.4	65.0
Valid N	6	5	4	6	6	6	6	6	6
Median	21.8	2.7	132.4	92	-100	-27.6	88.4	-27.2	67.2
25th%ile	20.5	2.7	113.1	83	-104	-34.7	20.7	-28.6	48.2
75th%ile	22.0	2.8	152.4	98	-94	-9.4	187.2	-21.3	101.5

*these values were outside the manufacturer's published range for the transducer (-37.5 to 262.5 mmHg), but within the range of the data acquisition card. Linearity in this range was verified against a reference transducer in the laboratory.

2.3.1 Contusion injury characteristics

Group B had a wider range of impact velocity than Group C, but the nominal 2.6 m/s impact velocity was not significantly different between them (p=0.177) (Table 2-2). The peak load for Group B ranged 46.8-82.0 N, and for Group C ranged 101.1-165.2 N. The median maximum load was 145% greater for the 100 g Group C injuries than for the 50 g Group B injuries (p=0.016) (Table 2-2). Although the device did not have a mechanism to eliminate weight bounce, the impactor tip did not rebound above the original height of the spinal cord in any of the tests. In some tests the impact tip resided lateral to the spinal cord after the impact (i.e. not on the dorsal surface of the dura), despite all attempts being made to align the impact centrally. In these cases the spinal cord was apparently deflected laterally due to the rounded shape of the impactor tip.

2.3.2 CSF pressure

The distance between the injury site and the transducer tip was significantly different between Groups B and C for the cranial-far transducer (p=0.004), but not the caudal-far transducer (p=0.065).

In most animals the fluid pressure profile measured at the "far" location at the time of injury consisted of a small negative pressure pulse followed immediately by a positive pressure pulse (Figure 2-4 and Figure 2-5). The magnitudes of peak negative and positive pressures had considerable variation between animals within each injury group (Table 2-2). The magnitude of median peak negative pressure was greater for Group C (100 g) than Group B (50 g) for both cranial-far (6 times greater) and caudal-far transducers (4.7 times greater); however, the difference was significant for the caudal location only (cranial-far p=0.093, caudal-far p=0.004). The median peak positive pressures were not significantly different for Group B and Group C (cranial-far p=0.818, caudal-far p=0.699).
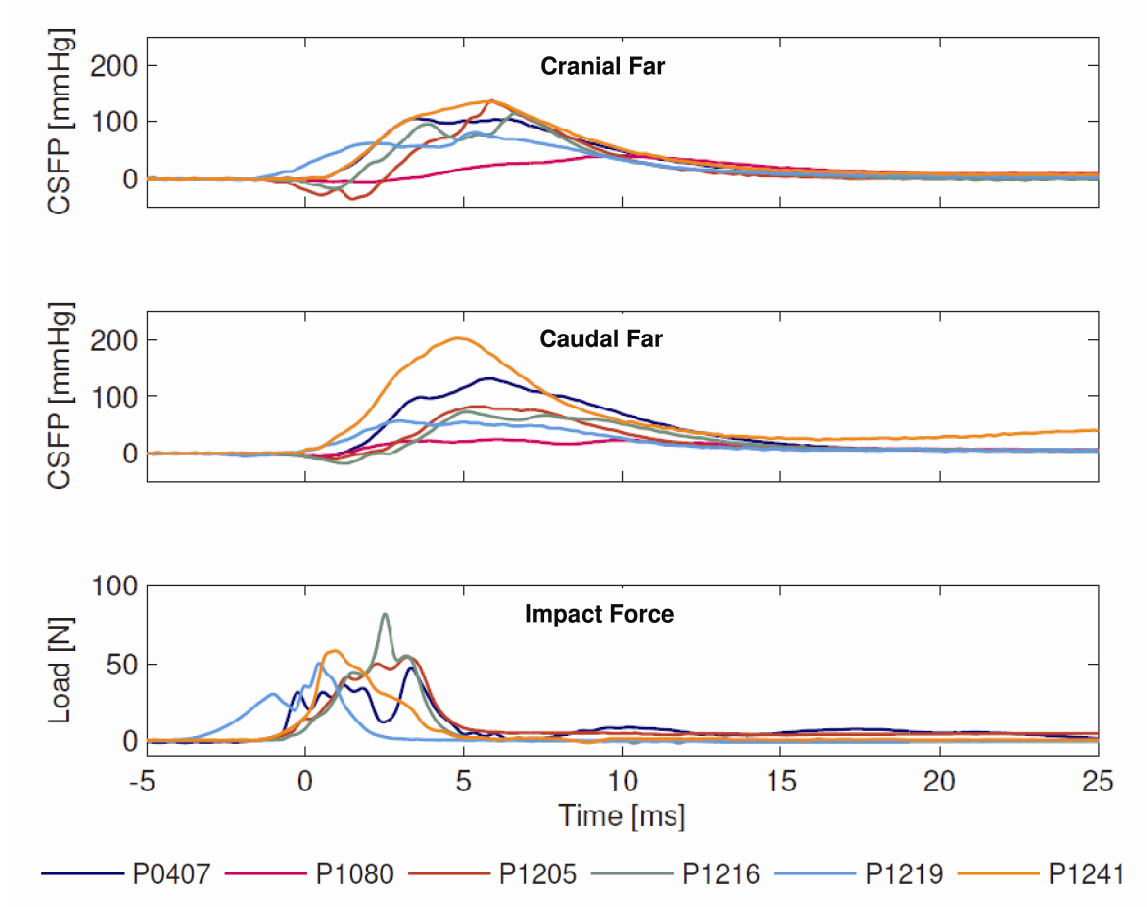
Figure 2-4 CSF pressure: cranial-far (top) and caudal-far (middle), and load (bottom) for the Group B (50 g injury) animals. Zero time is arbitrarily aligned at Caudal-far = ±3mmHg. There were no significant differences between the peak pressures (positive and negative) measured at Cranial-far and Caudal-far locations. The early rise of the impact force, relative to the CSF pressure, for P1219 may indicate contact between the impactor and the sides of the laminectomy prior to dura contact.
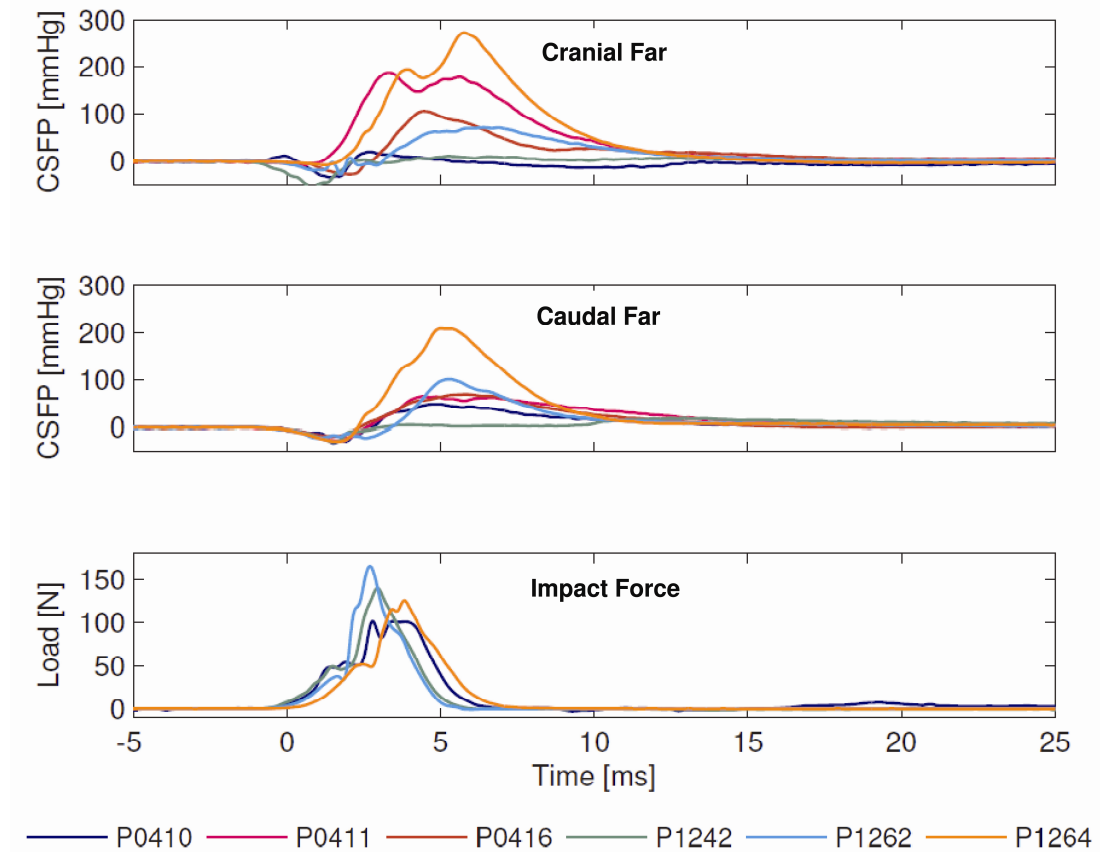
Figure 2-5 CSF pressure: cranial-far (top) and caudal-far (middle), and load (bottom) for the Group C (100 g injury) animals. Zero time is arbitrarily aligned at caudal-far = ±3 mmHg. There were no significant differences between the peak pressures (positive and negative) measured at Cranial-far and Caudal-far locations. There was considerable variability in the pressure profiles; for example P1242 showed very little pressure change while P1264 exhibited a large fluctuation, yet the impact force profiles are fairly similar.

In the two animals in which additional pressure transducers were placed approximately 20 mm from the injury epicentre, the peak positive pressure recorded at the cranial- and caudal-near transducer locations exceeded the upper range of the pressure transducers and data acquisition system. This was approximately 300 mmHg above the baseline CSF pressure. Negative pressure pulses were not observed at either the cranial or caudal locations at the near measurement sites (Figure 2-6).
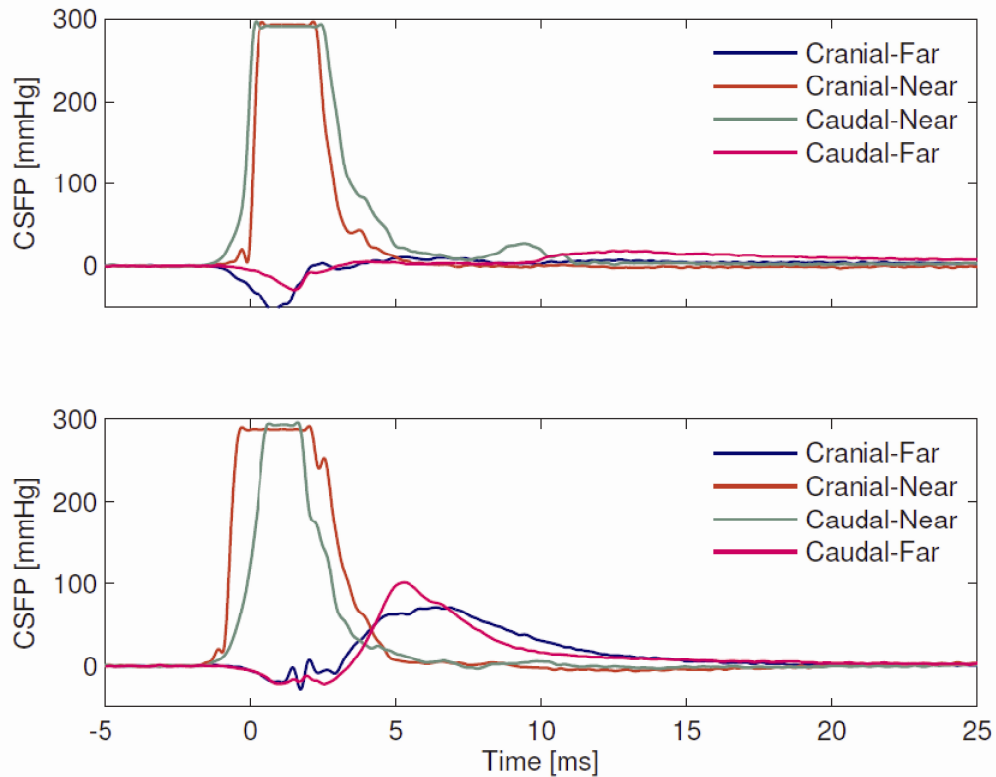
Figure 2-6 Plots of CSF pressures for the two tests from Group C in which two "near" transducers were implanted (top: P1242; bottom: P1262). The pressures at the "near" location exceeded the upper range of the pressure transducers.

Across groups B and C, on average the far-caudal transducer was placed slightly further away from the injury epicentre than the far-cranial transducer (p=0.002). However, there was no significant difference between the peak pressures recorded caudal versus cranial to the injury site for experimental groups B and C (negative pressure p=0.583, positive pressure p=0.308). (Table 2-2)

2.4 Discussion

A large animal model of traumatic SCI has the potential to more closely represent the scale and physiology of the human spinal cord, and therefore may be an important step in elucidating primary and secondary injury mechanisms, and evaluating the efficacy of treatments. In this study the human-like size of the porcine thoracic spinal cord and intrathecal space (Section 7.3) was exploited to measure CSF pressures associated with spinal cord injuries from a novel weight drop device, by inserting miniature pressure sensors into the intrathecal space adjacent to the injury site. The results suggest the miniature Yucatan pig is an appropriate model for studying CSF, spinal cord and dura interactions during injury and that with further development it may be an appropriate *in vivo* large animal model of SCI for many basic science applications where human-like dimensions and physiology are important.

101

2.4.1   Injury model

Although previous SCI research has used a variety of medium-to-large species, contemporary work predominantly uses well established rodent models that are less ethically contentious and have less cost and complexity associated with surgery and care. Pigs are well established as paediatric and adult models in TBI research [376] and as models of chronic spinal cord pathology [502-504]. They have also been used for ischaemic models of SCI [e.g. 379]. Isolated reports of mechanical SCI models in the pig include weight-drop [383], pneumatic impactor [382] and clip compression [384,389] techniques; however, to our knowledge, these models have not been characterised mechanically. In our opinion, pigs are a suitable SCI model because their CNS is similar to humans in several respects including blood supply and flow characteristics [388,505], white and grey matter distribution, brain and spinal cord growth and development [506] and spinal skeletal similarities [386,464,507]. Specifically, the miniature Yucatan is an ideal breed for both acute and chronic studies as it is bred disease-free, and has a slow growth rate and low weight at full maturity [375]. However, there are also some notable deviations from human spine anatomy including a greater number of vertebrae [375] and, according to our observation and estimation, a greater amount of epidural fat and larger epidural vessels than in many humans.

There are several challenges associated with the required surgery – it is technically demanding and lengthy, requiring trained surgical staff and close veterinary monitoring throughout. Care must be taken to avoid the large epidural veins which are prominent in the anterolateral canal, and to avoid breach of the canal wall when placing the pedicle screws. There is potential for considerable CSF loss during transducer placement; care must be taken to minimise the size of the puncture hole, and to introduce the transducer and apply sealant rapidly. The bone wax "plug" was essential to form a patent seal and to prevent damage to the transducer upon its removal. Larger animals are also more susceptible to infection than rodents, a consideration that is particularly important for protocols with long-duration anaesthetic and for survival studies. All components of the injury device that reside in the surgical field can be autoclaved or soaked in cold sterile solution.

Mounting the device to the spine served two purposes. Firstly, it located the weight at a fixed distance from the dural surface throughout the large dorsal excursion associated with respiration in the ventilated animal. Hung et al. [369] induced a unilateral pneumothorax to reduce this motion in cats, but the methodology used to combat this motion is otherwise rarely described for apparatus that were fixed to the operating table. This feature also makes the injury device well suited to experiments in which prolonged compression of a consistent magnitude is desired after the dynamic injury. Secondly, the pedicle screw and rod construct eliminated relative motion between the fixed vertebra and likely improved consistency of the energy delivered to the spinal cord; others have placed a saddle under the spinal cord [296] or rigid supports under the transverse processes [396].

The impactor tip had approximately the same diameter as the maximum lateral diameter of the cord; it is not known how this compares to other devices because cord dimensions were not commonly reported. The spherical tip ensured maximum tip advancement without impingement on the lateral canal walls; however, the relative instability of the contact between the convex impactor tip and dural surface may have caused lateral displacement of the spinal cord relative to the tip. Although great care was taken to centre the guide cylinder relative to the lateral borders of the dura, this instability would have been exaggerated by any lateral misalignment of the guide cylinder. While the final resting position might not be indicative of alignment during the impact event, the lateral motion may have influenced the resultant injury in some animals. Previously reported weight-drop devices commonly used a secondary "impounder" resting on the cord [e.g. 294] presumably to aid alignment of the falling weight. However, this reduces the energy transferred from the falling weight to the spinal cord [364] and even light weight static impounders alter the size and shape of the intrathecal space and spinal cord prior to injury [369], which was undesirable in the current study.

It is difficult to compare the impact velocities and peak loads obtained in this study with previous published results because very few large animal studies report velocity, peak impact force and spinal cord dimensions. In our study the load cell provides valuable information regarding the relative force profiles applied for the two injury severities; the significant difference between peak impact forces for Groups B (50 g) and C (100 g) was expected due to the larger mechanical energy associated with the larger mass. Due to space and weight restrictions, the impactor did not incorporate an accelerometer for inertial compensation; however, the mass of the impactor tip (below the load cell) was 3.45 g and therefore from Newton's second law this would require a correction of less than 8%. Variation of peak force within the experimental groups can be attributed to factors such as differing tissue mechanical responses due to variation in the size of the spinal cord, dura and ligamentous tissues, presence of different amounts of CSF, and any deviations of the impactor tip from the centerline. We did not report a measure of dural displacement in this study because we thought that any lateral deviations of the impactor tip would confound the measurement.

2.4.2   CSF pressures

While the CSF likely provides mechanical protection for the central nervous system during minor whole body perturbations, a mechanical insult which imparts a large energy to the system may produce a pressure wave in the CSF and in the fluid and solid constituents of the spinal cord that transfers energy (and deformation) away from the site of the injury, thus disrupting cellular function at locations remote from the injury. Despite early recognition of this potential [1,3] further focus in published reports is limited to very few descriptions of diffuse axonal injury (DAI) remote to the site of mechanical insult. DAI has been observed in the cervical spinal cord following experimental TBI in ferrets subjected to

cortical impacts [508] and in rabbits subjected to rotational head acceleration [509]. Human occurrences are limited to anecdotal evidence of DAI in the cervical cord associated with shaken baby syndrome [156,157], and evidence of axonal injury at sites remote from the focal injury in SCI patients who died between 4 hours and 6 weeks after injury has been reported [163]. Recently, Czeiter et al. [162] observed that impact induced TBI was capable of evoking traumatic axonal injury in the cervical and thoracolumbar spinal cord of rats. Observing that the majority of the injured cells in the thoracolumbar region were close to the surface of the cord, they proposed that in addition to the commonly cited axonal stretch mechanism, a shock wave travelling through the CSF could have contributed to this cellular injury.

The peak CSF pressures measured in the current study were several orders of magnitude higher than normal resting pressures. Baseline CSF pressures have been measured in the rat cisterna magna 6-8 mmHg [496] and lumbar intrathecal sac 0.7-7.4 mmHg [105], 4.18 mmHg [104]; in cats, 8.7 mmHg [101] and in dogs: cervical 8.8 mmHg and lumbar 10.0 mmHg [100]. Transient pressure increases in humans are associated with the Valsalva manoeuvre, 10.5 mmHg [64] and coughing, 40 mmHg [63]. To the authors' knowledge, there is no established pressure tolerance value for the bulk spinal cord or its cellular constituents. However, animals exposed to external blast overpressures ranging from 75 to 7500 mmHg have exhibited reduced performance in physical tests and degeneration of cerebral cortex neurons [340], injury to neuronal and glial cells, and brain edema [344-349], brain haemorrhage and edema [342], morphological changes to neurons [351], damage to central visual pathways [343] and elevated intracranial pressure and impaired cognitive function [341]. While neural tissue in different locations may have different injury susceptibility due to differences in microvasculature, metabolic processes and cellular distribution, these studies suggest that the peak pressures observed in the current study may approach or exceed pressure tolerances and thus may contribute to the overall injury severity sustained by the animals.

To our knowledge there have been only two single measurements of spinal CSF pressure during an *open* experimental SCI. Hung et al. [1] reported a peak pressure of 50 mmHg approximately 25 mm cranial to the injury site in a cat weight-drop model using a 15g-25cm injury, with a 5 mm diameter cylindrical weight. The same group, using a similar weight-drop cat model, reported a 150 mmHg peak pressure at 15 mm caudal and cranial to the injury site, in response to a 20g-15cm injury [2]. Differences in animal size, weight-drop parameters and pressure transducer placement make direct comparison to our data difficult; however, it is noted that the peak CSF pressures measured at 100 mm from the epicentre in our experiments were of similar or greater magnitude to those measured previously. The peak pressures in the current study exhibited wide variation which may be due to variation in the peak impact load, baseline CSF pressure, CSF layer thickness and the nature of the contact between the spherical impactor tip and the dura. In the two animals with transducers 20 mm from the epicentre, the "out-of-range"

104

readings imply that the pressures at the equivalent distance were at least an order of magnitude higher than those measured in the cats. This may be due to the higher injury energy used in the current study, and also the differing size of the cat and pig anatomy. Further, in those studies the CSF pressure was measured via an implanted "fluid filled needle" and tube attached to an external pressure transducer. This liquid measurement path probably caused attenuation of the pressure signal which did not occur in the current study because the sensing face was in direct contact with the CSF. The pressure trace provided in Hung et al. [1] indicates that the positive pressure pulse was followed by a smaller negative pressure pulse of around -16 mmHg. It is not known why negative pressures occurred *after* the initial positive peak in Hung's study, while in our study the negative trough *preceded* the positive peak.

The most comprehensive published study of spinal CSF pressure transients used a closed-spine lateral weight-drop SCI model in dogs [3]. Pressures ranging from -630 mmHg to 1960 mmHg were measured at 60 mm from the impact site, with diminishing ranges of approximately -400 to 288 mmHg at 150 mm, and -28 to 19.0 mmHg at 440 mm from the impact site. These pressures are considerably higher than those of the present study, particularly at the measurement locations closest to the impact. The closed-spine model imparts the SCI by dropping a large mass on the intact spinal column and so it is difficult to compare the injury severity to that of the current study or to human SCI. Wennerstrand et al. [3] also used a fluid-filled catheter attached to an external transducer and accounted for the damping by applying a correction factor determined from a synthetic model of the system; however, it is unclear how well this replicated the animal tests and therefore if the correction factor produced accurate estimates of the CSF pressure within the thecal sac.

Other studies that have measured spinal pressure associated with injury have either used physical models without CSF, or have not replicated the kinetics and/or kinematics that produce human SCI. Yoganandan and colleagues [469] placed a pressure transducer instrumented gelatine spinal cord in cadaver cervical spines with a C4 laminectomy and subjected them to a number of weight-drop tests. They recorded pressures between 240-400 kPa (1800-3000 mmHg) at the injury epicentre, and 30-50 kPa (225-375 mmHg) at one vertebral level rostral/caudal, for 200-600 g-cm impacts. The authors did not provide separate weight and height measures for the weight-drop, but the pressure values reported are of similar magnitude to the current study. Other researchers have measured cervical CSF pressures in whiplash models using pigs [287,288] and post mortem human subjects [289]. The former recorded pressures from -100 to 150 mmHg and observed that higher pressures were associated with the location of neuron membrane leakage; these values are within the range measured in the current study. The latter study reported similar pressure amplitudes (0 and 220 mmHg); however, the vascular and CSF systems were not pressurised in these post mortem human subject tests.

In characterising biomechanical systems it is desirable to alter the natural state as little as possible. In this experiment, a long narrow laminectomy and subsequent removal of ligamentum flavum and epidural fat were required. This, along with the addition of cyanoacrylate gel to the dural surface, alters the dorsal boundaries of the system and may influence the dynamic response of the dura and CSF. However, the open surgical approach allowed the introduction of miniature pressure sensors which permitted measurement of pressure in direct contact with the fluid. The transducers' size, weight and flexibility minimised possible effects of transducers on the mechanical response of the system. It is possible that soft tissue came into contact with the pressure sensor face during the injury; however, the sensing face on the cross-section of the fibre was some distance from the injury site where large tissue deformations are less likely, and its small size and flexibility probably allowed it to bend in a similar manner as the soft tissue. The effect of the anaesthetic protocol on the process of CSF formation and resorption is unknown but it is unlikely that this affected the pressure transients. Finally, the weights used to impart the injury were greater than would be expected of a bone fragment retropulsed into the canal during a burst fracture SCI, and reducing this weight would enable more human-like injury parameters to be used.

2.5 Conclusion

A large animal experimental SCI model and injury device were developed and successfully used to directly measure intrathecal CSF pressure at the instant of the injury event using miniature flexible pressure transducers. The peak magnitudes measured at approximately 100 mm from the injury epicentre were at least one order of magnitude above baseline. Pressures measured at 20 mm from the injury epicentre exceeded the range of the pressure transducer. Further studies utilising refined weight-drop parameters to better approximate a human-like SCI and pressure transducers with a higher range are needed to further evaluate the contribution of dynamic CSF pressure to primary injury.

Chapter 3   CSF Pressure during Contusion-type SCI[2]

3.1 Introduction

Despite concentrated research efforts over the past three decades, spinal cord injury (SCI) continues to be a devastating and permanent condition. While a number of treatments that showed promise in pre-clinical studies have been tested in human clinical trials, none has had demonstrable efficacy [374]. This lack of effective translation of treatments from laboratory models to bedside has been attributed, in part, to important differences between the human injury and the rodent models commonly used to represent it. While the rat contusion model replicates some features of human SCI [510], there are substantive differences in neuroanatomy and behavioural outcome [511]. One clear disadvantage of the rat model is the large discrepancy in scale relative to human anatomy [512]. Recognising this, there is a strong sentiment within the SCI research community that establishing pre-clinical treatment efficacy in a suitable large animal model would be an advantageous step in the appropriate pre-clinical evaluation of treatments [374]. This size discrepancy has implications for the selection of suitable injury parameters and the subsequent mechanical and biological response of the system to the injury and to treatment agents. We propose that an important and under-emphasised aspect of this scaling issue is the lack of a cerebrospinal fluid (CSF) layer of the same relative dimension as in humans.

Humans have a CSF layer surrounding the spinal cord that is on the order of 2-4 mm thick in the thoracic region [391,394]. Previous *ex vivo* and *in vivo* studies have noted the potential for this fluid layer to be both mechanically protective [e.g. 1,280,281] and potentially injurious [1,162,285] depending on the nature and magnitude of the mechanical loading. It has been proposed that a pressure wave of sufficient magnitude travelling away from the mechanical impact may injure cells some distance from the impact [1,162]. Axonal injury remote from the site of mechanical impact has been observed clinically [157,163], and *in vivo* and *in vitro* neural tissues are adversely affected by experimental fluid impulses [e.g. 313,332,342]. Further, some cases of post-traumatic ascending myelopathy [170,173,174] and SCIs which occur without evidence of bony or ligamentous abnormality [161] do not have a well defined origin and could be partly due to a pressure-induced primary injury mechanism occurring at, or some distance from, the main mechanical insult. Despite this potential "over-pressure" mechanism, animal, cadaver, and computational models that are used to study the mechanisms of SCI and treatment commonly do not include a fluid layer, and only two groups have measured CSF pressure during an experimental SCI [1-3].

---

[2] A version of Chapter 3 has been submitted for publication. Jones CF, Lee JHT, Burstyn U, Okon, E, Kwon BK and Cripton PA. Cerebrospinal fluid pressures during dynamic contusion-type spinal cord injury in a pig model.

The study presented in Chapter 2 demonstrated that measuring CSF pressure in a miniature pig model of SCI is feasible and provided some evidence that fluid pressures occurring at the instant of SCI may be sufficient to contribute to neural injury. However, that preliminary study had several limitations. Firstly, due to the requirements of concurrent studies using the same animals, the weight and height combinations used to impart the injury were not based on biomechanical studies of burst fracture processes. Secondly, only two animals had pressure transducers placed near to the injury site; furthermore, the pressures measured at this location exceeded the range of the transducers used. The previous study also highlighted several ways in which the injury device could be refined to improve its robustness and also the repeatability of the impact velocity obtained. Finally, the preliminary study did not include histological analysis of the spinal cord tissue viability. Therefore, the objective of this study was to characterise the CSF pressure waves associated with experimental SCIs with weight-velocity combinations approximating moderate and high human-like severity, at several locations, and to determine if these are sufficient to contribute to neural tissue injury some distance from the primary mechanical insult.

3.2 Methods

The experimental protocol was approved by the Animal Care Committee of the University of British Columbia and complied with the guidelines and policies of the Canadian Council on Animal Care.

3.2.1 Animals

Fourteen female Yucatan miniature pigs (~20 kg, Sinclair Bio-Resources, Windham, ME, USA) were group housed and acclimatised at the facility for at least one week before surgery. Animals were assigned to high severity injury (n=6), moderate severity injury (n=6) and sham (n=2) groups. Anaesthesia was induced with Telazol (4-6 mg/kg IM), xylazine (0.6 mg/kg) and atropine (0.02 mg/kg, IV), animals were intubated, and maintained on isoflurane (2-3.5% in O_2) with mechanical ventilation (10-12 breaths/min, tidal volume 10-12 mL/kg). Analgesics (hydromorphone 0.15 mg/kg IM or morphine 1 mg/kg IM) were administered before surgery and thereafter every 3-4 hours; antibiotics (cefazolin, 20 mg/kg IV) were administered before surgery and then every 4 hours. Blood pressure was monitored using Doppler ultrasound and a cuff on the forelimb. All animals received lactated Ringer's solution (IV). Temperature was monitored via a rectal probe and maintained at 37.5-38.5 °C with a circulating-water pad. Catheters were placed in the left carotid artery and external jugular vein to monitor central arterial and venous pressure. The urinary bladder was catheterised using an 8 French Foley catheter. Isoflurane concentration and fluid rate were adjusted as needed to maintain systolic arterial blood pressure within normal physiologic parameters.

3.2.2 Injury device

The SCI was imparted with a custom modified weight-drop device comprising a 20 g weight released from a height of 25 cm (moderate severity) or 125 cm (high severity), replicating the bone fragment weight and velocity associated with burst fractures [132,462]. The injury device (Figure 3-1) was attached to the spine unilaterally at T10-T13 with pedicle screws and a bridging titanium rod (screws: 4.0x26/28 mm; rod: 3.5 mm diameter/150 mm length; Vertex Reconstruction System, Medtronic, Minneapolis, MN, USA). This construct was fixed to the base of an articulating arm (Model 660 (modified), L.S. Starett, Athol, MA, USA) which enabled the aluminum guide rail (N17, Igus, Concord, ON, Canada) to be placed orthogonal to the spinal cord, resting on the remaining lateral borders of the vertebrae. Guide rails of length 0.6 m and 1.5 m were used. The weight consisted of a rapid-prototyped hollow cylinder (material: ABS-M30, sealed with acrylic lacquer) with a linear bearing attachment (aluminum/plastic, Drylin N17, Igus, Concord, ON, Canada) and was instrumented with a load cell (range ±222.41 N, LLB215, Futek Advanced Sensor Technology, Irvine, CA, USA) to which a 3/8" diameter cylindrical impact tip (material: ABS-M30, sealed with acrylic lacquer) with a 45°/1 mm bevelled edge was fixed. This diameter closely matched the lateral diameter of the thoracic dura, as measured by *in vivo* magnetic resonance imaging performed on three animals in a separate study (unpublished data). The impact tip height was set using a custom measuring tool and the weight was released by a latching solenoid (STA151082-234-1002, cage 81840, Saia-Burgess, Vandalia, OH, USA) with associated custom electronics.

A high speed camera (PhantomV9.1, Vision Research, Wayne, NJ, USA) was used to track quadrant markers rigidly attached to the weight and guide rail (field of view ~50×275 mm, 5500 frames per second, resolution 240×1344). The images were used to determine the impact velocity and the dorsal dura displacement during injury.
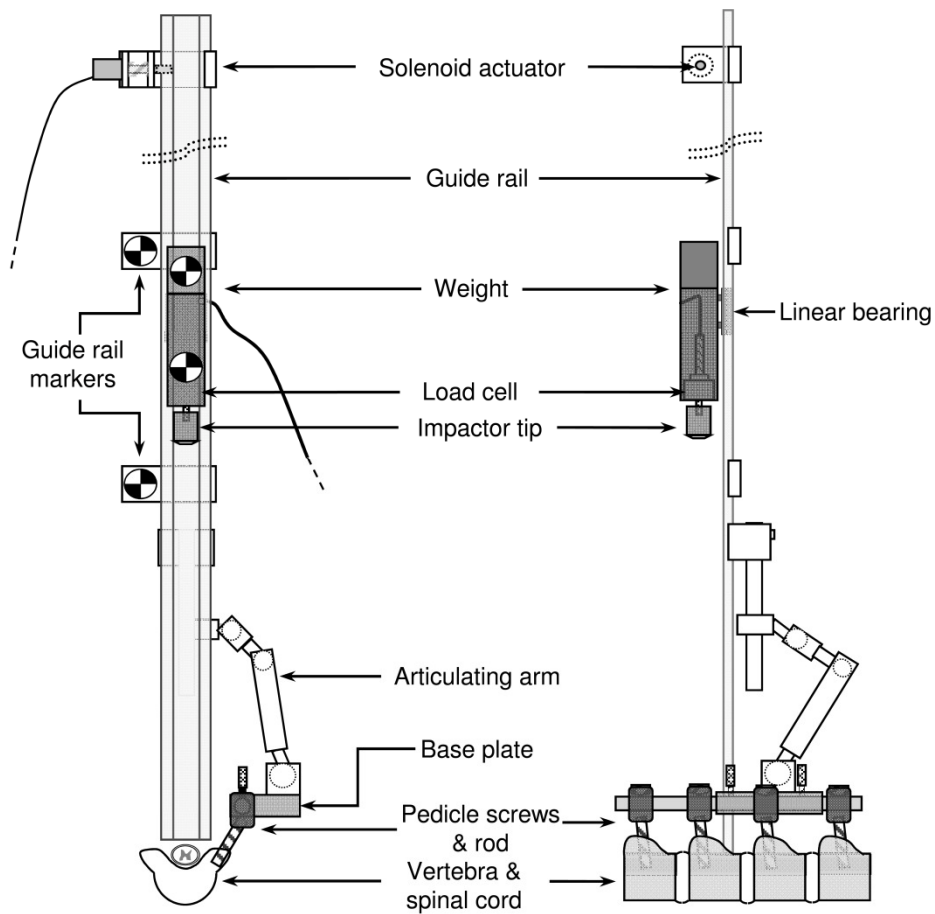
Figure 3-1 Schematic of front view (left) and side view (right) of the weight-drop injury device installed on vertebrae T10-T13; the injury was centred on the T11 vertebral level.

3.2.3 Pressure transducers

CSF pressure was measured at four locations with miniature fibre-optic pressure transducers (Preclin 420LP/360HP with Samba202 control unit, Samba Sensors, Sweden) (Table 3-1). The frequency response of these transducers is not published by the manufacturer but they have been used previously to measure high rate *in vivo* and atmospheric pressure impulses during experimental blast and TBI [290,314,341,342]. The transducer consists of 50 mm of bare glass fibre, then 50 mm of Teflon coated fibre, and 6 metres of plastic coated cable. Two high range pressure transducers were placed at 30 mm from the injury site (cranial-, caudal-near), facing towards the impact locations, and two low range transducers were placed at 100 mm from the injury site (cranial-, caudal-far), facing away from the impact location (Figure 3-2). Low range transducers were also used to measure the arterial and venous pressures. The Samba 202 control units were sampled at 40 kHz, from which an analog signal was transmitted to a data acquisition system.

Table 3-1 Pressure transducer specifications (Samba Sensors, Gruvgatan 6, Sweden)

	Preclin420LP (low range)	Preclin360HP (high range)
Range (mmHg)	37.5 – 262.5	-75 – 3500
Accuracy (mmHg)	±0.38 plus ±2.5% of reading	± 4% of reading
Sensor tip diameter (mm)	0.42	0.36
Fibre diameter (mm)	0.25	0.40
Fibre length (mm)	50	50
Temperature coefficient (mmHg/ºC, 20-45ºC)	<0.15	<1.95
Coating	nil	radiopaque coating
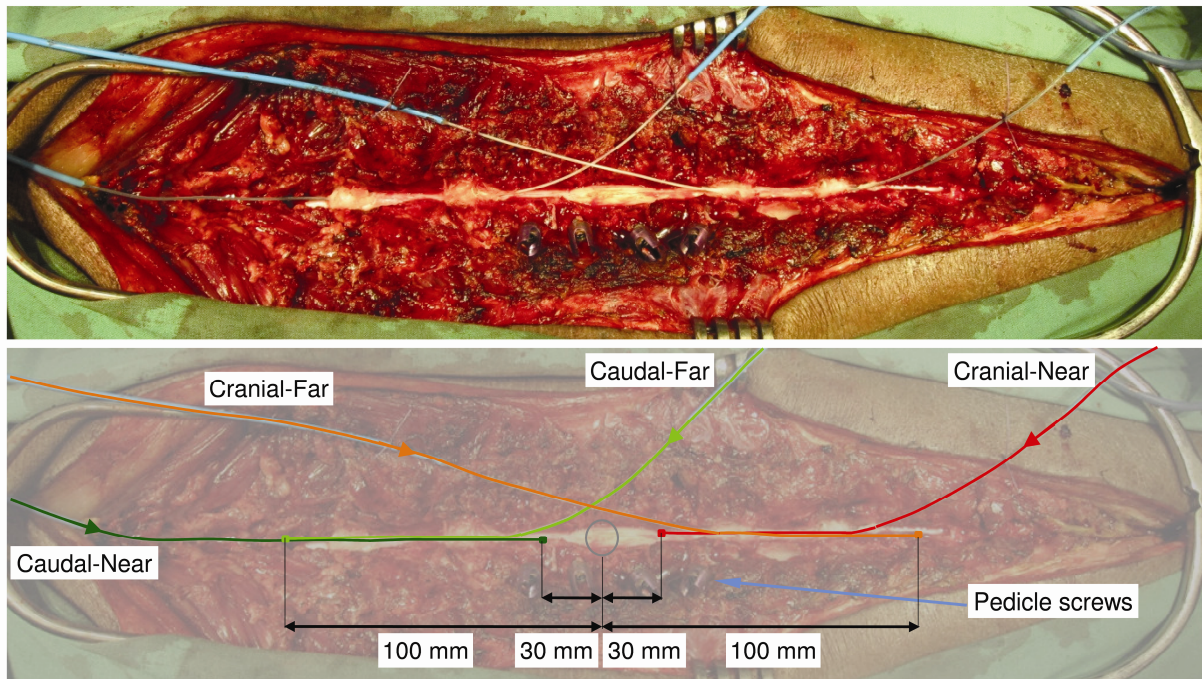
Figure 3-2 Photo (top) and overlay (bottom) indicating the location of the four intrathecal pressure transducers and pedicle screws; the injury was centred on the T11 vertebral level.

3.2.4   Experimental protocol

The animal was anaesthetised and the spinal cord was exposed via a laminectomy from T4 to L4. The laminectomy was widened at T10-T11 to ensure that the impactor tip did not strike the bony edges during impact. Pedicle screws were inserted and the articulating arm attached. The dura was exposed and the surgical table was tilted so that the animal's head was angled downwards to reduce hydrostatic pressure at the pressure transducer insertion point. The desired entry point for the subarachnoid pressure transducers was measured with callipers, then the dorsal dura was gently lifted with forceps at this

location and a small hole made with a needle tip. The transducer was rapidly introduced and advanced 50 mm into the intrathecal space (to the Teflon coated section), on the dorsal aspect of the cord. The dural hole was sealed around a small bone wax plug moulded to the transducer at the junction of the bare fibre and Teflon coating, using cyanoacrylate adhesive gel. After all four transducers had been placed, the animal's head was raised to bring the thoracic spinal cord into a horizontal position. The guide rail was attached and aligned vertically such that the weight tip was centred over the T11 vertebral level. The animal's ventilation was held to cease respiration motion and the solenoid was activated to impart the injury. The ventilation was resumed within three seconds after injury. As part of a separate protocol the animals remained under anaesthetic for 14 hours post-injury with 100 g compression for 8 hours and then 6 hours without compression. Animals were euthanised with an IV injection of sodium pentobarbital. The two sham animals received all surgical procedures except for the injury.

3.2.5   Histology

The spinal cord was harvested rapidly 14 hours after injury, and a 5 cm segment, with the dura intact and centered on the injury epicentre, was immersed in 4% phosphate buffered paraformaldehyde at 4 °C for 72 hr. Segments were cryoprotected in three 0.1 M phosphate buffered sucrose solutions (24%, 18% and 12%) for 2–3 days each, or until the tissue sank to the bottom of the container. The dura was dissected from the spinal cord and 1 cm segments were embedded in Tissue Tek OCT (Sakura Fintek Inc, Torrance, CA, USA). Transverse sections 200 μm thick were cut on a cryostat (Microm HM505E, Waldorf, Germany) and every second section mounted on slides, then stored at -80°C. Sections were stained with Eriochrome Cyanine and counter-stained with Neutral Red [513] to visualise the spared white and grey matter. For the analysis of lesion size, every fourth section (i.e. 1600 μm apart) starting from the estimated lesion centre was photographed at 5× objective with a microscope (DM5000B, Leica, Wetzlar, Germany), digital camera (DFC420, Leica) and software (Leica Application Suite, V3.1.0). Images for each section were merged in Adobe Photoshop (CS5, San Jose, CA, USA), the lesion area and total spinal cord area were manually segmented in the digital images using Analyse software (V10.0, Analyse Direct, Overland Park, KS, USA), and the percent "spared" tissue [(total-lesion)/total)] was calculated for each section. The "epicentre" was defined as the cross-section with the least amount of white and grey matter sparing (i.e. the greatest extent of parenchymal damage).

3.2.6   Data acquisition, analysis and statistics

Pressure, load and camera synchronisation data were acquired with custom Labview (V8.6, National Instruments, Austin, TX, USA) programs at 50 kHz then post-filtered and processed with custom Matlab (V2008b, The Mathworks, Matick, MA, USA) programs with a two-way 4th-order Butterworth filter with 5 kHz low-pass cut-off frequency. High speed video was captured with Phantom

(V9.0.640, Vision Research Inc., Wayne, NJ, USA) and distortion corrected with a camera calibration routine [514]. Markers were tracked using TEMA software (V3.2-024, Image Systems AB, Linköping, Sweden) using the quadrant marker setting (see Section 2.2.5).

For each test we determined mechanical parameters including peak impact force, force impulse, maximum dorsal dural displacement, impact velocity; and pressure parameters including peak positive and negative pressure, impulse, wave speed and attenuation ratio. All CSF pressures are reported relative to the pre-injury value to eliminate the effect of hydrostatic pressure variation [100] and respiratory and vascular pulsations. The wave speed was defined as the delay between the pressure peaks at the "near" and "far" locations, divided by the 70 mm transducer separation. The attenuation ratio was defined as the ratio of the "near" to "far" peak pressure. Contact between the dura and the impactor tip was defined to be when the jerk (i.e. the derivative of acceleration) of the impactor was a minimum, corresponding to the sharp change in velocity that occurred upon impact. This was found by fitting a spline to the filtered (two-way 4th-order Butterworth, 1 kHz low-pass cut-off frequency) velocity data, and differentiating the spline twice to obtain the jerk. The maximum dorsal dural displacement was defined as the difference between the impactor displacement at the time of dura contact and the maximum impactor displacement. This value includes the compression of the dura, CSF, spinal cord and anterior epidural contents; spinal cord compression alone could not be determined. The impact velocity was defined as the average velocity in the 10 ms prior to impact (i.e. over a distance of around 23 and 46 mm prior to impact for the two injury severities respectively).

The model (animal age, weight, pre-injury CSF pressure), injury and pressure parameters were assessed using non-parametric descriptive statistics. Differences between these parameters for the two experimental groups were assessed with Mann-Whitney U Tests. Wilcoxon Rank Sum matched-pairs tests were used to assess differences in the pressure profiles caudal and cranial to the injury. To compare tissue sparing between the high and moderate severity Mann-Whitney U Tests were performed at each location. Statistics were not performed on the histology of the sham animals because only two animals were used; the results are shown for comparison. A p-value of <0.05 was considered significant for all tests.

3.3   Results

3.3.1   Animals and injury characteristics

The age and weight of the pigs was consistent between the injury groups (Table 3-2). Due to technical issues high speed video data were not available for three animals, and force data were not available for one animal, all from the moderate-injury group. The model produced distinct and repeatable injury parameters for the moderate and high severity impacts. The high severity impacts had a median

peak impact force three times higher than that of the moderate severity impacts. The median load impulse and impact velocities were twice as high for the high severity impacts compared to the moderate severity impacts. These differences were statistically significant (Table 3-2). Although there was a trend towards lower median dural displacement for the moderate injury severity group, it was not significantly different from the high injury severity group probably due to the small number of results available for the moderate injury group. The pre-injury CSF pressure was within the normal range for both groups; however, there was a trend towards lower baseline pressures for the moderate severity group (Table 3-2).

Table 3-2 Descriptive statistics for model assessment parameters and results of Mann-Whitney U-tests comparing these parameters for the moderate and high severity injury groups. Statistically significant results (p<0.05) are in bold.

	Moderate Injury Severity		High Injury Severity		p-value
	Median	Quartiles	Median	Quartiles	
Age (days)	121.5	(115.0,133.0)	124	(121.0,130.0)	0.521
Weight (kg)	20	(20,20)	21.3	(19.5, 24.0)	0.415
Pre-injury Cranial CSFP (mmHg)	5.1	(4.4,7.0)	7.8	(5.5,8.2)	0.109
Pre-injury Caudal CSFP (mmHg)	4.4	(2.7,6.8)	7.6	(6.5,8.9)	**0.037**
Peak impact force (N)	20.8*	(18.4, 21.1)	62.1	(52.6, 65.2)	**0.006**
Load impulse (N.ms)	53.9*	(53.0, 57.9)	101.5	(98.3,101.8)	**0.006**
Impact velocity (m/s)	2.32**	(2.30, 2.36)	4.55	(4.44, 4.71)	**0.020**
Dural displacement (mm)	3.8**	(3.3, 5.4)	5.4	(5.0, 5.6)	0.197

n=6 except: *n=5 **n=3

3.3.2   CSF pressure

In all animals distinct pressure pulses of magnitudes greater than normal physiologic values were observed at the four pressure transducer locations. The pulse at the "near" transducers had greater peak magnitude, greater impulse and shorter duration than the "far" transducers, both caudal and cranial, and for both injury severities (Table 3-3). The peak negative pressures were similar in magnitude to the noise level of the signal and are therefore not reported. A typical response is shown in (Figure 3-3).
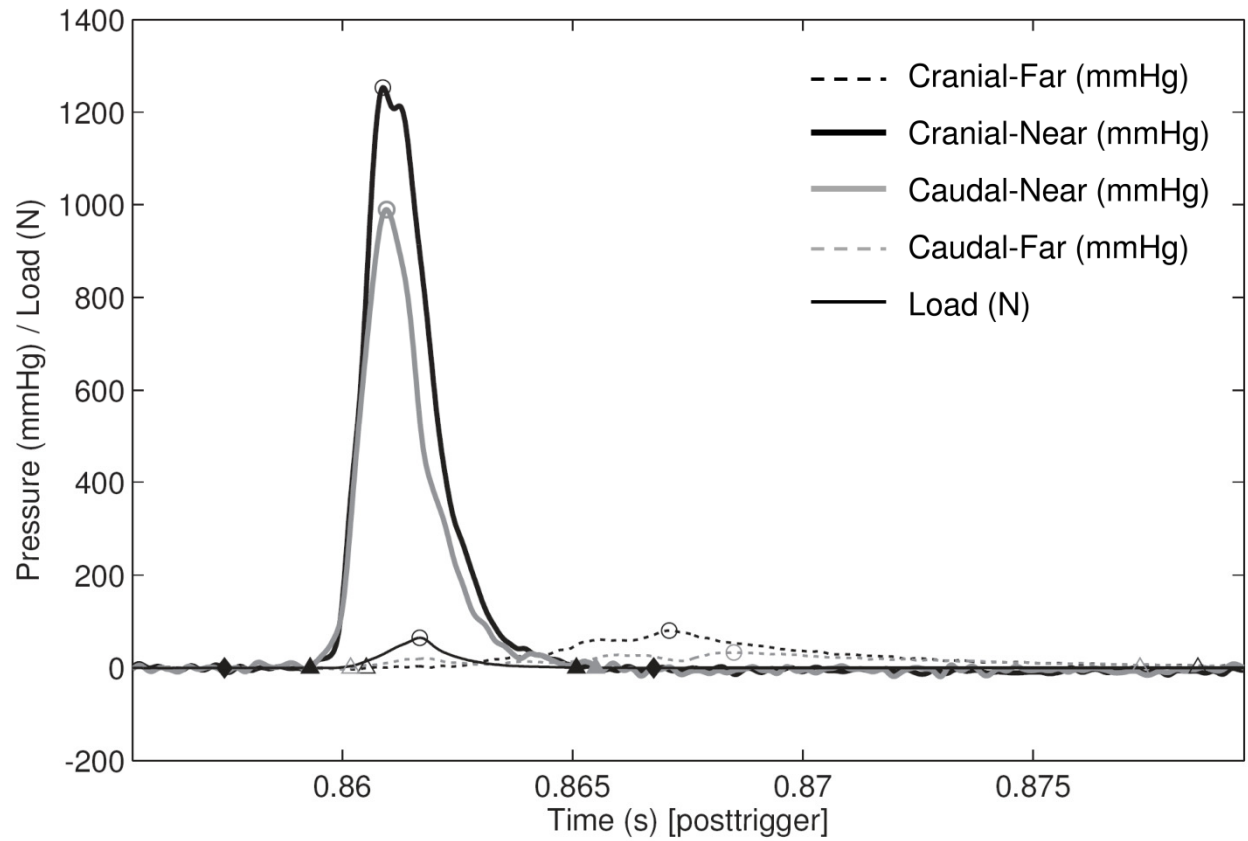
Figure 3-3 Typical response for a single injury (#P1805); CSF pressure at four locations, and load versus time. Open circles indicate peak pressure or load, triangles and diamonds indicate impulse calculation bounds.

Table 3-3 Descriptive statistics and results of the Mann-Whitney U-test comparisons for the moderate and high severity injury groups: peak positive pressure, pressure impulse, peak pressure, wave speed and attenuation ratio. Statistically significant results (p<0.05) are in bold.

	Moderate Injury Severity					High Injury Severity					p-value
	Median	Quartiles		Range		Median	Quartiles		Range		
Peak positive pressure (mmHg)											
Cr-Far	7.2	4.7	7.6	3.8	39.2	33.7	22.9	80.5	18.5	83.7	**0.025**
Cr-Near	565.6	403.0	611.0	96.7	625.6	1069.0	836.0	1253.0	615.6	1430.3	**0.007**
Ca-Near	446.5	370.4	630.5	155.6	680.2	841.7	784.1	989.6	740.3	1015.4	**0.004**
Ca-Far	21.5	9.2	42.3	1.7	67.6	46.5	33.3	67.1	23.5	93.0	0.109
Pressure impulse (mmHg.msec)											
Cr-Far	57.7	42.1	266.8	9.6	372.9	351.2	151.5	432.7	106.1	479.5	**0.037**
Cr-Near	1329.5	896.0	1547.5	351.0	1587.2	1743.7	1553.4	2232.9	1365.7	2504.2	**0.025**
Ca-Near	969.1	869.2	1470.6	539.3	1836.3	1572.7	1506.3	1660.1	1046.1	1757.6	0.078
Ca-Far	209.9	71.2	313.1	12.5	488.1	402.0	301.2	521.5	188.3	600.4	0.109
Wave speed (m/s)											
Cranial	3.4	2.7	9.4	2.5	9.9	7.2	7.1	11.3	6.7	13.4	0.109
Caudal	10.0	7.0	11.0	4.0	12.6	9.2	8.7	11.0	7.1	15.5	0.810
Attenuation ratio											
Cranial	78.2	20.6	83.0	15.6	106.6	29.7	17.1	33.2	15.6	41.7	0.150
Caudal	19.9	16.1	46.4	9.3	93.1	16.5	13.0	29.7	10.9	34.3	0.522

The high severity injury was associated with greater positive peak pressures and impulses; however, due to considerable variation in specimen response this was not statistically significant for all transducer locations (Figure 3-4). The estimated wave speeds had an overall range of 2.5-15.5 m/s and a statistically non-significant trend towards higher wave speeds for the high severity injury. The attenuation ratio between the near and far locations ranged from 9.3 to 106.6 and there was no significant difference in its magnitude between the injury groups (Table 3-3).
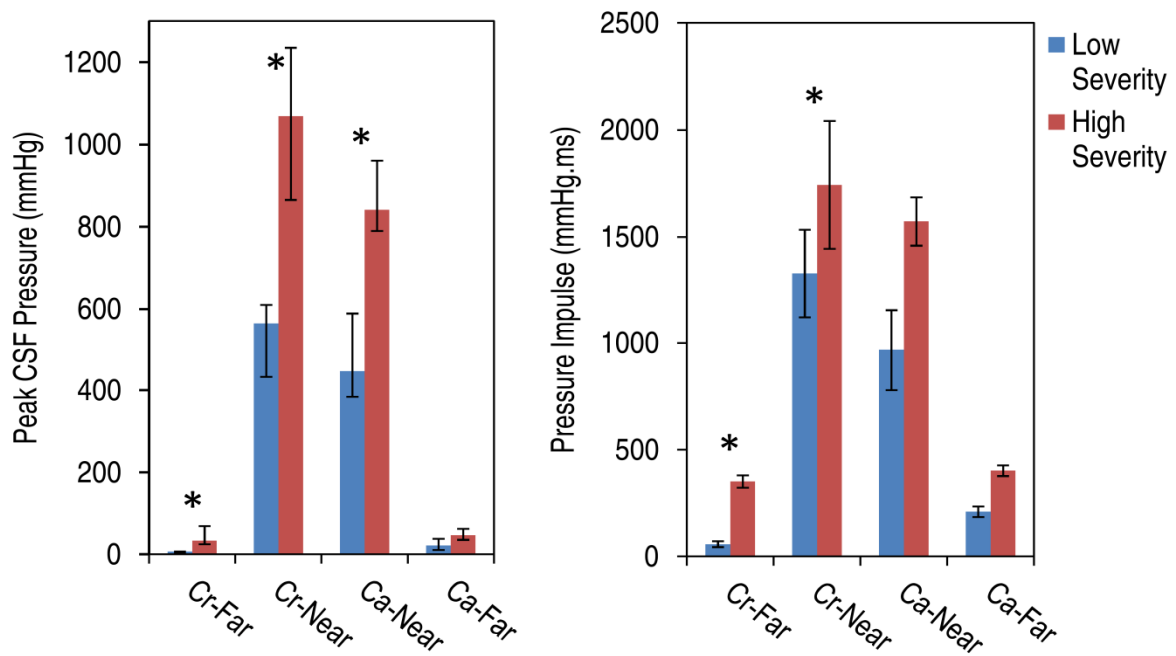
Figure 3-4 Peak positive CSF pressure and pressure impulse at each transducer location, for the two injury groups. Bar is median value, error bars are 25th%ile/75th%ile. * indicates statistical significance (p<0.05).

There was no significant association between the cranial/caudal location and the magnitude of the pressure peak or impulse at either the "near" or "far" transducers. Wave speed was significantly greater on the caudal than the cranial side (mean 1.2-1.8 times), while attenuation factor tended to be greater for the cranial side, but did not reach significance (Table 3-3, Table 3-4).

Table 3-4 Results of the Wilcoxon Rank Sum (matched-pairs) tests comparing the cranial and caudal test parameters. Statistically significant results (p<0.05) are in bold.

Parameter	p-value
"Far" peak positive pressure	0.100
"Far" pressure impulse	0.272
"Near" peak positive pressure	0.136
"Near" pressure impulse	0.071
Wave speed	**0.010**
Attenuation Ratio	0.084

3.3.3　Histology

The high injury severity animals had less white and grey matter sparing at and around the injury epicentre than the moderate severity animals; however, this difference was statistically significant only at the injury epicentre and 1.6 mm cranial and caudal to the epicentre (Figure 3-5, left). The longitudinal extent of the tissue damage did not appear to be different for the two injury severity groups. The cumulative sparing between 8 mm cranial and 8 mm caudal to the epicentre was higher for the moderate severity group than the high severity group, but the difference was not statistically significant (p=0.109) (Figure 3-5, right). Example photographs of microscope images are shown in Figure 3-6.
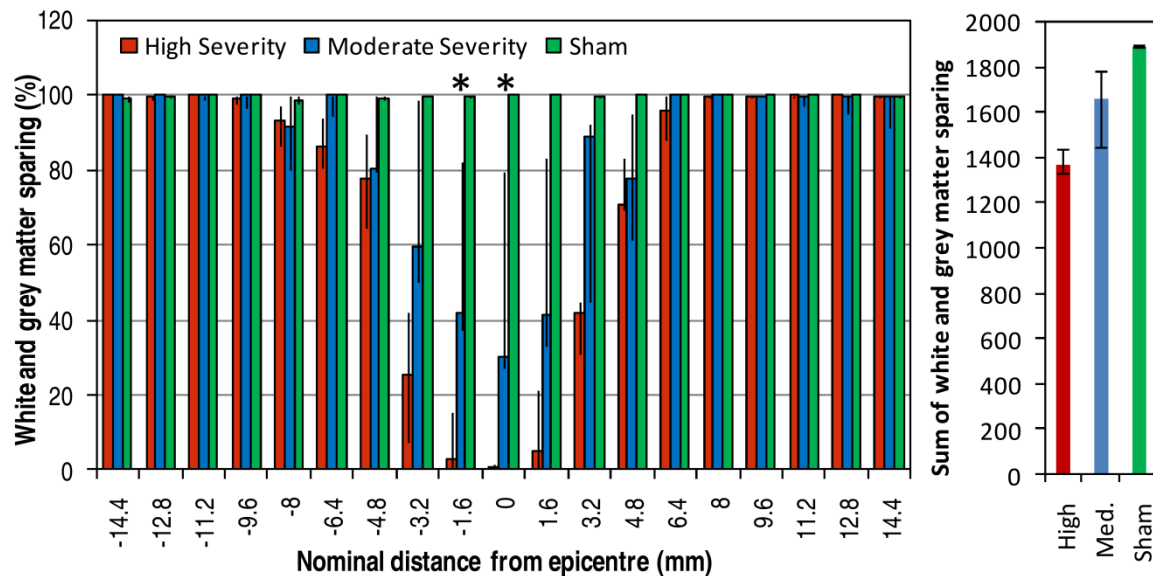
Figure 3-5 White and grey matter sparing (%) for the high, moderate and sham animals (left) and cumulative white and grey matter sparing from 8mm cranial and caudal of the epicentre (right). Data are presented as median ± $25^{th}/75^{th}$ percentile. * indicates significant difference (p<0.05) between the high and moderate injury severity as per Mann-Whitney U-test. Sham animals are shown but no statistics were performed on this group due to low numbers.
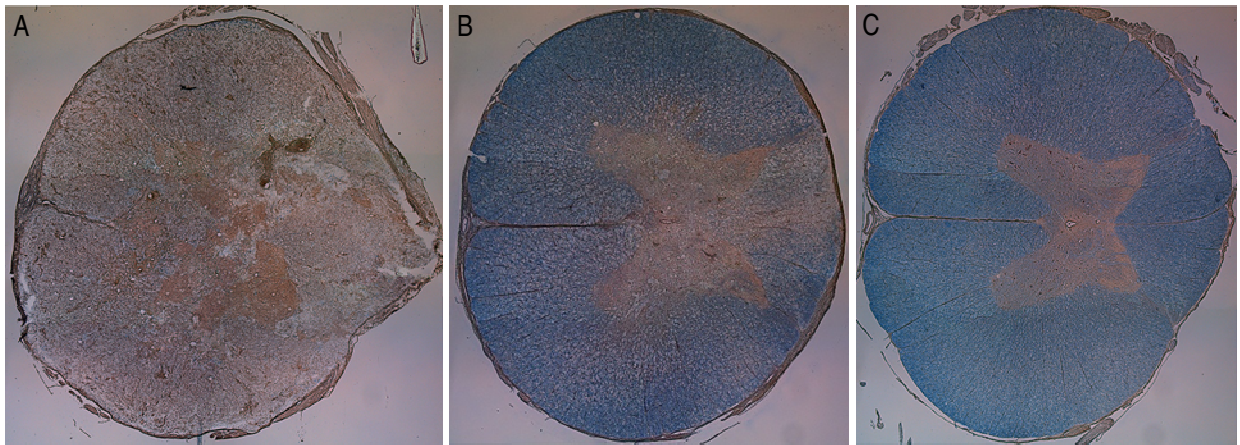
Figure 3-6 Photographs of microscope sections stained with eriochrome cyanine: (A) High severity injury animal (P1805) at epicentre, 0% tissue sparing; (B) Moderate severity animal (P1697) 3.2 mm caudal of epicentre, 60% tissue sparing; (C) Sham animal (P1628) at epicentre, 100% tissue sparing.

3.4 Discussion

Pressure transients propagating away from the injury site in the CSF may contribute to tissue damage at locations away from the mechanical insult, but this fluid response has not been well characterised in a model which accurately replicates the mechanical characteristics and scale of human SCI. In this study we have demonstrated the utility and repeatability of a novel large animal model of thoracic contusion SCI, and have measured the cranial and caudal CSF pressure variation associated with two simulated bony impingement velocities approximating moderate and high severity human SCI. We described the injury with parameters of impact velocity, dural displacement, peak force and impulse. The CSF pressure wave was characterised with the parameters of peak pressure, pressure impulse, attenuation ratio and wave speed.

To the authors' knowledge, CSF pressures relating to the acute SCI event have been investigated only in synthetic/cadaver models [469,515], in two cats subjected to a weight-drop experimental SCI [1,2] and in dogs receiving a closed-column impact [3]. Dynamic CSF and neural parenchyma pressures have also been measured intracranially in various models of TBI [290,313,314,342,486,490], and in the spine during simulated whiplash [e.g. 287,289]. In general, the form of the pressure profiles measured in this study was similar to those reported for impact of the brain and spinal cord. A notable difference was the absence of an appreciable negative pressure trough preceding the positive pressure peak at both locations. We observed this at the far location in previous tests using a similar injury model when 1) transducers were implanted at each far location only, 2) more severe injuries were applied and, 3) a spherical impactor tip was used [516]. It is not apparent if these or other factors contributed to this difference.

The peak pressures measured at the "near" locations were in excess of normal values that have been recorded in recumbent large animals, 8.8-10 mmHg [100,101] and humans, 6.6-20.6 mmHg [60,64,517]. Comparing our closest condition of the "near" transducers with the moderate severity injury, our peak pressure range of 96.7-680.2 mmHg, is considerably higher than the 50 and 150 mmHg peaks recorded by Hung [1] and Albin [2] at 25 and 15 mm, respectively, from the injury. This may be due to differences in animal size, injury parameters (15g-25cm, 20g-15cm compared to 20g-32cm) and pressure transducer configuration. Wennerstrand et al. [3] report a peak pressure of 1960 mmHg at 60 mm from the injury site for a dog subjected to an external lateral impact. This is around three-fold higher than the present study, but it is difficult to reconcile these 2kg-20m closed-spine impacts with our open weight-drop SCI. All of these studies used a pressure transducer that was coupled to the subarachnoid space via a catheter and tubing which can cause damping of the signal; the latter attempted to adjust for this by applying correction factors determined with a bench model and reference transducer [3]. Our transducers were indwelling and therefore probably gave a more accurate measure of the pressure acting on the neural tissue.

The reduction in peak pressure and impulse, and increase in pulse duration, from the "near" to "far" locations was expected and is predominantly due to damping of the wave via energy absorption and dissipation in the spinal cord, fluid and dural tissues. A small contribution could also be due to the orientation of the "near" and "far" transducers. The length of the pig spine and the transducers meant that the "far" transducers had to face away from the injury site, while the "near" transducers were able to face towards the site. Hence the pressure recorded by the "near" transducers likely included a dynamic pressure component, proportional to the fluid velocity squared, while the "far" transducers did not. However, in this closed system the fluid bulk velocity induced by the impact is probably small, particularly at the "far" location, and so the pressure difference caused by transducer direction is probably minimal. In general, the pressure peaks measured at the "far" location (range 1.7-93.0 mmHg, relative to pre-injury baseline) were of a similar order of magnitude to increases measured in humans during transient increased intra-abdominal pressure (10.5 mmHg Valsalva manoeuvre [64]), jugular occlusion (10.7 mmHg, Queckenstedt's test), and coughing (~50 mmHg) [63]. These have no physiologic effect when performed transiently and normal autoregulation mechanisms are functioning. Therefore, it would be reasonable to conclude that pressure-induced injury is unlikely at the "far" location. The 10 to 100-fold attenuation ratios also indicate that for the injury severities used in this study, sufficient energy is absorbed from the fluid into the cord and dura by at least 100 mm from the injury site. Rapid wave amplitude damping with distance from the mechanical insult was reported by Wennerstrand [3] - pressures of around 2000 mmHg were recorded at 60 mm from the site of impact, and were reduced to 30 mmHg at 450 mm away. Attenuation ratios of 0.4-1.8 per cm can be derived from those data; the

generally higher attenuation in our study (1.3-15.4 per cm) may be because of the very different injury mechanism used, and because the dorsal spinal canal and epidural contents were partially removed.

The pressure wave speed exhibited large variation and its magnitude appeared independent of the injury parameters. The speed of the wave propogation may have been influenced by the material properties of the spinal cord and dura, the thickness of the dural layer, and any stress wave or motion that propagated within the spinal cord and epidural contents. The modest differences in caudal and cranial response, although limited to wave speed and marginally attenuation ratio, may indicate that the end condition (cranially the ventricles and brain, and caudally the lumbar cistern) has a limited effect on the fluid wave propagation.

To the authors' knowledge, there is no established pressure tolerance value for the bulk spinal cord or its cellular constituents. However, two techniques that are used to study TBI induce the injury using fluid pressures that are transmitted through the CSF, without direct contact with the brain; these are the blast overpressure and fluid percussion models. We recognise that tissue tolerance can be specific to the conditions of the external loading, the geometry of the anatomy and local tissues differences such as vasculature, metabolic processes and cellular distribution. Despite these limitations, the TBI studies provide evidence that the pressure measured in the current study may have sufficient magnitude and duration to elicit an injury response in neural tissue. Recent studies investigating diffuse axonal brain injury due to blast overpressure exposure have indicated that pressure-related injury thresholds may be lower for neural tissue than other soft tissue and organs [351]. Animals exposed to external blast overpressures ranging from 75 to 7500 mmHg have exhibited reduced performance in physical tests and degeneration of cerebral cortex neurons [340], injury to neuronal and glial cells, and brain edema [344-349], brain haemorrhage and edema [342], morphological changes to neurons [351], damage to central visual pathways [343] and elevated intracranial pressure and impaired cognitive function [341].

With the fluid percussion TBI model the pressures resulting in a moderate to severe mixed focal and diffuse injury typically range from 1000 to 3000 mmHg, with an impulse duration of around 20 ms [e.g. 313,314,319]. Mild injuries are reported for pressures as low as 300 mmHg [312,316,317]. Several studies have measured pressures in the brain parenchyma, ventricles and intracranial space that are similar to the applied external pressure for both the blast [337,338] and fluid percussion [313-315] models. All of the pressures measured at the "near" location, and some at the "far" location were within the ranges associated with blast and fluid percussion TBI. *In vitro* cell preparations have also been subjected to pressure impulses to induce injury, with magnitudes similar to those recorded in our study. Neuronal and glial cells exposed to fluid pressure impulses of 1550 mmHg [331] and 362-3050 mmHg [332] show cell damage and reduced viability. These preparations typically restrict the ability of the

tissue to undergo concomitant strain deformation [307], which provides support for the mechanism of pressure induced injury in the absence of other mechanical loading.

The pressure *impulse* (as opposed to the peak pressure) for the various models discussed above is not commonly reported. However, it has been noted that pressure impulse may be a superior injury determinant than peak pressure for some cells [518], and load impulse is commonly used in injury biomechanics as tissue tolerance is often better expressed by both the magnitude of a load and the duration of its application. For the fluid percussion model in cats, Hayes et al. [312] reported irreversible apnoea with a fluid impulse in the brain of 7600 mmHg.ms, while Saljo et al. [342] measured impulses ranging 37-590 mmHg.ms and reported cellular damage in the brain of pigs subjected to low impulse noise from firearms. The impulses recorded at the "near" location in our study are between these two ranges, and at the "far" location are generally within the range of Saljo et al. [342]. The paucity of data makes it difficult to draw definitive conclusions about the likelihood of cellular injury with a pressure impulse criterion, but these limited data indicate that a diffuse cellular injury may occur.

The histology results indicate that the higher velocity injury caused greater tissue damage at and around the epicentre, as expected. Both the high and moderate severity animals had a further eight hours of static compression after the dynamic injury and it is not possible to separate damage that occurred due to the initial impact and post-injury ischaemia due to the compression. Although the tissue damage appeared to have a greater cranial-caudal extent in the high severity animals compared to the moderate severity animals, this was not statistically significant and cannot be specifically attributed to the differences in dynamic CSF pressure parameters. The small difference in tissue sparing between the moderate and high severity animals, despite the significant differences in peak impact force, load impulse, impact velocity, peak CSF pressure and pressure impulse, may be due to the eight hours of sustained compression that was applied to both groups (see section 3.2.4). It should be noted that the histological methods employed in this study were not intended to be sufficient to observe any diffuse or subtle cellular damage that may have occurred, either at or remote to the injury epicentre, as a result of fluid loading. Due to financial constraints we were not able to complete histological analysis of the tissue remote to the impact site and chose to focus instead on providing evidence that the injury model had similar lesion characteristics to human contusion SCI. Future studies may elect to utilise immunohistochemistry methods specifically focussed on diffuse axonal injury and other more subtle cellular dysfunction in the more remote tissue.

The pig injury model faces challenges common to all large animal studies; most notably time, cost and complexity. However, it offers many advantages over the conventional rat SCI models, the most pertinent being the approximate human scale, the associated presence of CSF, and the similarities to human anatomy and physiology. Specific limitations include the necessary alteration of the

biomechanical system by laminectomy, removal of the ligamentum flavum and dorsal epidural fat, and insertion of the transducers. The laminectomy width and length was minimised, and by using small and flexible transducers we minimised their effect on mechanical response. While the transducer faces were not shielded, each fibre ran parallel to the cord in the intrathecal space and the sensing face was on the cross-section of the fibre thus minimised the possibility of contact with the dura or spinal cord. There was a learning curve associated with transducer insertion which probably led to the differing pre-injury CSF pressure between the two groups; however, this is unlikely to have altered the observed trends due to the large difference in the injury parameters for the two groups. An accelerometer was not mounted on the impactor due to space and mass limitations, so the impact forces were not inertially compensated. The mass of the impactor tip (below the load cell) was 1.39 g and according to Newton's second law this would require a correction of less than 10%.

3.5 Conclusion

The magnitudes of the transient peak CSF pressure and the CSF pressure impulse resulting from experimental contusion SCIs are dependent on the injury velocity and distance from the injury site. When compared to previous studies that have found a relationship between exposure to pressure impulses and cellular damage in the brain, the peak pressures measured at 30 mm from the injury site indicate that the severity of primary tissue damage may be affected by the propagating fluid pressure wave. The cranial-caudal extent of cellular damage may be limited by the damping effect of the neural and dural tissue, which in this study reduced the pressure close to normal ranges within 100 mm of the injury site. These data suggest that the design and implementation of future animal, cadaver and computational models that seek to accurately replicate the biomechanics of human SCI should consider the inclusion of CSF, and these data will be valuable for validating such models.

Chapter 4 The CSF Layer, Impact Velocity and Mechanical Indicators of Injury Severity[3]

4.1 Introduction

The cerebrospinal fluid (CSF) is thought to protect the spinal cord from injurious loading by the spinal canal during everyday activities of living. However, during spinal fractures such as burst fractures bone fragments can be forced into the canal at high velocity and it is unclear the extent to which CSF provides protection in this scenario. Biomechanical studies of burst fracture have shown that the maximum canal encroachment is greater than that seen on post-injury imaging [133,461]. Clinically, post-injury spinal canal encroachment does not correlate well with initial paralysis severity [519] and is not a good predictor of neurological outcome [136,520]. In addition, the physical mechanism with which load is applied to the spinal cord (i.e. through contusion, dislocation or distraction of the spinal column or cord) can affect the nature and extent of the tissue damage [142,422]. A better understanding of the contribution of the various anatomic components to the biomechanics of the injury event may inform the limitations of current SCI models and lead to improved risk metrics, prevention strategies, prognostication and targeted therapies.

Current risk metrics for SCI such as the Torg ratio [145,146] and the proposed "space available for cord" [147] are based on the sagittal dimension of the canal and the canal plus cord, respectively, and do not consider the amount of CSF surrounding the cord. However, the dimensions of the canal at levels adjacent to an SCI have been found to have limited predictive value for SCI risk in the thoracolumbar spine [135,136]. Incorporating a measure of the thecal sac may improve the predictive value of such SCI risk metrics. The thickness of the CSF layer varies along the length of the spine, as does the size of the cord and canal [391,394]. Furthermore, some researchers have suggested that pressure waves propagated in CSF at the time of injury may contribute to neural damage away from the primary injury site [1,3,162,285]. Because estimating pre-injury tissue dimensions is challenging in SCI patients, and because the extent of protection offered by various thicknesses of CSF layers is unknown, biomechanics studies may provide valuable new information on the role of the CSF in SCI.

The biomechanics of the SCI event have been investigated with respect to anatomical components such as the CSF, dura and spinal ligaments, using animal, cadaver, and physical models. Dynamic CSF

---

[3] A version of Chapter 4 is in preparation for publication. Jones CF, Kwon BK and Cripton PA. CSF pressure transients, cord deformation and load transmission are affected by CSF thickness and impact velocity in a bench-top model of contusion type SCI.

pressures associated with experimental SCIs have also been measured in cats [1,2], dogs [3] and pigs (Chapter 2&3), with peaks ranging from 50 [1] to 2000 mmHg [3]. Spinal canal pressure transients associated with burst fracture events from axial impacts have been measured in a lumbar cadaveric model with fluid filled dura but no spinal cord [473], and in a cadaver head-neck model with a synthetic spinal cord but no fluid component [515]. The former recorded pressure waves of 217-2415 mmHg associated with burst fractures [473], and in the latter, pressures ranging from 83 to 1500 mmHg corresponded to compression and burst fractures [515].

Several biomechanical models have sought to characterise spinal cord compression and strain response to simulated burst fracture type injuries. Synthetic spinal cords made from silicone gel [471,521] or gelatin [469] and placed within synthetic or cadaver head-neck models have been used to visualise cervical cord strain [471,521] and spinal cord loading [469] during head-first impacts. However, these models did not incorporate a fluid component. Models of burst fracture SCIs using suspended e*x vivo* bovine spinal cords [462] and silicone elastomer surrogates [280,281] impacted with a synthetic bone fragment projectile, have shown that the posterior longitudinal ligament [462], the presence of CSF [280,281] and increased bone fragment contact area [281] all reduce maximum spinal cord compression, but dura alone (without CSF) does not [280,462]. In these studies the spinal cord could not be directly visualised with the high speed camera because it was encased in dura and the researchers assumed that the fluid was displaced prior to cord compression.

Generally, animal and cadaver models generate a limited amount of data due to ethical and economic considerations. Further, in such experiments it is difficult to control and/or measure some of the injury parameters, such as the baseline dimensions and transient compression of the spinal cord and CSF layer. Therefore, we constructed a physical model of the spinal neural system, including spinal cord, dura and CSF elements, with mechanical properties that approximated the native tissues. The aim of this study was to investigate the effect of thecal sac size and impact velocity on CSF pressure, impact forces and cord compression. We hypothesised that these parameters would be inversely proportional to thecal sac size and directly proportional to impact velocity.

4.2 Methods

4.2.1 Surrogate cord and dura

The model consisted of a synthetic spinal cord with round cross-section (diameter 10 mm, length 55 cm) made from QMSkin30 [470] dosed with barium sulphate to make it radiopaque with an Aluminum equivalent of 8.8 mm. We had previously selected this material as an appropriate surrogate for perfused, *in vivo,* spinal cord material, and characterised its mechanical response in quasistatic uniaxial tension and compression [470], and dynamic transverse compression [280]. A synthetic dura was

made from polyethylene plastic (4361NN40, 4.0 gauge lay flat tubing, Buyers Packaging Group, Delta, BC, Canada) formed into tubes 60 cm length and nominal diameters of 12, 18 and 24 mm using a heat sealer. The ratios of the synthetic dura to cord diameter were 1.2, 1.8 and 2.4, respectively. To the authors' knowledge, no studies have reported paired measurements of cord and dura diameter; however, the ratios of mean dura to mean cord diameter in the human thoracic region ranges from 1.6 to 2.4 [391,394,522]. If the standard deviations are applied to the means, then limits of the dura:cord ratio expand to 1.1 to 4.0 [391,394,522].

Tensile tests of the dura material were performed on 40x5 mm rectangular samples of the plastic with a materials testing machine (Dynamite 8841, Instron, Canton, MA, USA) with using a 22.24 N range load cell (31 Mid, Honeywell, Morristown, NJ, USA; linearity ±0.15% full scale) and the built-in linear variable displacement transducer (position accuracy 0.25 mm). A preload of 0.1 N was applied, followed by a preconditioning protocol of 15 sinusoidal cycles to 0.8 mm (2% strain) at 1.25 Hz, and then a constant strain of 0.166 mm/sec (0.4/s) until 200% strain. Data were acquired at 200 Hz. The thickness of the plastic was measured on 10 samples using Vernier callipers (G06089154, STM, Kitchener, ON, Canada). We compared the behaviour under tensile loading to published data for human and bovine spinal dura, and unpublished data from our laboratory for Yucatan Miniature pig spinal dura.

4.2.2   Physical model and weight-drop device

The spinal cord and dura were fixed horizontally in a custom device consisting of a series of stands that could be moved in the axial direction and therefore allowed the two materials to be tensioned independently (Figure 4-1, Figure 4-2). The dura was connected at either end to an acrylic reservoir with a volume of 250 mL and diameter 56 mm, which was fitted with an inlet matching the dura diameter. The reservoir at the right was fixed, and that on the left could be adjusted axially. The spinal cord was connected at either end to a shaft that passed through the reservoir, a seal and a bearing. The shaft was attached to a fixed stand on the left, and to a load cell which is referred to herein as the "tether" load cell (22.24 N, Model 31Mid, Honeywell, Morristown, NJ, USA; linearity ±0.15% full scale) and adjustable stand on the right. The adjustable stands were mounted on linear sliders with calibrated lag screws (UniSlide A2506Q1-S2.5, Velmex, Bloomfield, NY, USA) to allow specific strains to be applied to the cord and dura independently. A strain of 7% was applied to the cord; this was similar to other synthetic models [280,281,462] and *in vivo* strains measured in humans [523] and animals [259]. The surrogate dura was fixed at approximately 1% strain, because its stiffness approximated that of native dura in the upper linear portion, rather than the extended linear "toe-region", of the tensile stress-strain curve. The space between the spinal cord and dura was filled with distilled water, and air was expelled from the system, via the ports in each reservoir. Distilled water has similar rheological properties to CSF [264,265]. A hydrostatic pressure of 10 mmHg, representative of human physiologic mean CSF pressure

126

[54,57-60], was applied with a sealed water column attached to one reservoir. The underside of the dura was supported with three flat plates to simulate the spinal canal. The height of the plates was adjusted for each dura size such that they just contacted the underside of the dura with minimal deformation of its circular cross-section. The smaller central plate was fitted with a load cell (222.41 N, WMC-50-456, Bose, Eden Prairie, MN, USA) which is referred to herein as the "base" load cell. Tests were completed at room temperature (21 °C).
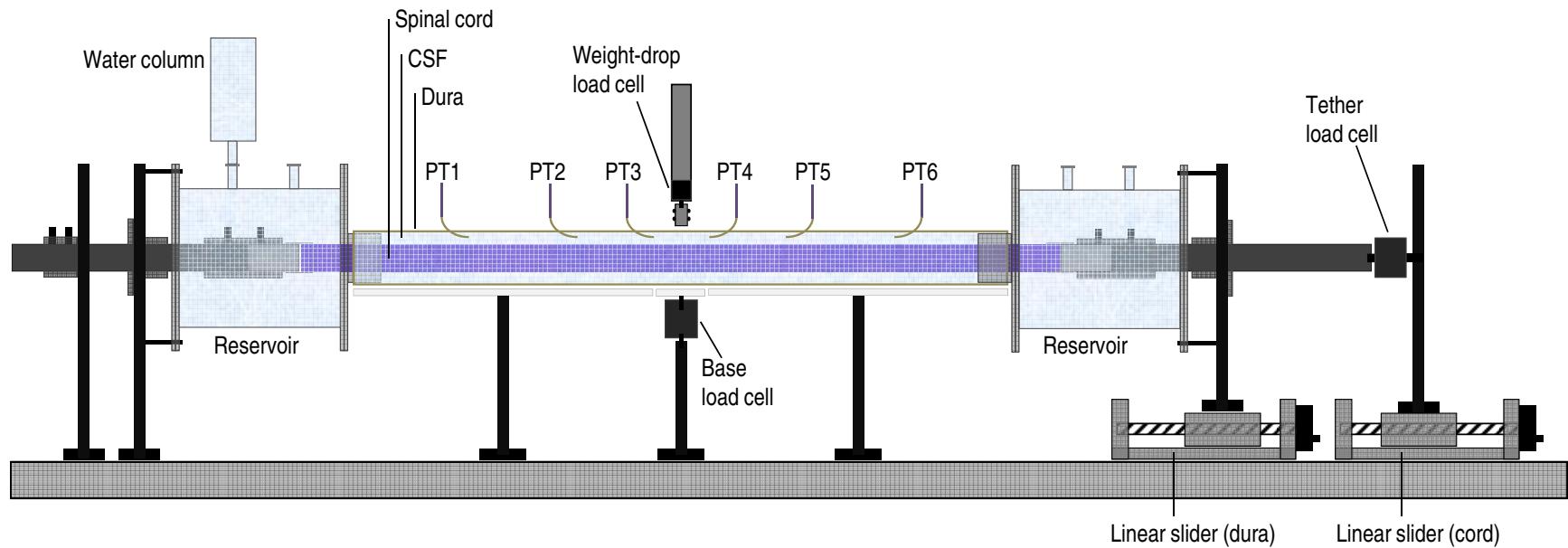
Figure 4-1 Schematic of the synthetic spinal cord and dura model (not to scale). For clarity, only the impactor of the weight drop device is shown, and the high speed x-ray is not depicted. PT= pressure transducer.
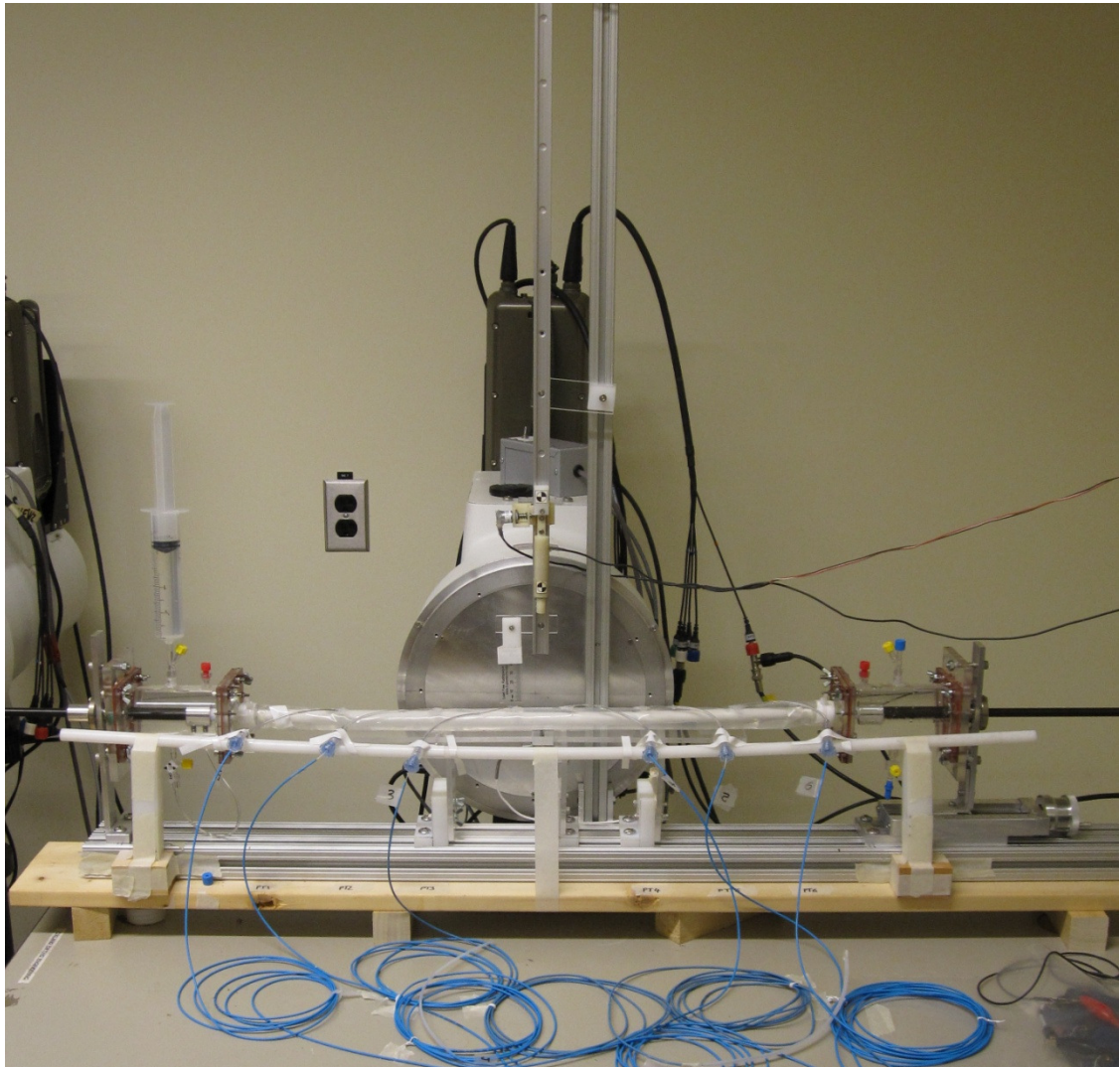
Figure 4-2 Photograph of the experimental setup. The x-ray source was directly below the position of the camera for this photo.

The spinal cord-dura construct was impacted with a modified weight-drop SCI device that was described in detail in Chapter 3. Briefly, an impactor instrumented with a load cell was released from heights of 10, 32, 75 and 125 cm and travelled down a guide rail positioned orthogonal to the spinal cord. These heights were selected to produce theoretical impact velocities of 1.6, 2.5, 3.8 and 4.9 m/s, which are within the range estimated for burst fractures [132,134,460] and the velocities used for large animal weight-drop models of SCI (Section 1.6.4). The upper and lower velocities also corresponded to those used in the *in vivo* pig studies (Chapter 3). The guide rail was modified so that it could be mounted on the table, and four 1 mm diameter steel balls were added to the impactor tip so that high speed x-ray could be used to determine the impactor velocity. The beads were placed bilaterally in the mid-plane at 6 and 11 mm from the tip of the impactor.

4.2.3   High speed x-ray

High speed x-ray was used to visualise the impactor, dura and spinal cord. The high-speed x-ray system consisted of an x-ray tube and generator (Comet MXR-160, TSG X-ray, Atlanta, GA; Gulmay FC-160 640W, TSG X-ray, Atlanta, GA) operated at 40- 45 kV / 7.5-8 mA and an image intensifier (PS93QX-P20, Precise Optics, Bay Shore, NY) with an integrated high-speed camera (Phantom V12, Vision Research, Wayne, NJ). The image intensifier was operated at 4 inch magnification and the camera at 6000 frames per second and 512x512 resolution. With these settings the x-ray system has a resolution of 2.2 lp/mm (0.23 mm/pixel) (Appendix B). The source to image intensifier distance was 106 cm, with the model approximately 6 cm in front of the intensifier. High speed x-ray video was captured with Phantom software (v675, Vision Research Inc., Wayne, NJ, USA). The pixel-to-mm scale was determined with a radiopaque ruler (15 mm, 1 mm graduations) suspended in the central plane of the spinal cord and impactor. The impact location was situated in the centre of the image intensifier where image distortion is minimal.

4.2.4   Pressure transducers

Pressure transducer ports, consisting of 19 Ga catheter, 2 mm diameter pressure tubing and a compression fitting (Tuohy Borst adapter 84044/80369, Quosina, NY, USA), were attached to the superior aspect of the dura at 30, 100 and 200 mm from the centre of the dura, using flexible plastic adhesive. CSF pressure was measured at the six locations with miniature fiber-optic pressure transducers (Preclin 420LP/360HP with Samba202 control unit, Samba Sensors, Sweden) (Table 3-1). Low range transducers were placed at locations 1 and 6 (200 mm from epicentre) and high range pressure transducers were placed at locations 3 and 4 (30 mm) for all tests. At locations 2 and 5 (100 mm from epicentre) high and low range transducers were used depending on the pressure range required for the particular drop height. All transducers were aligned approximately parallel with the axis of the spinal cord and were directed towards the impact site. The Samba 202 control units sampled at 20 kHz, from which an analog signal was produced and output to a data acquisition system. The pressure data were synchronised with the load data and high speed x-ray camera trigger signal, and all were acquired at 10 kHz.

4.2.5   Test protocol

Five replicate tests were carried out for each combination of dura size (small, medium, large) and drop height (10, 32, 75, 125 cm). Five tests were also completed at each height with dura but no CSF present, using the medium size dura.

4.2.6   Data and image analysis and statistics

All data processing and analysis was completed with custom Matlab programs (V7.11.0 R2010b, The Mathworks, Matick, MA, USA), unless otherwise specified.

For the surrogate dura tensile tests, the load and displacement data were filtered with a two-way 4th-order low-pass Butterworth filter with a cut-off frequency of 5 Hz. The specimen area used to determine the stress was the specimen width multiplied by the average of the measured thicknesses. For each specimen the elastic modulus was determined as the slope of the line of best fit between zero and around 4% strain.

For the impact tests the load and pressure data were filtered with a two-way 4th-order low-pass Butterworth filter with a cut-off frequency of 2 kHz to remove high frequency noise. The baseline pressure was determined (from transducer location 6) for one second before impact. The peak positive and negative pressure was determined at each transducer location. The peak load was determined for the impactor, base and tether load cells.

The x-ray images were undistorted using open source software XrayProject (V2.1.8, www.xromm.org, [524]) (Appendix B) and denoised using custom 3D curvelet image denoising software developed with the open source CurveLab toolkit (V2.0, www.curvelet.org, [525]). The location of the steel balls on the impactor tip was tracked using TEMA (V3.2-024, Image Systems AB, Linköping, Sweden). The instantaneous velocity of each ball for each data point before impact was determined using the central differences method. The impact velocity was defined as the average velocity of the four balls. The locations of the superior and inferior aspects of the spinal cord were manually segmented in the high speed video images (Figure 4-3). The baseline dura and cord diameters were defined as the average diameter in the ten images prior to contact between the impactor tip and the dura. The maximum cord compression was defined as the minimum distance between the inferior cord surface and the impactor tip (as determined from the steel markers). The superior surface of the cord was not used for this parameter because there was not sufficient contrast between the impactor tip and the spinal cord to distinguish the border between the two. The percent cord compression was calculated as the maximum cord compression divided by the baseline cord diameter.
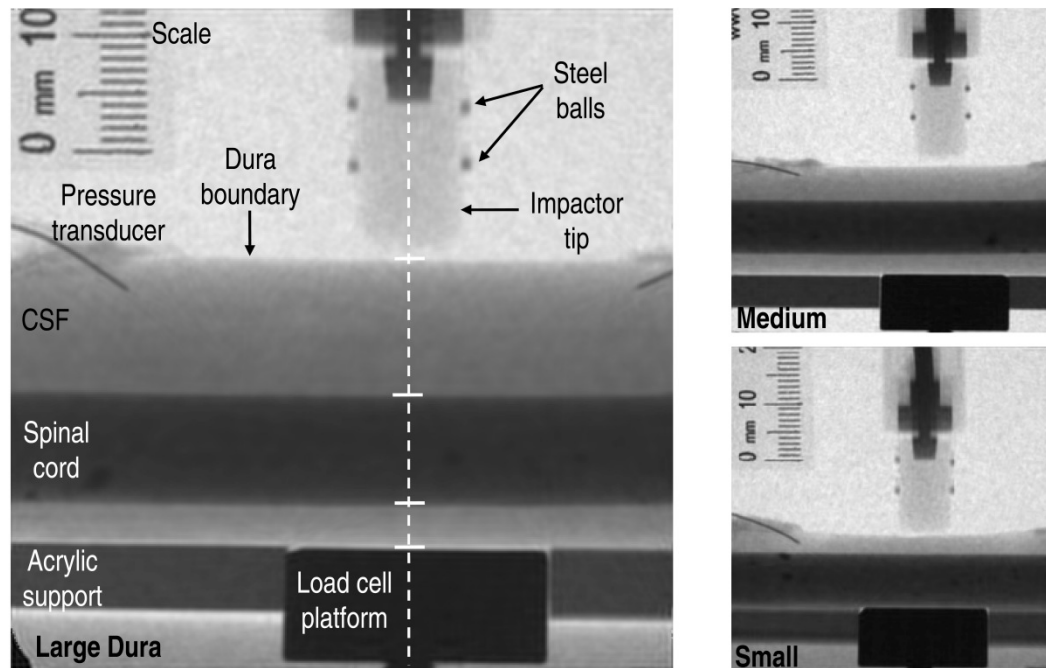
Figure 4-3 Typical high speed x-ray images with the large dura (left), medium (top right) and small (bottom right), immediately prior to contact between the impactor tip and the dura surface. In the image on the left, the solid horizontal lines on the dashed white line (central to the impactor) indicate the boundaries that were manually segmented to determine the baseline cord and dura diameters, and the maximum cord compression.

To demonstrate the relationships between the independent and dependent variables, a multiple regression model was determined for each independent variable: cord compression; impactor, base and tether loads; and the peak CSFP at each transducer location. The dependent variables were impact velocity, CSF dimension (i.e. dura diameter – cord diameter), and baseline CSFP. The models for the cord compression and loads included the "no CSF" case; this was excluded from the models for the CSF pressure. The baseline CSFP was not included as an independent variable for the cord compression and load models because it was not a relevant measure for the "no CSF" condition. It was initially included for the peak CSFP models, but was removed because it was not significantly different from zero ($p<0.05$).

4.3   Results

4.3.1   Tensile testing of synthetic dura

The plastic material used for the surrogate dura had an elastic modulus, between zero and 4% strain, of 188 MPa (SD 12 MPa) (Figure 4-4), which placed it within the upper range that has been reported for fresh-frozen human, bovine and porcine spinal dura (Table 4-1). The plastic thickness was 0.13 mm (SD 0.01 mm), which is at the lower end of that reported for human and porcine spinal dura (Table 4-1).

132
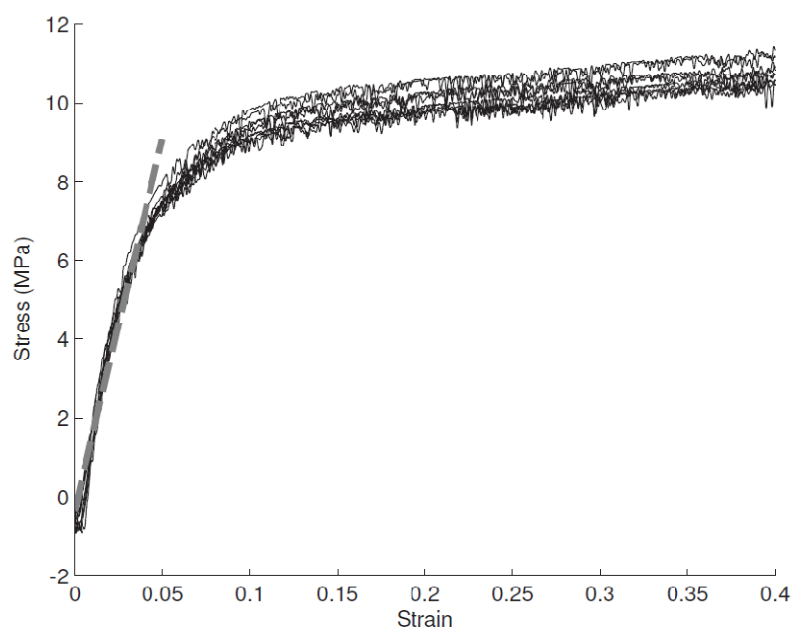
Figure 4-4 Stress vs. strain plot for tensile tests on 10 samples (black solid lines) of the plastic used to construct the surrogate dura. Dashed grey line is the mean line of best fit between zero and 4% strain.

Table 4-1 Elastic modulus (MPa) and thickness (mm) of human, bovine and porcine spinal dura from published data.

	Specimen Type	Average	Minimum	Maximum
Elastic modulus (MPa)				
Tencer 1985 [250]	Human	150.0*	67.8	238.7
Runza et al., 1999 [249]	Human	86.2†	43.0	143.6
Runza et al., 1999 [249]	Bovine	64.0‡	26.7	85.6
Unpublished§	Porcine	79.7	29.5	154.5
Thickness (mm)				
Tencer 1985 [250]	Human	0.27‖	-	-
Zarzur et al., 1996 [253]	Human	0.18¶	0.10	0.25
Leung et al.§ [526]	Porcine - Dorsal	0.26	0.11	0.48
Leung et al.§ [526]	Porcine - Ventral	0.15	0.10	0.31

*Mean and range derived from plots for cervical, upper and lower thoracic and lumbar dura.

†Average of minimum and maximum derived from plots of ranges for tissues tested fresh or frozen for 24 and 120 hr at -4°C.

‡ Average of minimum and maximum derived from plots of ranges for tissues tested fresh or frozen for 96 hr at -4°C or 4°C.

§Unpublished data (manuscript in preparation) from tests on cervical, thoracic and lumbar dura from Yucatan miniature pigs

‖ Presumed average of cervical, upper and lower thoracic and lumbar dura, range not given.

¶N=3

4.3.2   Model results

The impact velocity, cord and dura diameters, and baseline CSF pressure for all groups are listed in Table 4-2. The 10, 32, 75 and 125 cm drop heights resulted in mean impact velocities of 1.2, 2.4, 3.7 and 4.8 m/s, respectively. The impact velocity for the large dura at 10 cm drop height showed more variation than other test groups; the reason for this is not apparent. The mean cord size ranged from 8.96 to 9.69 mm, and the three dura diameters were a nominal 12.8, 19.2 and 24.8 mm. In general the cord was positioned below the centreline of the dura, but was raised off the lower border of the dura (Figure 4-3). The mean baseline CSFP ranged from 9.9 to 10.7 mmHg.

Table 4-2 Descriptive statistics for impact velocity, cord and dura diameter, and baseline CSF pressure for each combination of dura size and drop height.

Drop height (cm)	Velocity (m/s)		Cord size (mm)		Dura size (mm)		Baseline CSFP (mmHg)	
	Mean	SD	Mean	SD	Mean	SD	Mean	SD
Small dura								
10	1.23	0.05	9.00	0.05	12.67	0.17	10.12	0.18
32	2.45	0.01	8.97	0.05	12.77	0.13	10.13	0.06
75	3.66	0.03	8.96	0.07	12.71	0.36	10.08	0.16
125	4.76	0.03	8.98	0.06	12.90	0.14	9.82	0.11
Medium dura								
10	1.24	0.02	9.17	0.03	19.10	0.05	10.57	0.38
32	2.31	0.03	9.04	0.10	19.19	0.08	10.68	0.22
75	3.68	0.02	9.23	0.10	19.29	0.08	10.13	0.21
125	4.85	0.07	9.27	0.09	19.38	0.12	9.90	0.04
Large dura								
10	0.93	0.15	9.61	0.04	24.72	0.04	10.33	0.15
32	2.27	0.04	9.69	0.07	24.90	0.07	10.11	0.22
75	3.66	0.01	9.62	0.06	24.78	0.11	10.10	0.24
125	4.79	0.04	9.59	0.04	24.82	0.24	10.04	0.23
No CSF								
10	1.26	0.02	8.99	0.12	-	-	-	-
32	2.40	0.03	9.04	0.13	-	-	-	-
75	3.73	0.01	9.41	0.20	-	-	-	-
125	4.81	0.03	9.21	0.14	-	-	-	-
Overall								
10	1.16	0.16	8.98	0.06	-	-	-	-
32	2.36	0.08	9.18	0.12	-	-	-	-
75	3.68	0.03	9.63	0.06	-	-	-	-
125	4.80	0.05	9.16	0.22	-	-	-	-
Small dura	-	-	-	-	12.76	0.22	10.04	0.18
Medium dura	-	-	-	-	19.24	0.13	10.32	0.40
Large dura	-	-	-	-	24.80	0.14	10.14	0.22

Example data from a single impact on small dura with a 32 cm drop height is shown in Figure 4-5. The pressure transients were higher and earlier at locations closer to the impact site. The onset of loading appeared to be slightly delayed (~3 ms in this example) relative to the impactor-dura contact measured on the high-speed camera and the pressure rise at the 30 mm location. We speculate that this was due to elastic compression of the impactor tip.
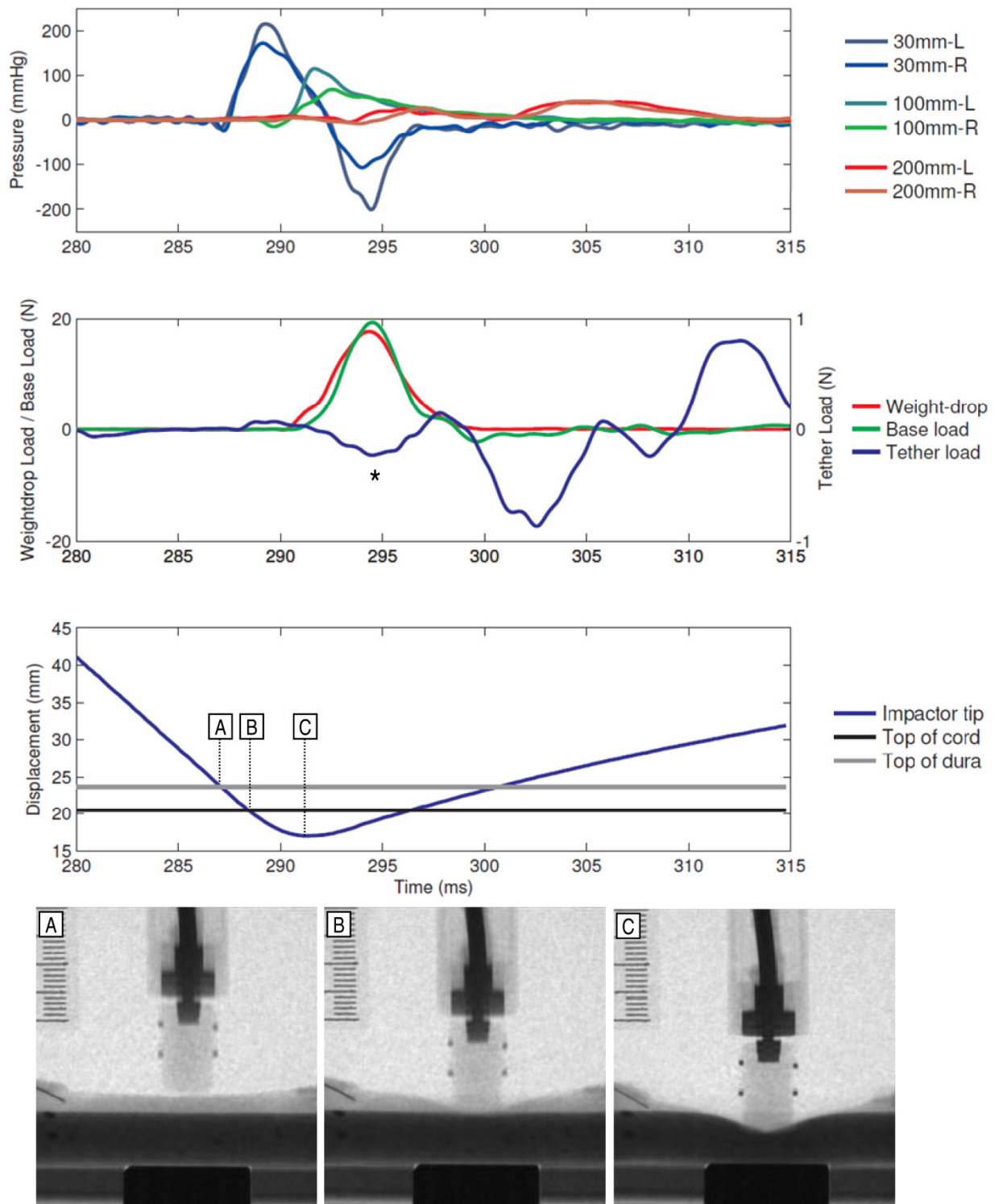
Figure 4-5 Representative data for one impact (small dura, 32 cm height drop), showing CSF pressure (top), loads (middle) and cord compression (bottom) versus time. Three frames of high speed x-ray illustrate (A) impactor-dura contact, (B) impactor-cord contact and (C) maximum cord compression. Note that in the central plot the Tether load is represented by the axis on the right, and the peak tensile tether load was taken at the location marked by *. Compressive load is positive and tensile load is negative.

Cord compression was directly proportional to drop height and inversely proportional to the thickness of the CSF layer. Compression did not occur at any drop height for the large dura size, or at the two lower drop heights for the medium dura size. Cord compression was greater than 18% for the no CSF condition and the small dura size for all drop heights. (Figure 4-6)
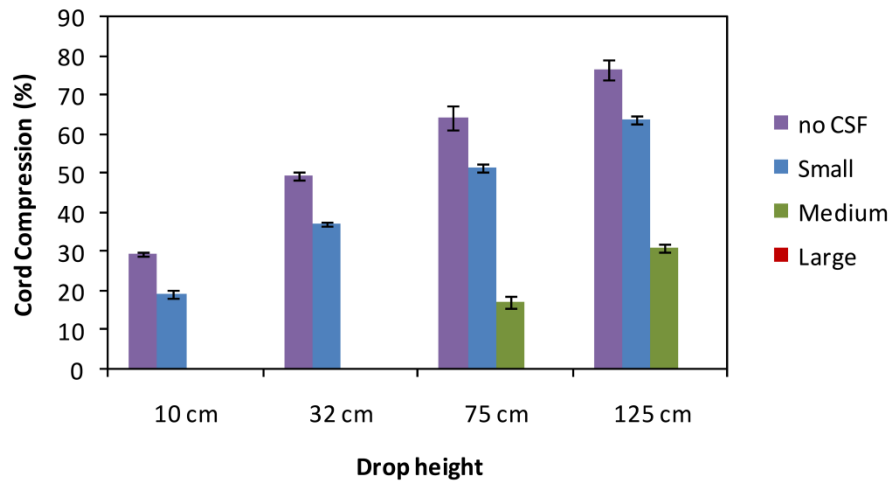
Figure 4-6 Cord compression (%) versus drop height for the noCSF condition and the small, medium and large dura sizes. (Mean ± SD). Note that there was no compression for the large dura at any drop height, nor for the medium dura at the 10 cm and 32 cm drop heights.

Both the peak impactor load (Figure 4-7) and the peak base load (Figure 4-8) were directly proportional to the drop height, and inversely proportional to the thickness of the CSF layer. The peak tether load increased with dura size and with drop height (Figure 4-9).
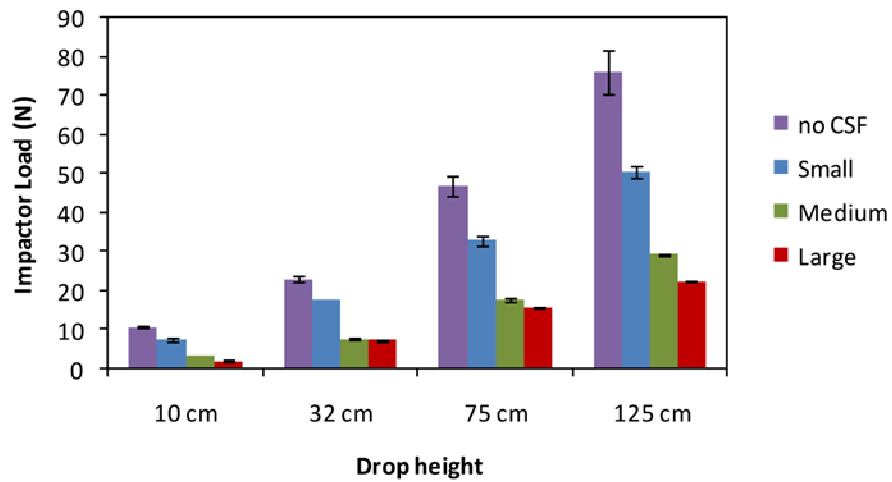
Figure 4-7 Impactor load versus drop height for the noCSF condition and the small, medium and large dura sizes. (Mean ± SD).
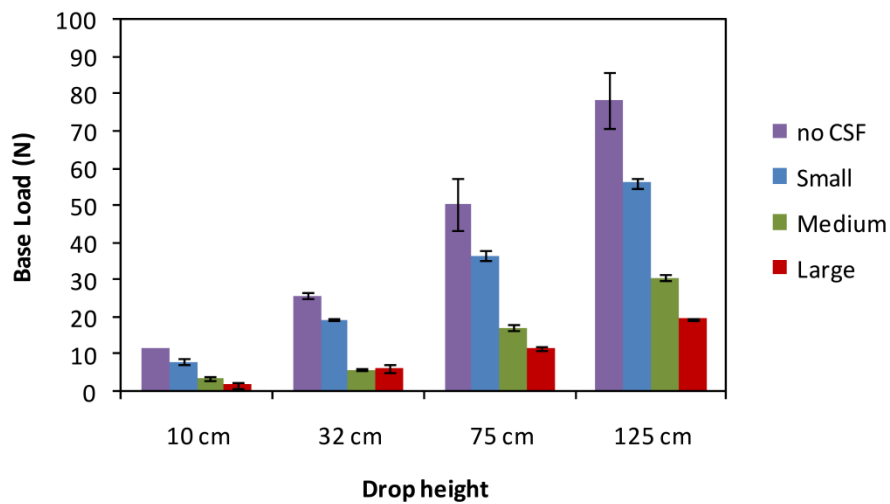
Figure 4-8 Base load versus drop height for the noCSF condition and the small, medium and large dura sizes. (Mean ± SD).
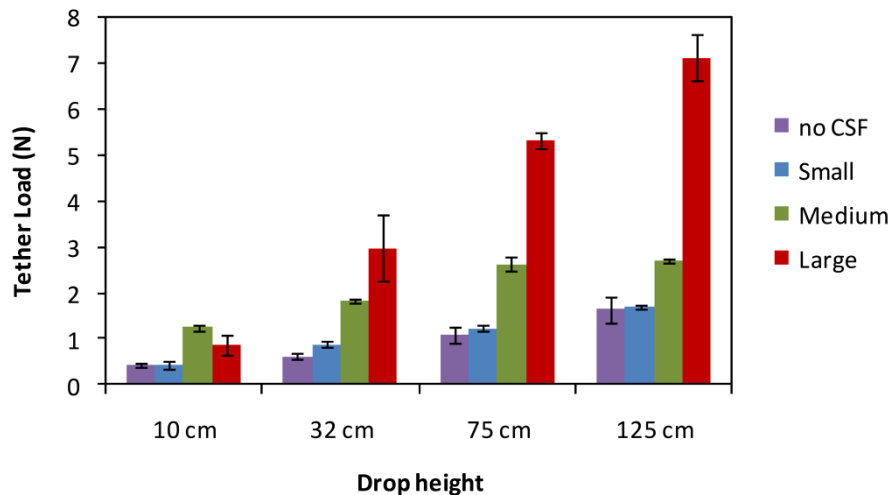
Figure 4-9 Spinal cord tether load versus drop height for the noCSF condition and the small, medium and large dura sizes. (Mean ± SD).

As expected, the impact velocity had a strong positive linear relationship with cord compression, impactor load, base load and tether load. There was a strong negative relationship between the CSF dimension and cord compression, impactor load and base load, i.e. increased CSF dimension resulted in decreased compression and loads at the impact site. In contrast, CSF dimension was directly proportional to tether load. In all cases the velocity had a dominant effect on the model, compared to the CSF dimension. The model accounted for between 74% and 83% of the variance in the four impact parameters (Table 4-3).

Table 4-3 Regression model coefficients for cord compression and impactor, base and tether loads. The models are based on the equation: $y = \alpha + \beta_1$ (impact velocity, m/s) $+ \beta_2$ (CSF dimension, mm). The p-values express the probability that the regression coefficient is equal to zero. The coefficient of determination, R^2, expresses the percentage of variance in y that is explained by the model.

	Coefficient	95%CI		p-value	R^2
Cord Compression (%)					
β_1 (velocity)	10.06	9.05	12.08	<0.0005	
β_2 (CSF dimension)	-3.31	-3.79	-2.84	<0.0005	0.80
α	19.54	11.99	27.09	<0.0005	
Impactor Load (N)					
β_1 (velocity)	10.49	9.13	11.84	<0.0005	
β_2 (CSF dimension)	-1.72	-2.04	-1.40	<0.0005	0.82
α	4.10	-0.99	9.19	0.113	
Base Load (N)					
β_1 (velocity)	10.81	9.35	12.26	<0.0005	
β_2 (CSF dimension)	-2.05	-2.39	-1.71	<0.0005	0.83
α	6.25	0.78	11.73	0.026	
Tether Load (N)					
β_1 (velocity)	0.72	0.57	0.87	<0.0005	
β_2 (CSF dimension)	0.21	0.17	0.25	<0.0005	0.74
α	-1.63	-2.19	-1.06	<0.0005	

The peak CSF pressure at each location was proportional to the drop height (i.e. velocity) and inversely proportional to the dura size. The magnitude of the CSF pressure wave decreased with distance from the impact epicenter for all dura sizes; for each dura size the attenuation was proportional to the drop height and the attenuation was greatest for the small dura size (Figure 4-10).
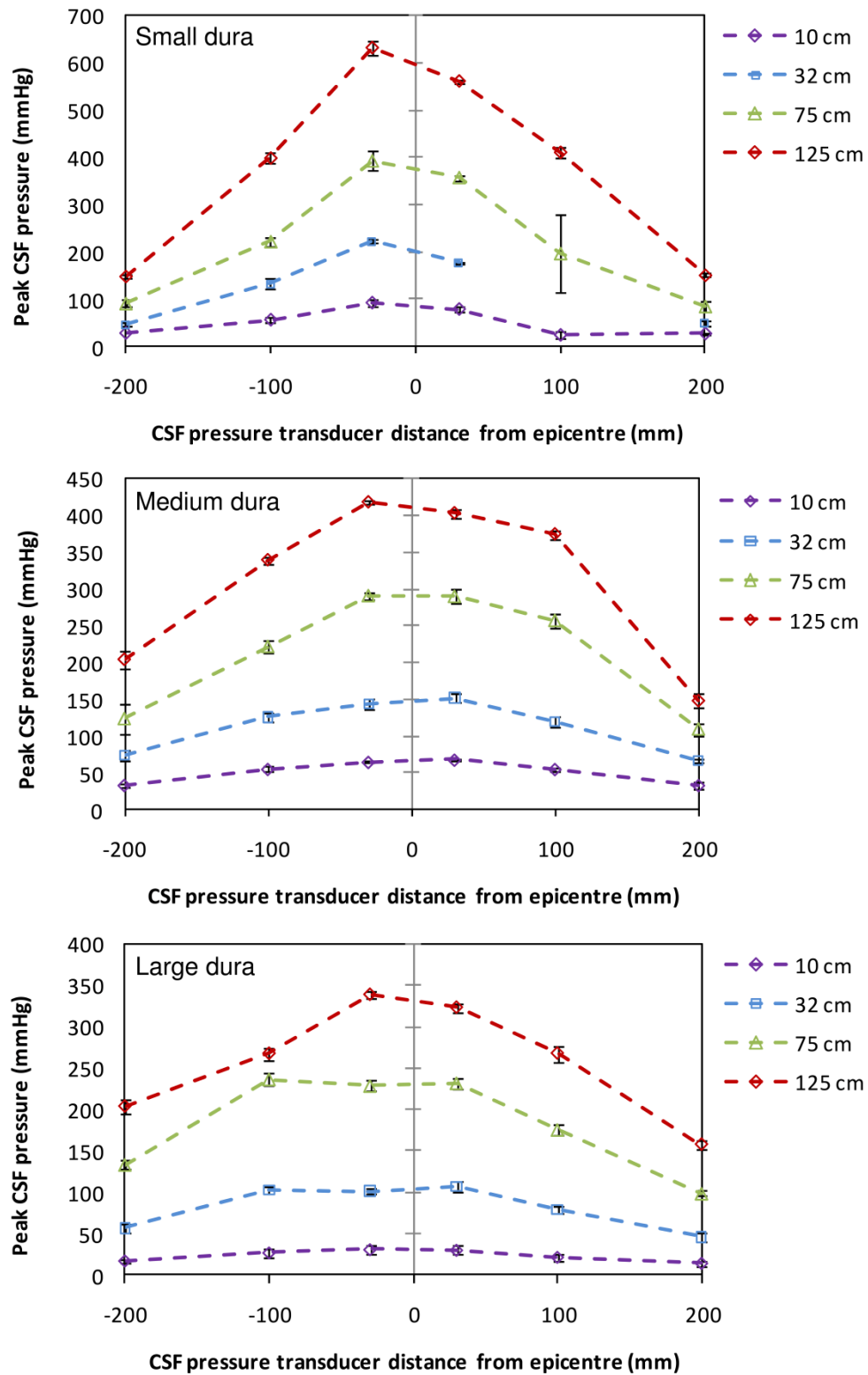
Figure 4-10 Peak CSF pressure (mmHg) versus distance from impact epicenter (mm) for each drop height. Small dura (top), Medium dura (middle), Large dura (bottom). Note that each vertical axis has a different scale.

The peak CSF pressure at each location was strongly and positively related to the impact velocity, i.e. peak pressure increased with higher impact velocities. Increased CSF dimension led to reduced peak CSF pressure at the 30 mm (CSF 3/4) and 100 mm (CSF 2/5) transducer locations. In contrast, increased CSF dimension was associated with increased peak CSF pressure at the 200 mm (CSF 1/6) locations, but the corresponding coefficient was not significantly different from zero at location CSF6. The multivariate linear regression model accounted for between 88 and 95% of the variance in the peak CSF values across the six transducer locations and in all cases the velocity term dominated the model (Table 4-4).

Table 4-4 Regression model coefficients for the peak CSF pressure at each transducer location. The models are based on the equation: $y = \alpha + \beta_1$ (impact velocity) $+ \beta_2$ (CSF dimension). Baseline CSFP was excluded from the model as the corresponding coefficient was not significantly different from zero. The p-values express the probability that the particular regression coefficient is equal to zero. The coefficient of determination, R^2, expresses the percentage of variance in y that is explained by the model.

		Coefficient	95%CI		p-value	R^2
30 mm from epicentre	CSF3					
	β_1	108.37	99.13	117.60	<0.0005	
	β_2	-13.07	-15.80	-10.33	<0.0005	0.92
	α	49.06	8.40	89.72	0.019	
	CSF4					
	β_1	101.23	93.48	108.98	<0.0005	
	β_2	-9.58	-11.88	-7.29	<0.0005	0.93
	α	21.91	-12.24	56.06	0.204	
100 mm from epicentre	CSF2					
	β_1	78.54	73.34	83.74	<0.0005	
	β_2	-3.06	-4.60	-1.52	<0.0005	0.94
	α	-22.84	-45.73	0.06	0.051	
	CSF5*					
	β_1	83.96	75.20	92.73	<0.0005	
	β_2	-4.44	-7.23	-1.65	0.002	0.88
	α	-29.42	-71.63	12.80	0.168	
200 mm from epicentre	CSF1					
	β_1	43.47	40.17	46.76	<0.0005	
	β_2	2.59	1.61	3.56	<0.0005	0.93
	α	-58.20	-72.70	-43.69	<0.0005	
	CSF6					
	β_1	34.50	32.29	36.70	<0.0005	
	β_2	0.45	-0.20	1.10	0.252	0.95
	α	-25.12	-34.84	-15.40	0.129	

*CSF5 – measurements for the small dura with 32 cm drop height were removed because they were strong outliers.

141

4.4 Discussion

The CSF which surrounds the spinal cord within the thecal sac is widely thought to reduce the load transmitted to the cord during everyday activities. However, the extent to which this is true during traumatic events such as burst fractures is largely unknown, and some researchers have proposed that pressure transients in the CSF may even contribute to injury severity. Understanding the biomechanical response of the CSF and dura in SCI may help to improve current animal and computational models of SCI, and improve our understanding of factors which contribute to elevated risk of SCI. Several synthetic models of contusion SCI have measured cord compression with and without CSF, but none have visualised the cord directly or concurrently measured CSF pressure transients. We constructed a synthetic model of the spinal cord and dura to investigate the effect of impact velocity and CSF dimension on cord compression, CSF pressure transients and load transfer to the spinal cord.

The elastic modulus of the surrogate dura (prior to plastic deformation) was in the upper range that has been reported for fresh-frozen human and bovine dura [249,250]. However, the thickness of the plastic was at the lower end of that which has been reported for humans [250,253] and that we have measured for dura specimens harvested from the same species of pigs used in our animal model (unpublished data). Thus, the structural stiffness of the surrogate dura was probably within the mid-range of that of native dura. Because the surrogate dura material did not exhibit the biphasic hyperviscoelastic "J"-shaped stress-strain behaviour observed for native dura, i.e. it lacked the initial low stiffness linear region, we applied only 1% strain to it in our model. This is also consistent with the observation that dura exists *in vivo* with a "pre-strain" such that the elastic fibres within the tissue appear stretched to the limit of their elasticity [259], a condition which would be achieved at the end of the low stiffness region, similar to other connective tissues which are composites containing elastin and collagen fibres [527].

Increased impact velocities resulted in higher peak impactor and base loads, and greater cord compression; this is consistent with basic physical concepts of load transmission and energy transfer. It is also consistent with the expectation that human and experimental animal SCIs with higher energy input in general result in more severe injury at the site of the bone-spinal cord contact. The peak impactor loads for the small dura, which is closest to the pig dura size, were approximately 50 and 80% of the loads measured for the 1.25 and 4.6 m/s impact velocities in the animals (Chapter 3). This disparity is probably due to differing material properties and the simplified geometries of the model.

The tether load increased with both impact velocity and pseudo-CSF thickness. The tether load is an indicator of the amount of axial tension in the surrogate cord, and may be related to the amount of strain induced in the material. Axial strain of around 20% or greater have been associated with transient or permanent nervous tissue damage [e.g. 219,302] (see also Section 1.5.4.3). We speculate that increased pseudo-CSF thickness caused increased cord tension (and strain) because of the greater

downward travel of the cord prior to contact with the inferior support; in the case of the largest dura size this contact did not occur.

Increased thickness of the pseudo-CSF layer, and an associated larger synthetic dura, was associated with lower peak impactor and base forces. This implies that a thicker fluid layer may reduce the load imparted to the spinal cord, and therefore the stress induced in the tissue. Decreased stress is associated with decreased tissue damage; a stress threshold of around 2 kPa has been derived for axons [309]. Increased pseudo-CSF thickness was also associated with lower cord compression, which is likely to result in less tissue damage. Transverse compression tolerance of the spinal cord, in terms of percent diametral compression, has been estimated to be around 25 [271] to 50% [269], depending on the rate and duration of compression. In this study, no CSF was associated with the most compression (30-75%), and no cord compression was observed with the largest dura size. Increasing from no CSF to the medium dura size decreased the cord compression 2.5 to 4.5 times at the higher impact velocities, and eliminated it at the lower velocities. This is consistent with previous synthetic, *in vitro* bovine, and computational models in which removing pseudo-CSF from the construct resulted in greater compression of the cord [280,281,528]. However, these studies were unable to visualise the cord directly, and relied on an assumption of full CSF collapse before beginning cord compression.

The peak pressure magnitudes were lower than we have previously measured *in vivo* in pigs using the same weight-drop apparatus (Chapter 3). At 30 mm from the epicentre the *in vivo* median peak pressure ranged from around 370 to 630 mmHg at 1.25 m/s impact velocity, and 780 to 1250 mmHg at 4.6 m/s impact velocity (the latter is slightly lower than the velocity in the synthetic model). These values are around 4-6 and 1.2-2 times higher than measured for the equivalent impact velocities in the model construct with the smallest dura size, which most closely replicates the dimensions of the animals. This disparity could occur due to the simplified geometry of the model. Firstly, we noted above that the peak pressure increased with thinner pseudo-CSF layers; in the synthetic model the diametral thickness of the pseudo-CSF layer was 3.74 mm (SD 0.24 mm) while in the pigs the diametral layer ranged from 0.75 to 2 mm (Chapter 6). Furthermore, very little of the CSF was located ventral to the spinal cord in the animals, whereas in the synthetic model, the cord tension always raised the spinal cord off the inferior support plate. Secondly, the spinal cord is not perfectly cylindrical, although the cross-section does more closely match a circle in the thoracic region than in the cervical and lumbar regions. We did not attempt to model the geometry of the spinal canal. Hall et al. showed that using either a flat plate or an anatomic model of the posterior canal had no effect on maximum cord compression or internal pressure in an *in vitro* model [462]. However, pressures measured inside surrogate cords during weight-drop tests were higher when the cord resided in narrow rather than wide cadaver cervical spines [468]. Thirdly, it could be because the synthetic materials did not completely replicate the viscoelastic mechanical behaviour of the biological tissues. The surrogate cord used in the present study is the most rigorously validated model of

which we are aware; however, there are known discrepancies between this cord and *in vivo* canine and feline cord and *ex vivo* bovine cord mechanical data.

The peak pressures measured inside *ex vivo* bovine spinal cords, at the impact site, subjected to impacts of 2.5 - 7 m/s ranged 300-2700 mmHg with various simulated posterior longitudinal ligament tensions [462]. Synthetic cords with internal pressure transducers and subjected to 100-600 g-cm weight drops (separate weight and height not given) ranged 1425-3075 mmHg at the impact site and 225-450 mmHg at the adjacent spinal level [468,469]. The pressures measured in the pseudo-CSF in our model were generally at the lower range of these impact-site measurements; it is likely that these pressures are highly dependent on the cross-sectional area of the impactor. Researchers have measured pressures ranging 80 to 2415 mmHg in surrogate cords [469] or water [473] placed in cadaver spines subjected to axial impacts inducing burst and compression fractures (more detail in Section 1.6.5). The results of the present study again fall at the lower end of this range, but neither of the previous studies modelled all of the cord, dura and CSF components. There is a paucity of literature regarding the pressure tolerance of the spinal cord; however, changes in brain tissue and neurological deficit have been observed in animals subjected to fluid percussion impulses [316] and external blast pressures [341] as low as around 100 mmHg (see also Section 1.5.4.4).

This *in vitro* model has several features which distinguish it from the models that have been compared above and were introduced in Section 1.6.5. Foremost, it is the first which enables measurement of the pressure in the pseudo-CSF, as well as the impactor, base and tethering loads, and cord compression. The clamp fixtures held the construct in horizontal alignment, thereby avoiding "pooling" of the pseudo-CSF which occurs at the bottom of vertically oriented models. The fixtures allowed independent tensioning of the spinal cord and dura, specimens of any length can be used (unlike some that utilise materials testing machines), and it would also be well suited to be used with *ex vivo* materials. The pseudo-CSF pressure can be easily varied. The weight-drop apparatus provides highly repeatable impact velocities on a continuous scale, limited only by the length of the guide-rail. The velocities that we used represent the range estimated in biomechanics studies for burst fractures [132,134,460]. The high-speed x-ray and radiopaque cord enable visualisation of the cord within the dura, which is not possible with video alone due to the visual distortion created by the fluid layer.

Like all *ex vivo* and physical models of biomechanical events and processes, this model has several limitations. The cord and dura had a simplified cylindrical geometry without nerve root or ligamentous tethering, and the posterior canal was simulated with a flat plate; however, some of these features are shared by previous synthetic [280,281,462] and computational models [495,499]. The spinal cord was around 2-3 mm larger than human thoracic cord, and the large dura (relative to the cord) was larger than reported human values [391,394]. It was not possible to reduce the thecal sac diameter beyond that of the

small dura size without risking impinging on the pressure transducers. Nonetheless, these geometries were suitable for illustrating the effect of velocity and thecal sac dimension. The spinal cord generally sat slightly below the centre of the dural sac because it was slightly denser than water, unlike the native cord that has neutral buoyancy in CSF. As mentioned above, the material properties of the cord and dura are key determinants of the model response. The biofidelity of the model would be improved by using a surrogate dura with direction-dependent hyperelastic properties – a composite material that mimics the anisotropic arrangement of collagen and elastin fibres in the native spinal dura [246,248,249,261] may be successful. Due to the complexity of the setup, we did not alternate between different dura sizes, although the velocity groups were randomised within dura groups. Finally, we did not investigate the sensitivity of the model to cord and dura strain, end reservoir volume and compliance, baseline pressure, and these may shed more light on the effects of CSF and impact velocity.

4.5 Conclusion

In this synthetic model, cord compression, peak CSF pressure at several locations along the cord, and loads imparted to the cord, were strongly dependent on the impact velocity and CSF thickness. The reduced cord compression, CSF pressure and loads associated with the large dura size suggest that larger CSF layers reduce the energy transferred to the spinal cord, and therefore severity and/or extent of resultant neurological damage. This suggests that clinical metrics of SCI risk may be more accurate if they incorporate measures of the thecal sac and spinal cord. Computational, synthetic, cadaveric and animal models of SCI may better simulate the biomechanics of the human injury event if fluid interaction is incorporated.

Chapter 5   CSF Pressure Distribution after Acute SCI [4]

5.1 Introduction

Despite significant advancements in acute care and rehabilitation which have greatly improved the survival and quality of life of spinal cord injured patients [529], a treatment resulting in significant improvements in neurological outcome after acute injury is lacking [153,494,530]. Vascular compromise and local tissue ischaemia are major contributors to the secondary pathophysiologic cascade that occurs immediately after the acute mechanical insult to the spinal cord [153,177]. Therefore, maintaining adequate tissue perfusion is one of the main objectives of post-trauma care. Systemic hypotension is common after acute spinal cord injury (SCI), particularly in the cervical spine, leaving the cord vulnerable to further ischaemic damage [182]. To avoid this, physicians commonly strive to maintain the mean arterial pressure (MAP) at approximately 85-90 mm Hg for 7 days post-injury [182], although current treatment guidelines acknowledge the lack of evidence to support a specific target MAP [183,184]. Nevertheless, the careful monitoring and management of MAP to ensure adequate spinal cord perfusion is a fundamental component of the medical management of acute SCI patients.

While there is justifiable emphasis on monitoring the MAP, this approach to haemodynamic support fails to recognise the potential effect of cerebrospinal fluid (CSF) pressure on spinal cord perfusion. The CSF that surrounds the spinal cord applies a hydrostatic pressure to the cord, and thus the spinal cord perfusion pressure (SCPP) is defined as the difference between the mean distal aortic arterial pressure (MAP) and the hydrostatic CSF pressure (CSFP), i.e. SCPP=MAP-CSFP [531]. CSF pressure is therefore inversely proportional to spinal cord perfusion pressure, i.e. as CSFP increases the SCPP decreases, provided that the MAP remains constant. Conversely, reducing CSFP by draining CSF would theoretically lead to increased perfusion pressure and greater oxygen delivery to the damaged area. Such CSF drainage is one approach used to lower elevated intracranial pressure (ICP) and increase cerebral perfusion pressure in patients with TBI [190]. Additionally, recent studies have provided evidence that reducing CSFP with controlled CSF drainage can reduce the risk of ischaemic damage to the spinal cord during thoracoabdominal aortic aneurysm repair [532-535].

For acute traumatic SCI, the drainage of CSF may also reduce CSFP and improve SCPP, but little is known about how SCI affects the CSFP distribution along the rostro-caudal length of the cord, particularly when there is residual extradural cord compression that may be occluding the subarachnoid

---

[4] A version of Chapter 5 is in preparation for publication. Jones CF, Newell RS, Lee JHT, Cripton PA and Kwon BK. The pressure distribution of cerebrospinal fluid responds to residual compression and decompression in an animal model of acute spinal cord injury.

space at the site of injury. In the acute SCI setting, CSF drainage protocols have recently been assessed for efficacy in animal models [196] and assessed for safety in acute SCI patients [91].

Horn et al. [196] evaluated the effect of hourly lumbar drainage of CSF to 10 mmHg pressure on tissue perfusion and neurophysiological outcomes in a rabbit model of acute SCI. Although histological analysis showed less tissue damage in the CSF drainage group, tissue perfusion was decreased and motor and electrophysiological measures were not improved, compared to animals not receiving drainage. Horn et al. [196] did not concurrently measure the CSF pressure cranial to the injury site. While lumbar pressure reflects intracranial and proximal spinal pressure in normal individuals [56], this may not be true after SCI. Residual bony compression of the spinal cord may cause subarachnoid occlusion, and since CSF is formed in the cranial vault, the proximal spinal compartment may experience increased pressure. In 22 acute SCI patients enrolled in a 72-hr lumbar CSF drainage trial, Kwon et al. [91] noted a sharp increase in mean lumbar CSF pressure and pulse pressure amplitude upon surgical decompression. This provides indirect clinical evidence that a system of higher pressure exists cranial to the injury when the thecal sac is occluded. Unfortunately, obtaining pressure measurements and/or draining CSF proximal to the injury would be difficult in SCI patients since ventricular drains are not indicated unless there is concomitant brain injury. This may limit our ability to define an appropriate pressure threshold for drainage and limit the effectiveness of lumbar CSF drainage prior to surgical decompression.

Pressure differentials are observed across subarachnoid obstructions due to cerebellar herniation [67,68] and spinal cord mass lesions [71,72,77], and this differential was exploited by the early Queckenstedt's test for spinal block [70,536]. In the only direct study of cranial-caudal pressures after experimental acute SCI that we are aware of, Shapiro et al. [211] reported increased pressures in the cisterna magna CSF and slightly reduced pressures in the lumbar CSF of a cat, which then recovered close to baseline over the 4-6 hour experiment. However, in this model the CSF pressures were measured for a limited duration and this study did not model a residual bony compression and subsequent surgical decompression, both of which are typical features of SCI patient presentation and course of treatment.

A better understanding of the cranial-to-caudal pressure differentials associated with acute SCI and surgical decompression will inform future experimental and clinical protocols for the maintenance of SCPP via CSF drainage and for the decompression of the spinal cord and thecal sac. The aims of our study were to determine if, after a human-like spinal cord injury: (1) a CSF pressure differential develops over the lesion site with an occluded subarachnoid space; (2) this pressure differential is resolved upon decompression of the intrathecal sac; (3) the resolution is sustained in the hours after decompression; and, (4) if a change in lumbar CSF pulse pressure amplitude is associated with compression and decompression.

5.2 Methods

The experimental protocol was approved by the University of British Columbia Animal Care Committee and complied with the guidelines and policies of the Canadian Council on Animal Care.

5.2.1 Pressure transducers and drift assessment

CSF, arterial and venous pressures were measured with miniature fibre optic pressure transducers (Preclin 420LP with Samba202 control unit, Samba Sensors, Sweden) with a sensor tip diameter 0.42 mm, bare fibre diameter 0.25 mm and length 50 mm. The transducers have a range of -37.5 to 262.5 mmHg, an accuracy of ±0.38 mmHg plus ±2.5% of reading, and temperature coefficient of <0.15 mmHg/°C. For transducers that cannot be re-zeroed *in vivo,* measurement drift is an important consideration [477,482]. Because the manufacturer reported long term stability (<0.5% range) in air at room temperature rather than in liquid at body temperature, and as the drift behaviour can vary between particular transducers of the same type, we characterised the drift of each transducer using conditions that mimicked the experimental environment. A water-filled test chamber was held stationary in a temperature controlled water bath (38.0 +0.1 °C) and all electronics were stabilised for at least one hour prior to beginning the test. The transducer was zeroed to atmospheric pressure, in air at room temperature, then immediately inserted into the chamber. The transducer was advanced to a depth giving a hydrostatic pressure of around 10 mmHg and a compression fitting was tightened around the transducer cable to seal the chamber. Pressure data were sampled continuously at 1Hz for at least 15 hours. The test was repeated nine times for the CSF transducers and six times for the blood transducers. The data were filtered with a 1000-tap FIR Blackman window filter with cut-off frequency 0.001 Hz, and the maximum pressure deviation between 30 min and 15 hours was determined for each test.

5.2.2 Animals

Fourteen female Yucatan miniature pigs (Sinclair Bio-Resources, Windham, ME, USA) were group housed and acclimatised at our facility for at least one week before surgery. The animals were divided into three experimental groups with the following demographics at surgery (mean ± standard deviation): sham: N=2, 133/142 days, 21.5/22 kg; moderate severity injury: N=6, 123.7±11.3 days, 20.2±1.0 kg; high severity injury: N=6, 125.3±6.5 days, 21.7±2.9 kg. Animals were fasted overnight before surgery. All surgical procedures were completed in a sterile field. Anaesthesia was induced with an intramuscular (IM) injection of Telazol 4-6 mg/kg, xylazine 0.6 mg/kg and intravenous (IV) atropine 0.02 mg/kg. Animals were endotracheally intubated, and maintained on isoflurane (2-3.5% in oxygen during surgery; 1.5-2.5% in oxygen post-injury as required) for the procedure. Mechanical ventilation was maintained at 10-12 breaths/min with a tidal volume of 10-12 mL/kg, and end tidal CO_2 was

maintained at 30-40 mmHg. Subcutaneous injections of ketoprofen (3 mg/kg) and bupivocaine (1-2 mg/kg) were given before the incisions for the central line and the laminectomy, respectively. Analgesics were administered before the surgery and as needed during the procedure (hydromorphone 0.15 mg/kg IM or morphine 1 mg/kg IM). Antibiotics were given immediately before surgery and every four hours thereafter (cefazolin, 20 mg/kg IV). Hydration was maintained with intravenous lactated Ringer's solution. Fluids were replaced with isotonic saline to counter respiratory alkylosis and/or dosed with 1-2.5% dextrose to counter hyperkalemia. Core temperature was monitored with a rectal temperature probe and maintained at 37.5-38.5 °C with a circulating-water heating pad. The urinary bladder was catheterised using an 8 French Foley catheter. Heart rate was monitored with ECG, blood oxygen saturation with a pulse oximeter on the tongue, and blood pressure with a forelimb cuff. Ventilation and anaesthetic level were adjusted to maintain normal heart rate and blood pressure. Central arterial and venous catheters were placed surgically in the left carotid artery and external jugular vein. This catheter configuration allowed for introduction of, and sealing around, the fibre-optic pressure transducer (described below) while maintaining a parallel access port for sampling and flushing. We used a 16 Ga, 15 cm length catheter (Arrow/Teleflex Medical, Markam, Ontario, Canada) fitted with a Y-connector. One side of the Y was fitted with a Tuohy Borst adapter (84044/80369, Quosina, NY, USA) to seal over the pressure transducer cable, and the other side with a standard IV needle access port. The line was locked with heparin saline and flushed periodically to maintain patency. Blood gases and electrolytes were analysed periodically.

5.2.3   Experimental protocol

A detailed description of the injury device is given in Chapter 3. Briefly, the modified weight-drop injury device consisted of a pedicle screw mounted articulating arm attached to a guide rail. A 20 g weight was released from the desired height, and guided by the rail on a linear bearing to impact the spinal cord. The release height determined the impact velocities (moderate severity 32 cm, ~2.3 m/s; high severity injury 125 cm, ~4.6 m/s). These parameters approximately replicated the bone fragment weight and velocity associated with burst fractures [132,462]. The impacting tip of the weight was a 9.53 mm diameter cylinder with a flat face and 45°/1 mm bevelled edge. The impact force and velocity, and spinal cord displacement were determined from the impactor load cell and high speed video images, as described in Chapter 3. After the injury, a stainless steel 100 g cylindrical weight with 9.53 mm diameter was placed at the injury site to mimic residual spinal cord compression by a bony fragment, as is typical in burst fracture or fracture-dislocation injuries.

The animal was anaesthetised and catheters were placed in the carotid artery and jugular vein. The spine was exposed and pedicle screws were inserted at T10-T13. The spinal dura was exposed via a laminectomy from T4 to L4. The laminectomy was widened at T10-T11 to ensure that the impactor tip

did not strike the bony edges during impact. The pressure transducers were zeroed in the atmosphere prior to insertion. Two transducers were placed with the sensing face a nominal 100 mm from the injury site, at approximately C7/T1, L5/6. Two similar high range transducers were placed close to the injury site for the study reported in Chapter 3; the data from these transducers were not used in the current study. To insert the sensors the surgical table was tilted to lower the animal's head and the desired location on the dura was measured with callipers and marked. The dorsal dura was gently lifted with forceps at this location and the tip of an 18 gauge needle was used to puncture it. The transducer was rapidly introduced and advanced 50 mm into the intrathecal space, on the dorsal aspect of the cord. The dural hole was sealed with cyanoacrylate gel to prevent further CSF leakage. After all four transducers had been placed the table was tilted to bring the thoracic spinal cord into a horizontal position. The arterial and venous pressure transducers were placed in their respective catheters. The articulating arm and guide rail were attached to the pedicle screws and the rail aligned vertically. The animal's ventilation was held to cease respiration motion, the solenoid was activated to impart the SCI and the ventilation was resumed within three seconds after injury. The impact weight was removed immediately and the 100 g weight for sustained compression was placed slowly and gently at the same location, supported by the guide rail. The weight remained in place for eight hours and then was removed to emulate a surgical decompression. Monitoring continued for a further six hours. All animals remained anaesthetised for 14 hours post-injury. The animal was not moved during the post-injury time, unless absolutely necessary for the animal's care, as raising or lowering the head could affect the hydrostatic pressure in the intrathecal sac. The two sham animals received all surgical procedures, including mounting of the injury device, with the exception of the dynamic injury and the post-injury compression.

5.2.4   Data acquisition, processing and statistical analysis

The analog output of each Samba202 pressure transducer control unit was connected to National Instruments data acquisition hardware. All pressure data were collected at 200 Hz using custom LabVIEW programs (V8.6, National Instruments, Austin, TX, USA). Baseline pressure data were collected for five minutes approximately 20 minutes before injury. After the injury, the pressure data were collected continuously for 14 hours, with 15 minute blocks were defined to facilitate animal care. The first five minutes of each block was designated as undisturbed data collection, followed by 10 minutes in which animal care procedures were carried out. The latter period was also used to take ultrasound images of the spinal cord once per hour (data reported in Chapter 6), and to maintain the patency of the arterial and venous transducer's catheters as required.

All post-processing of the data was completed using custom programs in Matlab (2009b, The Mathworks, Matick, MA, USA). We extracted the first five minute section of each 15 minute block and applied several digital filtering routines with 2000-tap FIR Blackman window filters to remove the

respiratory artifact [537] (which is patient specific and varies with end tidal volume and ventilation rate in mechanically ventilated subjects [81]) and high frequency noise while maintaining arterial pulsation [537] (Figure 5-1A). An example of the raw CSF pressure data and each step of the filtering sequence are shown for 30 seconds of a typical CSF pressure signal in Figure 5-1. Firstly, the mean heart rate (HR) was determined by filtering the central arterial pressure with low-pass cut-off of 10 Hz, and using a custom peak-trough detector. Then all pressure data were band-pass filtered with high and low-pass cut-off frequencies of 0.8*HR and 10 Hz, respectively (Figure 5-1B), to remove high frequency noise and the respiratory artifact. The original (raw) pressure data were also subjected to a low-pass filter with a cut-off frequency of 0.8*HR to remove the arterial pulsations (Figure 5-1C). The mode of the resultant signal (corresponding to the lower plateau of the low-pass signal) was determined from a histogram with bin size of 0.2 mmHg for central arterial pressure (CAP), and 0.1 mmHg for central venous pressure (CVP) and CSF pressure (CSFP) (Figure 5-1D). The mode was then added to the initial band-pass data to restore the correct mean offset, (Figure 5-1E) producing a "regenerated" signal. The mean CVP and CSFP were determined as the average of all the regenerated data points in the five minute period. Mean arterial pressure was determined by applying peak-trough detection to the regenerated signal and then by the relation MAP=(2*diastole + systole)/3, where systole and diastole corresponded to the detected peaks and troughs, respectively. CSF pulse pressure amplitude was determined as the mean of the peak-to-peak amplitudes in the regenerated signal.
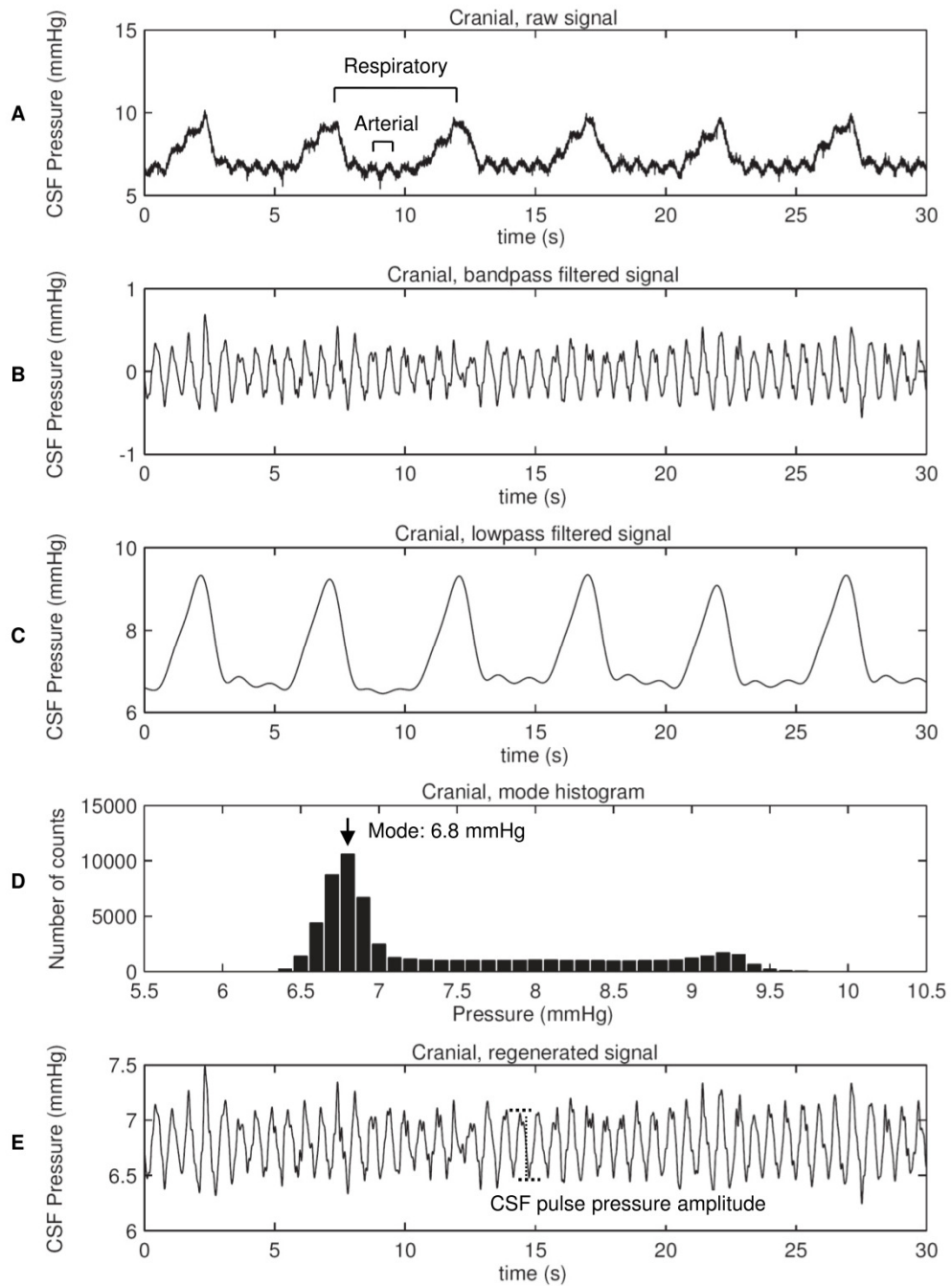
Figure 5-1 Example of filtering process for 30 seconds of Cranial pressure data (P1836, t=0-15min). (A) raw signal; (B) signal after band-pass filtering with Fc1=0.8HR, Fc2=10 Hz to remove respiratory artifact; (C) signal after low-pass filtering with Fc=0.8HR to remove arterial pulsation but maintain DC offset; (D) mode histogram of low-pass filtered signal; (E) regenerated data from the addition of the mode (6.8 mmHg) and the band-pass filtered signal from (B).

We assessed the longitudinal trends of the cranial and caudal CSF pressures for the moderate and high severity injury groups, to determine if these data could be pooled into a single group for statistical analysis. A linear mixed model (LMM) was used to describe the longitudinally measured change in the

cranial-to-caudal pressure differential during the compression period [538]. Time was the fixed effect and pig was the random effect, to represent the variation in baseline pressure across the animals. Paired t-tests were used to test the null hypothesis that the "step" change in the cranial and caudal CSF pressure from immediately before decompression to immediately after decompression was equal to zero. The alternative hypotheses were that the change was less than zero (i.e. negative) and greater than zero (i.e. positive) for the cranial and caudal locations, respectively. A LMM was used to describe the change in cranial-to-caudal CSF pressure differential (i.e. CSFPcranial – CSFPcaudal) after decompression, again with pig as the random effect for the random intercept model. The same LMM and paired t-tests, with equivalent alternative hypotheses, were applied to assess the change in pulse pressure amplitude during compression, decompression and post-decompression. Note that although the data presented in Figure 5-3 (Section 5.3.2) have been zeroed to the initial pressure for ease of visualising the trends (zeroing removes bias due to differing hydrostatic pressure and transducer zeroing) statistical analysis was performed on uncorrected data. A LMM was also used to assess the change in blood pressure over the entire experimental period for all 14 animals.

5.3 Results

5.3.1   Pressure transducer drift assessment

In the pressure transducer drift tests an initial temperature equilibration occurred within 1-2 minutes after immersion, and this was followed by a drift that tapered substantially within about 30 minutes (Appendix C). In the following 14.5 hours the pressure tended to drift in one direction, with small positive and negative fluctuations. The mean maximum deviation from the initial pressure between 30 min and 15 hours was 0.5±0.10 mmHg and 0.4±0.11 mmHg for the CSF transducers, and 0.25±0.11 mmHg and 0.70±0.31 mmHg for the venous and arterial transducers, respectively.

5.3.2   CSF pressure and pulse pressure amplitude

Thirteen animals completed surgery and post-injury monitoring without complications. The impact force and velocity, and spinal cord displacement for these animals were reported in Chapter 3. The mean time between induction of anaesthesia and injury was 5.9 hr (SD 0.6) and the mean time between start of spine surgery and injury was 3.6 hr (SD 0.5). One animal (P1676) from the high severity group exhibited cardiac arrhythmia and bradycardia at 2.5 hours post-injury, was treated with atropine and epinephrine and stabilised, then had a second cardiac event at 4.5 hours post-injury, which was fatal at 5 hours post-injury; the data from this animal are included in the analysis until 2.5 hours. Animals P1700 and P1642 from the moderate severity group exhibited similar arrhythmias at four and six hours post-injury respectively; they were treated with epinephrine and atropine, were subsequently stabilised and had no

further complications. The data obtained during these cardiac events was excluded from the statistical analysis.

In some animals we experienced difficulty with clot formation around the tip of the central arterial and venous pressure transducers, leading to variations that were not physiologic. This variation did not occur in the CSF pressure measurements. The systolic blood pressure, measured with the forelimb Doppler ultrasonic cuff, was therefore a more reliable indicator of the trend in blood pressure and is reported instead. In most animals the systolic blood pressure gradually declined over the 14 hrs post-injury (Figure 5-2) and the rate of decline was significantly different from zero (Table 5-1).
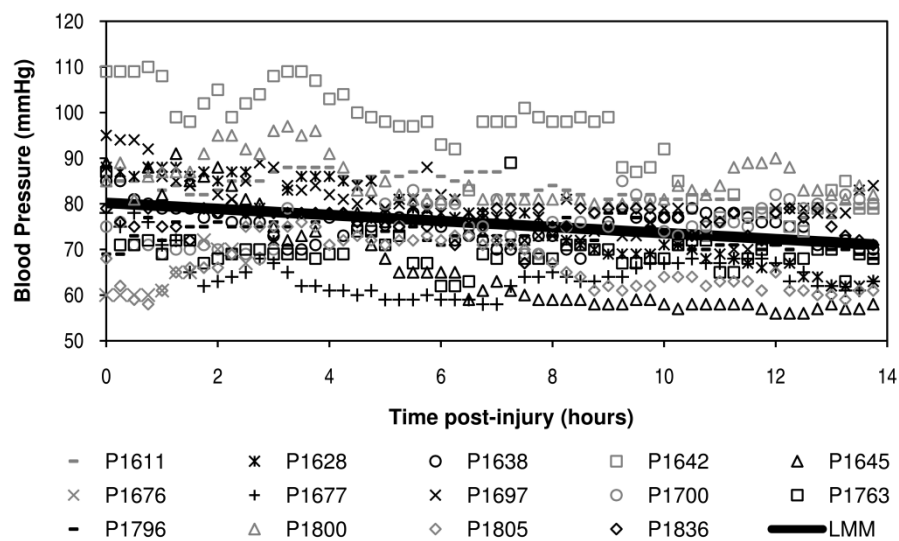
Figure 5-2 Linear mixed model and raw data for blood pressure (from cuff measurements) over compression and decompression. Both the intercept term (β_0) and the slope term (β_1) were significantly different from zero.

Table 5-1 Coefficients and 95% confidence interval for the linear mixed model for blood pressure.

Test Period	β_0 (y intercept, mmHg)		β_1 (slope, mmHg/hr)		N
	Estimate	95%CI	Estimate	95%CI	
Compression & Post-Decompression (14 hours)	80.20	(73.83, 86.56)	-0.66**	(-1.21, -0.12)	14

**p<0.001

There was no observable difference in the pre- and post-injury pressure profiles between the moderate and high injury severity groups, so they were combined for analysis (Figure 5-3). The mean baseline CSF pressure was 4.5 mmHg (SD 2.1) and 5.1 mmHg (SD 1.4) for the cranial and caudal

154

transducer, respectively, at 25.0 min (SD 9.1) before injury. The cranial baseline pressure was higher than the caudal baseline pressure in about half of the animals. Immediately after injury both pressures were slightly higher at 5.1 mmHg (SD 2.6) and 5.8 mmHg (SD 2.0) for the cranial and caudal transducer, respectively. The transducers for animal P1700 were incorrectly zeroed and were not included in these baseline averages.

The cranial pressure tended to increase during the eight hours of compression for all animals. The response of the caudal pressure was stratified into three groups: in five animals it decreased or was predominantly constant and appeared to be independent of the cranial pressure (Figure 5-3A); in three animals it decreased or was predominantly constant and showed similarity in parts to the cranial pressure (Figure 5-3B); and, in three animals it followed the same pattern as the cranial pressure (Figure 5-3C). After decompression the cranial and caudal pressure equalised in four animals, and in the remaining seven they did not equalise but followed the same trajectory and fluctuations as the cranial pressure (Figure 5-3). Descriptive statistics for the changes in the cranial and caudal CSFP over the compression, decompression and combined compression-decompression periods are shown in Table 5-2.
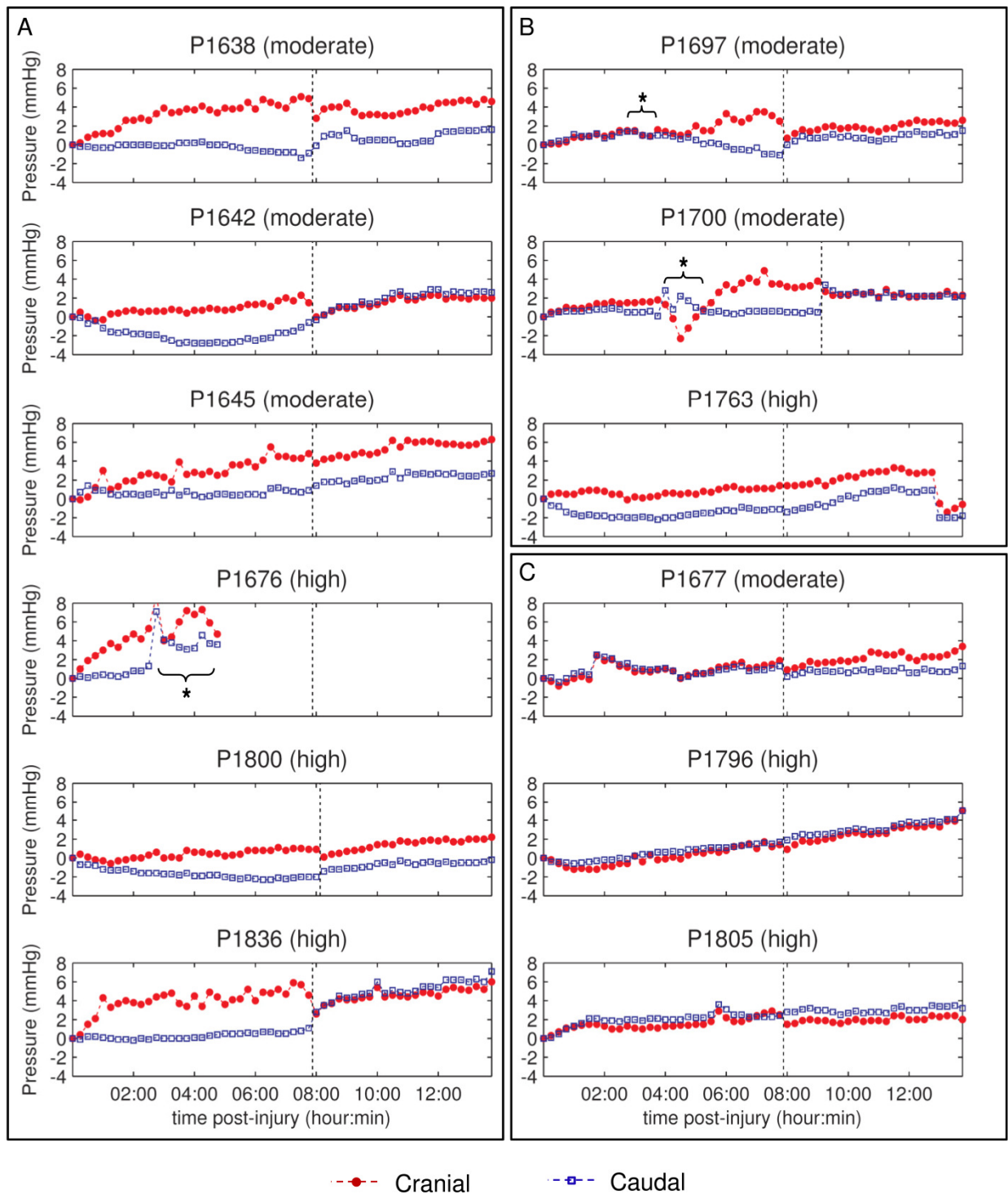
Figure 5-3 Cranial (red) and Caudal (blue) CSF pressures for 14 hours post-injury, divided into groups exhibiting distinct pre-decompression behaviour (A) consistent and increasing cranial-caudal pressure differential, (B) partial cranial-caudal pressure differential, and (C) little or no cranial-caudal differential. Vertical black dashed line indicates the time at which decompression occurred; note decompression time of 9:00 hr for P1700 to allow stabilisation time after epinephrine/atropine. *these data were not included in statistical analysis due to noticeable effects of cardiac arrhythmia and bradycardia, with administration of atropine and epinephrine.

Table 5-2 Descriptive statistics for the changes in CSF Pressure at the cranial and caudal location during the compression, post-decompression and combined compression – post-decompression periods (N=11 for all rows).

	Mean	Standard Deviation	95% Confidence Interval
CSF Pressure change during compression (8 hours)			
Cranial	2.75	1.51	(1.73, 3.76)
Caudal	0.20	1.41	(-0.74, 1.14)
CSF Pressure change during post-decompression (6 hours)			
Cranial	1.67	1.73	(0.51, 2.83)
Caudal	1.45	1.57	(0.39, 2.50)
CSF Pressure change during compression & post-decompression (14 hours)			
Cranial	3.25	2.05	(1.88, 4.63)
Caudal	2.29	2.38	(0.69, 3.89)

The cranial-caudal CSF pressure differential increased by approximately 0.4 mmHg per hour during the compression period. This increase was mostly attributable to a mean 2.75 mmHg cranial CSF pressure elevation in the eight hours after injury. The rate of increase was significantly different from zero (Figure 5-4A, Table 5-3). At the time of decompression, the cranial pressure decreased for all animals except one with an average reduction of 1.2 mmHg; conversely, the caudal pressure increased for all animals except one, with an average elevation of 0.65 mmHg (Figure 5-5A). These immediate changes in cranial and caudal CSFP were significantly different from zero (Table 5-2). In the six hours after decompression, the cranial-caudal CSF pressure differential decreased marginally, but the rate was not significantly different from zero (Figure 5-4B, Table 5-3).
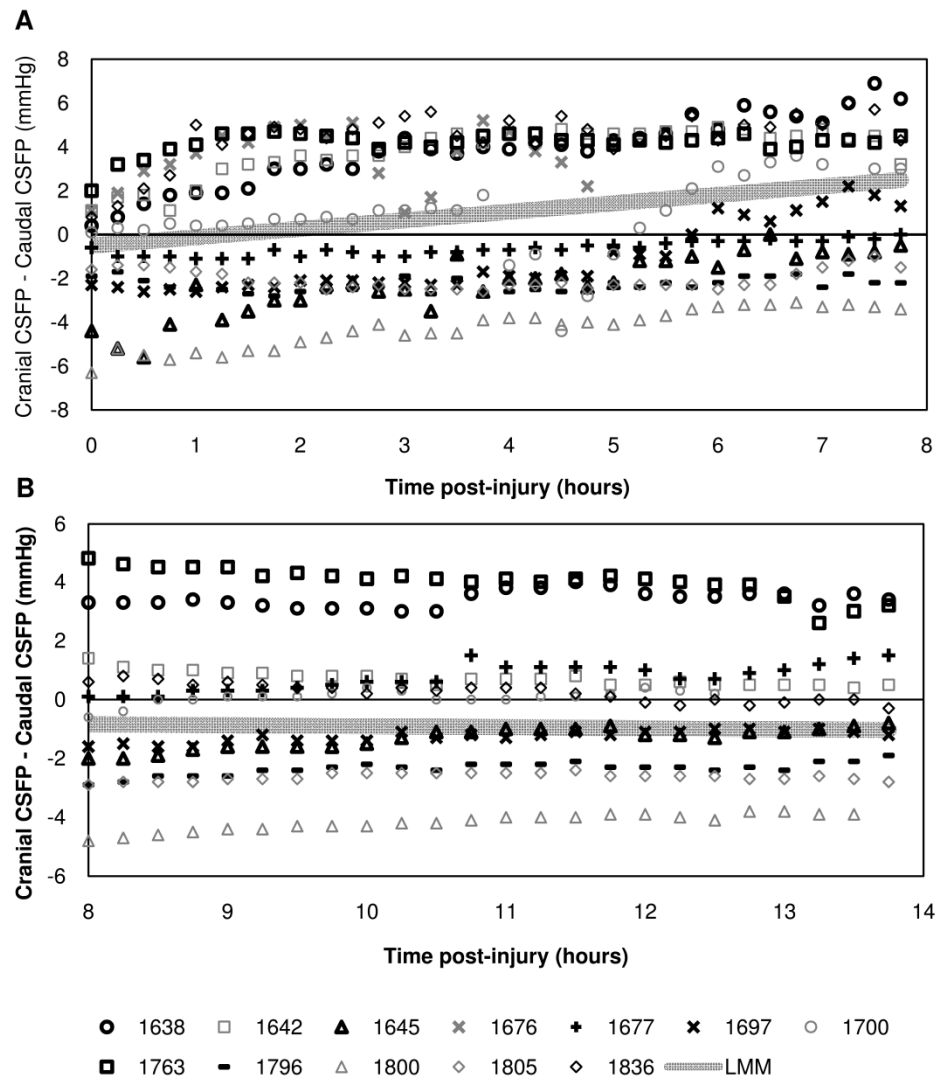
Figure 5-4 Linear mixed model and individual animals' data points for cranial-caudal CSF pressure differentials for periods of (A) Compression and (B) Post-decompression. The intercept term (β_0) was not significantly different from zero for either group and the slope term (β_1) was significantly different from zero for the Compression period.

158

Table 5-3 Coefficients and 95% confidence interval for the linear mixed models for cranial-caudal CSF pressure differential and cranial-caudal pulse pressure amplitude differential.

Test Period	β_0 (y intercept, mmHg)		β_1 (slope, mmHg/hr)		N
	Estimate	95%CI	Estimate	95%CI	
Cranial-caudal CSF pressure differential					
Compression (8 hours)	-0.51	(-2.21, 1.19)	0.387**	(0.207, 0.566)	12
Post-Decompression (6 hours)	-0.59	(-2.57, 1.40)	-0.033	(-0.049, 0.002)	11
Cranial-caudal pulse pressure amplitude differential					
Compression (8 hours)	0.51**	(0.28, 0.73)	0.005	(0.023, 0.034)	12
Post-Decompression (6 hours)	0.16	(-0.04, 0.36)	0.033*	(0.004, 0.063)	11

*p<0.05

**p<0.001
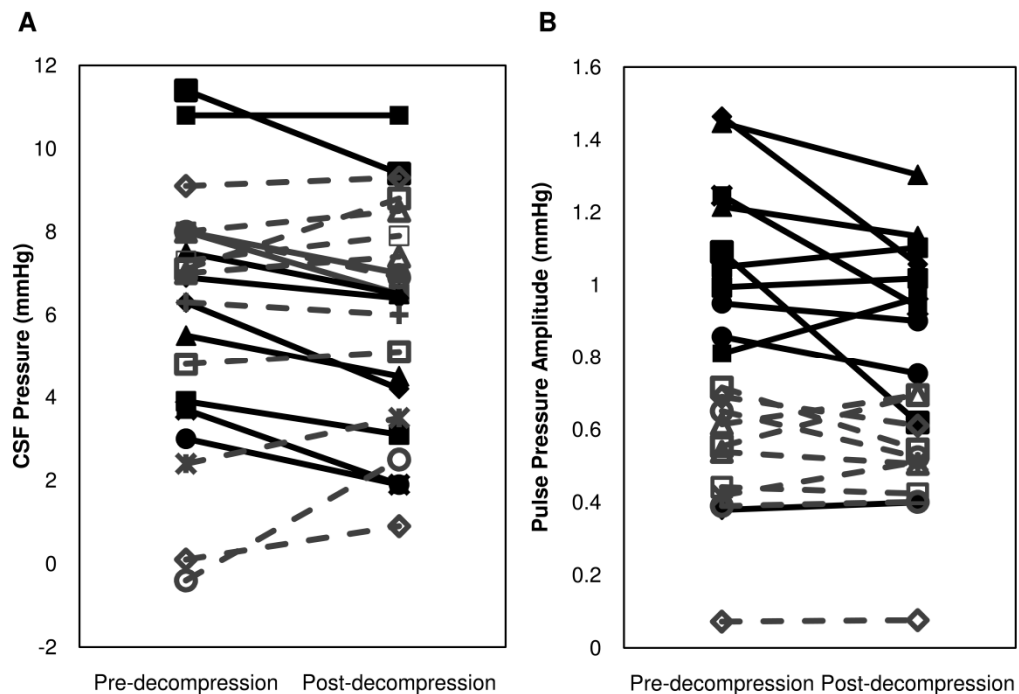
Figure 5-5 Comparison CSF pressure (A) and pulse pressure amplitude (B) at the cranial (solid black line) and caudal (dashed grey line) location immediately before (pre-) and after (post-) decompression.

Table 5-4 Descriptive statistics and t-test results for the change in CSF pressure and pulse pressure amplitude at the time of decompression (N=11 for all rows). H_0: null hypothesis, H_a: alternate hypothesis.

	Mean	Standard Deviation	95% Confidence Interval	Paired t-test (H_0: mean=0)
CSF pressure change at time of decompression				
Cranial	-1.16	0.64	(-1.59, -0.73)	H_a: mean < 0 p = 0.0001
Caudal	0.65	1.04	(-0.05, 1.34)	H_a: mean > 0 p = 0.0325
Pulse pressure amplitude change at time of decompression				
Cranial	-0.12	0.20	(-0.25, 0.01)	H_a: mean < 0 p = 0.0373
Caudal	-0.01	0.10	(-0.07, 0.06)	H_a: mean > 0 p = 0.6265

A pulsatile waveform, with frequency components attributable to both arterial and respiratory origins (e.g. Figure 5-1A), was observed in all CSF pressure signals. The CSF pulse pressure amplitude differential was significantly different from zero immediately following the injury (i.e. the cranial CSFPPA was consistently greater than the caudal CSFPPA), but the rate of change over the compressed time was not significant (Table 5-3). At the time of decompression, the cranial CSFPPA decreased in seven and increased in four animals. The caudal CSFPPA decreased in five and increased in six animals (Figure 5-5B). The mean immediate decrease in CSFPPA due to decompression was significantly different from zero at the cranial location but not at the caudal location (Table 5-4). After decompression the cranial-caudal CSFPPA increased on average at 0.03 mmHg per hour, and this rate was significantly different from zero (Table 5-3).

The results for the sham animals were inconclusive because they exhibited different pressure patterns. For one animal the cranial pressure increased steadily throughout the first five hours and then appeared to plateau. The caudal pressure, in this animal, remained relatively constant for five hours then began to rise, and reached a plateau at around seven hours, but did not equalise with the cranial pressure within the experimental period. For the second sham animal, the cranial pressure remained approximately constant throughout the 14 hours; caudal results were not obtained in this animal due to transducer malfunction (Figure 5-6).
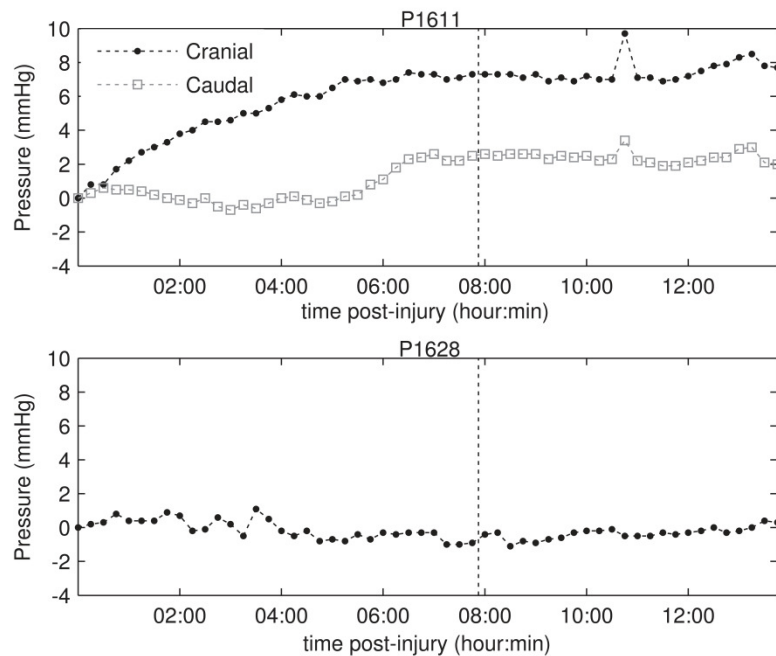
Figure 5-6 Cranial and Caudal CSF pressures for 14 hours post-injury, for the two sham animals (P1611, P1628). Vertical black dashed line indicates the time at which decompression *would* have occurred had these animals been in the experimental group.

5.4 Discussion

While ventricular and lumbar drainage of CSF has been a first tier treatment for intracranial hypertension of traumatic or pathological origin for some time [189,190,539], recognition of the potential impact of elevated CSFP on spinal cord perfusion has been relatively recent. Manipulating perfusion pressure via CSF drainage during thoracoabdominal aortic aneurysm surgery is reported to reduce the risk of iatrogenic ischaemic SCI [193-195], but the results of two studies of lumbar drainage after traumatic SCI [91,196] have raised questions regarding the distribution of pressure cranial and caudal to the injury site, particularly in the presence of subarachnoid occlusion. In this study we profiled the response of the CSF pressure and pulse pressure amplitude cranial and caudal to an experimental acute SCI followed by an eight hour sustained compression and six hours of decompression.

The porcine model was appropriate for assessing CSF pressures after SCI; the similar anatomy and human-like scale of this model are described in detail in Chapter 6. The animals were largely stable throughout the surgery; the gradually declining blood pressure is common during extended periods of anaesthesia [540]. In the pressure transducer drift characterisation test, the pressure transducer drift over 14.5 hours was acceptably low compared to the observed CSF pressure changes in the animals. The experimental SCI occurred at least 30-60 min after the last pressure transducer was implanted, well after the initial temperature equilibration and stabilisation period of the transducer.

We observed increased cranial CSF pressure and slightly decreased caudal CSF pressure during the sustained subarachnoid occlusion. To our knowledge, only one other animal study has measured CSF pressure cranial and caudal to a SCI in the hours after injury. In cats receiving a single contusive injury with no residual compression, Shapiro et al. found that the CSF pressure in the cisterna magna increased by a maximum of approximately 3.7 mmHg, and in the lumbar intrathecal sac pressure decreased by approximately 1.3 mmHg in four hours [211]. This is approximately three times the rate of change observed in the current study. In the majority of their 16 animals the pressure changes began within 15 minutes following injury, reaching statistical significance over baseline at 30 minutes, and then trended back towards baseline at around three to four hours. This differs from the general trend of continuous divergence from baseline that we observed for the entire eight hours of our "artificial" compression. Shapiro et al. [211] did not provide an artificial means of subarachnoid occlusion and did not assess spinal cord swelling, so it cannot be confirmed that the subsequent pressure differential in their experiment was a consequence of subarachnoid occlusion. Similarly, in our experiment, even with the static weight placed on the cord, we were unable to confirm with absolute certainty that the subarachnoid space was completely occluded in all animals, and this could certainly have contributed to some of the variability observed.

CSF pressure is determined by the balance of the fluid formation and absorption rates, the latter being determined by the resistance to outflow and the venous pressure [541]. The current knowledge regarding the uneven distribution of CSF formation and absorption sites in the cranial and spinal compartments supports the increased cranial and decreased caudal pressures observed during compression causing a subarachnoid occlusion. The primary location of formation is the choroid plexus of the lateral, 3rd and 4th ventricles [6,542]; while nonchoroidal sources such as the brain parenchyma contribute up to 20% of fluid production [13]. A *spinal* CSF production site has not been detected in any mammal tested [16-19,27]. CSF absorption is a passive process driven by a pressure differential between the subarachnoid and venous systems [45] and in normal individuals the absorptive capacity is thought to be much greater than that needed to maintain mass balance [38]. The primary CSF absorption sites are the cranial and spinal arachnoid granulations and villi [42,45,543] and the lymphatic pathways, specifically via the cribriform plate into the cervical lymph and via lymphatic channels in the dura [43,48]. Lymphatic absorption accounts for 40-48% of CSF clearance in sheep [30] and humans [544,545], and the lymphatic mechanism predominates at lower gradients while the arachnoid villi are secondarily recruited at higher pressures [48]. Spinal absorption has been demonstrated to account for 25% of total absorption in sheep [49] and 50% in cats [27]. In humans spinal absorption is estimated to occur at ~10 mL/hr [35] accounting for around 50% of total absorption. To the author's knowledge, CSF formation and absorption has not been evaluated in pigs. From a mass balance approach these observations support the observations that during compression the cranial pressure rises due to reduced

CSF absorption and continued formation in the cranial compartment, and the caudal pressure falls or remains static due to continued CSF absorption but lack of formation in the spinal compartment.

The caudal pressure increased and the cranial pressure decreased in immediate response to decompression. Kwon et al. [91] measured lumbar CSF pressure before and immediately after surgical decompression of SCI patients. They reported a mean increase in lumbar pressure of 7.9 mmHg at the time of decompression for 22 patients which is considerably larger than the mean increase observed in the current study (1.16 mmHg). The difference may be because the patients had a greater time between injury and decompression (mean 21.6 hrs) than the animals in the current study (8 hrs), and therefore more CSF accumulation cranial to the injury. Also, 17 of these patients had cervical injuries, compared to our lower thoracic injury model, which may lead to a greater cranial pressure increase due to the lower spatial volume available to compensate for the increasing fluid volume, and reduced availability of spinal absorption pathways. Further, human CSF pressure is generally higher than that reported in animals [100-102,104]. Early decompression is thought to improve patient outcome by reducing ischaemic effects from persistent cord compression [200]. The changes in cranial-caudal pressure differential observed in the current study indicate that another benefit of decompression may be the reduction of subarachnoid occlusion leading to decreased cranial compartment pressure (and therefore increased cord perfusion cranially), and reduced resistance to CSF outflow.

In the six hours after decompression both the cranial and caudal CSF pressures increased, but the pressure differential did not change. Kwon et al. [91] reported a significant mean peak increase (10.3 mmHg) in postoperative lumbar CSF pressure compared to the peak pressure recorded during decompression surgery. This is around five times higher than the mean increase in caudal pressure observed in the six hours after decompression in the present study. The disparity could be because pressures were recorded for longer after decompression in the patients (mean 56.3 hours) than our animals or because of the initial loss of CSF in our animals during pressure transducer insertion. In the aforementioned study of Shapiro et al., four animals were re-catheterised at 18-24 hours post-injury and pressures were not different to baseline [211]. That result contrasts distinctly with our observation that pressures at both the cranial and caudal sites were substantially different from baseline at 14 hours post-injury and may be due to differences in the severity of the induced injury, a species dependent response to injury, or that their study did not actively provide residual compression. Our results indicate that the resolution of the cranial-caudal pressure differential that occurred during decompression was generally maintained over the six hours after decompression.

Kwon et al. [91] reported peak lumbar CSF pressures above normal levels (i.e. >20 mmHg) following decompression in their SCI patients. The pressures that we observed in this animal model would generally not be considered to be above normal in an animal of this size [100-103]. This may be

because the loss of CSF (estimated to be 1-3 mL) during insertion of the pressure transducers artificially reduced the baseline pressure, and because the anaesthetic caused a progressive decline in blood pressure throughout the experiment.

We had expected that for the sham animals the cranial and caudal CSFP would be similar throughout the 14 hour test period, and that both pressures would gradually increase as the fluid lost during pressure transducer was re-formed. The increasing cranial-caudal differential observed during the first 5 hours for animal P1611 is difficult to explain, especially given that the histology and ultrasound confirmed that no spinal cord damage (Section 3.2.5) or thecal occlusion (Section 6.3), respectively, occurred as a result of the surgery alone. Data collection began approximately 15 minutes after pressure transducer insertion, compared to 30-60 min after insertion for the experimental animals, and this time period may represent the most rapid flow of CSF from the cranial to the spinal subarachnoid space resulting in the steep pressure recovery seen in animal P1611. The lack of concordance between cranial and caudal transducers until 5 hours may have been due to cranial-caudal compartments caused by the thoracic kyphosis. In animal P1628 only the cranial transducer produced reliable data, and in contrast to the other sham animal the pressure remained fairly constant for 14 hours. Unfortunately, financial constraints did not allow further sham animals to be tested. Despite the disparate results obtained in the two sham animals, we believe that the conclusions drawn from the experimental animals remain compelling.

In the current study caudal CSFPPA was generally lower than cranial CSFPPA, and this is consistent with previous observations that pulse pressure amplitude decreases along the cranio-vertebral axis [89,90]. This difference was more pronounced during compression than after decompression. In the six hours after decompression there was a small but significant increase in the cranial-caudal CSFPPA differential per hour. Although the magnitude (0.03 mmHg/hr) was smaller than the variation in the CSFPPA seen over a 30 second period (Figure 5-1E), the statistical model (LMM) was based on 5-minute averages each 15 minutes for all animals. Changes in caudal and cranial CSFPPAs appeared to be associated with the CSF pressures, which is consistent with previous observations when mean CSF pressure was increased experimentally [94,546,547], or by pathology [67,548]. The CSFPPA is known to be sensitive to acute systemic blood pressure elevation as shown with administration of epinephrine [549] and we observed this in animals that required treatment for cardiac arrhythmia.

Kwon et al. [91] noted that in some of their SCI patients the lumbar CSFPPA was essentially zero prior to decompression, but became distinct after decompression. In some of these patients the pulse pressure declined again in the 48 hours after decompression, and this was associated with MR imaging findings of residual compression of the thecal sac. Those authors suggested that the phenomenon of changing CSFPPA may be used to determine whether decompression of the cord and subarachnoid space

has been achieved. In our study all animals had a visible caudal CSF pulse pressure waveform during the compressed period. This may be because of the better resolution of our transducers and data acquisition system compared to the clinical monitors. Also, this may have been caused by incomplete occlusion of the subarachnoid space, as we were unable to confirm that the static weight that we left on the dura completely occluded this space and prevented fluid flow across the injury site. In our animals, the amplitude was generally lowest immediately before decompression, which occurred earlier in our study (8 hr after injury) than in the patient group (mean 23 hr after injury). In our study six animals had increased caudal CSFPPA upon decompression (mean 0.06 mmHg), but across all eleven animals the mean change was -0.01 mmHg. The representative data provided by Kwon et al. [91] indicates a threefold increase in CSFPPA after decompression. The small CSFPPA change we observed may largely reflect the small change in caudal CSF pressure at decompression, as per the mean pressure – amplitude association described above. The ability to detect small amplitude changes is probably also dependent on the method used to eliminate the respiratory artifact. No previous study that we are aware of has assessed CSFPPA as an indicator of decompression. Others have suggested that it may be an indicator of severity of hydrocephalus [98,550], and TBI [92,99]; however, caution in interpretation of CSFPPA changes has been urged as the parameter depends on many interacting physiological factors [551]. Although intraoperative ultrasound data indicated that removing the compressive weight restored subarachnoid space at the injury site (see Chapter 6) we did not consistently observe an association with caudal CSFPPA therefore this was not an indicator of decompression status in these animals.

There are several limitations in the methodology of this study. Firstly, we apparently did not achieve occlusion in three animals (Group C). We had expected the combination of the 100 g weight compression and cord swelling from the dynamic injury to provide subarachnoid occlusion; Yeo et al. [218] reported that in sheep receiving a severe T10 injury (50g – 20cm), there was no flow past the injury site between one and 24 hours post-injury, and this continued up to 44-100 hours after injury. We were not able to directly assess occlusion during the compressed condition. Other researchers have used subarachnoid kaolin injections [78,552,553], compression clips [554,555] extradural balloon catheters [292,445,556,557] or beads [558] and ligatures [209], to affect SCI and/or intrathecal occlusion in decompression or hydrocephalus studies in various animals. However, we felt that our method reasonably replicated the human situation wherein the malaligned canal or a bone fragment causes residual spinal cord and thecal compression.

The post-injury monitoring period was limited to 14 hours for practical constraints and to ensure the health of the animal under prolonged anaesthetic. The time from injury to decompression was shorter than reported for some clinical settings [202], but injury-to-surgery times of eight hours and less have been reported [202,559], and the observed trends are nonetheless indicative of the clinical sequelae. The delicate nature of the pressure transducers did not allow for continued measurement in a conscious

animal; however, pressure measurements in an ambulating animal are likely to be erroneous due to the changes in head and spine posture, and therefore would require serial sedation of the animal. The animals remained under general anaesthetic throughout; there is no published data directly reporting the influence of the drugs we used on CSF formation, absorption and pressure. Ketamine can induce increased brain metabolism and decreases cerebral blood flow [560]; however, it was only used for induction, reduces ICP only transiently in mechanically ventilated swine [561] and washout is expected in one hour [562]. Isoflurane has a rapid washout rate [563], minimal effects on ICP and cerebral blood flow [564] and reduces MAP but does not change CSFP in humans [565]. We were unable to avoid loss of CSF during pressure transducer insertion so while the pressure trends observed are indicative of what would happen in a SCI patient, the magnitude of the pressures and pressure changes are lower than might be expected clinically.

5.5 Conclusion

In the presence of a sustained full or partial intrathecal occlusion after an acute experimental SCI, the cranial spinal CSF pressure became progressively higher than the caudal CSF pressure. Decompression of the subarachnoid space resulted in redistribution of fluid pressure and this "equalisation" of pressure was largely maintained in the six hours after decompression. There was no consistent association between spinal cord decompression and increased caudal CSF pulse pressure amplitude. The results of this animal study suggest that CSF drainage by a lumbar intrathecal catheter is likely to be most applicable after surgical decompression relieves the occlusion of the subarachnoid space and the pressure differential across the injury site is resolved. Decompression may contribute to increased perfusion in the spinal cord cranial to the injury site, compared to the compressed state.

Chapter 6 Gross Morphological Response to Decompression[5]

6.1 Introduction

Decompression, the alleviation of spinal cord impingement from a malaligned or fractured spinal column, is recognised as an important procedure in the immediate post-injury phase of the treatment of acute traumatic spinal cord injury (SCI) [200]. Relieving pressure on the spinal cord is thought to promote the restoration of blood flow to the affected area, thereby reducing secondary degradation processes associated with ischaemia [566]. The optimal timing of surgical decompression remains uncertain [200]. Numerous animal studies have shown that early decompression can reduce secondary damage and/or improve functional outcome [207-209,554,567]. However, published clinical studies to date have been less conclusive regarding the merits of early decompression, in part due to ambiguity around the definition of "early" [200,559]. Improved understanding of the neural tissue's response to decompression may help to define appropriate indications, optimal timing and expected prognosis for decompression surgery for traumatic SCI.

Spine surgeons commonly utilise ultrasound imaging to intra-operatively confirm the adequacy of spinal cord decompression in traumatic and non-traumatic conditions. Ultrasound can provide a circumferential view of the spinal cord to demonstrate that it is free from mechanical compression, and is particularly useful for visualising the ventral side of the spinal cord (where compression is common, and is impossible to appreciate from a dorsal approach) [197,198]. Using ultrasound, the spinal cord is generally deemed to be decompressed when it appears to move freely within the dura with a patent subarachnoid space [199]. Despite intra-operative confirmation of spinal cord decompression, post-operative magnetic resonance imaging studies done within the acute (24-48 hrs post-surgery) and subacute (48 hrs – 7 days) periods often reveal that the cord has swelled up against the dura, filling the subarachnoid space. The development of this response is poorly understood.

The spinal cord's response to decompression has been studied with various imaging modalities; however, few studies pertain to traumatic SCI and none has monitored the cord dimensions in the immediate postoperative period. In patients with chronic cervical myelopathy, cross-sectional area and sagittal and coronal diameter have been quantified at preoperative, intraoperative and medium-term postoperative time points, and the observed pattern of residual deformation or increased dimension [568-

---

[5] A version of Chapter 6 is in preparation for publication. Jones CF, Kwon BK and Cripton PA. Gross morphological changes of the spinal cord immediately after surgical decompression in a large animal model of traumatic spinal cord injury.

571] had good prognostic value in some studies [568,571,572]. Mihara et al. [573] report a classification system for the intraoperative assessment of anterior subarachnoid space decompression for myelopathic conditions. With respect to traumatic injury, several studies have retrospectively measured the length of parenchymal edema and haemorrhage as indicated by hyperintensity of T2- and T1-weighted MR images, respectively, and reported some level of prognostic value [574-576]. Anatomical measurements have concentrated on bony measurements such as spinal cord compression and canal size at the injury level [577,578] but these do not distinguish between dura and spinal cord. The majority of clinical imaging studies are retrospective, and therefore the interval between injury, pre-operative scans and surgery is uncontrolled and varies widely within studies. Shimada et al. [576] included serial imaging studies, but these were in the chronic phase and only patients receiving conservative treatment were included, while Boldin et al. [575] studied postoperative images taken 5-12 days after surgical decompression. MR signal changes have been observed in rodents in the hyperacute (<6 hr) [579] and acute phase [580] after injury, but there was no period of sustained compression in these studies and gross morphology changes were not assessed.

To our knowledge, no study has previously described the gross morphology and sonographic features of the injured spinal cord and subarachnoid space, nor has any study been able to study the time-varying nature of these responses immediately following surgical decompression of a traumatic SCI. Such information would give insights into the temporal development of the acute secondary injury response and may explain how CSF flow obstruction at the injury site contributes to intrathecal pressure changes after injury. Additionally, expansion of the injured spinal cord up against the dura may result in further compression of the spinal cord, which could negate the potential benefits of the surgical decompression; and the dynamics of spinal cord swelling may shed light on this issue as well. We recently completed a series of SCI experiments in a large animal (porcine) model which had a spinal cord diameter that was representative of that of a human and that had a measurable, human-like, subarachnoid space. During these experiments, we had the opportunity to perform ultrasound imaging on the spinal cord at the site of the injury for six hours after decompression. The objective of this study was to quantify the changes in the spinal cord and subarachnoid space sagittal diameter and to describe the changes in ultrasound signal at the injury site for six hours after decompression following acute experimental SCIs of moderate and high severity.

6.2 Methods

All experimental procedures were approved by the University of British Columbia Animal Care Committee and complied with the guidelines and policies of the Canadian Council on Animal Care.

6.2.1   Animals and animal care

Thirteen female Yucatan miniature pigs (Sinclair Bio-Resources, Windham, ME, USA) were group housed and acclimatised at our facility for at least one week before surgery. The animals were divided into three experimental groups with the following demographics at surgery: sham: N=1, 142 days, 22 kg; moderate severity injury: N=6, 123.7 days (SD 11.3), 20.2 kg (SD 1.0); high severity injury: N=6, 125.3 days (SD 6.5), 21.7 kg (SD 2.9). Animals were fasted overnight before surgery. All surgical procedures were completed in a sterile field. Anaesthesia was induced with an intramuscular (IM) injection of Telazol 4-6 mg/kg, xylazine 0.6 mg/kg and intravenous (IV) atropine 0.02mg/kg. Animals were endotracheally intubated, and maintained on isoflurane (2-3.5% in oxygen during surgery; 1.5-2.5% in oxygen post-injury as required) for the procedure. Mechanical ventilation was maintained at 10-12 breaths/min with a tidal volume of 10-12 mL/kg, and end tidal CO_2 was maintained at 30-40 mmHg. Subcutaneous injections of ketoprofen (3 mg/kg), and bupivocaine (1-2 mg/kg) were given before the incisions for the central line and the laminectomy, respectively. Analgesics were administered before the surgery and as needed during the procedure (hydromorphone 0.15 mg/kg IM or morphine 1 mg/kg IM). Antibiotics were given immediately before surgery and every 4 hours thereafter (cefazolin, 20 mg/kg IV). Hydration was maintained with intravenous lactated Ringer's solution. Fluids were replaced with isotonic saline to counter respiratory alkylosis and/or dosed with 1-2.5% dextrose to counter hyperkalemia. Core temperature was monitored with a rectal temperature probe and maintained at 37.5-38.5 °C with a circulating-water heating pad. The urinary bladder was catheterised using an 8 French Foley catheter. Heart rate was monitored with ECG, blood oxygen saturation with pulse oximeter on the tongue, and blood pressure with a forelimb cuff, and ventilation and anaesthetic level were adjusted to maintain normal heart rate and blood pressure. Central arterial and venous catheters were placed surgically in the left carotid artery and external jugular vein. Blood gases and electrolytes were analysed periodically.

6.2.2   Injury protocol

The thecal sac was exposed via a laminectomy from T4 to L4. For a separate experimental protocol, four miniature flexible pressure transducers were implanted in the subarachnoid space, and the dura sealed with cyanoacrylate glue, prior to injury; these remained *in situ* for the whole experiment. The tips of the closest transducers were 30 mm cranial and caudal to the injury epicentre and did not interfere with ultrasound imaging. A SCI was carried out on the exposed cord at T11 using a weight-drop apparatus that was rigidly attached to the T10-T13 vertebra with pedicle screws. The injury device has been described in detail in Chapter 3. The moderate injury consisted of a 20 g weight dropped from 32 cm (impact velocity: 2.3 m/s) and the severe injury consisted of a 20 g weight dropped from 125 cm (impact velocity: 4.6 m/s). These parameters approximated the bone fragment weight and velocity

associated with burst fractures [132,462]. Immediately after injury, the impact weight was removed and a 100 g weight with a 9.53 mm diameter flat circular tip, supported by the guide rail, was slowly and gently placed at the injury site to mimic ongoing compression of a bony fragment, as is typical in burst fracture or fracture-dislocation injuries. After eight hours of compression, the 100 g weight was removed and monitoring continued for another six hours. This duration was chosen as a compromise between what would be clinically relevant and what was experimentally feasible for the animal model. The sham animal received all surgical procedures (i.e. laminectomy, cord exposure, pedicle screw and pressure transducer insertion) and ultrasound imaging, and was monitored for the same 14 hour period. The injury and post-injury sustained compression were not applied in the sham animal.

6.2.3 Ultrasound

Mid-sagittal plane B-Mode ultrasound images were obtained at the injury site with a 14 MHz linear array probe (L14-5W/60, 60 mm linear array, centre frequency 9.5 Hz; Ultrasonix RP, Ultrasonix Medical Co., Richmond, BC, Canada). The 480×640 images had a length of 73.6 mm and a resolution of 0.115 mm. For the experimental animals, sets of five images were obtained prior to injury, immediately (within ten minutes) after decompression, and then every hour for six hours thereafter. For the sham animal, sets of five images were obtained every two hours over the 14-hour experiment. The surgical site was filled with sterile saline to provide coupling between the probe (with a sterile cover and ultrasound gel) and tissue, with a standoff distance of 5-10 mm, and dorsal-to-ventral images were obtained in the mid-sagittal plane. This plane was determined by maintaining a vertical and midline probe alignment relative to the spinal column and by ensuring that the central canal was visible in the image. The pulsatile motion of the dura was visible [581]; the operator acquired the image at the point in the cycle corresponding to maximum dura distension to provide the most consistent and also the greatest measure of subarachnoid space. All ultrasound scans were performed by a single investigator (CFJ), except the pre-injury images, which were performed by the surgeon under instruction of CFJ.

6.2.4 Image analysis

The anterior and posterior borders of the spinal cord and dura were manually segmented in every image using Analyse software (Analyse 8.0, Analyse Direct, Overland Park, KS, USA). For the dura the inner (cord side) surface was segmented. The approximate centre of three intervertebral discs and the centre of the visible lesion were also delineated. All images were segmented by one investigator (CFJ) who was blinded to the animal and the time point. This coordinate data was then post-processed in Matlab (2009b, The Mathworks, Mattick, MA, USA). The sagittal diameters of the spinal cord and dura (subarachnoid space) were defined as the distance between each point on the anterior border and the corresponding point on the posterior border with the same caudal-cranial coordinate. The diameters were

also calculated using a minimum Euclidean distance criterion which would account for cord/dura curvature, but this gave very similar results and so is not reported.

The minimum and maximum diameter of the spinal cord and the thecal sac within 10 mm rostral and caudal to the lesion epicentre (approximately twice the impounder diameter) were determined for each image. In the same region, the diameter of the thecal sac at the minimum and maximum cord diameter was determined as a measure of subarachnoid space patency (Figure 6-1). The mean value for each set of five images was then calculated, to give one value for each variable at each time point.
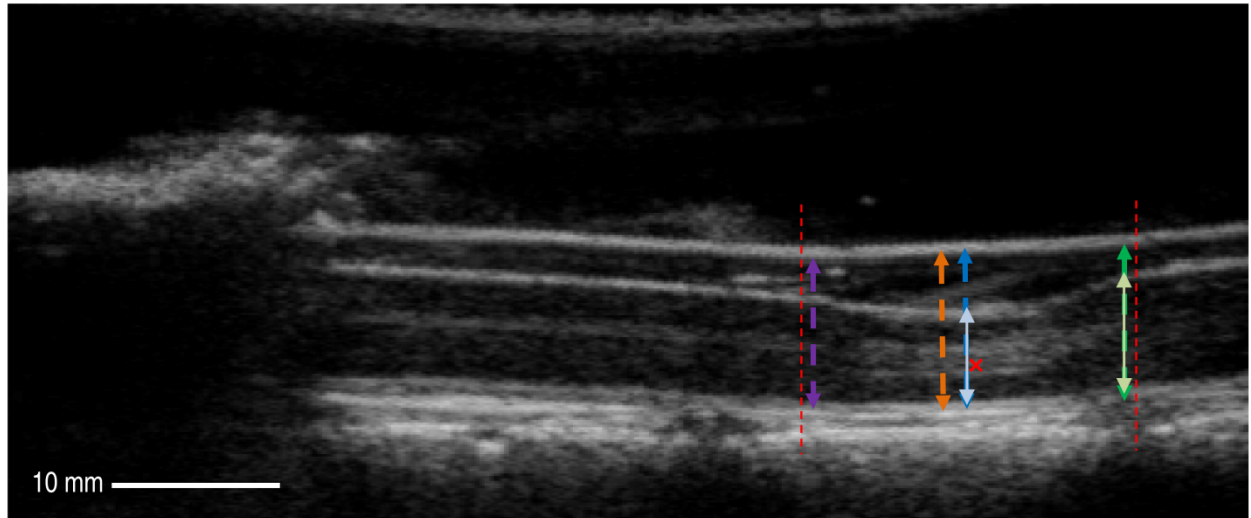
Figure 6-1 Representative post-injury ultrasound image indicating the location of the parameters determined for each image. Approximate centre of the lesion (red cross), outer borders of the length in which the diameters were determined (dashed red lines), minimum spinal cord diameter (light blue arrow) and dura diameter at that location (dark blue arrow) used to determine maximum subarachnoid space diameter, maximum spinal cord diameter (light green arrow) and dura diameter at that location (dark green arrow) used to determine minimum subarachnoid space diameter, minimum dura diameter (purple arrow) and maximum dura diameter (orange arrow).

To assess the intra-reader reliability of the image segmentation, a set of eight images (one for each time point) was randomly selected from different animals, and segmented once each day for ten consecutive days. For each image the standard deviation of the mean for the minimum and maximum spinal cord and dura diameters, and subarachnoid spaces was calculated. The root mean squared of the eight standard deviations [RMSSD$= \sqrt{SD^2/8}$] was then calculated for each measure.

The changes in minimum and maximum spinal cord diameter, thecal sac diameter, and subarachnoid space from pre-injury to six hours post-decompression were assessed. Differences in immediate and longitudinal response between the two injury groups and the sham animal were examined. We defined effective subarachnoid occlusion to be a subarachnoid space of less than 0.5 mm.

The lesion site was graded qualitatively according to the extent of abnormal (increased) parenchymal echogenicity relative to the surrounding parenchyma using the images taken immediately and six hours after decompression. A five-point scale, adapted from [582], was used (Table 6-1).

Table 6-1 Qualitative grading scale for increased parenchymal echogenicity on ultrasound images

Grade	Description
Grade 0	no area of altered echogenicity
Grade 1	diffuse non-specific altered echogenicity (small change in brightness, texture change)
Grade 2	focal increased echogenicity <0.5 cord diameter
Grade 3	focal increased echogenicity >0.5 and <1 cord diameter
Grade 4	increased echogenicity = 1 cord diameter
Grade 5	increased echogenicity = 1 cord diameter plus local hypogenic formations within echogenic area

6.3 Results

One animal (P1676) from the high injury severity group died five hours after injury and was excluded from the analysis. Animals P1700 and P1642 from the moderate severity group exhibited cardiac arrhythmia and bradycardia at four and six hours post-injury respectively; they were treated with epinephrine and atropine, were subsequently stabilised and had no further complications. Ultrasound data was not collected at one time point for two animals (P1800, P1697) and two points for one animal (P1700).

The features observed in the images were qualitatively similar to those previously described for ultrasound studies of the normal and injured spinal cord [581,583]. The borders of the spinal cord and dura were visible in all images. The central canal was generally visible, except at the lesion site after injury. The anterior border of the spinal canal and the epidural fat were both highly reflective and therefore not distinguishable. Intervertebral discs appeared as anechoic masses ventral to the dura, and in some cases reflections from the pedicle screws were also observed (Figure 6-2).
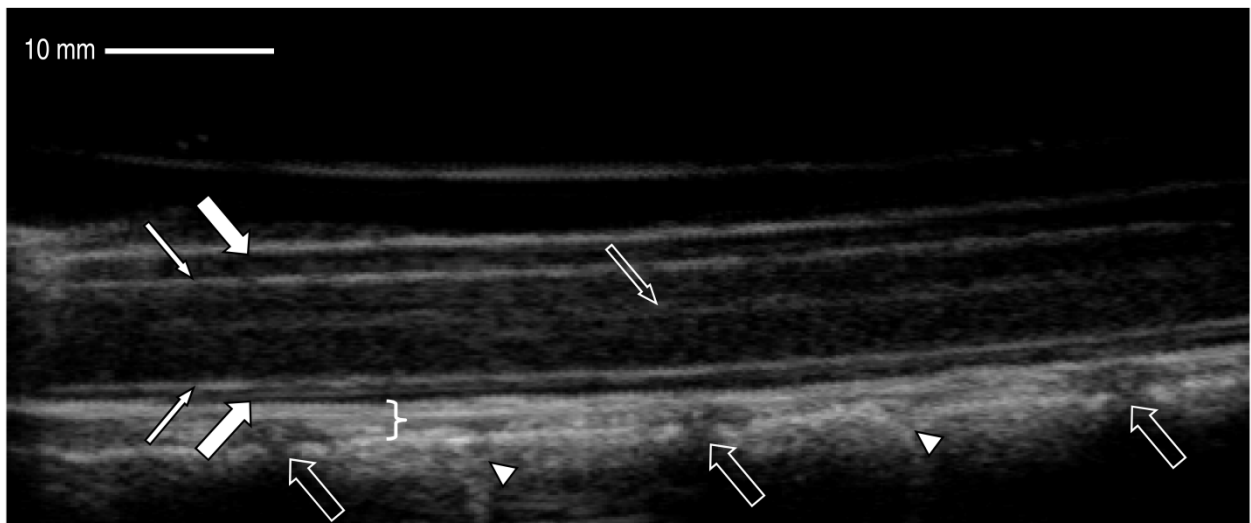
Figure 6-2 Pre-injury ultrasound image indicating the location of spinal cord anatomy visible on the ultrasound images. Dorsal and ventral inner boundary of the dura (large filled arrows), outer border of the spinal cord (thin filled arrows), central canal (thin open arrow), epidural fat and posterior border of vertebral bodies (bracket), intervertebral discs (large open arrows) and reflection from pedicle screws (filled arrowheads).

The intra-reader repeatability of the segmentation method, expressed as the root mean squared standard deviation (RMSSD) of ten repeats of eight images, ranged from 0.08 to 0.10 mm for the parameters requiring two data points (minimum and maximum diameter for spinal cord and dura). For the subarachnoid space measurements, which required four data points, the RMSSD was 0.14 mm.

The mean pre-injury spinal cord diameter was 5.6 ± 0.4 mm and that of the thecal sac was 7.0 ± 0.5 mm, for all experimental and sham animals. The difference between cord and thecal sac diameter (i.e. subarachnoid space) at the location of the minimum pre-injury cord diameter was 1.5 ± 0.4 mm, and at the location of the maximum pre-injury cord diameter was 1.3 ± 0.4 mm.

For the sham animal, the mean minimum spnal cord diameter over seven samplings in 14 hours was 5.7 ± 0.1 mm (range 5.6-5.8 mm), and the mean maximum diameter was 6.0 ± 0.1 mm (range 5.9-6.1 mm). The minimum and maximum thecal sac diameters showed slightly more variation, 6.8 ± 0.1 mm (range 6.6-6.9 mm) and 7.2 ± 0.2 mm (range 7.0-7.4 mm) (Figure 6-5F).

The physical response of the spinal cord to decompression following acute injury and eight hours of sustained compression varied among animals and was characterised by localised residual deformation and/or increased diameter (swelling) of the spinal cord (Figure 6-3). In seven (four moderate/three high injury severity) of 11 animals, there was a residual deformation of up to 0.6 mm within ten minutes after decompression, with a length approximately equal to the impactor diameter (Figure 6-4A,B,C,F; Figure 6-5 A,D,E). This deformation resolved to the diameter of the surrounding unaffected cord within one to

three hours after decompression (Figure 6-3A) in all but one case. In four of these cases, although a localised depression at the point of impactor contact was visible on the image, the minimum cord diameter was not smaller than the pre-injury value. This was probably because the cord had swollen both at the injury site, and rostral and caudal to the static weight during the eight hours of compression. This is referred to as a "general swelling" in the remainder of the manuscript. To capture this observation, qualitative grades (small/medium/large) were assigned to the residual deformation. In addition, the time at which the residual deformation was resolved (i.e. the lesion site diameter appeared to match the diameter of the rostral and caudal cord) was established. Qualitative grades of local swelling (small/medium/large) and rate of local swelling (immediate or gradual) were also assigned (Table 6-2).
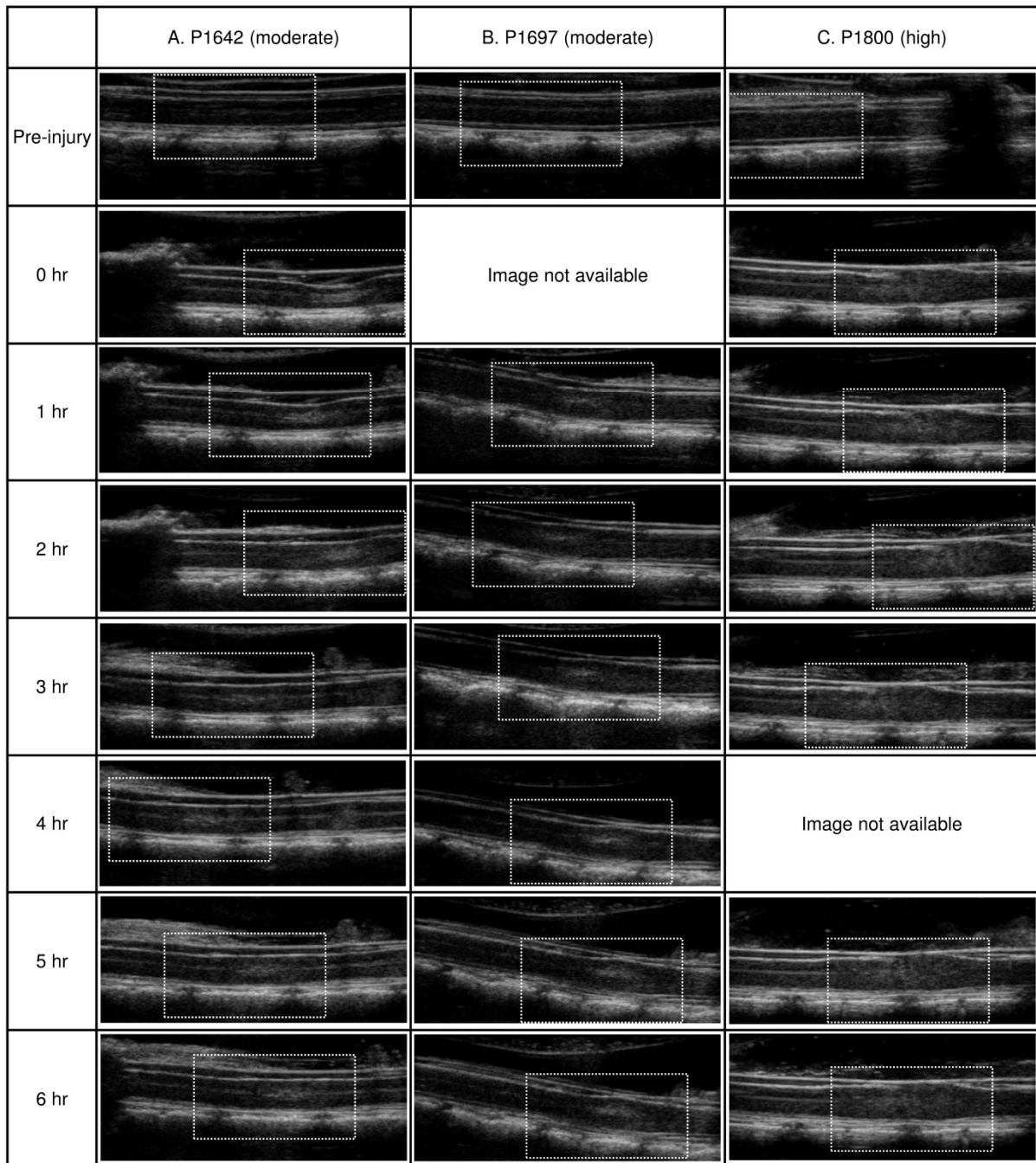
Figure 6-3 Example ultrasound images depicting three typical responses, in three subjects, to decompression following an acute injury with eight hours sustained compression. The 0 hr image was taken within 10 minutes of decompression. (Column A) Residual deformation followed by swelling, in a moderate injury severity animal (P1642, moderate injury severity); (Column B) Gradual swelling leading to subarachnoid space <0.5 mm at4 hr, in a moderate injury severity animal (P1697, moderate injury severity); (Column C) Rapid swelling and interruption of the anterior pia/spinal cord, in a high severity animal (P1800, high injury severity). White rectangle indicates location of injury and approximate area used for analysis.
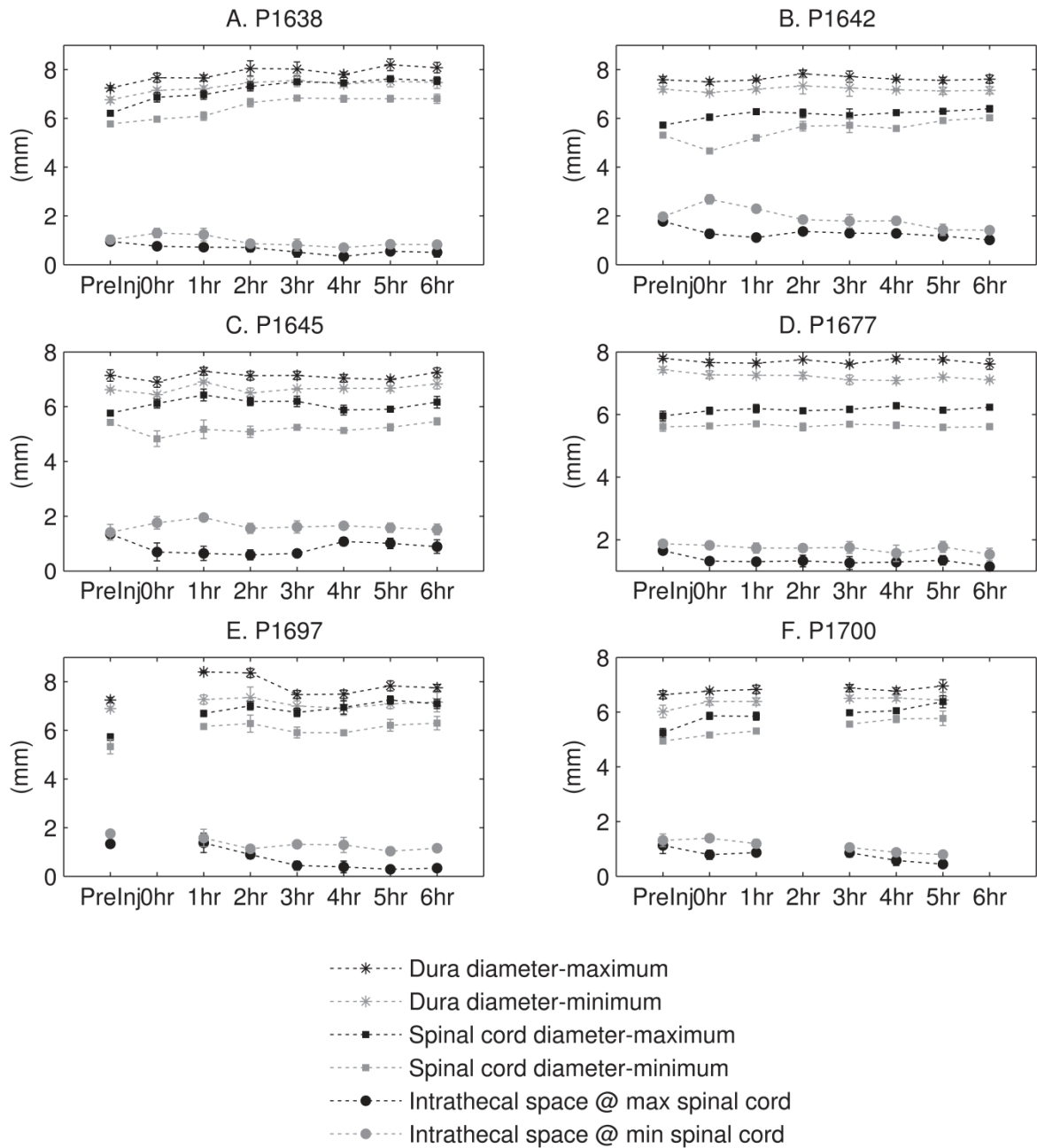
Figure 6-4 Moderate Injury Severity Animals (panel A-F). Maximum and minimum dura diameter, spinal cord diameter, and subarachnoid space at the maximum and minimum spinal cord diameter, for pre-injury, immediately after decompression (following eight hours sustained compression), and once per hour thereafter until six hours post-decompression. Ultrasound images not available for P1697 (0 hr) and P1700 (2 hr). Values are mean (of five ultrasound images) ± standard deviation.
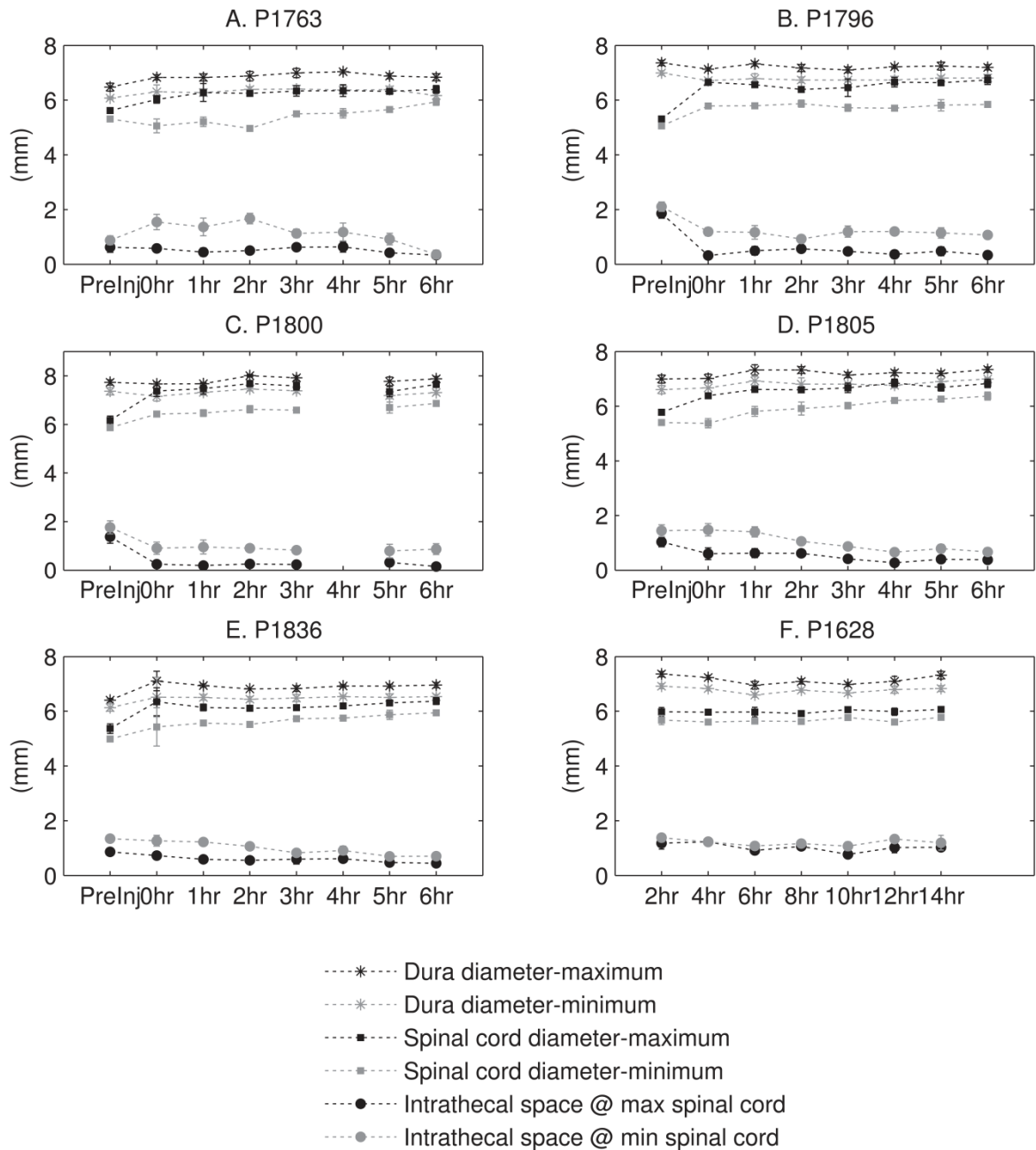
Figure 6-5 High injury severity animals (panel A-E) and sham animal (panel F). Maximum and minimum dura diameter, spinal cord diameter, and subarachnoid space at the maximum and minimum spinal cord diameter, for pre-injury, immediately after decompression (following eight hours sustained compression), and once per hour thereafter until six hours post-decompression. Ultrasound images not available for P1800 (4 hr). Values are mean (of five ultrasound images) ± standard deviation.

In six of eight cases with residual deformation, the resolution of the deformation was followed by swelling of the spinal cord centered around the injury site (Figure 6-3B). In three (one moderate/two high injury severity) of the four remaining cases, a large increase in cord diameter of up to 1.3 mm was

apparent immediately after decompression (Figure 6-3C; Figure 6-4E; Figure 6-5B,C). The final animal (moderate injury severity) exhibited only a small increase in cord diameter over six hours (Figure 6-4D).

The maximum and minimum thecal sac diameters tended to be stable over six hours, with the greatest changes generally being an increase between pre-injury and immediately after decompression. There was no detectable residual deformation of the dura at the injury site immediately after decompression. For two animals, the standard deviation of the maximum and minimum dura diameter over six hours exceeded that of the sham animal, and these increases trended closely with large increases in cord diameter that were immediate (P1697) and gradual (P1638) (Figure 6-4A,E).

Eight animals (three moderate/five high injury severity) obtained a subarachnoid space of <0.5 mm within six hours after decompression (Figure 6-4A, E, F; Figure 6-5A-E; Table 6-2). This threshold was considered to represent subarachnoid occlusion due to the accuracy with which the cord and dura materials could be distinguished when in close proximity on the images. It is noted that the presence of a patent lateral thecal sac, due to lateral dura "bulging" or a lack of lateral cord swelling, could not be confirmed on these mid-sagittal plane images; however, it is likely that swelling occurred in a radial manner rather than uni-directionally.

Table 6-2 Summary of qualitative and quantitative spinal cord morphology and lesion ultrasound grade for each animal.

Animal	Injury	Residual Deformation	Swelling	Subarachnoid space <0.5mm	Grade@ 0/6hrPD	Comment
		none/small/med/large (time at resolution)	none/small/med/large (gradual/immediate)	Time (min. space, mm)		-
P1628	Sham	None	None	N/A	0 / 0	No ultrasonic evidence of injury or changes.
P1638	Mod.	Medium (1hr PD)*	Large (gradual)	4hr PD (0.4)	3 / 4	Dorsal surface interrupted. Central canal not visible.
P1642	Mod.	Large (2hr PD)	Small (gradual)	NA (1.0)	2 / 1	Central canal not visible.
P1645	Mod.	Large (>6hr PD)	Small (gradual)	NA (0.5)	1 / 0	-
P1677	Mod.	None	Small (gradual)	NA (1.1)	1 / 1	-
P1697	Mod.	Small	Large (immediate)	3hr PD (0.3)	2 / 2	-
P1700	Mod.	Small (1hr PD)*	Medium (gradual)	5-6hr PD (0.4)	3 / 3	Central canal not visible.
P1763	High	Large (3hr PD)	Large (gradual)	6hr PD (0.3)	4 / 4	Dorsal surface interrupted. Central canal not visible.
P1796	High	None	Large (immediate)	0hr PD (0.3)	4 / 4	Dorsal surface interrupted. Central canal not visible.
P1800	High	None	Large (immediate)	0hr PD (0.1)	4 / 4	Dorsal surface interrupted. Central canal not visible.
P1805	High	Small (1hr PD)*	Medium (gradual)	4hr PD (0.3)	4 / 4	Central canal not visible.
P1836	High	Small (2h PD)*	Large (edges immediate, centre gradual)	5-6hr PD (0.4)	4 /4	Dorsal surface interrupted. Central canal not visible.

Mod.= moderate; PD=post-decompression; *local residual deformation not indicated by minimum spinal cord diameter due to general swelling.

Note that animal P1676 was excluded from the analysis because it died before decompression.

Increased parenchymal echogenicity at the injury site following decompression was observed in all animals. All animals in the high injury severity group had Grade 4 changes both immediately after decompression and at the end of the experiment, while those in the moderate severity group had Grades 1 to 3 (Figure 6-6). In general the hyperechogenic area did not change substantially in diameter or length over the six hours. In four of five high severity animals the dorsal surface of the cord (potentially the pia mater) had an interrupted appearance at the lesion site (Figure 6-3C; Table 6-2); this occurred in only one moderate severity animal. In general, the central canal became indistinguishable at the injury site (Table 6-2), probably in part due to the increased echogenicity at the lesion site. Two animals from the high injury severity group (P1805, P1836) had small hypoechogenic formations with the echogenic lesion area (Figure 6-6D).
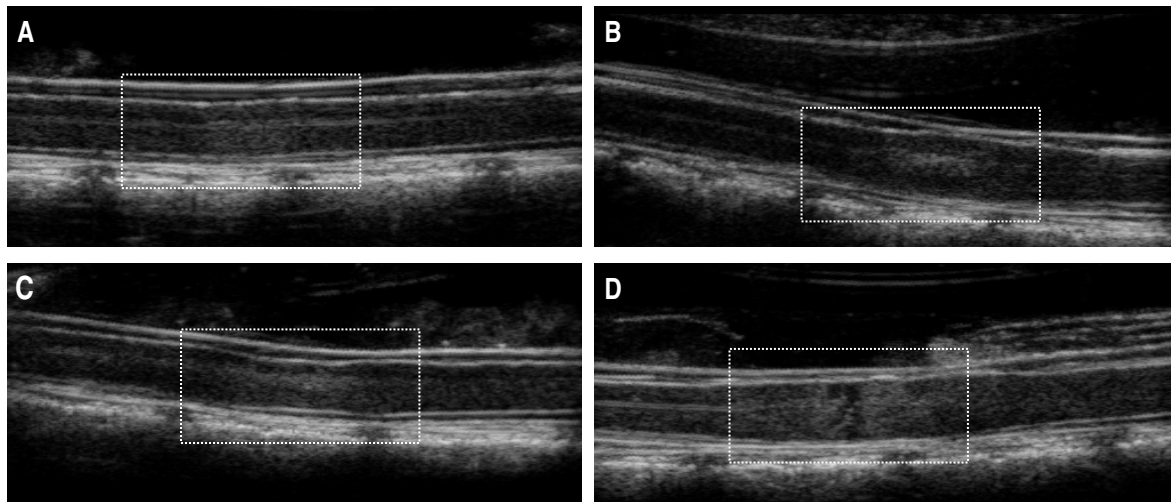
Figure 6-6 Ultrasound images showing examples of graded echogenic changes. (A) Grade 1 (P1677, 1hr); (B) Grade 2 (P1697, 6hr); (C) Grade3 (P1700, 6hr); (D) Grade4, with hypoechogenic area (P1805, 6hr). White rectangle indicates location of injury.

6.4 Discussion

In this study, serial ultrasound images of the lesion site were employed to quantify the change in gross morphology of the spinal cord, thecal sac, and subarachnoid space after decompression following an acute contusive SCI with eight hours of sustained compression in a pig model. We observed several morphologic patterns after decompression, including residual local tissue deformation, gradual tissue relaxation and swelling, and immediate cord swelling, which were generally dependent on the initial injury severity.

The human-like ultrasound features, human-like scale, and good measurement reliability indicated that the pig spinal cord represents a reasonable model for characterising the spinal cord and dural response to decompression. Although the accuracy and repeatability of this method have not been completely characterised, the resolution and repeatability measures indicate that the imaging was suitable for within-specimen comparisons. Both the pre- and post-injury ultrasound images showed features consistent with ultrasound investigations of human and other animal spinal cords. The sagittal diameter of the cord was very similar to the average human thoracic cord (4-8 mm) [391,393,394] but the dura diameter was relatively smaller than reported for humans (9-16 mm) [391,394]. This was at least partially attributable to the loss of CSF that was inevitable during the placement of the pressure transducers used in the partner investigation of CSF pressure during and after contusion SCI (Chapter 3 and Chapter 5). The variation in spinal cord and thecal sac diameter for the sham animal over 14 hours was of the same order of magnitude as the measure of intra-reader reliability, indicating that changes are not induced by the surgical procedure in the absence of injury and compression/decompression.

The observation of local residual deformations (from the tip of the weight) of up to around 10-15% of the pre-injury cord diameter was unexpected. This delay in recovery of the normal shape may be attributed to a combination of the viscoelastic material behaviour of the tissue [e.g. 226,228], essentially due to the gradual re-uptake of fluids which were previously expelled by the compressive force, and physiological responses to the injury such as haemorrhage and inflammation, ultimately resulting in edema. *Ex vivo* compression tests have shown that an intact pia helps restoration of spinal cord shape after decompression [235]. In some cases a visible residual deformation on the ultrasound image was not associated with a reduced minimum spinal cord diameter compared to the pre-injury value, indicating that there was a general swelling of the cord across the analysed region during the sustained compression phase.

The low injury severity animals were more likely to have a larger residual deformation, and these did not usually swell to occlude the subarachnoid space. However, animals with a moderate or small residual deformation commonly exhibited subsequent cord swelling that approached complete subarachnoid occlusion (<0.5 mm diameter difference) in the sagittal plane. This indicates that a spinal cord that appears unobstructed during intraoperative assessments after surgical decompression may not remain so for a substantial amount of time.

The lack of residual deformation of the thecal sac is unsurprising, since the dura exists under a physiologic longitudinal strain [250] due to nerve root and ligament tethering and possibly a fluctuating radial strain due to the pulsating hydrostatic pressure of the CSF. Furthermore, visual inspection of the dura surface did not reveal macroscopic damage which we would expect to be associated with irreversible

plastic deformation of the tissue. Its shape is probably also influenced by the redistribution of cerebrospinal fluid after decompression (see Chapter 5).

The dural membrane is elastic [e.g. 246,249,260], and therefore the variation in diameter of the thecal sac after decompression can be attributed to changes in the contained volume and pressure, from a combination of CSF volume and pressure changes, and local spinal cord volume changes. The former was likely as some fluid was lost during insertion of pressure transducers that were inserted for the study reported in Chapter 5 in which we measured CSF pressure before and after decompression. In general, a gradual increase in the CSF pressure was observed during the six hours after decompression. This may have been partly due to swelling of the spinal cord (in addition to continuous CSF formation), and the increased pressure would also likely cause some distension of the dura. A small step change in available subarachnoid volume may also occur at the time of decompression due to the removal of the weight.

The high injury severity group tended to exhibit extensive swelling immediately after the decompression – an observation that is consistent with the notion that this morphologic response is related to injury severity. Additionally, in some of these animals we noted that the reflectivity of the pial surface on ultrasound was no longer uniform, suggesting that the pia mater was disrupted (and that this too is likely a reflection of injury severity).

The rapid swelling observed suggests that there is a need for early interventions after SCI that reduce tissue swelling and maintain parenchymal perfusion. The reduction in tissue swelling with hyper-osmotic agents such as mannitol has been studied extensively in TBI [584], although its use in SCI is uncommon. The fact that the spinal cord may swell to fill the subarachnoid space and potentially exert pressure upon the dural membrane has led some to surgically open the dura and expand the intrathecal space around the cord, although this is not a commonly accepted clinical practice [212-217].

Although our primary goal was to measure the morphological response to decompression, we also noted changes in the intraparenchymal signal after injury and these were consistent with those seen previously in human SCI [582] and experimental animal SCI [583]. The increased echogenicity of the parenchyma that was observed has been attributed to contusion, edema and haemorrhage in traumatic injuries in the acute and subacute phases [582,585]. An obscured central canal, which was observed in most of the animals, is commonly associated with intra- and extra-medullary lesions [581]. The data showed a distinct difference in ultrasound features for the two injury severities – the high severity group tended to have greater alteration of echogenicity over a larger area. This is consistent with the observation that edema and haemorrhage seen on pre- and post-operative MR images correlate to some extent with medium- and long-term clinical neurological deficit after SCI [575-577,586]. Two animals had small areas of decreased echogenicity within the lesion area; localised anechoic features are associated with cysts in other spinal pathologies [582], but cysts would not be expected until the late

phases of injury [151] so the significance of this observation is unclear. Finally, in some animals the signal appeared disrupted on the anterior surface of the cord and this may indicate that the pial membrane was damaged during the mechanical insult.

There are challenges associated with modeling a clinically relevant injury for which the mechanical parameters are largely unknown and the timing of events is highly variable, as is the case in SCI. The sustained compression was achieved with a 100 g weight which was selected to mimic occlusion of the subarachnoid space by a bone fragment; it is not known how well this represents the force imparted by a bony impingement. Although dural compression was visually confirmed, the cord and thecal sac dimension were not measureable with the weight in position. We feel that our acute SCI with sustained compression model is more clinically relevant compared to some models that have applied static compression without a primary dynamic injury or that have used very short periods of compression [reviewed in 200]. The eight hour time period from injury to decompression in this experiment is shorter than reported for some clinical settings [e.g. 91,203,204] but similar and shorter injury-to-surgery times have been reported or are likely achievable in some centers [202,559] and transfer time between the injury scene and tertiary care admission is consistently decreasing [205]. There is ongoing debate regarding the optimal timing of decompression [200]. The use of the pig for this SCI model is also unique in that its spinal cord is close to human scale, so that gross morphology changes are probably directly translatable to humans and human-like injury parameters could be approximated without need for scaling.

There are several limitations associated with the protocol and ultrasound measurements. As noted above, the subarachnoid space was probably slightly smaller than normal, particularly in the pre-injury scans, because of CSF loss during pressure transducer insertion. Further, the diameter of the thecal sac may have been modified by the water bath placed around it; however, this is likely minimal and a uniform volume of water was used for each scan. The laminectomy may have allowed the dura and cord more mobility than if they were constrained by the dorsal spinal canal, and also precluded assessment of extradural occlusion. Due to the size and shape of the ultrasound transducer, the dura and cord morphology were assessed in the sagittal plane only; however, it is probably reasonable to assume that swelling occurs in a radial manner. Finally, we did not calibrate our measurements specifically for the speed of sound in spinal cord tissue, but all results are comparative.

6.5 Conclusion

Following decompression after an acute experimental SCI, the changes in spinal cord morphology over six hours were characterised by (1) residual deformation followed by gradual swelling, (2) gradual swelling leading to subarachnoid occlusion, or (3) immediate swelling with associated subarachnoid occlusion. The profile of residual deformation and swelling appeared to be dependent on the severity of

the initial injury. This may partly explain the variable response seen in clinical studies of early decompression and may point to a patient subset in which the benefits of the typical surgical decompression may be negated or attenuated by subsequent swelling. The rapid onset of subsequent intrathecal occlusion may have implications for the biodistribution of biologic therapies administered intrathecally.

Chapter 7   Integrated Discussion

7.1 Overview

Five studies were undertaken in three phases to assess the roles and characteristics of CSF in SCI. In phase 1, a novel large animal model was developed that enabled, for the first time, the characterisation of CSF pressure transients associated with contusion type SCI. In phase 2, a novel bench-top model was designed and constructed to explore the relationship between the CSF layer and mechanical parameters determining the severity of injury. Finally, in phase 3, the animal model was used to conduct a novel investigation of post-injury CSF pressure distribution and morphological response to decompression. The work presented in this thesis demonstrates that the CSF and the thecal sac contribute to the biomechanics of the SCI at the instant of injury and respond to subsequent thecal occlusion and decompression in a manner that may have implications for the clinical management of SCI.

7.2 Summary of findings

A contusion SCI model in the Yucatan miniature pig was developed and provided preliminary evidence for the potential of CSF pressure transients to contribute to SCI. A novel injury device, based on the weight-drop technique and with the ability to measure impact load and velocity, was designed, built and used to create a new large animal SCI model. A technique for implanting miniature pressure transducers into the thecal sac was developed. Preliminary data were collected to support the further investigation of CSF pressure transients as contributors to SCI. The injury model was also used, after device modifications, for the studies presented in Chapters 3, 5 and 6.

CSF pressure transients associated with experimental spinal cord injuries of moderate and high human-like severities are of a magnitude comparable to pressure transients associated with neural tissue damage reported in the literature. The injury device and animal model developed in Chapter 2 were further refined and used in Chapter 3 to measure CSF pressures at multiple locations along the cord length at the instant of injury. For both 2.3 m/s and 4.6 m/s impact velocities, the peak CSF pressures measured at 30 mm from the injury epicentre were within the upper range of pressures associated with experimental brain injuries induced by fluid percussion techniques and external blast overpressures. Because pressure thresholds for spinal cord tissue damage have not been defined, these brain injury metrics were used to indicate pressures at which neural tissue is affected. The CSF pressure wave was rapidly attenuated such that within 100 mm of the injury epicentre the peak pressures were in the lower range associated with experimental TBI and, for the 2.3 m/s impact velocity, approached the level of transients induced by everyday activities.

The dimension of the CSF layer, and the velocity of impact, affects the magnitude of the peak CSF pressure, impact load, tether load and cord compression in a bench-top model of SCI. In Chapter 4, a novel bench-top model was used to assess the effect of CSF layer thickness and impact velocity on the key mechanical parameters which determine the severity of an SCI. Increased CSF layer thickness and/or decreased impact velocity led to reduced peak pressure, lower impact loads, slightly higher tether loads and less cord compression. This suggests that researchers should consider using models of SCI with human-like CSF dimensions and impact velocities particularly if mechanical biofidelity at the neural tissue level is desired. SCI risk metrics may have more predictive strength if a measure of CSF layer thickness is incorporated.

The CSF pressures cranial and caudal to a SCI lesion are affected by sustained thecal occlusion and subsequent decompression. CSF pulse pressure amplitude is not affected substantially by these conditions. Haemodynamic support and early decompression are two clinical management options for SCI that aim to maintain spinal cord perfusion. Draining CSF via a lumbar catheter has been proposed as an adjunct to these. However, it is unclear how the distribution of CSF is affected by thecal occlusion and subsequent decompression since this cannot be assessed in patients. In Chapter 5 it was demonstrated, using the large animal model, that prior to decompression the cranial CSF pressure increased and caudal CSF pressure either decreased or remained the same. Thus, the cranial-caudal differential increased steadily over eight hours of thecal sac occlusion. At the time of decompression, the cranial CSF pressure decreased and the caudal CSF pressure increased immediately, thereby reducing or eliminating the differential. The differential was then largely unchanged for six hours after decompression. In contrast to some observations in patients, the caudal pulse pressure amplitude did not change significantly at the time of decompression in the animal model.

The spinal cord's morphological response to decompression is dependent on the severity of the initial injury; for more severe injuries, swelling subsequent to decompression may occlude the thecal sac. Post-surgical MR images of SCI patients often reveal cord swelling and thecal sac occlusion at 24-48 hours after decompression surgery. In Chapter 6 ultrasound images were taken to assess the changing morphology of the spinal cord and dura at the injury site in the six hours immediately following decompression in the pig model. The response of the cord after decompression was dependent on the impact velocity. Residual deformation of the cord occurred for the moderate injury severity but tissue relaxation and/or enlargement gradually resolved this within six hours. For higher severity injuries the cord swelled immediately upon decompression and tended to lead to thecal occlusion as assessed in the mid-sagittal plane.

7.3 Modelling considerations

In the pursuit of viable treatments for SCI, numerous animal, cadaver, bench-top and computational models have been developed and optimised to examine specific biomechanical or neuroscientific hypotheses. Evaluations that are feasible in the experimental setting are often not possible in the clinical setting because patient wellbeing must not be compromised. Large animal models, in addition to playing an important role in basic science investigations, can therefore provide invaluable information to guide the priorities of clinical research.

The SCI animal model developed for this thesis was based on a weight-dropping technique which is historically the most common method of creating a contusion type SCI in large animals such as dogs, cats and NHPs. However, compared to methods previously reported, the pig model described in this thesis has several unique features which make it particularly suited to the objectives of the studies. Few SCI models have been developed using the pig, despite it presenting fewer ethical concerns than domestic pets and NHPs (Section 1.6.1). The Yucatan miniature pig has spinal cord and dural dimensions more similar to human (see below) than the predominant rat models and the small NHPs that are sometimes used as intermediaries for pre-clinical studies [295,361]. The miniature species is also well suited to chronic studies because the animals have a slow growth rate and low weight at maturity, thereby reducing the complexity of post-injury care and handling.

Previous reports of large animal weight-drop models have not explicitly demonstrated that the height and weight used to create the injury was based on the kinematics and kinetics of the bone-cord interaction in a human SCI. This is in contrast to TBI work in which researchers have often attempted to scale the injury parameters to the size and age of the animal used [376,587]. Figure 7-1 illustrates the height and weight settings that have been used for weight-drop induced SCIs in large animals. The 50 and 100 g weights (Figure 7-1, solid red circles) used in the preliminary study presented in Chapter 2 were higher than would be expected of burst fracture bone fragments [460,462] (see Section 1.6.4). In the present case, these weights were selected based on the requirements of two separate studies of pharmacological biodistribution and chronic injury which were undertaken concurrently on these animals. Nevertheless, similar weights have been used for cat, sheep and small NHP SCIs, and both weights were below the estimated wet weight of human thoracolumbar vertebra (250-550 g) [465]. The impactor used to create the SCI in the second study of CSF transients (Chapter 3) (Figure 7-1, solid red squares) and employed for the bench-top model (Chapter 4) was only slightly heavier than bone fragments resulting from experimental burst fractures in bovine spines [462].

The drop heights selected for all three studies (Figure 7-1, red markers) corresponded to a range of bone fragment velocities derived from experimental burst fractures [132,134,460], whereas previous models have generally used velocities at the lower end of this range. The impact velocity of experimental

contusion injuries has been demonstrated to influence the electrophysiological response [272], haemorrhage [269,275] , blood-spinal cord barrier disruption [274] and overall tissue damage and behavioural recovery [267].
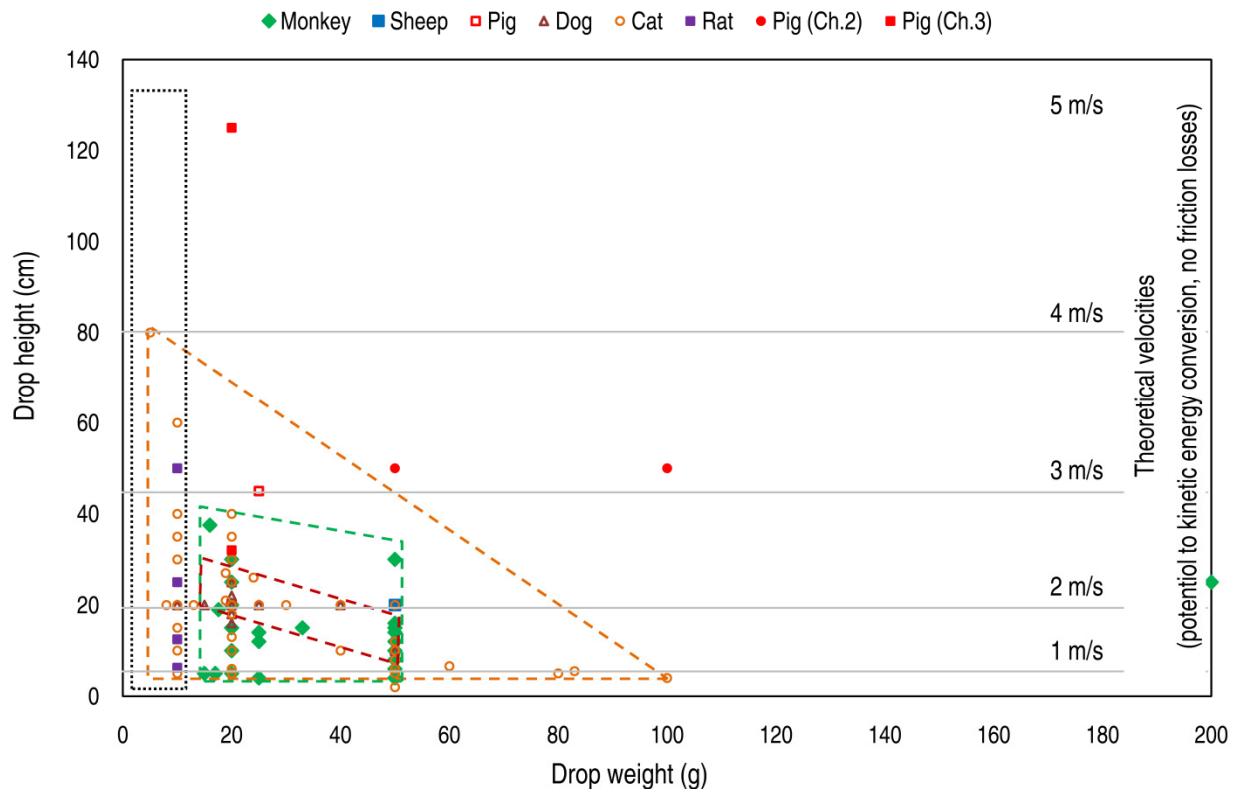
Figure 7-1 Injury parameters (height and weight) reported to induce transient or permanent paresis in various large animal weight-drop models, including the parameters used for the studies in Chapter 2 and 3 (red filled markers). The data was collated from all available large animal studies that used an open weight-drop model and reported separate drop weight and height information, from 1968 to present. Dashed areas indicate nominal "injury corridors" for cat (orange), dog (dark red) and monkey (green) models. The dotted black rectangle indicates the range of heights that would theoretically produce occlusion velocities measured for burst fracture and dislocation events observed in biomechanical experiments, and an aproximate range of bone fragment weights that have been reported for experimental burst fractures. The grey lines indicate theoretical estimates of velocities based on assuming complete conversion of potential to kinetic energy, i.e. no friction or other losses.

To produce an injury with similar biomechanics to the human scenario without the need to scale the mechanical input parameters, an animal with similar spinal cord and dural diameter is required. A similar length spinal cord is also desirable for biomechanical studies concerned with the propagation of pressure or stress waves in fluid or tissue and the distribution of tissue damage, such as the studies in this thesis. Because the majority of researchers do not report dimensions for the cord of the animal used, and size can vary appreciably between strains and with the age of the animal species used, it is difficult to evaluate the current model against previous models. There is also a lack of systematic studies of animal

spinal cord and dura dimensions in the published literature. For humans, spinal cord dimension, and to a lesser extent dura dimension, have been measured using a variety of *ex vivo* techniques including calliper measurements of fresh and fixed tissue and histology cross-sections, and *in vivo* CT myelography and MRI (Figure 7-2). The values reported have a fairly wide range due to natural variability as well as inherent inaccuracies in these measurement and imaging techniques. The sagittal diameter of the thoracic spinal cord of the 20-22 kg, 4-5 month old Yucatan miniature pigs used in this thesis (assessed with *in vivo* ultrasound, Chapter 6) was within the mid-range reported for the human thoracic cord (Figure 7-2). In a series of pre-surgical MR scans taken during the planning phase of this thesis the sagittal diameter of the thoracic dura was lower than the average human values and at the lower limit of the range (Figure 7-2 and Figure 7-3). The diameter was slightly lower when measured by ultrasound during the surgery since some CSF loss occurred during pressure transducer insertion (Figure 7-2). Based on the mean ultrasound measurements in which the internal dura diameter was measured, the pig dura:cord ratio was approximately 1.26 (7.2:5.7 mm) compared to the human value of approximately 1.6 (10.8/6.8 mm) in the mid-thoracic region based on the data of Zaaroor et al. [394]. The pig MRI data (n=1) gave a ratio of 1.44. Therefore the sagittal CSF layer thickness relative to the cord diameter was lower in these Yucatan miniature pigs than in humans.
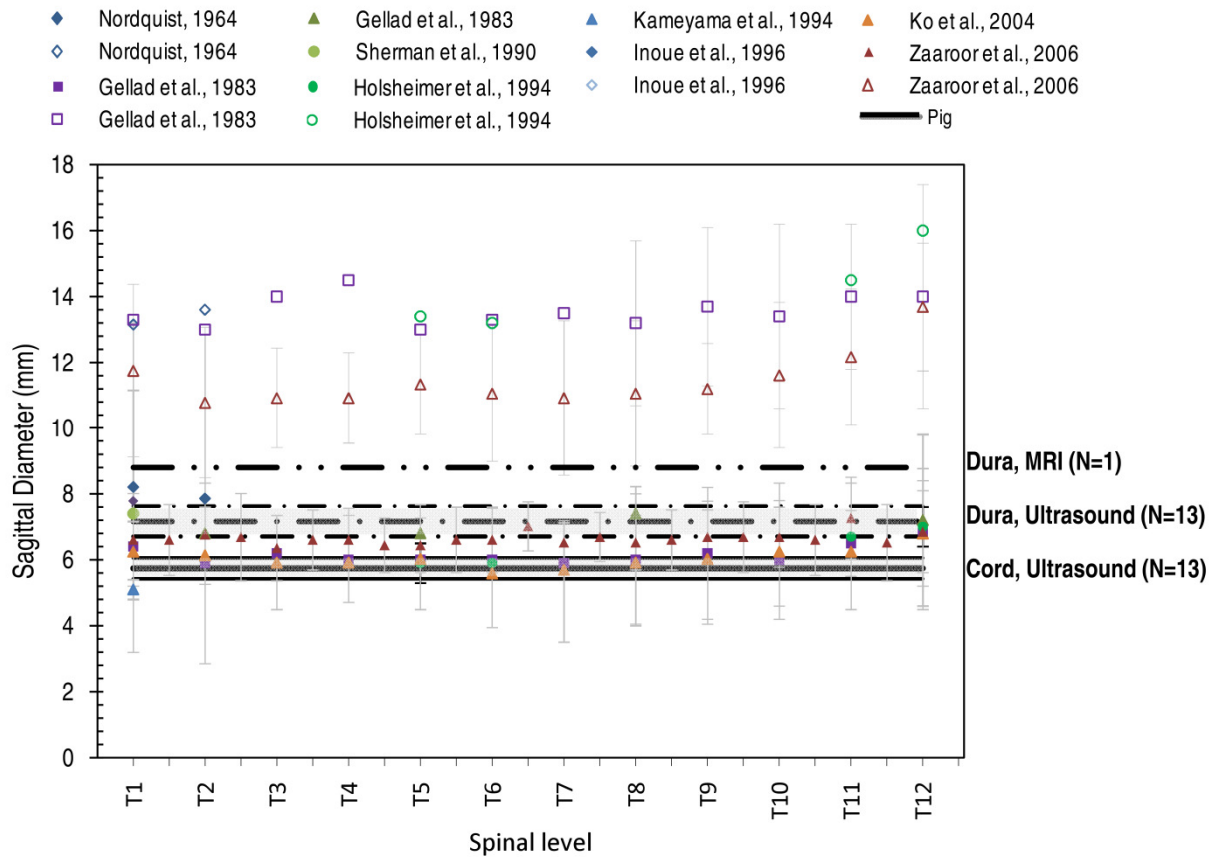
Figure 7-2 Sagittal diameter of human spinal cord (closed markers) and dura (open markers), from vertebral level T1 to T12; mean±SD or range, as available. Thoracic sagittal diameter of spinal cord (solid black line) and dura (dashed black line) as measured for 13 Yucatan miniature pigs with ultrasound after pressure transducer insertion; mean±SD (Chapter 6). Thoracic sagittal diameter of dura (dot-dash black line) measured axial MRI of 20 kg Yucatan miniature (N=1, unpublished data). Human data is compiled from studies that utilised a number of different techniques including: magnetic resonance imaging [394,522,588], computed-tomography myelography [391,589], and post-mortem physical [393], radiographic [590] and histological [392] measurements.
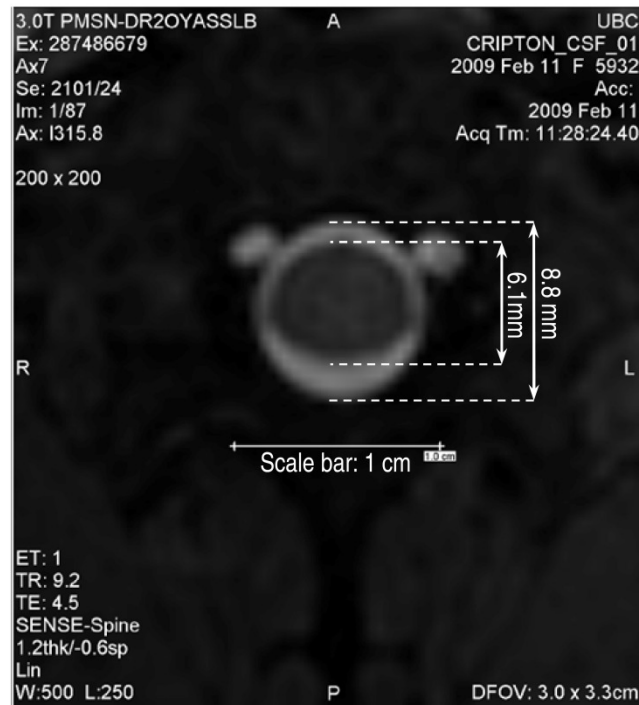
Figure 7-3 Axial magnetic resonance image of thoracic spine of 20 kg Yucatan miniature pig (unpublished data). 3 Tesla MR (Intera, Philips, the Netherlands) three dimensional fast field echo (3D FFE) T1-weighted scan sequence optimised for cord and CSF: acquired in-plane resolution 0.6 mm, reconstructed in-plane resolution 0.47 mm, field of view 30x33 mm, acquired slice thickness 1.2 mm, reconstructed slice thickness 0.6 mm, matrix size 200x200, repetition time 9.2 ms, echo time 4.5 ms, flip angle 35 °, water-fat shift 1.5 pixels, spine coil.

7.4   The role of CSF in the biomechanics of SCI

Spinal cord injuries involve complex mechanical events in which many physical variables contribute to the initial injury characteristics and severity. In order to study SCI, researchers employ a variety of *in vivo* (animal), *ex vivo*, bench-top and computational models. Many assumptions and simplifications are made in order to create practical and repeatable model "systems", and it is important that researchers are aware of the effects that these may have on the study results. A thorough understanding of the individual biomechanical contributions of the spinal, paraspinal and nervous system tissues is therefore essential to the appropriate design and use of these models.

Although the potential importance of CSF in SCI biomechanics was recognised in the 1970s [1-3,285], very few studies have since attempted to advance understanding in this area. Contemporary work investigating the fluid's role has been limited to bench-top models using *ex vivo* tissues and synthetic materials [280,281], and computational models [495,528]. In this thesis an animal model and a bench-top model were used to investigate the biomechanical role of CSF at the instant of a SCI. This thesis presents the first dataset of pressure transients measured at the time of experimental SCI using transducers placed

191

directly in the spinal CSF. Previous measures of CSF pressure transients during SCI are extremely sparse, and these were limited by the pressure transducer technology of the time. The bench-top model was used to identify the manner in which the dimension of the CSF layer influences the magnitude of these transients, as well as spinal cord compression and load transmission.

7.4.1 Peak pressure

The studies in Chapters 2, 3 and 4 showed that, as expected, pressure transients in the CSF have the highest magnitude at sites closest to the impact site. In this animal model, the transients reached over 1000 mmHg for the higher injury severity and over 500 mmHg for the moderate injury severity. The peak pressure near to the injury site for both injury severities was much higher than the two single pressure measurements reported for open experimental SCI in the cat (Figure 7-4, green triangle and purple circle) [1,2]. As discussed in Sections 2.4.2 and 3.4, this may reflect differences in the animal model or the pressure measurement technique. The "near" peak pressure for the high severity animals was similar to that recorded at 80 mm cranial to the impact site, but much lower than at 60 mm caudal to the site (Figure 7-4, teal circles with dashed line) in the closed-spine canine model of Wennerstrand et al. [3]. These measurement positions were only reported for a single animal and it is difficult to speculate on the specific reason for the lack of symmetry around the impact site in that model. The closed-spine lateral impact model of Wennerstrand et al. may have produced a different biomechanical response within the caudal and cranial canal due to differences in spine flexibility in the thoracic and lumbar regions, or different distribution of paraspinal tissues which would contribute to damping.

The paraspinal and nervous tissues appeared to be very efficient at damping the pressure wave produced by the impact to within the range associated with normal everyday fluctuations that are non-injurious. A similar damping of CSF pressure transients during SCI has only been shown once before and this was in a canine model [3]. In the current tests, the pressure at the "far" location appeared to be reduced to much the same value regardless of the weight, velocity, or "near" peak pressure associated with the impact (Figure 7-4). It is noted that the study using closed-spine impacts on dogs did not achieve pressures similar to normal transients until around 350 mm from the impact site [3], over three times the distance required for similar reduction in the current open pig model. In Chapter 3 an attenuation ratio was defined as the ratio of the "near" and "far" peak magnitudes. Normalised by distance, it ranged quite widely from 1.3-15.4 per cm in the current study and did not have a strong association with injury severity despite the similar "far" pressures for both groups. Attenuation ratios of 0.4-1.8 per cm were derived from the data of Wennerstrand and colleagues [3]. It is speculated that the generally higher attenuation in the current study may be due to the open canal allowing more distension of the dura which may dissipate the energy faster than the enclosed canal.
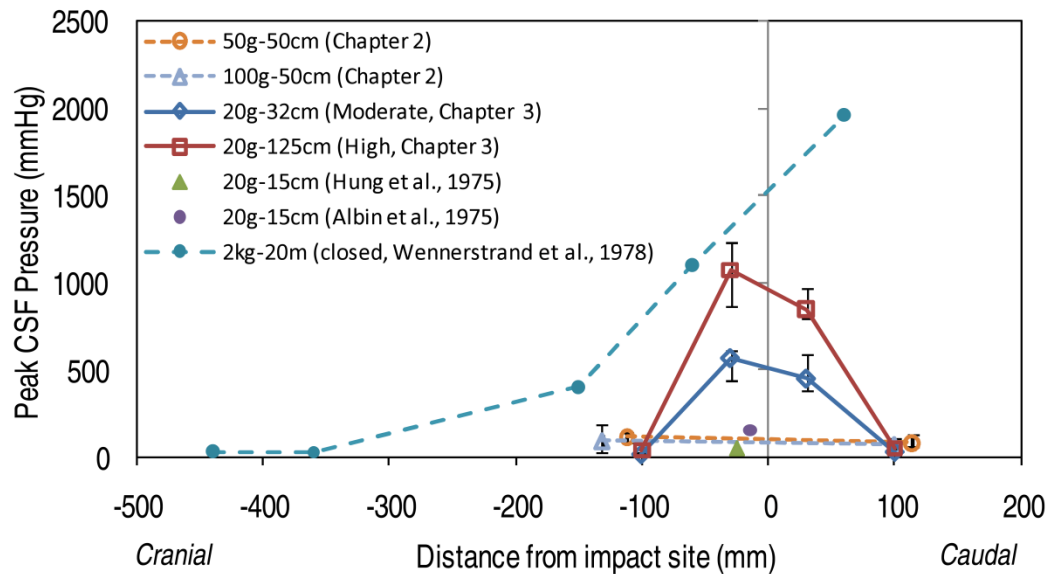
Figure 7-4 Peak CSF pressure versus distance from the impact site for the current studies (open markers) and reported values compiled from the literature (filled markers).

7.4.2   Pressure impulse

The impulse of the pressure wave, which is the integral of the pressure magnitude over the time in which it acts, was reported in Chapter 3. Soft tissues are viscoelastic, exhibiting a physical response to mechanical loading that is time (i.e. strain rate and duration) dependent, due to their water content and their complex composite structure comprising collagen, elastin and ground substance [527]. Injury criteria that include a time component, for example the impulse of an applied impact load, are often better predictors of gross mechanical failure than peak load or deformation for cells, tissues and body parts [272,518,591,592]. In Section 3.4 it was noted that the pressure impulse at both 30 mm and 100 mm from the injury site was within the range of impulses reported to cause cellular damage in animal brains [312,342]. The pressure impulse was not reported in the three studies that reported spinal CSF pressure during SCI [1-3]. To aid in determining whether pressure impulse is more closely correlated with cellular damage, researchers should consider reporting the impulse or duration, in addition to the peak magnitude, of pressure transients applied to or measured within the CSF.

7.4.3   Could a CSF pressure transient contribute to SCI?

No study to date has sought to detect *in vivo* tissue damage due to a fluid impulse in the spinal CSF. The researchers that have measured spinal CSF transients speculated that the pressures may contribute to injury [1-3]; however, similar to the current study, no direct evidence of cellular disruption

could be obtained because the injury mechanism used included direct mechanical impingement of the spinal cord. Deformations caused by impingement, and the secondary cellular response to these defoamtions, may overwhelm or confound histological findings at and remote to the injury site because the evidence of pressure impulse mediated injury may be more subtle. As discussed in Section 1.4.6.2, other researchers have observed spinal cord tissue damage remote from a focal injury site and some have speculated that it may be caused by CSF pressure waves. Such data is scarce but includes diffuse axonal injury in the spinal cord of infants with shaken baby syndrome [156,157], in the thoracolumbar spinal cord of rats subjected to head impact and fluid percussion TBI [162], and up to 24 vertebral levels from the lesion epicentre in the spinal cords of 17 patients who died between 30 minutes and 6 weeks after injury [163]. Other SCI observations that have not been fully explained, and for which there may be some contribution from a CSF pressure impulse, include post-traumatic ascending and descending myelopathy [165-178,593], transient spinal shock or concussion [164], and SCIWORA without MRI abnormalities [161]. Although alternative mechanisms have been proposed for some of these observations, it is possible that such tissue damage is initiated by CSF pressure transients during the primary injury event.

There is no established pressure tolerance for spinal cord tissue. In Chapters 2 and 3 the measured peak pressures were compared to non-injurious spinal transients that occur during everyday activities and clinical exams, and to cranial pressures associated with several experimental TBI models (see Section 1.5.4.4). While the former are specific to the spine, the latter are for the brain and the comparisons were made with the recognition that tissue tolerances are mechanism and location specific. Figure 7-5 illustrates that in this pig model, the peak pressures at 30 mm from the impact site (solid blue and purple lines) were much higher than transients associated with everyday activities (green bars), while those at 100 mm from the impact site (dashed blue and purple) were of the same order of magnitude. At the near location, peak pressures were in the mid- to upper ranges of peak pressures that have been measured in the spinal and cranial CSF and parenchyma during various SCI, TBI and whiplash experiments, while those at the "far" location in both of the pig studies were at the lower end of this range (Figure 7-5, orange and yellow bars). Details of these experiments and the transducers that were used were provided in Sections 1.5.4.2, 1.5.4.4 and 1.7.2.
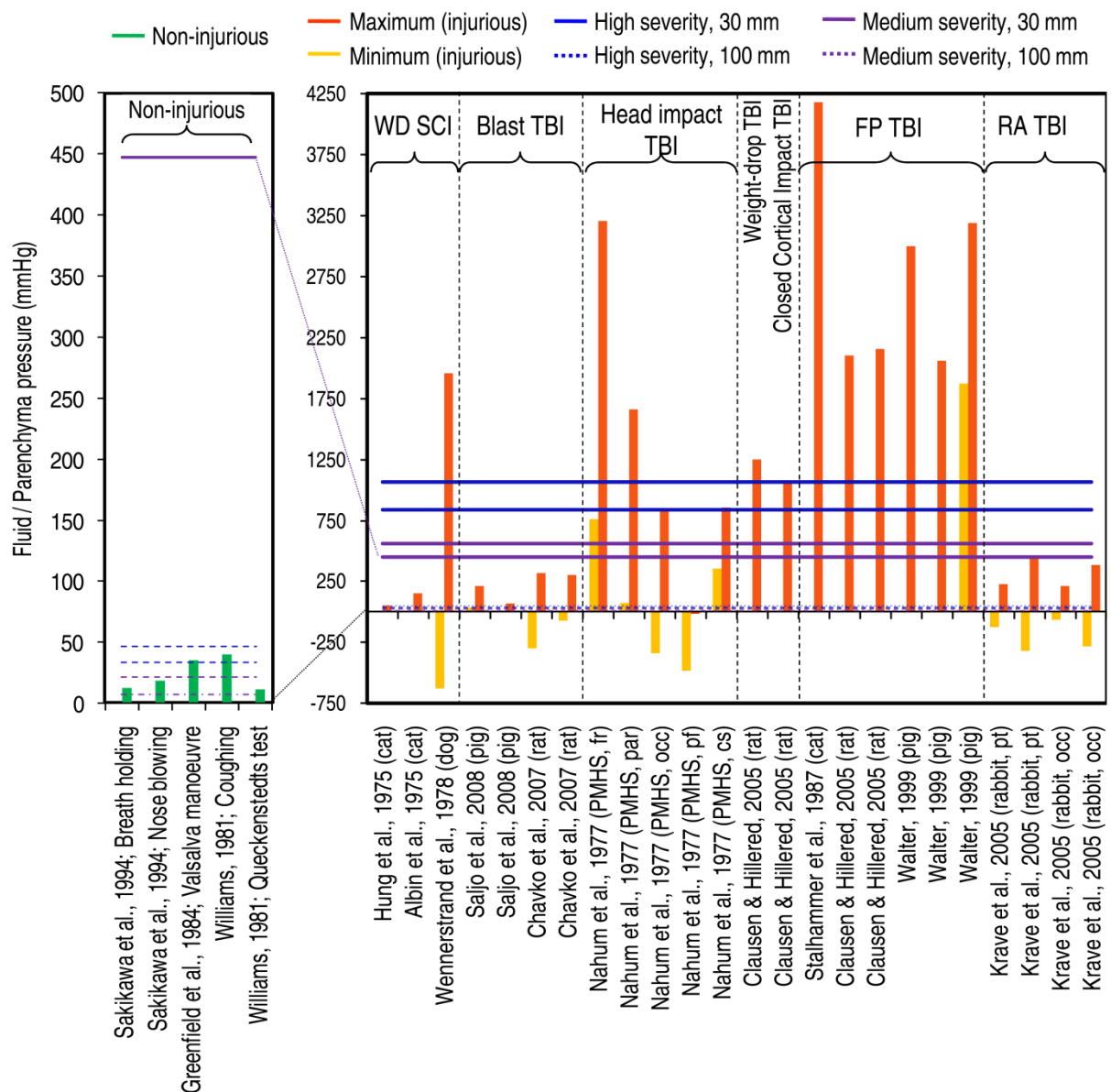
Figure 7-5 **Non-injurious (green vertical bars) and injurious CSF/parenchyma pressure transients measured during with experimental SCI and TBI events (vertical bars) compared to median CSF transients measured in pigs at 30 mm and 100 mm cranial and caudal to the injury epicentre for high and medium severity injuries (horizontal lines) (Chapter 3).** WD=weight-drop; SCI = spinal cord injury; TBI=traumatic brain injury; FP=fluid percussion; RA= rotational acceleration. [1-3,62-64,290,313,314,319,337,342,486]

Although the comparative data presented in Figure 7-5 were measured at the time that the injuries occurred, the injury could not be directly attributed to the pressure itself. Cellular injury attributable to pressure waves transmitted through the cranial CSF to the brain tissue has been demonstrated in blast TBI experiments in animals, and fluid percussion insults on *in vitro* cell preparations have shown similar

responses. These are not threshold values, but serve to show the range of pressures that may induce different degrees of temporary and permanent cell damage. Figure 7-6 illustrates that the pressures measured at 30 mm from the impact (blue and purple solid lines) were in the mid-range of the incident pressures, and those measured at 100 mm from the impact (blue and purple dashed lines) were within the lower range of the incident pressures (orange vertical bars). This suggests that the pressure wave may contribute to injury close to the site, but that such an effect would be diminished at more remote locations.
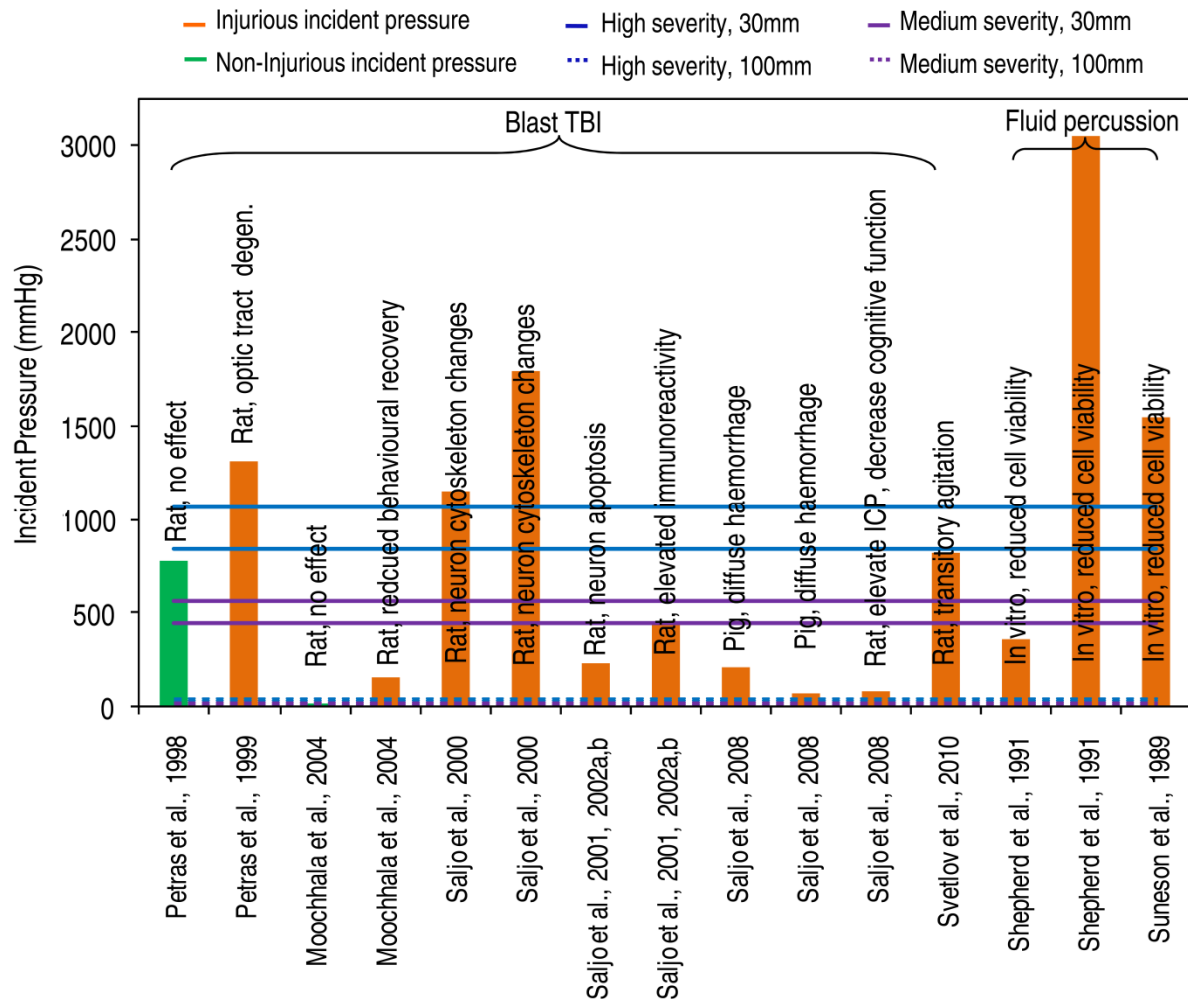
Figure 7-6 Pressure transients incident on animals or *in vitro* cell preparations subjected to blast or fluid percussion injury, with evidence of subsequent tissue/cell damage (vertical bars), compared to median CSF transients measured in pigs at 30 mm and 100 mm cranial (upper) and caudal (lower) to the injury epicentre for high (blue) and medium (purple) severity injuries (Chapter 3).
[331,332,340-343,345,347-349]

The majority of the aforementioned studies report only peak pressures. However, as noted above, due to the time-dependent nature of viscoelastic tissues' mechanical and damage response, injury is often

196

better represented by the impulse of load rather than its peak. Kato et al. noted that pressure impulse may be a superior injury determinant than peak pressure for some cells [518]. Irreversible apnoea was observed in cat subjected to a fluid impulse in the cranial vault of 7600 mmHg.ms [312] and impulses ranging 37-590 mmHg.ms were associated with cellular damage in the brain of pigs subjected to low impulse noise from firearms [342]. The impulses recorded at the "near" location in the current study are between these two ranges, and at the "far" location are generally within the range of Saljo et al. [342]. The paucity of data makes it difficult to draw definitive conclusions about the likelihood of cellular injury with a pressure impulse criterion, but these limited data indicate that a diffuse cellular injury may occur, but with diminishing probability with distance from the impact site.

7.4.4   Effect of CSF layer thickness on mechanical descriptors of SCI

The layer of CSF that surrounds the spinal cord has long been regarded as a protector of the neural tissue. While there has been some attention to the action of the cranial CSF during TBI, there have been very few investigations of the spinal CSF mechanics during SCI. In this thesis, the effect of the thickness of the CSF layer on CSF pressure, peak cord compression, impact load and tether load was demonstrated for the first time, using a model constructed of synthetic materials (Chapter 4).

The bench-top model produced lower peak pressures than the animal model, but near the impact site the peak pressures were similar to those measured inside *ex vivo* bovine cords subjected to 5 m/s, 7 g impacts [462](Figure 7-7, left). Pintar and colleagues [594] also measured surrogate cord pressures resulting from impacts, but the individual weights and heights (i.e. velocity) used were not reported. The peak pressures in the current study were also within the range measured in a surrogate cord in the cervical spine [469], and in a water filled dural case in the lumbar spine [473], of cadaveric specimens subjected to axial impact inducing burst and other fractures. This suggests that some of the variability in the pressure results in the animal studies may have been due to variation in the size of the CSF layer.

Figure 7-7 Peak CSF pressure measured at various locations in the current bench-top model and a previous simulation of Hall et al. [462] utilising bovine and surrogate spinal cords and dura (left); Peak CSF pressures measured inside cadaver spinal canals (with [469] and without [473] surrogate cord) subjected to axial impacts (right); compared to median CSF transients measured in pigs at 30 mm (dashed horizontal lines) and 100 mm (solid horizontal lines) cranial and caudal to the injury epicentre for high (blue) and medium (purple) severity injuries (Chapter 3).

The current study showed that progressively increasing the CSF layer thickness from no CSF, through small, medium and large CSF layers, while maintaining the same baseline CSF pressure and cord diameter, resulted in a significant reduction in percent cord compression. Previous studies using surrogate and bovine spinal cord and dura suspended in a materials testing machine have demonstrated that the presence of CSF (as opposed to an absence) resulted in reduced maximum cord compression in burst fracture simulations [280,281], and similar trends have been shown with a finite element model [528]. The percent cord compression observed in the current study at 4.6 m/s impact velocity was similar to the simulation of Persson et al. [281] which used an impactor of comparable diameter and similar impact velocity (4.5 m/s) to the current study, but with a weight of only 7 g (Figure 7-8). The increased CSF layer also led to a decreased peak impact load, but a slightly higher axial tether load; no previous studies have reported this finding.

Figure 7-8 Bar graph comparing the % cord compression measured during 4.6 m/s impacts for the noCSF, small, medium and large dura cases in the current study (blue bars) (mean±standard deviation), and the % cord compression measured for 4.5 m/s impacts using a 7 g impactor with similar impactor:cord diameter ratio for bovine and surrogate cords with and without CSF (purple bars) (median±standard deviation, where available); data derived from [281].

7.4.5 Implications for SCI models in basic science research

The current investigation of the characteristics of the CSF pressure during SCI provides preliminary evidence that CSF pressure transients may play a part in SCI severity and distribution along the cord. This may have implications for models that are used for basic neurotrauma research, depending on the nature of the research question to which an answer is sought.

Using the synthetic model, it was confirmed that maximum cord deformation is reduced with increasing dimension of the CSF layer. This is consistent with previous studies that compared CSF and no-CSF conditions using *in vitro* preparations of bovine cord and dura [280,281]. In addition, the maximum impact load at the site of the mechanical insult, and the CSF pressure at locations adjacent to, and far from, the impact site were reduced with increasing CSF thickness; these relationships have not been shown previously. It is known that for dynamic impacts, displacement and load are proportional to injury severity (Section 1.5.4.1), and this thesis has provided evidence that CSF pressure transients may also contribute to tissue damage (Chapter 2 and 3). Based on these observations, it is likely that the dimensions of the CSF layer around the spinal cord will have an effect on the severity and /or extent of the injury sustained. This suggests that more biofidelic mechanical models, whether they are computational, synthetic or animal, may be achieved with the inclusion of an appropriately sized CSF layer.

Finite element models have been used extensively in injury biomechanics. They have been used to predict the stress and strain distribution in the cord, to determine the effect of changing mechanical input parameters and to refine estimates of the mechanical properties of spinal tissues. The importance of including the CSF in computational models appears to have been recognised relatively early for TBI research [595], but is a very recent addition to computational models of SCI. Several finite element models have been developed to simulate various aspects of the biomechanics of SCI. Earlier models did not include a fluid layer component [461,499,596] but models of experimental rat SCI [495] and bovine-scale SCI [528] with a CSF layer have been reported more recently. Computational models of SCI will likely provide more accurate results if they incorporate fluid elements. For example, following from the observation in Chapter 4 that the size of the CSF layer affects the magnitude of cord compression and the peak load imparted to the cord, computational models that include CSF would be expected to produce tissue strain and stress distributions more closely approximating the real scenario. A recent bovine-scale computational model showed that including fluid-structure interactions altered stress and strain profiles and overall cord compression [528]. As the processing power of computers and the sophistication of modeling software increases, it is anticipated that more models will incorporate fluid-structure interactions. The data presented in Chapters 2, 3 and 4 will be an important source of information for the validation of such models.

These results also suggest that bench-top models or cadaver studies incorporating surrogate cords for dynamic investigation of SCI mechanics, similar to those described in Section 1.6.5, should consider including CSF. This is particularly the case if the outcome measures include spinal cord deformation or load, which are dependent on CSF layer thickness (Chapter 4), as well as internal cord pressure or transient canal occlusion. Such models would also require a surrogate dura material with appropriate material properties. Previous bench-top models have used excised bovine dura [280,281] and plastics [281] (Chapter 4), while no cadaver model has included dura around a spinal cord. Excised natural dura is difficult to harvest in large sections, it is not easily modified to form different diameters, and it is challenging to seal nerve root sleeves adequately. The plastics that have been used have elastic moduli similar to the upper linear region of the dura stress-strain relationship (although at much lower strains), but do not mimic the "two-tiered" hyperelastic non-linear behaviour of the dura. Furthermore, they do not have the anisotropic and viscoelastic properties that often dominate the material response at higher strain rates. Development of a mechanically-similar surrogate material could refine such models considerably.

As noted in Section 1.6.2, and subsequent chapters of this thesis, the biological aspects of SCI and the pre-clinical development of potential treatments are largely reliant on models in the rat [597] which has a CSF layer only 50-80 μm thick [495]. The findings in this thesis suggest that the large animal models that dominated biomechanical (and biological) studies of SCI prior to around 1980 may have been

advantageous with respect to the more human-like scale of their cord and CSF layer. However, this benefit was largely unacknowledged and in some cases removed by the use of relatively heavy static impounders which compressed the dura prior to impact (Section 1.6.3.1). The contemporary rodent models are well developed, a great deal is understood about the pathophysiology of acute SCI in these animals, and a large battery of histological and behavioural techniques have been established to test their response to treatments [598]. Due to these and other advantages concerning efficiencies of cost, time and complexity, rodents will quite obviously remain the dominant vehicle of SCI research. Nonetheless, the findings of this thesis suggest that the subset of these studies that concentrate on the *in vivo* biomechanics of SCI, depending on the effect or phenomena they seek to understand, may consider utilising an animal with a substantial CSF layer. For example, the existence of a CSF layer alters the load transmitted to the cord at the impact site, and may alter the stress distribution within the tissue at more remote sites due to the propagation of a pressure wave. This may be important for a study which seeks to determine the relationship between injury parameters and internal cord strain. Furthermore, while it is recognised that the current thesis did not provide direct histological evidence of a pressure-mediated injury mechanism, previous studies have shown that different deformation magnitudes and modes are associated with specific cell damage characteristics [142,143]. Therefore, the results of Chapters 2 to 4 suggest that after potential treatments have shown efficacy in rodent models, it may be advantageous to undertake intermediate pre-clinical studies using animals with a more human-like CSF space prior to non-human primate and clinical trials, both of which are considerably more expensive.

7.4.6   Implications for clinical research

The results of this investigation of the characteristics of the CSF pressure during SCI, combined with previously reported TBI-inducing fluid percussion and blast incident pressures, provide support for the notion that CSF pressure transients may play a part in SCI severity and extent. Evidence of remote and diffuse cellular injury after SCI is quite scarce in the clinical and scientific literature; however, these studies suggest that this potential injury mechanism should be investigated in the future.

The dependence of the CSF peak pressure, cord compression and impact load on CSF thickness suggests that a metric of SCI risk including a measure of dural size may have higher predictive value. The most established risk measure is the Torg ratio, which considers only the size of the canal [145]; the "space available for cord" measure has been proposed and is based on the cross-sectional area of the canal and of the cord [147]. Current MR imaging technology is approaching appropriate resolution to allow visualisation of the relatively small CSF layer. However, care must be taken to ensure the selected sequence is suitable and optimised to minimise the over- or under-estimation of CSF content.

7.5 CSF pressure differentials and cord morphology

7.5.1 Discussion

This thesis has demonstrated for the first time the changes in cranial and caudal CSF pressure associated with a dynamic SCI with residual cord compression, and an eventual decompression. It also provided the visualisation of cord and dura morphology in the immediate post-decompression phase, which has not been reported previously. The results presented in Chapters 5 and 6 provide an important insight into two aspects of the physiological response to SCI that cannot currently be measured in SCI patients.

During the period of residual cord compression we observed an increase in the cranial CSF pressure while the caudal CSF pressure decreased or remained static, resulting in an increasing pressure differential of approximately 0.4 mmHg per hour over the eight hours of compression (Chapter 5). While the trend was convincing and statistically significant, it was nonetheless smaller than anticipated. In their study of parenchymal and CSF pressures after experimental SCI in cats, Shapiro and colleagues noted that fluid pressures in the cisterna magna increased while those in the lumbar cisterne decreased slightly for about two hours after injury, such that a differential was obtained at a rate of about 2.14 mmHg/hr [211]. The differential then remained fairly constant for 1-1.5 hrs, before decreasing gradually. Kwon et al. also provided indirect evidence for an increasing cranial compartment CSF pressure, observing a mean increase in caudal pressure of 7.9 mmHg at the time of decompression in SCI patients undergoing surgical decompression [91]. Because the pressure-volume compliance of each subarachnoid space compartment is unknown, it is difficult to estimate the cranial-caudal pressure differential for the patients immediately prior to decompression. However, it is noted that the mean caudal pressure elevation upon decompression was around 12 times larger in the patients (7.9 mmHg) than the pigs (0.65 mmHg), while the mean time to decompression was only 2.7 times longer (21.6 hr and 8 hr, respectively). This may suggest that the rate at which the differential increased in the pigs was smaller than occurred in the SCI patients. However, the disparity may also be due to differences in the subarachnoid space compliance of humans and pigs due to differences in natural anatomy and physiology, and perhaps induced by the laminectomy which may have allowed greater distension of the pigs' spinal dura than would otherwise occur in a closed canal. Furthermore, the mean caudal pressure elevation value for the pigs included animals in which the subarachnoid occlusion was probably not complete – perhaps due to incomplete occlusion of the lateral thecal sac – and as a result had less significant differentials established prior to decompression.

Kwon and colleagues [91] noted that substantial changes in CSF pulse pressure amplitude occurred at the time of decompression in some patients, and hypothesised that this may be related to the degree to which the decompression restored the thecal sac. Although small changes in both caudal and cranial

CSFPPA were detected in most animals at the time of decompression, the changes were not consistent in direction and were therefore not statistically significant. The small CSFPPA changes observed may have been due to the relatively small change in mean CSF pressure magnitude seen at the time of decompression – a larger pulse pressure amplitude is generally associated with higher mean CSF pressure [67,94,96,546-548]. The current study demonstrated that if CSF pressure measurements are made with transducers and data acquisition systems of sufficient resolution, very small changes in CSFPPA can be detected. The filtering strategy used to decouple the arterial pulsations from the respiratory artefact also contributes to detection of small changes in CSFPPA. The relatively simple filtering procedure used in the current study was detailed in Chapter 5; few studies have detailed the methods used to remove the respiratory "artefact" from the raw pressure data [83,599] and future investigations might benefit from developing more sophisticated filtering strategies to maximise the information obtained from the signal.

In the period after decompression, distinct patterns of spinal cord residual deformation and swelling were observed and were generally dependent on the severity of the delivered impact. A similar relationship was indirectly reported by Shapiro et al., although that study did not provide sustained cord compression. They noted that in cats injured with 20g-20cm and 30g-20cm impacts a tissue pressure differential did not occur, which they interpreted as an indication that these injury energies did not cause sufficient swelling to result in loss of communication between the cranial and caudal compartments [211]. However, when the impact energy was increased to 40g-20cm the natural cord swelling was sufficient to create an occlusion, and in those animals the pressure differentials indicated that occlusion occurred within 30 minutes of injury and was maintained until around three hours post-injury [211]. The time course of thecal sac patency due to cord swelling has been measured more directly for experimental SCI in sheep (50g-20cm injury at T10) using contrast myelography. This methodology identified complete subarachnoid block within one hour of injury in three of four animals, which persisted for between 72 and 192 hrs in all animals [218]. However, neither of these studies included a period of residual cord compression, which is common in SCI patients and often requires decompression by traction or by surgical means.

Due to the relatively low number of animals studied, the variety of pressure responses observed in the pre- and post-decompression periods, and the relatively short post-decompression observation period, it was not possible to draw an association between the post-decompression ultrasound and pressure measurements in the current study. The cord swelling led to the appearance of a fully occluded thecal sac within six hours after decompression in half of the animals; this reponse may be expected to dictate the cranial and caudal CSF pressures after decompression. For example, for animals in which the cord swelled to touch the dura, a differential might be re-established, while in those in which swelling was less substantial would probably maintain a cranial-to-caudal equilibrium. Future investigations of the relationship between time, swelling and pressure differential might seek to measure the intraparenchymal

pressure or the contact pressure between the cord and dura at injury site, to quantify CSF flow across the injury, and to obtain three-dimensional serial ultrasound, MR or CT myelogram images with which to quantify the morphology of the cord and dura.

Both the CSF pressure differentials before decompression and the ultrasound observations after decompression suggest that the thecal sac may be divided into cranial and caudal compartments after SCI due to both bony impingement and cord swelling. The delivery of biologics [180] or other therapies into the intrathecal space should consider the potential effect of such a compartmentalisation on the diffusion and dispersion of the therapy along the length of the cord. Evaluations of such drugs and their delivery methods should be undertaken in animals injured with a SCI severity that causes spinal cord swelling with a similar time course and magnitude to human SCI.

7.5.2   Implications for clinical management of SCI: CSF drainage and decompression

The results in Chapter 5 and 6 of this thesis highlight the importance of early post-traumatic intervention. In particular, the CSF pressure distribution and cord morphology results suggest that early pharmaceutical intervention should aim to reduce cord swelling. The results showed that if thecal occlusion occurs at the injury site, this may lead to a CSF pressure differential between the cranial and caudal compartments. Such differentials have been observed in the past for other conditions with thecal sac occlusions, such as cerebellar herniations and spinal cord tumours (Section 1.3.3.2), but have not been reported for the SCI population. The ultrasound imaging showed that depending on the severity of the mechanical insult, cord swelling may be fast and of sufficient magnitude to occlude the thecal sac within hours after decompression.

7.5.2.1   CSF drainage

Acute neurotrauma such as TBI and SCI initiates a cascade of pathophysiological events including ischaemia, oxidative cellular injury, apoptosis, inflammation and edema [152]. Standard clinical management of acute severe TBI patients involves placing an intraventricular drain for ICP monitoring and to facilitate fluid drainage for perfusion pressure management. For SCI patients, perfusion pressure management is achieved by haemodynamic support alone with no CSF pressure monitoring or drainage. One of the primary reasons for this disparity is the concern that releasing CSF below a swollen compressed cord could result in neurological deterioration [600], because of a pressure differential that may be created by releasing the caudal fluid. However, while Hollis et al. [71] showed an increased risk of neurological deterioration in patients with subarachnoid block from malignancies, there have been no reports of similar complications in the case of acute SCI. Recently, Kwon and colleagues found no evidence of neurological deterioration in a group of eleven acute SCI patients undergoing lumbar drainage; however, because the protocol did not allow CSF to be drained at times when the patients'

neurological function could not be monitored (i.e. when they were asleep or sedated), very little CSF was actually drained [91].

On the basis of large lumbar pressure rises observed at decompression, Kwon and colleagues hypothesised that the compression on the spinal cord caused by canal malalignment or displaced disc and bone fragments may have led to a pressure gradient across the injury site [91]. The current study is the first to demonstrate this differential directly by taking CSF pressure measurements in the cranial and caudal compartments caused by sustained cord impingement. The finding has several implications for the practice of lumbar CSF drainage in the acute SCI patient population. Firstly, it indicates that increased CSF pressure after SCI with thecal occlusion is largely restricted to the cranial compartment. Due to the aforementioned restrictions on catheter placement in SCI patients, the fluid in this subarachnoid compartment cannot be either monitored for pressure or drained, and this probably limits the feasibility of employing CSF drainage in SCI patients, at least prior to decompression. Furthermore, targeted hypertensive therapy (without CSF drainage) to maintain perfusion pressure above a threshold would also need to be based on CSF pressure measurements in the cranial compartment. In the future, advancements in miniature transducer technology and minimally invasive surgical techniques may allow safe access to the proximal subarachnoid space, but this lack of access currently limits CSF drainage or monitoring as a clinical management option prior to decompression.

The rise in lumbar pressure observed at the time of decompression in both the current study and that of Kwon et al. [91] implies that once the thecal pathway is restored, lumbar CSF drainage is more likely to achieve the desired depression of CSF pressure throughout the entire spinal thecal sac. Measuring the change in lumbar CSF pressure at the time of decompression may be of prognostic value. There is a known association between the magnitude and duration of elevated ICP, and the prognosis of TBI patients [539,584]. Similarly, the lumbar CSF pressure change, in addition to the delay between injury and decompression, may correlate with the amount of ischaemic damage cranial to the level of the injury. The rapid appearance of cord swelling after decompression indicates that the window of opportunity for lumbar monitoring and drainage may be limited in some cases, although the sample size in the current study was not sufficient to discern an association between swelling and post-decompression CSF pressure trends.

7.5.2.2 *Decompression*

The principal justification for surgical decompression is that removing bony material impinging on the spinal cord will increase the local blood flow to the tissue. However, the "equalisation" of the pressure differential observed after decompression (Chapter 5) may provide evidence of a secondary mechanism by which early decompression assists in restoring or improving tissue perfusion. This does not appear to have been recognised previously, and may warrant further study. Occlusion of the thecal

sac led to steadily increasing cranial CSF pressure in the current study; similar was observed in cats receiving a dynamic SCI where the occlusion is presumed to have occurred as a result of cord swelling [211]. There is also indirect evidence that this occurred in the clinical series of Kwon and colleagues [91], although they were unable to measure CSF pressure cranial to the injury in their patients. Although there was no measure of tissue perfusion in these three studies, it is probably reasonable to assume that increased cranial CSF pressure would result in a decreased spinal cord perfusion in this region provided that the blood pressure remained constant. This notion is supported by studies which have demonstrated that reduced CSF pressure induced by draining CSF during TAAA surgery results in reduced risk of ischaemic paraplegia, and also the understanding that elevated ICP is detrimental to the recovery of TBI patients (Section 1.4.7.1). Thus when decompression alleviates the thecal occlusion, the CSF is able to flow from the "high pressure" cranial region to the "low pressure" caudal region, reducing the cranial pressure and increasing the tissue perfusion. This suggests that a complementary benefit of decompression may be the reduction of CSF pressure cranial to the level of the injury, provided that subsequent cord swelling does not immediately re-occlude the thecal sac. Re-establishing a pathway to the spinal CSF resorption sites may also have implications for the transport of nutrient and waste products in the CSF, but this is purely speculative.

The clinical evaluation of the efficacy of early decompression is complicated by issues such as spontaneous neurological recovery [597], difficulties reaching concensus on what is considered an "early" timepoint and can be achieved logistically [200], and the heterogeneity of injury mechanisms and severities. In Chapter 6 it was shown that in this animal model, the timing and extent of spinal cord swelling after decompression appeared to be dependent on the severity of the mechanical insult. This swelling response may contribute to the aforementioned heterogeneity observed in human SCI. A higher energy injury was generally associated with a quicker and more extensive focal swelling, which potentially negates any beneficial effect of the decompression. This result, combined with the observed differences in CSF pressure differential both before and after decompression, suggests that clinical assessment of the value of decompression may be more conclusive if the cases are stratified according to estimates of the energy associated with the injuries. This could possibly be done with accident reconstruction methodology, or by classification of the fractures and ligamentous disruptions, although there are well recognised limitations to the extrapolation of injury "energy" from these factors. Emerging early measures of injury severity such as magnetic resonance signal change [601] or CSF biomarkers [597] could also be considered once they are better established.

7.6 Limitations

It is well recognised that animal models of SCI only approximate a highly idealised human SCI [494]. As indicated in Section 1.4.3, there are many different fracture and loading mechanisms that can

impart complex combinations of compression, distraction, torsion and shear loads to the dura and spinal cord. Furthermore, even if a single injury mechanism is selected for simulation (e.g. burst fracture) it is extremely difficult to determine the mechanical parameters necessary to accurately replicate the biomechanics of SCI (Section 1.6.4). Similar to all other contusion models, the pig model presented here applies the load to the dorsal aspect of the spinal cord, while a typical burst fracture involves contact between a bone fragment and the ventral aspect of the spinal cord. In addition, experimental SCIs are carried out with the animal in the prone position, while it has been shown that both the location of the spinal cord in the canal and the dorsal/ventral distribution of CSF are sensitive to body position in humans [522]. The influence of injury mechanism (i.e. contusion, dislocation, distraction) on the type of tissue damage sustained has been highlighted by several researchers in recent years [142,143,602]. It is likely that these different injury mechanisms also interact differently with the CSF layer; this thesis has not sought to investigate these different mechanisms.

The potential for the surgical procedures to alter the biomechanical and physiological response to SCI is recognised. Ideally CSF pressure changes would be assessed without modification of the bony and ligamentous structure, loss of CSF during pressure transducer insertion, or the use of anaesthesia; however, this was not possible with current technology. To optimise the use of resources, the same animals were used for the studies presented in Chapter 3, 5 and 6. Therefore, the surgical procedures undertaken were a combination of the requirements for each of the three studies. The spinal surgery was quite extensive, and as noted in Section 7.4.1 removing the posterior canal, ligaments and epidural fat may have affected the transmission of the pressure wave in the spinal cord and CSF (Chapter 3). Future technology may enable pressure transducers to be implanted with minimally invasive surgery, and with reduced CSF loss. Anaesthetic drugs have the potential to alter brain metabolism and cardiovascular physiology, which may affect the formation and resorption of CSF. It has been reported that CSF pressure is an average of 8.6 mmHg lower in young patients when under general anaesthetic [517], although there is not similar information for animals. As noted in Section 5.4, the selected anaesthetics were not expected to have such effects, but the mechanisms of CSF formation and resorption are not completely understood (Section 1.3.2) and thus, the possibility cannot be disregarded.

Relatively little is known about the neuroanatomy of the pig spinal cord compared to that of humans and rats. There may be differences such as tract locations and cellular response to injury, which could have implications for the secondary pathophysiology of the model. Phase 1 of the research (Chapter 2 and 3) was concerned with the mechanical response of the system for which similar gross anatomy and tissue mechanical properties are adequate. As noted in Section 7.3, the size of the pig's thoracic cord was similar to human, but the dura was at the lower range measured in humans by MRI and CT myelography. The *in vitro* compression behaviour of the pig spinal cord is reportedly similar to human, porcine and bovine brain [237]; there is no published data for its tensile behaviour. The

mechanical properties of pig dura have not been reported; however, unpublished data collected in this laboratory indicates that the quasistatic elastic modulus, failure stress and failure strain of pig dura is similar to humans and other animals. The characteristics studied in Phase 3 (Chapter 5 and 6) relied on similarity in the pathophysiological response of the cerebrospinal fluid and the spinal cord. The pig was deemed appropriate for this research program because the species has been used previously for studies of intrathecal drug delivery after SCI [383] as well as ischaemic [377,378,505] and traumatic SCI [382,385,389], and as a model of TBI [376]. While there is no evidence to suggest that the pig's primary physiological response to SCI would be dissimilar to human, studies to ensure that it shares the characteristics of human SCI pathology, such as central haemorrhage, spreading ischaemia and necrosis, and subsequent infarction and cavitation [494], are required to ensure that this assumption is correct.

The histology data presented in Chapter 3 provided a basic assessment of the injury severity and extent centred on the lesion epicentre. This analysis confirmed the presence of a central lesion similar to other contusion models [494], and that the higher injury severity resulted in less spared tissue (see Section 3.3.3). However, the thesis did not include an extensive analysis of histological data or an assessment of the animals' behavioural function after injury. A more detailed immunohistochemistry analysis may allow assessment of diffuse and remote cellular damage. Specific immunohistochemistry analyses are suggested in Section 7.7.4 below. As previously mentioned, because this is a new animal model there was no existing tool to assess behavioural recovery, and this was being developed in a separate parallel study [501,603].

The post-injury period was limited to 14 hours due to the challenges associated with maintaining the animals under prolonged anaesthesia and the logistics of continuous monitoring. The eight hour thecal occlusion period matched the proposed accident-to-surgery time limit for the definition of *early* decompression in clinical studies of decompression efficacy [201,202], and appears to be achievable for some tertiary care centres [202,205]. It was also much longer than previous animal studies of "early" decompression [200]. Finally, due to the time and cost intensive nature of the animal experiments, the number of animals in each experimental group was relatively low. Since no data was available to perform *a priori* power analyses, the sample size was selected according to that which is generally regarded as acceptable for spine biomechanics research [604].

As with all bench-top models of biological systems, the major limitations of the model were associated with the mechanical properties of the synthetic materials, the simplified geometry of the components and the uncertainty in the boundary conditions applied to mimic the *in vivo* condition; these were discussed in Section 4.4. Briefly, the cord and dura had cylindrical geometry without nerve root or ligamentous tethering, the posterior canal was simulated with a flat plate and the lateral and superior canal boundaries were not modelled; the minimum dura size was limited by the need to provide adequate

space for the pressure transducers; the dura did not have anisotropic hyperviscoelastic material properties, and the model was not subjected to a rigorous sensitivity analysis. These limitations were likely reflected in the disparity between the magnitudes of transient pressure peaks measured in the bench-top model versus the animal model. The advantages of the current model over previous models incorporating dura and CSF were outlined in Section 4.4.

7.7 Recommendations

Each of the studies in this thesis has illustrated areas in which further investigations may be warranted. Given the relative paucity of literature relating to the role of CSF in both the primary mechanical insult and the subsequent pathophysiologic sequelae, there are many opportunities for improving upon and extending the scope of the research in this thesis to further the current understanding of the role of CSF in SCI.

7.7.1 Improving the injury apparatus

There are several improvements that could be made to the weight-drop SCI apparatus to improve the accuracy and efficiency of data collection and analysis. The accuracy of cord compression and velocity measures derived from high speed camera images is dependent upon accurate correction of lens distortion; in addition, small errors may arise due to possible misalignment of the vertical guide rail and the post-processing of images is time consuming. A more accurate and immediate measure of cord compression could probably be obtained if a low-friction linear variable displacement transducer or high speed non-contact laser or ultrasound displacement transducer were able to be employed; this was not possible with the current configuration. Accuracy could also be improved using two cameras and a calibration algorithm to obtain displacement data in three dimensions; however, this would increase the post-processing time further. Using an active motion capture system may also be possible but the data capture rates of those commonly used in orthopaedic applications do not appear to be sufficient.

The current impactor design allows for dropped weights of 20 g and higher. By further optimising the design of the impactor, the weight could probably be reduced to around 12 g. The weight of the load cell is currently the limiting factor; we used the smallest commercially available load cell at this time. The cable of the load cell may contribute to the variability in the force delivered to the cord; however, a wireless load cell of this weight and size is not currently available. As noted in Section 1.6.3.1, thorax compression has been identified as a source of variability in other weight-drop models. Clamping the vertebra on either side of the pedicle screw and rod construct and fixing them to the operating table or a floor-mounted frame may be advantageous.

The method used to obtain sustained compression on the cord in the post-injury period did not allow quantification of compression or thecal occlusion (Section 5.4). Quantifying the degree of occlusion reached and/or measuring CSF flow across the injury site may reduce variability and assist in the interpretation of the response to sustained compression and decompression.

7.7.2 Defining the mechanical inputs

The process of designing the injury device highlighted the paucity of data existing on which to base experimental SCI parameters (see Section 1.6.4). Furthermore, the bench-top model study clearly showed that CSF pressure, cord compression and impact loads are highly dependent on the impact velocity (Section 4.3.2), which highlights the need for accurate estimates of injury velocity. Previous attempts to visualise burst fracture bone fragments have used mirrors and a high speed camera [133] and discrete sensors placed in the canal [132], but both of these approaches required removing the spinal cord, which probably affected the biomechanical response. In recent years uni- and bi-planar high speed x-ray systems capable of capturing images at more than 1000 frames per second and with improved resolution, such as the system used in Chapter 4, have emerged. Revisiting the question of the speed of canal encroachment in burst and other spinal fractures with this technology may yield improved data to assist device and model design. In the case of a burst fracture, such studies should also endeavour to determine the weight and cross-sectional area of the bony fragment produced.

7.7.3 Animal model development

Although not necessary for the studies presented here, a survival model based on the miniature Yucatan pig would be invaluable to answer further basic science questions as well as to be an intermediary pre-clinical assessment tool. The need for such a model has been identified by the clinical and research community [374]. Some development studies have been carried out in parallel with this thesis, and behavioural scales for the objective assessment of recovery have been reported [501,603]. With rigorous characterisation to define the behavioural recovery associated with specified injury parameters and the type and extent of the cellular damage and lesion resulting from secondary pathophysiology, the model has the potential to become a valuable intermediary for the pre-clinical evaluation of pharmacological and biologic treatments.

7.7.4 Pressure transients and injury thresholds

This study showed that the pressures occurring in the CSF during injury are within the range known to cause at least temporary changes in brain cells, particularly near the site of the impact. However, because this contusion model also produced substantial cord compression, it was not possible

to distinguish between tissue damage caused by the mechanical compression and damage caused by the pressure transients. Producing a pressure impulse without direct cord compression could be achieved by providing a mechanical stop on the weight-drop (or other) injury device, so that the dura and CSF are dynamically compressed, but the spinal cord is not. Using an iterative approach, perhaps aided by a numerical simulation, the impact parameters could be adjusted until the pressure profile achieved was similar to that reported in Chapter 2 and 3. Any tissue damage observed in histological sections could then be attributed to the fluid pulse alone. Immunohistopathology techniques suitable for observing diffuse cellular dysfunction remote from the site of the injury should be used. Such antibodies may include microtubule associated protein-2 (MAP-2) [605] and neuronal nuclei (NeuN) [605] for neurons, neurofilament [143] for white matter, and glial fibrillary acidic protein (GFAP) for astrocytes [606].

While the above approach would be necessary to demonstrate the extent of tissue damage remote to the injury site, it may be an inefficient manner in which to determine injury threshold. Determining injury thresholds is recognised as one of the more difficult tasks in injury biomechanics, due to a high degree of variability in injury mechanism and individual response. An *in vitro* cellular approach using barochambers or weight-drop apparatus capable of applying impulsive loads (described briefly in Section 1.5.4.4) may be a complementary method to determine a pressure threshold for the constituents of spinal cord tissue. However, these methods are not without their own inherent limitations including a lack of cellular connectivity and extracellular matrix [307,332].

A validated finite element model that incorporates fluid-solid interactions could provide a more detailed map of the pressure wave propagation and the associated stress distribution in the tissues; CSF has been included in only two SCI models to date [495,528]. In animal and bench-top models the number of pressure transducers that can be placed and their location are limited, whereas in computational models the output parameters can be obtained at numerous locations and at any desired position. Such a model may help to clarify the profile of the pressure wave propagation, the distance from the impact at which the cellular injury threshold is crossed, and the effect of the pressure wave on fluid motion and spinal cord and dura deformation.

7.7.5 Post-injury pressure and spinal cord swelling

This is the first study to highlight that the redistribution of CSF between the cranial and caudal compartments may be a key benefit of decompression. Further research is needed to determine whether this redistribution has a tangible effect on tissue perfusion and nutrient/waste transport. A study of CSF drainage following SCI in rabbits found that, contrary to expectation and in contradiction to the histology results, spinal cord perfusion at the injury site *decreased* relative to controls during the periods of induced intrathecal hypotension [196]. However, perfusion was measured with a non-invasive laser Doppler

tissue perfusion probe which, according to the authors, is not able to measure perfusion in the deeper parenchyma. Radio-labelled tracers [607] and invasive electrode techniques [608] have demonstrated increased blood flow during CSF drainage (with lowered CSFP) for TAAA surgery in various animals, and most recently the use of non-invasive near-infrared spectroscopy sensors to detect tissue oxygen saturation has been described in a TAAA surgery patient [609]. While spinal cord perfusion pressure is the only clinically available measure of tissue perfusion, it is derived from other measurable quantities. Therefore it is only a gross regional representation of true perfusion and localised differences are likely at the microvascular level [91]. Therefore, examining the effect of subarachnoid occlusion and subsequent decompression on local tissue perfusion measured along the length of the spinal cord would provide valuable information to support, or oppose, continued exploration of the therapeutic potential of early decompression and/or CSF drainage to accompany haemodynamic support for traumatic SCI.

Both of the previous studies of CSF drainage for SCI have drained the CSF from a catheter inserted in the lumbar cisterne [91,196]. The current findings suggest that to achieve reduced CSF pressure when there is an impingement on the spinal cord, the fluid may need to be drained from the cranial compartment since this is the compartment of increased pressure. Future studies in animals should consider assessing the effect of draining the CSF *cranial* to the injury using local tissue perfusion measures, histological evidence of tissue damage and functional outcome. Increasing the study duration may help to magnify the effect; however, this would probably require waking the animals from anaesthesia. If successful, translation to clinical practice is likely to be challenging since cranial drainage is not currently indicated unless there is an accompanying TBI. Advances in technology and surgical techniques may someday lower the risk of catheterising the proximal intrathecal space in SCI patients to an acceptable limit.

This thesis provided the first quantitative analysis of cord response to decompression. However, the study was limited in that only the mid-sagittal dimension was measured and there was no complementary measurement of cross-lesion fluid flow or parenchymal pressure. As mentioned in Section 7.5.1, a more comprehensive analysis of three-dimensional morphology, flow and pressure over an extended duration could shed more light on the benefits or detriments of early decompression. It may also help to determine those factors that indicate the likelihood of improved prognosis following decompression surgery. The parenchymal pressure readings in particular may also improve understanding of the results that have been reported for dural decompression in animals and patients [212-217] (Section 1.4.7.2).

7.7.6   Improving the bench-top model

The bench-top model apparatus has the potential to perform adequately for future studies of SCI mechanics although the biofidelity of the model would be improved by the refinement of several elements. There is currently no surrogate dura material that accurately replicates the hyperviscoelastic properties of native dura. The response of a viscoelastic material is dependent on the rate of load and strain application; therefore, proper characterisation of these properties is important for the high speed impacts used to simulate SCI. Although the surrogate spinal cord material replicates the quasi-static *in vivo* modulus of spinal cord under tensile and transverse compressive loading [470], it has not been optimised at low strains [470] or for high strain rate transverse compression [280]. Increased biofidelity could also be obtained by more accurate replication of cord, dura and canal geometry, including nerve roots and tethering elements. A more detailed strain distribution within the cord might be obtained by utilising bi-planar x-ray and a surrogate containing a three-dimensional grid of radiopaque markers.

7.8   Contributions

This thesis addressed several contemporary questions in SCI research that have implications for both basic science and clinical research. The studies brought about new models, methods and knowledge about the role of CSF in SCI, and in doing made a number of novel contributions to the field:

1. In Chapter 2 a new large animal model of SCI based on the weight-drop method was introduced. There are few contemporary large animal models based on a contusion injury mechanism and this is the first which is capable of measuring impact load, velocity and displacement. This study also reports, for the first time, measurements of CSF pressure transients during experimental SCI utilising pressure transducers placed directly in the spinal thecal sac. The model is suitable for studying many aspects of the biomechanics of SCI because the pig spinal cord is a similar size to the human spinal cord. With further development it also has the potential to become an important pre-clinical intermediary for the assessment of SCI treatments.

2. The study in Chapter 3 presented a refined injury device design, and a comprehensive characterisation of CSF pressure transients in response to SCIs designed to mimic moderate and high severity human SCIs. This is the first study to measure CSF pressure at multiple locations along the length of the spine with an open SCI model utilising human-like injury parameters and indwelling pressure transducers. The study demonstrated that peak pressures near the SCI site are within the range associated with cellular damage in experimental TBI models, and that there is rapid damping of the pressure wave within 100 mm from impact site. This unique dataset of pressure profiles, in conjunction with the corresponding description of the impact (velocity, load and compression) will be valuable for the validation of computational, bench-top and cadaveric models.

3. A novel bench-top model that was designed and used to explore the effect of CSF layer thickness and impact velocity on the CSF and cord response is described in Chapter 4. This is the first such model that incorporates dura and cord that can be tensioned independently and allows direct x-ray visualisation of the cord during the impact. The study demonstrated that thecal sac dimension (CSF layer thickness) is inversely proportional to peak CSF pressure, cord compression and impact load, but directly proportional to tether load. The impact velocity is directly proportional to peak CSF pressure, cord compression, impact load and tether load. These results suggest that researchers should, depending on their particular research objectives, consider using animal, cadaver, benchtop and computational models with appropriately sized CSF layers to improve the models' biofidelity.

4. The study detailed in Chapter 5 measured CSF pressure trends cranial and caudal to the SCI site in response to eight hours of sustained thecal sac occlusion and a further six hours subsequent to decompression. The study demonstrated for the first time that a thecal sac occlusion caused by a pseudo-bony fragment leads to a CSF pressure differential between the cranial and caudal compartments, and that this may be relieved by decompression. This study makes a significant contribution as such measurements are not currently possible in patients, and because the results have implications for, and have the potential to be translated directly to, CSF pressure measurement and drainage protocols as well as intrathecal drug delivery.

5. The changes in cord and dura morphology after surgical decompression following an acute SCI were described and quantified for the first time in Chapter 6. The study demonstrated that swelling of the spinal cord can be rapid and in some cases appear to occlude the thecal sac within six hours. The residual deformation that was observed in animals with a moderate injury severity has not been reported previously. These findings are important because such measurements are not possible in a clinical population and they may provide some insight into the challenges associated with demonstrating benefits of early decompression in patients with widely varying injury severities.

7.9 Conclusion

The CSF that fills the thecal sac and surrounds the spinal cord is assumed to offer protection for the neural tissue during everyday activites. In contrast, some clinical and experimental evidence suggests that it may contribute to a remote diffuse injury during SCI by way of a pressure wave transmitted away from the mechanical insult. Further, there has been clinical interest in manipulating CSF pressure as a means of haemodynamic support in acute SCI patients. The role of CSF in the biomechanics of the SCI event and its immediate pathophysiology has only been studied in a limited fashion. This thesis describes a series of studies exploring various ways in which CSF contributes to SCI mechanics.

A model of contusion SCI in a large animal was developed along with a technique for measuring spinal CSF pressure with indwelling miniature pressure transducers. The results showed that substantial

pressure transients in the CSF were created by experimental contusion SCI events with human-like impact energies. The magnitude of these pressure waves were within the range of pressures associated with cellular damage in TBI models at around 30 mm from the impact site, but significantly damped by 100 mm away. The high magnitude travelling wave may help to explain some experimental and clinical evidence of diffuse tissue damage remote from the injury epicentre. A bench-top model of the spinal cord and dura was constructed and used to demonstrate that the thickness of the CSF layer, as well as the impact velocity, affect mechanical measures related to injury severity such as peak CSF pressure, impact load and cord compression. These findings suggest that animal, bench-top and computational models that lack human-like thecal sac dimensions may have limited biofidelity and that the mechanical parameters (e.g. velocity) used to study SCI biomechanics and pathophysiology should be carefully selected, and scaled if necessary, to match the human scenario. Finally, the response of the CSF pressure and spinal cord and thecal sac morphology was studied after acute SCI with sustained occlusion of the thecal sac and after decompression. Sustained thecal occlusion caused an increased cranial pressure and consequential pressure differential between the cranial and caudal compartments that was at least partially resolved by decompression. This finding demonstrates that CSF pressure monitoring and fluid drainage for acute SCI patients, in whom intrathecal access is limited to lumbar catheterisation, may be of limited value in those with residual bony compression of the cord. The changes in morphology of the spinal cord after decompression appeared to be related to the primary injury severity. Further, swelling often led to apparent thecal occlusion within six hours of decompression. These results demonstrate that swelling of the spinal cord may re-occlude the subarachnoid space within hours and this may attenuate the benefits of surgical decompression, thus suggesting that it may be important to reduce cord swelling to optimise the clinical outcome after acute traumatic SCI.

References

1. Hung TK, Albin MS, Brown TD, Bunegin L, Albin R, and Jannetta PJ (1975) Biomechanical responses to open experimental spinal cord injury. *Surgical Neurology*. **4**(2):271-6.

2. Albin MS, Hung TK, Brown TD, Jannetta PJ, Bunegin L, and Albin RL (1975) Experimental spinal cord injury biomechanics. *Neuroscience Abstracts*. **1**:697.

3. Wennerstrand J, Jonsson A, and Arvebo E (1978) Mechanical and histological effects of transverse impact on the canine spinal cord. *Journal of Biomechanics*. **11**(6-7):315-31.

4. Drake RL, Vogl W, and Mitchell AWM, *Gray's anatomy for students*. 2005, Philadelphia: Elsevier: Churchill Livingston.

5. Nicholas DS and Weller RO (1988) The fine anatomy of the human spinal meninges. A light and scanning electron microscopy study. *Journal of Neurosurgery*. **69**(2):276-82.

6. Brown PD, Davies SL, Speake T, and Millar ID (2004) Molecular mechanisms of cerebrospinal fluid production. *Neuroscience*. **129**(4):957-70.

7. Last RJ and Tompsett DH (1953) Casts of the cerebral ventricles. *British Journal of Surgery*. **40**(164):525-43.

8. Rubin RC, Henderson ES, Ommaya AK, Walker MD, and Rall DP (1966) The production of cerebrospinal fluid in man and its modification by acetazolamide. *Journal of Neurosurgery*. **25**(4):430-6.

9. Cutler RW, Page L, Galicich J, and Watters GV (1968) Formation and absorption of cerebrospinal fluid in man. *Brain*. **91**(4):707-20.

10. Milhorat TH, *Cerebrospinal fluid and the brain edemas*. 1987, New York: Neuroscience Society of New York.

11. Johanson CE, Duncan JA, 3rd, Klinge PM, Brinker T, Stopa EG, and Silverberg GD (2008) Multiplicity of cerebrospinal fluid functions: New challenges in health and disease. *Cerebrospinal Fluid Res*. **5**:10.

12. McConnell H, *Cerebrospinal fluid dynamics*. 1st ed. Cerebrospinal fluid in neurology and psychiatry, ed. Mcconnell, H. and Bianchine, J. 1994, London: Chapman and Hall. Chapter 2.

13. McComb JG (1983) Recent research into the nature of cerebrospinal fluid formation and absorption. *Journal of Neurosurgery*. **59**(3):369-83.

14. Segal MB and Pollay M (1977) The secretion of cerebrospinal fluid. *Experimental Eye Research*. **25 Suppl**:127-48.

15. Milhorat TH (1976) Structure and function of the choroid plexus and other sites of cerebrospinal fluid formation. *International Review of Cytology*. **47**:225-88.

16. Akhtar AZ, Pippin JJ, and Sandusky CB (2008) Animal models in spinal cord injury: A review. *Reviews in the Neurosciences*. **19**(1):47-60.

17. Hammerstad JP, Lorenzo AV, and Cutler RW (1969) Iodide transport from the spinal subarachnoid fluid in the cat. *American Journal of Physiology*. **216**(2):353-8.

18. Lux WE, Jr. and Fenstermacher JD (1975) Cerebrospinal fluid formation in ventricles and spinal subarachnoid space of the rhesus monkey. *Journal of Neurosurgery*. **42**(6):674-8.

19. Coben LA and Smith KR (1969) Iodide transfer at four cerebrospinal fluid sites in the dog: Evidence for spinal iodide carrier transport. *Experimental Neurology*. **23**(1):76-90.

20.   Speake T, Whitwell C, Kajita H, Majid A, and Brown PD (2001) Mechanisms of CSF secretion by the choroid plexus. *Microscopy Research and Technique*. **52**(1):49-59.

21.   May C, Kaye JA, Atack JR, Schapiro MB, Friedland RP, and Rapoport SI (1990) Cerebrospinal fluid production is reduced in healthy aging. *Neurology*. **40**(3 Pt 1):500-3.

22.   Chen CP, Chen RL, and Preston JE (2010) The influence of cerebrospinal fluid turnover on age-related changes in cerebrospinal fluid protein concentrations. *Neuroscience Letters*. **476**(3):138-41.

23.   Nilsson C, Stahlberg F, Thomsen C, Henriksen O, Herning M, and Owman C (1992) Circadian variation in human cerebrospinal fluid production measured by magnetic resonance imaging. *American Journal of Physiology*. **262**(1 Pt 2):R20-4.

24.   Rudick RA, Zirretta DK, and Herndon RM (1982) Clearance of albumin from mouse subarachnoid space: A measure of CSF bulk flow. *Journal of Neuroscience Methods*. **6**(3):253-9.

25.   Baudrie V, Roullet JB, Goureau Y, Chaouloff F, and Elghozi JL (1990) Determination of cerebrospinal fluid production rate using a push-pull perfusion procedure in the conscious rat. *Fundamental and Clinical Pharmacology*. **4**(3):269-74.

26.   Curran RE, Mosher MB, Owens ES, and Fenstermacher JD (1970) Cerebrospinal fluid production rates determined by simultaneous albumin and inulin perfusion. *Experimental Neurology*. **29**(3):546-53.

27.   Lorenzo AV, Hammerstad JP, and Cutler RW (1970) Cerebrospinal fluid formation and absorption and transport of iodide and sulfate from the spinal subarachnoid space. *Journal of the Neurological Sciences*. **10**(3):247-58.

28.   Bering EA, Jr. and Sato O (1963) Hydrocephalus: Changes in formation and absorption of cerebrospinal fluid within the cerebral ventricles. *Journal of Neurosurgery*. **20**:1050-63.

29.   Chen RL, Kassem NA, Redzic ZB, Chen CP, Segal MB, and Preston JE (2009) Age-related changes in choroid plexus and blood-cerebrospinal fluid barrier function in the sheep. *Experimental Gerontology*. **44**(4):289-96.

30.   Boulton M, Flessner M, Armstrong D, Hay J, and Johnston M (1998) Determination of volumetric cerebrospinal fluid absorption into extracranial lymphatics in sheep. *American Journal of Physiology*. **274**(1 Pt 2):R88-96.

31.   Chodobski A, Szmydynger-Chodobska J, Cooper E, and McKinley MJ (1992) Atrial natriuretic peptide does not alter cerebrospinal fluid formation in sheep. *American Journal of Physiology*. **262**(5 Pt 2):R860-4.

32.   Payne R, Madsen J, Harvey RC, and Inturrisi CE (1986) A chronic sheep preparation for the study of drug pharmacokinetics in spinal and ventricular CSF. *Journal of Pharmacological Methods*. **16**(4):277-96.

33.   Pappenheimer JR, Heisey SR, Jordan EF, and Downer Jd (1962) Perfusion of the cerebral ventricular system in unanaesthetized goats. *American Journal of Physiology*. **203**:763-81.

34.   Heisey SR, Held D, and Pappenheimer JR (1962) Bulk flow and diffusion in the cerebrospinal fluid system of the goat. *American Journal of Physiology*. **203**:775-81.

35.   Edsbagge M, Tisell M, Jacobsson L, and Wikkelso C (2004) Spinal CSF absorption in healthy individuals. *American Journal of Physiology. Regulatory, Integrative and Comparative Physiology*. **287**(6):R1450-5.

36.   Hochwald GM and Sahar A (1971) Effect of spinal fluid pressure on cerebrospinal fluid formation. *Experimental Neurology*. **32**(1):30-40.

37. Calhoun MC, Hurt HD, Eaton HD, Rousseau JE, Jr., and Hall RC, Jr. (1967) Rates of formation and absorption of cerebrospinal fluid in bovine hypovitaminosis a. *Journal of Dairy Science*. **50**(9):1489-94.

38. Katzman R and Hussey F (1970) A simple constant-infusion manometric test for measurement of CSF absorption. I. Rationale and method. *Neurology*. **20**(6):534-44.

39. Nilsson C, Lindvall-Axelsson M, and Owman C (1992) Neuroendocrine regulatory mechanisms in the choroid plexus-cerebrospinal fluid system. *Brain Research. Brain Research Reviews*. **17**(2):109-38.

40. Kapoor KG, Katz SE, Grzybowski DM, and Lubow M (2008) Cerebrospinal fluid outflow: An evolving perspective. *Brain Research Bulletin*. **77**(6):327-34.

41. Johnston M and Papaiconomou C (2002) Cerebrospinal fluid transport: A lymphatic perspective. *News Physiol Sci*. **17**:227-30.

42. Kido DK, Gomez DG, Pavese AM, Jr., and Potts DG (1976) Human spinal arachnoid villi and granulations. *Neuroradiology*. **11**(5):221-8.

43. Bell WO (1995) Cerebrospinal fluid reabsorption. A critical appraisal. 1990. *Pediatric Neurosurgery*. **23**(1):42-53.

44. Silver I, Kim C, Mollanji R, and Johnston M (2002) Cerebrospinal fluid outflow resistance in sheep: Impact of blocking cerebrospinal fluid transport through the cribriform plate. *Neuropathology and Applied Neurobiology*. **28**(1):67-74.

45. Boulton M, Armstrong D, Flessner M, Hay J, Szalai JP, and Johnston M (1998) Raised intracranial pressure increases CSF drainage through arachnoid villi and extracranial lymphatics. *American Journal of Physiology*. **275**(3 Pt 2):R889-96.

46. Bering EA, Jr. and Salibi B (1959) Production of hydrocephalus by increased cephalic-venous pressure. *AMA Archives of Neurology and Psychiatry*. **81**(6):693-8.

47. Bedford THB (1935) The effect of increased intracranial venous pressure on the pressure of the cerebrospinal fluid. *Brain*. **58**(4):427-47.

48. Zakharov A, Papaiconomou C, Koh L, Djenic J, Bozanovic-Sosic R, and Johnston M (2004) Integrating the roles of extracranial lymphatics and intracranial veins in cerebrospinal fluid absorption in sheep. *Microvascular Research*. **67**(1):96-104.

49. Bozanovic-Sosic R, Mollanji R, and Johnston MG (2001) Spinal and cranial contributions to total cerebrospinal fluid transport. *American Journal of Physiology. Regulatory, Integrative and Comparative Physiology*. **281**(3):R909-16.

50. Tubbs RS, Hansasuta A, Stetler W, Kelly DR, Blevins D, Humphrey R, Chua GD, Shoja MM, Loukas M, and Oakes WJ (2007) Human spinal arachnoid villi revisited: Immunohistological study and review of the literature. *Journal of Neurosurgery. Spine*. **7**(3):328-31.

51. Lee RR, Abraham RA, and Quinn CB (2001) Dynamic physiologic changes in lumbar CSF volume quantitatively measured by three-dimensional fast spin-echo MRI. *Spine (Phila Pa 1976)*. **26**(10):1172-8.

52. Eckenhoff JE (1970) The physiologic significance of the vertebral venous plexus. *Surgery, Gynecology and Obstetrics*. **131**(1):72-8.

53. Lavinio A, Czosnyka Z, and Czosnyka M (2008) Cerebrospinal fluid dynamics: Disturbances and diagnostics. *European Journal of Anaesthesiology. Supplement*. **42**:137-41.

54. Smith M (2008) Monitoring intracranial pressure in traumatic brain injury. *Anesthesia and Analgesia*. **106**(1):240-8.

55. Hewett R and Counsell C (2010) Documentation of cerebrospinal fluid opening pressure and other important aspects of lumbar puncture in acute headache. *International Journal of Clinical Practice*. **64**(7):930-5.

56. Lenfeldt N, Koskinen LO, Bergenheim AT, Malm J, and Eklund A (2007) CSF pressure assessed by lumbar puncture agrees with intracranial pressure. *Neurology*. **68**(2):155-8.

57. Warrell DA, Cox TM, Cox JD, and Benz EJ, eds. *Oxford textbook of medicine*. 2005, Oxford University Press: Oxford, UK.

58. Gilland O, Tourtellotte WW, O'Tauma L, and Henderson WG (1974) Normal cerebrospinal fluid pressure. *Journal of Neurosurgery*. **40**(5):587-93.

59. Neville L and Egan RA (2005) Frequency and amplitude of elevation of cerebrospinal fluid resting pressure by the valsalva maneuver. *Canadian Journal of Ophthalmology*. **40**(6):775-7.

60. Whiteley W, Al-Shahi R, Warlow CP, Zeidler M, and Lueck CJ (2006) CSF opening pressure: Reference interval and the effect of body mass index. *Neurology*. **67**(9):1690-1.

61. Corbett JJ and Mehta MP (1983) Cerebrospinal fluid pressure in normal obese subjects and patients with pseudotumor cerebri. *Neurology*. **33**(10):1386-8.

62. Sakikawa Y, Kobayashi H, and Nomura Y (1994) Changes in cerebrospinal fluid pressure in daily life. *Annals of Otology, Rhinology and Laryngology*. **103**(12):959-63.

63. Williams B (1981) Simultaneous cerebral and spinal fluid pressure recordings. I. Technique, physiology, and normal results. *Acta Neurochirurgica*. **58**(3-4):167-85.

64. Greenfield JC, Jr., Rembert JC, and Tindall GT (1984) Transient changes in cerebral vascular resistance during the valsalva maneuver in man. *Stroke*. **15**(1):76-9.

65. Martins AN, Wiley JK, and Myers PW (1972) Dynamics of the cerebrospinal fluid and the spinal dura mater. *Journal of Neurology, Neurosurgery and Psychiatry*. **35**(4):468-73.

66. Lakke JPWF, *Queckenstedt's test; electromanometric examination of CSF pressure on jugular compression and its clinical value*. 1969, Amsterdam: Excerpta Medica Foundation. 194.

67. Langfitt TW (1975) Clinical methods for monitoring intracranial pressure and measuring cerebral blood flow. *Clinical Neurosurgery*. **22**:302-20.

68. Kaufmann GE and Clark K (1970) Continuous simultaneous monitoring of intraventricular and cervical subarachnoid cerebrospinal fluid pressure to indicate development of cerebral or tonsillar herniation. *Journal of Neurosurgery*. **33**(2):145-50.

69. Magnaes B (1982) Clinical recording of pressure on the spinal cord and cauda equina. Part 1: The spinal block infusion test: Method and clinical studies. *Journal of Neurosurgery*. **57**(1):48-56.

70. Pearce JM (2006) Queckenstedt's manoeuvre. *Journal of Neurology, Neurosurgery and Psychiatry*. **77**(6):728.

71. Hollis PH, Malis LI, and Zappulla RA (1986) Neurological deterioration after lumbar puncture below complete spinal subarachnoid block. *Journal of Neurosurgery*. **64**(2):253-6.

72. Komotar RJ, Zacharia BE, Mocco J, Kaiser MG, Frucht SJ, and McKhann GM, 2nd (2008) Cervical spine disease may result in a negative lumbar spinal drainage trial in normal pressure hydrocephalus: Case report. *Neurosurgery*. **63**(4 Suppl 2):315; discussion

73. Caviness JA, Tucker MH, Pia SK, and Tam DA (1998) Hydrocephalus as a possible early symptom in a child with a spinal cord tumor. *Pediatric Neurology*. **18**(2):169-71.

74. Porter A, Lyons MK, Wingerchuk DM, and Bosch EP (2006) Spinal cord astrocytoma presenting as "Idiopathic" Intracranial hypertension. *Clinical Neurology and Neurosurgery*. **108**(8):787-9.

75.	Prasad VS, Basha A, Prasad BC, and Reddy DR (1994) Intraspinal tumour presenting as hydrocephalus in childhood. *Child's Nervous System*. **10**(3):156-7.

76.	Rifkinson-Mann S, Wisoff JH, and Epstein F (1990) The association of hydrocephalus with intramedullary spinal cord tumors: A series of 25 patients. *Neurosurgery*. **27**(5):749-54; discussion 54.

77.	Purohit AK, Dinakar I, Sundaram C, and Ratnakar KS (1990) Anaplastic astrocytoma of the spinal cord presenting with features of raised intracranial pressure. *Child's Nervous System*. **6**(2):113-5.

78.	Klekamp J, Volkel K, Bartels CJ, and Samii M (2001) Disturbances of cerebrospinal fluid flow attributable to arachnoid scarring cause interstitial edema of the cat spinal cord. *Neurosurgery*. **48**(1):174-85; discussion 85-6.

79.	Nakamura K, Urayama K, and Hoshino Y (1997) Lumbar cerebrospinal fluid pulse wave rising from pulsations of both the spinal cord and the brain in humans. *Spinal Cord*. **35**(11):735-9.

80.	Magder S (2007) Invasive intravascular hemodynamic monitoring: Technical issues. *Critical Care Clinics*. **23**(3):401-14.

81.	Brumback RA, *Anatomic and physiological aspects of the cerebrospinal fluid space*, in *The cerebrospinal fluid*, Herndon, W. and Brumback, R., Editors. 1989, Kluwer Academic Boston. 15-43.

82.	Teplick RS (1987) Measuring central vascular pressures: A surprisingly complex problem. *Anesthesiology*. **67**(3):289-91.

83.	Mitchell MM, Meathe EA, Jones BR, Donch TE, Ricks WG, Benumof JL, and Saidman LJ (1987) Accurate, automated, continuously displayed pulmonary artery pressure measurement. *Anesthesiology*. **67**(3):294-300.

84.	Enzmann DR and Pelc NJ (1992) Brain motion: Measurement with phase-contrast MR imaging. *Radiology*. **185**(3):653-60.

85.	O'Connell JE (1970) Cerebrospinal fluid mechanics. *Proceedings of the Royal Society of Medicine*. **63**(5):507-18.

86.	Greitz D, Franck A, and Nordell B (1993) On the pulsatile nature of intracranial and spinal CSF-circulation demonstrated by MR imaging. *Acta Radiologica*. **34**(4):321-8.

87.	Lee E, Wang JZ, and Mezrich R (1989) Variation of lateral ventricular volume during the cardiac cycle observed by MR imaging. *AJNR: American Journal of Neuroradiology*. **10**(6):1145-9.

88.	Loth F, Yardimci MA, and Alperin N (2001) Hydrodynamic modeling of cerebrospinal fluid motion within the spinal cavity. *Journal of Biomechanical Engineering*. **123**(1):71-9.

89.	Bering EA, Jr. (1955) Choroid plexus and arterial pulsation of cerebrospinal fluid; demonstration of the choroid plexuses as a cerebrospinal fluid pump. *AMA Archives of Neurology and Psychiatry*. **73**(2):165-72.

90.	Takizawa H, Gabra-Sanders T, and Miller JD (1986) Spectral analysis of the CSF pulse wave at different locations in the craniospinal axis. *Journal of Neurology, Neurosurgery and Psychiatry*. **49**(10):1135-41.

91.	Kwon BK, Curt A, Belanger LM, Bernardo A, Chan D, Markez JA, Gorelik S, Slobogean GP, Umedaly H, Giffin M, Nikolakis MA, Street J, Boyd MC, Paquette S, Fisher CG, and Dvorak MF (2009) Intrathecal pressure monitoring and cerebrospinal fluid drainage in acute spinal cord injury: A prospective randomized trial. *Journal of Neurosurgery. Spine*. **10**(3):181-93.

92.   Eide PK and Sorteberg W (2006) Intracranial pressure levels and single wave amplitudes, Glasgow coma score and Glasgow outcome score after subarachnoid haemorrhage. *Acta Neurochirurgica*. **148**(12):1267-75; discussion 75-6.

93.   Carrera E, Kim DJ, Castellani G, Zweifel C, Czosnyka Z, Kasparowicz M, Smielewski P, Pickard JD, and Czosnyka M (2010) What shapes pulse amplitude of intracranial pressure? *Journal of Neurotrauma*. **27**(2):317-24.

94.   Avezaat CJ, van Eijndhoven JH, and Wyper DJ (1979) Cerebrospinal fluid pulse pressure and intracranial volume-pressure relationships. *Journal of Neurology, Neurosurgery and Psychiatry*. **42**(8):687-700.

95.   van Eijndhoven JH and Avezaat CJ (1986) Cerebrospinal fluid pulse pressure and the pulsatile variation in cerebral blood volume: An experimental study in dogs. *Neurosurgery*. **19**(4):507-22.

96.   Qvarlander S, Malm J, and Eklund A (2010) The pulsatility curve-the relationship between mean intracranial pressure and pulsation amplitude. *Physiological Measurement*. **31**(11):1517-28.

97.   Eide PK and Brean A (2006) Intracranial pulse pressure amplitude levels determined during preoperative assessment of subjects with possible idiopathic normal pressure hydrocephalus. *Acta Neurochirurgica*. **148**(11):1151-6; discussion 6.

98.   Schuhmann MU, Sood S, McAllister JP, Jaeger M, Ham SD, Czosnyka Z, and Czosnyka M (2008) Value of overnight monitoring of intracranial pressure in hydrocephalic children. *Pediatric Neurosurgery*. **44**(4):269-79.

99.   Holm S and Eide PK (2008) The frequency domain versus time domain methods for processing of intracranial pressure (ICP) signals. *Medical Engineering and Physics*. **30**(2):164-70.

100.   Carlson GD, Oliff HS, Gorden C, Smith J, and Anderson PA (2003) Cerebral spinal fluid pressure: Effects of body position and lumbar subarachnoid drainage in a canine model. *Spine*. **28**(2):119-22.

101.   Klarica M, Rados M, Draganic P, Erceg G, Oreskovic D, Marakovic J, and Bulat M (2006) Effect of head position on cerebrospinal fluid pressure in cats: Comparison with artificial model. *Croatian Medical Journal*. **47**(2):233-8.

102.   Johnston IH, Rowan JO, Park DM, and Rennie MJ (1975) Raised intracrannial pressure and cerebral blood flow, 5: Effects of episodic intracranial pressure waves in primates. *Journal of Neurology, Neurosurgery and Psychiatry*. **38**:1076-82.

103.   Rudehill A, Hjemdahl P, Sollevi A, Sylven O, and Owall A (1987) Changes in cardiac metabolism, perfusion, ECG and plasma catecholamines during increased intracarnial pressure in the pig. *Acta Anaesthesiology Scandinavica*. **31**:265-72.

104.   Budgell BS and Bolton PS (2007) Cerebrospinal fluid pressure in the anesthetized rat. *Journal of Manipulative and Physiological Therapeutics*. **30**(5):351-6.

105.   Barth KN, Onesti ST, Krauss WE, and Solomon RA (1992) A simple and reliable technique to monitor intracranial pressure in the rat: Technical note. *Neurosurgery*. **30**(1):138-40.

106.   Sweetman B and Linninger AA (2010) Cerebrospinal fluid flow dynamics in the central nervous system. *Annals of Biomedical Engineering*.

107.   Armonda RA, Citrin CM, Foley KT, and Ellenbogen RG (1994) Quantitative cine-mode magnetic resonance imaging of chiari I malformations: An analysis of cerebrospinal fluid dynamics. *Neurosurgery*. **35**(2):214-23; discussion 23-4.

108.   Higuchi H, Adachi Y, and Kazama T (2005) Effects of epidural saline injection on cerebrospinal fluid volume and velocity waveform: A magnetic resonance imaging study. *Anesthesiology*. **102**(2):285-92.

109. Carpenter PW, Berkouk K, and Lucey AD (2003) Pressure wave propagation in fluid-filled co-axial elastic tubes. Part 2: Mechanisms for the pathogenesis of syringomyelia. *Journal of Biomechanical Engineering*. **125**(6):857-63.

110. Kalata W, Martin BA, Oshinski JN, Jerosch-Herold M, Royston TJ, and Loth F (2009) MR measurement of cerebrospinal fluid velocity wave speed in the spinal canal. *IEEE Transactions on Bio-medical Engineering*. **56**(6):1765-8.

111. Bertram CD, Brodbelt AR, and Stoodley MA (2005) The origins of syringomyelia: Numerical models of fluid/structure interactions in the spinal cord. *Journal of Biomechanical Engineering*. **127**(7):1099-109.

112. Williams B (1976) Cerebrospinal fluid pressure changes in response to coughing. *Brain*. **99**(2):331-46.

113. Ackery A, Tator C, and Krassioukov A (2004) A global perspective on spinal cord injury epidemiology. *Journal of Neurotrauma*. **21**(10):1355-70.

114. van den Berg ME, Castellote JM, Mahillo-Fernandez I, and de Pedro-Cuesta J (2010) Incidence of spinal cord injury worldwide: A systematic review. *Neuroepidemiology*. **34**(3):184-92; discussion 92.

115. Dryden DM, Saunders LD, Rowe BH, May LA, Yiannakoulias N, Svenson LW, Schopflocher DP, and Voaklander DC (2003) The epidemiology of traumatic spinal cord injury in Alberta, Canada. *Canadian Journal of Neurological Sciences*. **30**(2):113-21.

116. Martins F, Freitas F, Martins L, Dartigues JF, and Barat M (1998) Spinal cord injuries--epidemiology in Portugal's central region. *Spinal Cord*. **36**(8):574-8.

117. Sekhon LH and Fehlings MG (2001) Epidemiology, demographics, and pathophysiology of acute spinal cord injury. *Spine*. **26**(24 Suppl):15.

118. O'Connor PJ (2005) Survival after spinal cord injury in Australia. *Archives of Physical Medicine and Rehabilitation*. **86**(1):37-47.

119. Varma A, Hill EG, Nicholas J, and Selassie A (2010) Predictors of early mortality after traumatic spinal cord injury: A population-based study. *Spine (Phila Pa 1976)*. **35**(7):778-83.

120. NSCISC, (2009) Annual statistical report for the spinal cord injury model systems 2009: Public version. National Spinal Cord Injury Statistical Center: Birmingham, Alabama.

121. Kannus P, Niemi S, Palvanen M, and Parkkari J (2000) Continuously increasing number and incidence of fall-induced, fracture-associated, spinal cord injuries in elderly persons. *Archives of Internal Medicine*. **160**(14):2145-9.

122. O'Connor PJ (2006) Trends in spinal cord injury. *Accident Analysis and Prevention*. **38**(1):71-7.

123. American Spinal Injury Association, (2006) Standard neurological classification of spinal cord injury. American Spinal Injury Association: www.asia-spinalinjury.org/publications/2006_Classif_worksheet.pdf.

124. Denis F (1983) The three column spine and its significance in the classification of acute thoracolumbar spinal injuries. *Spine (Phila Pa 1976)*. **8**(8):817-31.

125. Denis F (1982) Updated classification of thoracolumbar fractures. *Orthopaedic Transactions*. **6**:8-9.

126. Magerl F, Aebi M, Gertzbein SD, Harms J, and Nazarian S (1994) A comprehensive classification of thoracic and lumbar injuries. *European Spine Journal*. **3**(4):184-201.

127. Lee JY, Vaccaro AR, Lim MR, Oner FC, Hulbert RJ, Hedlund R, Fehlings MG, Arnold P, Harrop J, Bono CM, Anderson PA, Anderson DG, Harris MB, Brown AK, Stock GH, and Baron

EM (2005) Thoracolumbar injury classification and severity score: A new paradigm for the treatment of thoracolumbar spine trauma. *Journal of Orthopaedic Science*. **10**(6):671-5.

128. Vaccaro AR, Hulbert RJ, Patel AA, Fisher C, Dvorak M, Lehman RA, Jr., Anderson P, Harrop J, Oner FC, Arnold P, Fehlings M, Hedlund R, Madrazo I, Rechtine G, Aarabi B, and Shainline M (2007) The subaxial cervical spine injury classification system: A novel approach to recognize the importance of morphology, neurology, and integrity of the disco-ligamentous complex. *Spine (Phila Pa 1976)*. **32**(21):2365-74.

129. Aung TS and el Masry WS (1997) Audit of a British centre for spinal injury. *Spinal Cord*. **35**(3):147-50.

130. Pickett GE, Campos-Benitez M, Keller JL, and Duggal N (2006) Epidemiology of traumatic spinal cord injury in Canada. *Spine (Phila Pa 1976)*. **31**(7):799-805.

131. Karacan I, Koyuncu H, Pekel O, Sumbuloglu G, Kirnap M, Dursun H, Kalkan A, Cengiz A, Yalinkilic A, Unalan HI, Nas K, Orkun S, and Tekeoglu I (2000) Traumatic spinal cord injuries in Turkey: A nation-wide epidemiological study. *Spinal Cord*. **38**(11):697-701.

132. Panjabi MM, Kifune M, Wen L, Arand M, Oxland TR, Lin RM, Yoon WS, and Vasavada A (1995) Dynamic canal encroachment during thoracolumbar burst fractures. *Journal of Spinal Disorders*. **8**(1):39-48.

133. Wilcox RK, Boerger TO, Allen DJ, Barton DC, Limb D, Dickson RA, and Hall RM (2003) A dynamic study of thoracolumbar burst fractures. *Journal of Bone & Joint Surgery American*. **85**(11):2184-9.

134. Wilcox RK, Boerger TO, Hall RM, Barton DC, Limb D, and Dickson RA (2002) Measurement of canal occlusion during the thoracolumbar burst fracture process. *Journal of Biomechanics*. **35**(3):381-4.

135. Vaccaro AR, Nachwalter RS, Klein GR, Sewards JM, Albert TJ, and Garfin SR (2001) The significance of thoracolumbar spinal canal size in spinal cord injury patients. *Spine (Phila Pa 1976)*. **26**(4):371-6.

136. Korovessis P, Piperos G, Sidiropoulos P, Karagiannis A, and Dimas T (1994) Spinal canal restoration by posterior distraction or anterior decompression in thoracolumbar spinal fractures and its influence on neurological outcome. *European Spine Journal*. **3**(6):318-24.

137. Bohlman HH (1985) Treatment of fractures and dislocations of the thoracic and lumbar spine. *Journal of Bone and Joint Surgery. American Volume*. **67**(1):165-9.

138. Bensch FV, Koivikko MP, Kiuru MJ, and Koskinen SK (2006) The incidence and distribution of burst fractures. *Emergency Radiology*. **12**(3):124-9.

139. Valentini MC, Busch R, Ferraris MM, and Venturi F (2006) The role of imaging in the choice of correct treatment of unstable thoraco-lumbar fractures. *European Journal of Radiology*. **59**(3):331-5.

140. Gomes S, Rudkin S, Tsai F, and Lotfipour S (2009) Bilateral cervical spine facet fracture-dislocation. *Western Journal of Emergency Medicine*. **10**(1):19.

141. Schauer BA and Sokolove PE (2003) Severe cervical spine distraction. *Journal of Emergency Medicine*. **25**(4):445-7.

142. Choo AM, Liu J, Lam CK, Dvorak M, Tetzlaff W, and Oxland TR (2007) Contusion, dislocation, and distraction: Primary hemorrhage and membrane permeability in distinct mechanisms of spinal cord injury. *Journal of Neurosurgery. Spine*. **6**(3):255-66.

143. Choo AM, Liu J, Dvorak M, Tetzlaff W, and Oxland TR (2008) Secondary pathology following contusion, dislocation, and distraction spinal cord injuries. *Experimental Neurology*. **212**(2):490-506.

144. Bunge RP, Puckett WR, Becerra JL, Marcillo A, and Quencer RM (1993) Observations on the pathology of human spinal cord injury. A review and classification of 22 new cases with details from a case of chronic cord compression with extensive focal demyelination. *Advances in Neurology*. **59**:75-89.

145. Pavlov H, Torg JS, Robie B, and Jahre C (1987) Cervical spinal stenosis: Determination with vertebral body ratio method. *Radiology*. **164**:771-5.

146. Torg JS (2002) Cervical spinal stenosis with cord neurapraxia: Evaluations and decisions regarding participation in athletics. *Current Sports Medicine Reports*. **1**:43-6.

147. Tierney RT, Maldjian C, Mattacola CG, Straub SJ, and Sitler MR (2002) Cervical spine stenosis measures in normal subjects. *Journal of Athletic Training*. **37**(2):190-3.

148. Fassett DR, Harrop JS, Maltenfort M, Jeyamohan SB, Ratliff JD, Anderson DG, Hilibrand AS, Albert TJ, Vaccaro AR, and Sharan AD (2007) Mortality rates in geriatric patients with spinal cord injuries. *Journal of Neurosurgery. Spine*. **7**(3):277-81.

149. Tracy JA and Bartleson JD (2010) Cervical spondylotic myelopathy. *Neurologist*. **16**(3):176-87.

150. Jabbour P, Fehlings M, Vaccaro AR, and Harrop JS (2008) Traumatic spine injuries in the geriatric population. *Neurosurgical Focus*. **25**(5):E16.

151. Norenberg MD, Smith J, and Marcillo A (2004) The pathology of human spinal cord injury: Defining the problems. *Journal of Neurotrauma*. **21**(4):429-40.

152. Rowland JW, Hawryluk GW, Kwon B, and Fehlings MG (2008) Current status of acute spinal cord injury pathophysiology and emerging therapies: Promise on the horizon. *Neurosurgical Focus*. **25**(5):E2.

153. Kwon BK, Tetzlaff W, Grauer JN, Beiner J, and Vaccaro AR (2004) Pathophysiology and pharmacologic treatment of acute spinal cord injury. *Spine Journal*. **4**(4):451-64.

154. Hickey R, Sloan T, and Rogers J, *Functional organisation and physiology of the spinal cord*, in *Textbook of neuroanesthesia with neurosurgical and neuroscience perspectives*, Albin, M., Editor. 1997, McGraw-Hill: New York. 1027-81.

155. Krassioukov A (2009) Autonomic function following cervical spinal cord injury. *Respiratory Physiology and Neurobiology*. **169**(2):157-64.

156. Hadley MN, Sonntag VK, Rekate HL, and Murphy A (1989) The infant whiplash-shake injury syndrome: A clinical and pathological study. *Neurosurgery*. **24**(4):536-40.

157. Shannon P, Smith CR, Deck J, Ang LC, Ho M, and Becker L (1998) Axonal injury and the neuropathology of shaken baby syndrome. *Acta Neuropathologica*. **95**(6):625-31.

158. Silberstein M and McLean K (1994) Non-contiguous spinal injury: Clinical and imaging features, and postulated mechanism. *Paraplegia*. **32**(12):817-23.

159. Henderson FC, Geddes JF, Vaccaro AR, Woodard E, Berry KJ, and Benzel EC (2005) Stretch-associated injury in cervical spondylotic myelopathy: New concept and review. *Neurosurgery*. **56**(5):1101-13; discussion -13.

160. Yucesoy K and Yuksel KZ (2008) Sciwora in MRI era. *Clinical Neurology and Neurosurgery*. **110**(5):429-33.

161. Pang D (2004) Spinal cord injury without radiographic abnormality in children, 2 decades later. *Neurosurgery*. **55**(6):1325-42; discussion 42-3.

162. Czeiter E, Pal J, Kovesdi E, Bukovics P, Luckl J, Doczi T, and Buki A (2008) Traumatic axonal injury in the spinal cord evoked by traumatic brain injury. *Journal of Neurotrauma*. **25**(3):205-13.

163. Cornish R, Blumbergs PC, Manavis J, Scott G, Jones NR, and Reilly PL (2000) Topography and severity of axonal injury in human spinal cord trauma using amyloid precursor protein as a marker of axonal injury. *Spine (Phila Pa 1976)*. **25**(10):1227-33.

164. Zwimpfer TJ and Bernstein M (1990) Spinal cord concussion. *Journal of Neurosurgery*. **72**(6):894-900.

165. Marshall LF, Knowlton S, Garfin SR, Klauber MR, Eisenberg HM, Kopaniky D, Miner ME, Tabbador K, and Clifton GL (1987) Deterioration following spinal cord injury. A multicenter study. *Journal of Neurosurgery*. **66**(3):400-4.

166. Farmer J, Vaccaro A, Albert TJ, Malone S, Balderston RA, and Cotler JM (1998) Neurologic deterioration after cervical spinal cord injury. *Journal of Spinal Disorders*. **11**(3):192-6.

167. Harrop JS, Sharan AD, Vaccaro AR, and Przybylski GJ (2001) The cause of neurologic deterioration after acute cervical spinal cord injury. *Spine (Phila Pa 1976)*. **26**(4):340-6.

168. Frankel HL (1969) Ascending cord lesion in the early stages following spinal injury. *Paraplegia*. **7**(2):111-8.

169. Planner AC, Pretorius PM, Graham A, and Meagher TM (2008) Subacute progressive ascending myelopathy following spinal cord injury: MRI appearances and clinical presentation. *Spinal Cord*. **46**(2):140-4.

170. Belanger E, Picard C, Lacerte D, Lavallee P, and Levi AD (2000) Subacute posttraumatic ascending myelopathy after spinal cord injury. Report of three cases. *Journal of Neurosurgery*. **93**(2 Suppl):294-9.

171. Colterjohn NR and Bednar DA (1995) Identifiable risk factors for secondary neurologic deterioration in the cervical spine-injured patient. *Spine (Phila Pa 1976)*. **20**(21):2293-7.

172. Al-Ghatany M, Al-Shraim M, Levi AD, and Midha R (2005) Pathological features including apoptosis in subacute posttraumatic ascending myelopathy. Case report and review of the literature. *Journal of Neurosurgery. Spine*. **2**(5):619-23.

173. Kumar A, Kumar J, Garg M, Farooque K, Gamanagatti S, and Sharma V (2010) Posttraumatic subacute ascending myelopathy in a 24-year-old male patient. *Emergency Radiololgy*. **17**(3):249-52.

174. Aito S, El Masry WS, Gerner HJ, Lorenzo ND, Pellicano G, D'Andrea M, Fromm B, and Freund M (1999) Ascending myelopathy in the early stage of spinal cord injury. *Spinal Cord*. **37**(9):617-23.

175. Schmidt BJ (2006) Subacute delayed ascending myelopathy after low spine injury: Case report and evidence of a vascular mechanism. *Spinal Cord*. **44**(5):322-5.

176. Krishnan C, Malik JM, and Kerr DA (2004) Venous hypertensive myelopathy as a potential mimic of transverse myelitis. *Spinal Cord*. **42**(4):261-4.

177. Tator CH (1991) Review of experimental spinal cord injury with emphasis on the local and systemic circulatory effects. *Neuro-Chirurgie*. **37**(5):291-302.

178. Visocchi M, Di Rocco F, and Meglio M (2003) Subacute clinical onset of postraumatic myelopathy. *Acta Neurochirurgica*. **145**(9):799-804; discussion

179. Kwon BK, Okon E, Hillyer J, Mann C, Baptiste D, Weaver LC, Fehlings MG, and Tetzlaff W (2010) A systematic review of non-invasive pharmacologic neuroprotective treatments for acute spinal cord injury. *J Neurotrauma, -Not available-, Epub ahead of print. doi:10.1089/neu.2009.1149.*

180. Kwon BK, Okon EB, Plunet W, Baptiste D, Fouad K, Hillyer J, Weaver LC, Fehlings MG, and Tetzlaff W (2010) A systematic review of directly applied biologic therapies for acute spinal cord injury. *J Neurotrauma, -Not available-, Epub ahead of print. doi:10.1089/neu.2009.1150.*

181. Tetzlaff W, Okon EB, Karimi-Abdolrezaee S, Hill CE, Sparling JS, Plemel JR, Plunet WT, Tsai EC, Baptiste D, Smithson LJ, Kawaja MD, Fehlings MG, and Kwon BK (2010) A systematic review of cellular transplantation therapies for spinal cord injury. *J Neurotrauma, -Not available-Epub ahead of print. doi:10.1089/neu.2009.1177.*

182. Hadley MN, Walters BC, Grabb PA, Oyesiku NM, Przybylski GJ, Resnick DK, Ryken TC, and Mielke DH (2002) Guidelines for the management of acute cervical spine and spinal cord injuries. *Clinical Neurosurgery*. **49**:407-98.

183. Ploumis A, Yadlapalli N, Fehlings MG, Kwon BK, and Vaccaro AR (2010) A systematic review of the evidence supporting a role for vasopressor support in acute SCI. *Spinal Cord*. **48**(5):356-62.

184. Consortium for Spinal Cord Medicine (2008) Early acute management in adults with spinal cord injury: A clinical practice guideline for health-care professionals. *Journal of Spinal Cord Medicine*. **31**(4):403-79.

185. Levi L, Wolf A, and Belzberg H (1993) Hemodynamic parameters in patients with acute cervical cord trauma: Description, intervention, and prediction of outcome. *Neurosurgery*. **33**(6):1007-16; discussion 16-7.

186. Vale FL, Burns J, Jackson AB, and Hadley MN (1997) Combined medical and surgical treatment after acute spinal cord injury: Results of a prospective pilot study to assess the merits of aggressive medical resuscitation and blood pressure management. *Journal of Neurosurgery*. **87**(2):239-46.

187. No authors listed (2002) Blood pressure management after acute spinal cord injury. *Neurosurgery*. **50**(3 Suppl):S58-62.

188. Hutchinson PJ, Corteen E, Czosnyka M, Mendelow AD, Menon DK, Mitchell P, Murray G, Pickard JD, Rickels E, Sahuquillo J, Servadei F, Teasdale GM, Timofeev I, Unterberg A, and Kirkpatrick PJ (2006) Decompressive craniectomy in traumatic brain injury: The randomized multicenter rescueicp study (www.Rescueicp.Com). *Acta Neurochirurgica. Supplementum*. **96**:17-20.

189. Kerr ME, Weber BB, Sereika SM, Wilberger J, and Marion DW (2001) Dose response to cerebrospinal fluid drainage on cerebral perfusion in traumatic brain-injured adults. *Neurosurgical Focus*. **11**(4):E1.

190. Tuettenberg J, Czabanka M, Horn P, Woitzik J, Barth M, Thome C, Vajkoczy P, Schmiedek P, and Muench E (2009) Clinical evaluation of the safety and efficacy of lumbar cerebrospinal fluid drainage for the treatment of refractory increased intracranial pressure. *Journal of Neurosurgery*. **110**(6):1200-8.

191. Marmarou A, Anderson RL, Ward JD, Choi SC, Young HF, Eisenberg HM, Foulkes MA, Marshall LF, and Jane JA (1991) Impact of ICP instability and hypotension on outcome in patients with severe head trauma. *Journal of Neurosurgery (Suppl)*. **75**(1S):S59-S66.

192. Resnick DK, Marion DW, and Carlier P (1997) Outcome analysis of patients with severe head injuries and prolonged intracranial hypertension. *Journal of Trauma*. **42**(6):1108-11.

193. Bicknell CD, Riga CV, and Wolfe JH (2009) Prevention of paraplegia during thoracoabdominal aortic aneurysm repair. *European Journal of Vascular and Endovascular Surgery*. **37**(6):654-60.

194. Khan SN and Stansby G (2004) Cerebrospinal fluid drainage for thoracic and thoracoabdominal aortic aneurysm surgery. *Cochrane Database of Systematic Reviews* (1):CD003635.

195. Fedorow CA, Moon MC, Mutch WA, and Grocott HP (2010) Review articles: Lumbar cerebrospinal fluid drainage for thoracoabdominal aortic surgery: Rationale and practical considerations for management. *Anesthesia and Analgesia*. **111**(1):46-58.

196. Horn EM, Theodore N, Assina R, Spetzler RF, Sonntag VK, and Preul MC (2008) The effects of intrathecal hypotension on tissue perfusion and pathophysiological outcome after acute spinal cord injury. *Neurosurgical Focus*. **25**(5):E12.

197. Raynor RB (1997) Intraoperative ultrasound for immediate evaluation of anterior cervical decompression and discectomy. *Spine (Phila Pa 1976)*. **22**(4):389-95.

198. Lerch K, Volk M, Heers G, Baer W, and Nerlich M (2002) Ultrasound-guided decompression of the spinal canal in traumatic stenosis. *Ultrasound in Medicine and Biology*. **28**(1):27-32.

199. Jokich PM, Rubin JM, and Dohrmann GJ (1984) Intraoperative ultrasonic evaluation of spinal cord motion. *Journal of Neurosurgery*. **60**(4):707-11.

200. Furlan JC, Noonan V, Cadotte DW, and Fehlings MG (2010) Timing of decompressive surgery of spinal cord after traumatic spinal cord injury: An evidence-based examination of pre-clinical and clinical studies. *Journal of Neurotrauma*. **27**(8):1517-28.

201. Cengiz SL, Kalkan E, Bayir A, Ilik K, and Basefer A (2008) Timing of thoracolomber spine stabilization in trauma patients; impact on neurological outcome and clinical course. A real prospective (rct) randomized controlled study. *Archives of Orthopaedic and Trauma Surgery*. **128**(9):959-66.

202. Ng WP, Fehlings MG, Cuddy B, Dickman C, Fazl M, Green B, Hitchon P, Northrup B, Sonntag V, Wagner F, and Tator CH (1999) Surgical treatment for acute spinal cord injury study pilot study #2: Evaluation of protocol for decompressive surgery within 8 hours of injury. *Neurosurgical Focus*. **6**(1):e3.

203. Botel U, Glaser E, Niedeggen A, and Meindl R (1997) The cost of ventilator-dependent spinal cord injuries-patients in the hospital and at home. *Spinal Cord*. **35**(1):40-2.

204. Tator CH, Fehlings MG, Thorpe K, and Taylor W (1999) Current use and timing of spinal surgery for management of acute spinal surgery for management of acute spinal cord injury in North America: Results of a retrospective multicenter study. *Journal of Neurosurgery*. **91**(1 Suppl):12-8.

205. Pirouzmand F (2010) Epidemiological trends of spine and spinal cord injuries in the largest Canadian adult trauma center from 1986 to 2006. *Journal of Neurosurgery. Spine*. **12**(2):131-40.

206. Thienprasit P, Bantli H, Bloedel JR, and Chou SN (1975) Effect of delayed local cooling on experimental spinal cord injury. *Journal of Neurosurgery*. **42**(2):150-4.

207. Dimar JR, 2nd, Glassman SD, Raque GH, Zhang YP, and Shields CB (1999) The influence of spinal canal narrowing and timing of decompression on neurologic recovery after spinal cord contusion in a rat model. *Spine (Phila Pa 1976)*. **24**(16):1623-33.

208. Delamarter RB, Sherman J, and Carr JB (1995) Pathophysiology of spinal cord injury. Recovery after immediate and delayed decompression. *Journal of Bone and Joint Surgery. American Volume*. **77**(7):1042-9.

209. Rabinowitz RS, Eck JC, Harper CM, Jr., Larson DR, Jimenez MA, Parisi JE, Friedman JA, Yaszemski MJ, and Currier BL (2008) Urgent surgical decompression compared to methylprednisolone for the treatment of acute spinal cord injury: A randomized prospective study in beagle dogs. *Spine (Phila Pa 1976)*. **33**(21):2260-8.

210. Saadoun S, Bell BA, Verkman AS, and Papadopoulos MC (2008) Greatly improved neurological outcome after spinal cord compression injury in AQP4-deficient mice. *Brain*. **131**(Pt 4):1087-98.

211. Shapiro K, Shulman K, Marmarou A, and Poll W (1977) Tissue pressure gradients in spinal cord injury. *Surgical Neurology*. **7**(5):275-9.

212. Zhu H, Feng YP, Young W, You SW, Shen XF, Liu YS, and Ju G (2008) Early neurosurgical intervention of spinal cord contusion: An analysis of 30 cases. *Chinese Medical Journal*. **121**(24):2473-8.

213. Koyanagi I, Iwasaki Y, Isu T, Akino M, and Abe H (1989) Significance of spinal cord swelling in the prognosis of acute cervical spinal cord injury. *Paraplegia*. **27**(3):190-7.

214. Perkins PG and Deane RH (1988) Long-term follow-up of six patients with acute spinal injury following dural decompression. *Injury*. **19**(6):397-401.

215. Rivlin AS and Tator CH (1979) Effect of vasodilators and myelotomy on recovery after acute spinal cord injury in rats. *Journal of Neurosurgery*. **50**(3):349-52.

216. Tator CH and Deecke L (1973) Value of normothermic perfusion, hypothermic perfusion, and durotomy in the treatment of experimental acute spinal cord trauma. *Journal of Neurosurgery*. **39**(1):52-64.

217. Smith JS, Anderson R, Pham T, Bhatia N, Steward O, and Gupta R (2010) Role of early surgical decompression of the intradural space after cervical spinal cord injury in an animal model. *Journal of Bone and Joint Surgery. American Volume*. **92**(5):1206-14.

218. Yeo JD, Payne W, Hinwood B, and Kidman AD (1975) The experimental contusion injury of the spinal cord in sheep. *Paraplegia*. **12**(4):279-98.

219. Hung TK, Chang GL, Chang JL, and Albin MS (1980) Stress-strain relationship and neurological sequelae of uniaxial elongation of the spinal cord of cats. *Surgical Neurology*. **15**(6):471-6.

220. Hung TK, Chang G-L, Lin HS, Walter FR, and Bunegin L (1981) Stress-strain relationship of the spinal cord of anesthetized cats. *Journal of Biomechanics*. **14**(4):269-76.

221. Hung TK and Chang GL (1981) Biomechanical and neurological response of the spinal cord of a puppy to uniaxial tension. *Journal of Biomechanical Engineering, Transactions of the ASME*. **103**(1):43-7.

222. Chang G-L, Hung T-K, and Feng WW (1988) In-vivo measurement and analysis of viscoelastic properties of the spinal cord of cats. *Journal of Biomechanical Engineering, Transactions of the ASME*. **110**(2):115-22.

223. Gefen A and Margulies SS (2004) Are in vivo and in situ brain tissues mechanically similar? *Journal of Biomechanics*. **37**(9):1339-52.

224. Weaver JB, Perrinez PR, Bergeron JA, Kennedy FE, H. W, S.S. L, Doyley MM, Hoopes PJ, and Paulsen KD. (2007) The effects of interstitial tissue pressure on the measured shear modulus in vivo. In *Proceedings of the SPIE. Medical Imaging 2007: Physiology, function and structure from medical images*. 17-22 February 2007.San Diego, CA.

225. Mazuchowski EL and Thibault LE. (2003) Biomechanical properties of the human spinal cord and pia mater. In *2003 Summer Bioengineering Conference*. 25-29 June 2003.Key Biscayne, Florida.

226. Bilston LE and Thibault LE (1996) The mechanical properties of the human cervical spinal cord in vitro. *Annals of Biomedical Engineering*. **24**(1):67-74.

227. Oakland RJ, Hall RM, Wilcox RK, and Barton DC (2006) The biomechanical response of spinal cord tissue to uniaxial loading. *Proceedings of the Institution of Mechanical Engineers. Part H, Journal of Engineering in Medicine*. **220**(4):489-92.

228. Fiford RJ and Bilston LE (2005) The mechanical properties of rat spinal cord in vitro. *Journal of Biomechanics*. **38**(7):1509-15.

229. Bain AC, Shreiber DI, and Meaney DF (2003) Modeling of microstructural kinematics during simple elongation of central nervous system tissue. *Journal of Biomechanical Engineering*. **125**(6):798-804.

230. Cheng S, Clarke EC, and Bilston LE (2008) Rheological properties of the tissues of the central nervous system: A review. *Medical Engineering and Physics*. **30**(10):1318-37.

231. Ozawa H, Matsumoto T, Ohashi T, Sato M, and Kokubun S (2001) Comparison of spinal cord gray matter and white matter softness: Measurement by pipette aspiration method. *Journal of Neurosurgery Spine*. **95**(2):221-4.

232. Ichihara K, Taguchi T, Sakuramoto I, Kawano S, and Kawai S (2003) Mechanism of the spinal cord injury and the cervical spondylotic myelopathy: New approach based on the mechanical features of the spinal cord white and gray matter. *Journal of Neurosurgery Spine*. **99**(3):278-85.

233. Ichihara K, Taguchi T, Shimada Y, Sakuramoto I, Kawano S, and Kawai S (2001) Gray matter of the bovine cervical spinal cord is mechanically more rigid and fragile than the white matter. *Journal of Neurotrauma*. **18**(3):361-7.

234. Shreiber DI, Hao H, and Elias RA (2009) Probing the influence of myelin and glia on the tensile properties of the spinal cord. *Biomechanics and Modeling in Mechanobiology*. **8**(4):311-21.

235. Ozawa H, Matsumoto T, Ohashi T, Sato M, and Kokubun S (2004) Mechanical properties and function of the spinal pia mater. *Journal of Neurosurgery Spine*. **1**(1):122-7.

236. Galle B, Ouyang H, Shi R, and Nauman E (2007) Correlations between tissue-level stresses and strains and cellular damage within the guinea pig spinal cord white matter. *Journal of Biomechanics*. **40**(13):3029-33.

237. Sparrey CJ and Keaveny TM (2009) The effect of flash freezing on variability in spinal cord compression behavior. *Journal of Biomechanical Engineering*. **131**(11):111010.

238. Hung TK, Lin HS, Bunegin L, and Albin MS (1982) Mechanical and neurological reponse of cat spinal cord under static loading. *Surgical Neurology*. **17**(3):213-7.

239. Morriss L, Wittek A, and Miller K (2008) Compression testing of very soft biological tissues using semi-confined configuration--a word of caution. *Journal of Biomechanics*. **41**(1):235-8.

240. Galle B, Ouyang H, Shi R, and Nauman E (2010) A transversely isotropic constitutive model of excised guinea pig spinal cord white matter. *Journal of Biomechanics*.

241. Chang GL, Hung TK, Bleyaert A, and Jannetta PJ (1981) Stress-strain measurement of the spinal cord of puppies and their neurological evaluation. *Journal of Trauma*. **21**(9):807-10.

242. Clarke EC, Cheng S, and Bilston LE (2009) The mechanical properties of neonatal rat spinal cord in vitro, and comparisons with adult. *Journal of Biomechanics*. **42**(10):1397-402.

243. Fiford RJ and Bilston LE. (1998) Strain distribution and relaxation behaviour of rat spinal cord. In *Proceedings of the 1998 ASME International Mechanical Engineering Congress and Exposition*. 15-20 November 1998.Anaheim, CA, USA: ASME, Fairfield, NJ, USA.

244. Cheng S, Clarke EC, and Bilston LE (2009) The effects of preconditioning strain on measured tissue properties. *Journal of Biomechanics*. **42**(9):1360-2.

245. Galford J and McElhaney JH (1970) A viscoelastic study of scalp, brain and dura. *Journal of Biomechanics*. **3**:211-21.

246. Haupt W and Stofft E (1978) [elasticity and tensile strength of human spinal dura mater]. *Verhandlungen der Anatomischen Gesellschaft* (72):139-44.

247. McGarvey KA, Lee JM, and Boughner DR (1984) Mechanical suitability of glycerol-preserved human dura mater for construction of prosthetic cardiac valves. *Biomaterials*. **5**(2):109-17.

248.	Patin DJ, Eckstein EC, Harum K, and Pallares VS (1993) Anatomic and biomechanical properties of human lumbar dura mater. *Anesthesia and Analgesia*. **76**(3):535-40.

249.	Runza M, Pietrabissa R, Mantero S, Albani A, Quaglini V, and Contro R (1999) Lumbar dura mater biomechanics: Experimental characterization and scanning electron microscopy observations. *Anesthesia and Analgesia*. **88**(6):1317-21.

250.	Tencer AF, Allen BL, Jr., and Ferguson RL (1985) A biomechanical study of thoracolumbar spine fractures with bone in the canal. Part III. Mechanical properties of the dura and its tethering ligaments. *Spine*. **10**(8):741-7.

251.	van Noort R, Black MM, Martin TR, and Meanley S (1981) A study of the uniaxial mechanical properties of human dura mater preserved in glycerol. *Biomaterials*. **2**(1):41-5.

252.	van Noort R, Martin TR, Black MM, Barker AT, and Montero CG (1981) The mechanical properties of human dura mater and the effects of storage media. *Clinical Physics and Physiological Measurement*. **2**(3):197-203.

253.	Zarzur E (1996) Mechanical properties of the human lumbar dura mater. *Arquivos de Neuro-Psiquiatria*. **54**(3):455-60.

254.	Persson C, Evans S, Marsh R, Summers JL, and Hall RM (2010) Poisson's ratio and strain rate dependency of the constitutive behavior of spinal dura mater. *Annals of Biomedical Engineering*. **38**(3):975-83.

255.	Wilcox RK, Bilston LE, Barton DC, and Hall RM (2003) Mathematical model for the viscoelastic properties of dura mater. *Journal of Orthopaedic Science*. **8**(3):432-4.

256.	Galford JE and McElhaney JH (1970) A viscoelastic study of scalp, brain, and dura. *Journal of Biomechanics*. **3**(2):211-21.

257.	Liu Y, Chandran K, and Wickstrom J. (1976) In vivo dynamic material properties of the canine spinal cord (dura mater). In *Proceedings of the 29th ACEMB*. 6-10 November 1976.Boston, Massachusetts.

258.	Slucky AV, Sacks MS, Pallares VS, Malinin TI, and Eismont FJ (1999) Effects of epidural steroids on lumbar dura material properties. *Journal of Spinal Disorders*. **12**(4):331-40.

259.	Tunturi AR (1977) Elasticity of the spinal cord dura in the dog. *Journal of Neurosurgery*. **47**(3):391-6.

260.	Maikos JT, Elias RA, and Shreiber DI (2008) Mechanical properties of dura mater from the rat brain and spinal cord. *Journal of Neurotrauma*. **25**(1):38-51.

261.	Fink BR and Walker S (1989) Orientation of fibers in human dorsal lumbar dura mater in relation to lumbar puncture. *Anesthesia and Analgesia*. **69**(6):768-72.

262.	Reina MA, Dittmann M, Lopez Garcia A, and van Zundert A (1997) New perspectives in the microscopic structure of human dura mater in the dorsolumbar region. *Regional Anesthesia*. **22**(2):161-6.

263.	Leung C, Russell C, Cripton PA, and Jones CF (2010) Dura. *TBA*.

264.	Brydon HL, Hayward R, Harkness W, and Bayston R (1995) Physical properties of cerebrospinal fluid of relevance to shunt function. 1: The effect of protein upon CSF viscosity. *British Journal of Neurosurgery*. **9**(5):639-44.

265.	Bloomfield IG, Johnston IH, and Bilston LE (1998) Effects of proteins, blood cells and glucose on the viscosity of cerebrospinal fluid. *Pediatric Neurosurgery*. **28**(5):246-51.

266.	Anderson TE and Stokes BT (1992) Experimental models for spinal cord injury research: Physical and physiological considerations. *Journal of Neurotrauma*. **9**(1).

267.	Young W (2002) Spinal cord contusion models. *Progress in Brain Research*. **137**:231-55.

268.   Ghasemlou N, Kerr BJ, and David S (2005) Tissue displacement and impact force are important contributors to outcome after spinal cord contusion injury. *Experimental Neurology*. **196**(1):9-17.

269.   Anderson TE (1985) Spinal cord contusion injury: Experimental dissociation of hemorrhagic necrosis and subacute loss of axonal conduction. *Journal of Neurosurgery*. **62**(1):115-9.

270.   Nacimiento AC, Bartels M, and Loew F (1986) Acute changes in somatosensory evoked potentials following graded experimental spinal cord compression. *Surgical Neurology*. **25**(1):62-6.

271.   Kloos AD, Fisher LC, Detloff MR, Hassenzahl DL, and Basso DM (2005) Stepwise motor and all-or-none sensory recovery is associated with nonlinear sparing after incremental spinal cord injury in rats. *Experimental Neurology*. **191**(2):251-65.

272.   Kearney PA, Ridella SA, Viano DC, and Anderson TE (1988) Interaction of contact velocity and cord compression in determining the severity of spinal cord injury. *Journal of Neurotrauma*. **5**(3):187-208.

273.   Ma M, Basso DM, Walters P, Stokes BT, and Jakeman LB (2001) Behavioral and histological outcomes following graded spinal cord contusion injury in the c57bl/6 mouse. *Experimental Neurology*. **169**(2):239-54.

274.   Maikos JT and Shreiber DI (2007) Immediate damage to the blood-spinal cord barrier due to mechanical trauma. *Journal of Neurotrauma*. **24**(3):492-507.

275.   Sparrey CJ, Choo AM, Liu J, Tetzlaff W, and Oxland TR (2008) The distribution of tissue damage in the spinal cord is influenced by the contusion velocity. *Spine (Phila Pa 1976)*. **33**(22):E812-9.

276.   Koenig G and Dohrmann GJ (1977) Histopathological variability in 'standardised' spinal cord trauma. *Journal of Neurology, Neurosurgery and Psychiatry*. **40**(12):1203-10.

277.   Molt JT, Nelson LR, Poulos DA, and Bourke RS (1979) Analysis and measurement of some sources of variability in experimental spinal cord trauma. *Journal of Neurosurgery*. **50**(6):784-91.

278.   Dohrmann GJ and Panjabi MM (1976) Spinal cord deformation velocity, impulse, and energy related to lesion volume in "Standardised" Trauma. *Surgical Forum*. **27**(62):466-8.

279.   Viano DC and Lovsund P (1999) Biomechanics of brain and spinal-cord injury:Analysis of neuropathologic and neurophysiologic experiments *Journal of Crash Prevention and Injury Control*. **1**(1):35-43.

280.   Jones CF, Kroeker SG, Cripton PA, and Hall RM (2008) The effect of cerebrospinal fluid on the biomechanics of spinal cord: An ex vivo bovine model using bovine and physical surrogate spinal cord. *Spine (Phila Pa 1976)*. **33**(17):E580-8.

281.   Persson C, McLure SW, Summers J, and Hall RM (2009) The effect of bone fragment size and cerebrospinal fluid on spinal cord deformation during trauma: An ex vivo study. *Journal of Neurosurgery. Spine*. **10**(4):315-23.

282.   Pudenz R and Shelden C (1946) The lucite calvarium - a method for direct observation of the brain II. Cranial trauma and brain movement. *Journal of Neurosurgery*. **3**:487-505.

283.   Wycis H (1948) The mechanical role of the cerebrospinal fluid in cerebral concussion. *Confinia Neurology*. **8**:292-9.

284.   Ommaya A (1968) Mechanical properties of tissues of the nervous system. *Journal of Biomechanics*. **1**:127-38.

285.   Bunegin L, Hung TK, and Chang GL (1987) Biomechanics of spinal cord injury. *Critical Care Clinics*. **3**(3):453-70.

286. Lindgren S and Rinder L (1969) Production and distribution of intracranial and intraspinal pressure changes at sudden extradural fluid volume input in rabbits. *Acta Physiologica Scandinavica*. **76**(3):340-51.

287. Boström O, Svensson MY, Aldman B, Hansson HA, Haaland Y, Lövsund P, Seeman T, Suneson A, Säljö A, and Örtengren T. (1996) A new neck injury criterion candidate-based on injury findings in the cervical spinal ganglia after experimental neck extension trauma. In *Proceedings of the International Research Council on the Biomechanics of Impact*. 11-13 September 1996.Dublin, U.K.

288. Svensson MY, Aldman B, Hansson HA, Lovsund P, Seeman T, Suneson A, and Oertengren T. (1993) Pressure effects in the spinal canal during whiplash extension motion: A possible cause of injury to the cervical spinal ganglia. In *Proceedings of International Research Council on the Biomechanics of Impacts*. 8-10 September 1993.Eindhoven, Netherlands: International Research Council on Biokinetics of Impact, Bron, France.

289. Eichberger A, Darok M, Steffan H, Leinzinger PE, Bostrom O, and Svensson MY (2000) Pressure measurements in the spinal canal of post-mortem human subjects during rear-end impact and correlation of results to the neck injury criterion. *Accident Analysis and Prevention*. **32**(2):251-60.

290. Krave U, Hojer S, and Hansson HA (2005) Transient, powerful pressures are generated in the brain by a rotational acceleration impulse to the head. *European Journal of Neuroscience*. **21**(10):2876-82.

291. Vallfors B, Hansson HA, Larsson S, and Johansson G (1980) Suction in neurosurgery. *Acta Neurochirurgica*. **55**(1-2):35-42.

292. Tarlov IM (1954) Spinal cord compression studies: iii. Time limits for recovery after gradual compression in dogs. *AMA Arch Neurol Psychiatry*. **71**(5):588-97.

293. Basso DM, Beattie MS, and Bresnahan JC (1995) A sensitive and reliable locomotor rating scale for open field testing in rats. *Journal of Neurotrauma*. **12**(1):1-21.

294. Albin MS, White RJ, Acosta-Rua G, and Yashon D (1968) Study of functional recovery produced by delayed localized cooling after spinal cord injury in primates. *Journal of Neurosurgery*. **29**(2):113-20.

295. Iwanami A, Yamane J, Katoh H, Nakamura M, Momoshima S, Ishii H, Tanioka Y, Tamaoki N, Nomura T, Toyama Y, and Okano H (2005) Establishment of graded spinal cord injury model in a nonhuman primate: The common marmoset. *Journal of Neuroscience Research*. **80**(2):172-81.

296. Ford RW (1983) A reproducible spinal cord injury model in the cat. *Journal of Neurosurgery*. **59**(2):268-75.

297. Wrathall JR, Pettegrew RK, and Harvey F (1985) Spinal cord contusion in the rat: Production of graded, reproducible, injury groups. *Experimental Neurology*. **88**(1):108-22.

298. Kroeker SG, (2010) Neurological compromise as a result of a tension-extension injury in the cervical spine [PhD thesis], *Department of Mechanical Engineering*. University of Washington: Seattle. 161.

299. Maiman DJ, Myklebust JB, Ho KC, and Coats J (1989) Experimental spinal cord injury produced by axial tension. *Journal of Spinal Disorders*. **2**(1):6-13.

300. Cusick JF, Myklebust J, Zyvoloski M, Sances A, Jr., Houterman C, and Larson SJ (1982) Effects of vertebral column distraction in the monkey. *Journal of Neurosurgery*. **57**(5):651-9.

301. Bain AC and Meaney DF (2000) Tissue-level thresholds for axonal damage in an experimental model of central nervous system white matter injury. *Journal of Biomechanical Engineering*. **122**(6):615-22.

302. Galbraith JA, Thibault LE, and Matteson DR (1993) Mechanical and electrical responses of the squid giant axon to simple elongation. *Journal of Biomechanical Engineering*. **115**(1):13-22.

303. Shi R and Pryor JD (2002) Pathological changes of isolated spinal cord axons in response to mechanical stretch. *Neuroscience*. **110**(4):765-77.

304. Jarzem PF, Quance DR, Doyle DJ, Begin LR, and Kostuik JP (1992) Spinal cord tissue pressure during spinal cord distraction in dogs. *Spine (Phila Pa 1976)*. **17**(8 Suppl):S227-34.

305. Smith DH, Wolf JA, Lusardi TA, Lee VM, and Meaney DF (1999) High tolerance and delayed elastic response of cultured axons to dynamic stretch injury. *Journal of Neuroscience*. **19**(11):4263-9.

306. Laplaca MC and Prado GR (2010) Neural mechanobiology and neuronal vulnerability to traumatic loading. *Journal of Biomechanics*. **43**(1):71-8.

307. Morrison B, 3rd, Saatman KE, Meaney DF, and McIntosh TK (1998) In vitro central nervous system models of mechanically induced trauma: A review. *Journal of Neurotrauma*. **15**(11):911-28.

308. Kumaria A and Tolias CM (2008) In vitro models of neurotrauma. *British Journal of Neurosurgery*. **22**(2):200-6.

309. Ouyang H, Galle B, Li J, Nauman E, and Shi R (2008) Biomechanics of spinal cord injury: A multimodal investigation using ex vivo guinea pig spinal cord white matter. *Journal of Neurotrauma*. **25**(1):19-29.

310. Cernak I (2005) Animal models of head trauma. *Neurorx*. **2**(3):410-22.

311. Thompson HJ, Lifshitz J, Marklund N, Grady MS, Graham DI, Hovda DA, and McIntosh TK (2005) Lateral fluid percussion brain injury: A 15-year review and evaluation. *Journal of Neurotrauma*. **22**(1):42-75.

312. Hayes RL, Stalhammar D, Povlishock JT, Allen AM, Galinat BJ, Becker DP, and Stonnington HH (1987) A new model of concussive brain injury in the cat produced by extradural fluid volume loading: II. Physiological and neuropathological observations. *Brain Injury*. **1**(1):93-112.

313. Stalhammar D, Galinat BJ, Allen AM, Becker DP, Stonnington HH, and Hayes RL (1987) A new model of concussive brain injury in the cat produced by extradural fluid volume loading: I. Biomechanical properties. *Brain Injury*. **1**(1):73-91.

314. Clausen F and Hillered L (2005) Intracranial pressure changes during fluid percussion, controlled cortical impact and weight drop injury in rats. *Acta Neurochirurgica*. **147**(7):775-80; discussion 80.

315. Sullivan HG, Martinez J, Becker DP, Miller JD, Griffith R, and Wist AO (1976) Fluid-percussion model of mechanical brain injury in the cat. *Journal of Neurosurgery*. **45**(5):521-34.

316. McIntosh TK, Vink R, Noble L, Yamakami I, Fernyak S, Soares H, and Faden AL (1989) Traumatic brain injury in the rat: Characterization of a lateral fluid-percussion model. *Neuroscience*. **28**(1):233-44.

317. Rinder L (1969) "Concussive response" And intracranial pressure changes at sudden extradural fluid volume input in rabbits. *Acta Physiologica Scandinavica*. **76**(3):352-60.

318. Millen JE, Glauser FL, and Fairman RP (1985) A comparison of physiological responses to percussive brain trauma in dogs and sheep. *Journal of Neurosurgery*. **62**(4):587-91.

319. Walter B, Bauer R, Fritz H, Jochum T, Wunder L, and Zwiener U (1999) Evaluation of micro tip pressure transducers for the measurement of intracerebral pressure transients induced by fluid percussion. *Experimental and Toxicologic Pathology*. **51**(2):124-9.

320. Delahunty TM, Jiang JY, Gong QZ, Black RT, and Lyeth BG (1995) Differential consequences of lateral and central fluid percussion brain injury on receptor coupling in rat hippocampus. *Journal of Neurotrauma*. **12**(6):1045-57.

321. Hartl R, Medary MB, Ruge M, Arfors KE, and Ghajar J (1997) Early white blood cell dynamics after traumatic brain injury: Effects on the cerebral microcirculation. *Journal of Cerebral Blood Flow and Metabolism*. **17**(11):1210-20.

322. Marmarou A and Shima K (1990) Comparative studies of edema produced by fluid percussion injury with lateral and central modes of injury in cats. *Advances in Neurology*. **52**:233-6.

323. Hilton DL, Jr., Einhaus SL, Meric AL, 3rd, White RP, Schweitzer JB, Park MR, and Robertson JT (1993) Early assessment of neurologic deficits in the fluid percussion model of brain injury. *Journal of Neurotrauma*. **10**(2):121-33.

324. Pfenninger EG, Reith A, Breitig D, Grunert A, and Ahnefeld FW (1989) Early changes of intracranial pressure, perfusion pressure, and blood flow after acute head injury. Part 1: An experimental study of the underlying pathophysiology. *Journal of Neurosurgery*. **70**(5):774-9.

325. Armstead WM and Kurth CD (1994) Different cerebral hemodynamic responses following fluid percussion brain injury in the newborn and juvenile pig. *Journal of Neurotrauma*. **11**(5):487-97.

326. Fritz HG, Walter B, Holzmayr M, Brodhun M, Patt S, and Bauer R (2005) A pig model with secondary increase of intracranial pressure after severe traumatic brain injury and temporary blood loss. *Journal of Neurotrauma*. **22**(7):807-21.

327. Shreiber DI, Bain AC, Ross DT, Smith DH, Gennarelli TA, McIntosh TK, and Meaney DF (1999) Experimental investigation of cerebral contusion: Histopathological and immunohistochemical evaluation of dynamic cortical deformation. *Journal of Neuropathology and Experimental Neurology*. **58**(2):153-64.

328. Shreiber DI, Smith DH, and Meaney DF (1999) Immediate in vivo response of the cortex and the blood-brain barrier following dynamic cortical deformation in the rat. *Neuroscience Letters*. **259**(1):5-8.

329. Mathew P, Bullock R, Graham DI, Maxwell WL, Teasdale GM, and McCulloch J (1996) A new experimental model of contusion in the rat. Histopathological analysis and temporal patterns of cerebral blood flow disturbances. *Journal of Neurosurgery*. **85**(5):860-70.

330. Mathew P, Graham DI, Bullock R, Maxwell W, McCulloch J, and Teasdale G (1994) Focal brain injury: Histological evidence of delayed inflammatory response in a new rodent model of focal cortical injury. *Acta Neurochirurgica. Supplementum*. **60**:428-30.

331. Suneson A, Hansson HA, Lycke E, and Seeman T (1989) Pressure wave injuries to rat dorsal root ganglion cells in culture caused by high-energy missiles. *Journal of Trauma*. **29**(1):10-8.

332. Shepard SR, Ghajar JB, Giannuzzi R, Kupferman S, and Hariri RJ (1991) Fluid percussion barotrauma chamber: A new in vitro model for traumatic brain injury. *Journal of Surgical Research*. **51**(5):417-24.

333. Jayakumar AR, Rao KV, Panickar KS, Moriyama M, Reddy PV, and Norenberg MD (2008) Trauma-induced cell swelling in cultured astrocytes. *Journal of Neuropathology and Experimental Neurology*. **67**(5):417-27.

334. Panickar KS, Jayakumar AR, and Norenberg MD (2002) Differential response of neural cells to trauma-induced free radical production in vitro. *Neurochemical Research*. **27**(1-2):161-6.

335. Courtney MW and Courtney AC (2010) Working toward exposure thresholds for blast-induced traumatic brain injury: Thoracic and acceleration mechanisms. *Neuroimage*. **54** (Suppl 1):S55-61.

336. Leung LY, VandeVord PJ, Dal Cengio AL, Bir C, Yang KH, and King AI (2008) Blast related neurotrauma: A review of cellular injury. *Molecular and Cellular Biomechanics*. **5**(3):155-68.

337.   Chavko M, Koller WA, Prusaczyk WK, and McCarron RM (2007) Measurement of blast wave by a miniature fiber optic pressure transducer in the rat brain. *Journal of Neuroscience Methods*. **159**(2):277-81.

338.   Bauman RA, Ling G, Tong L, Januszkiewicz A, Agoston D, Delanerolle N, Kim Y, Ritzel D, Bell R, Ecklund J, Armonda R, Bandak F, and Parks S (2009) An introductory characterization of a combat-casualty-care relevant swine model of closed head injury resulting from exposure to explosive blast. *Journal of Neurotrauma*. **26**(6):841-60.

339.   Bauman RA, (2010) Personal communication.

340.   Moochhala SM, Md S, Lu J, Teng CH, and Greengrass C (2004) Neuroprotective role of aminoguanidine in behavioral changes after blast injury. *Journal of Trauma*. **56**(2):393-403.

341.   Saljo A, Svensson B, Mayorga M, Hamberger A, and Bolouri H (2009) Low levels of blast raises intracranial pressure and impairs cognitive function in rats. *Journal of Neurotrauma*. **268**(8):1345-52.

342.   Saljo A, Arrhen F, Bolouri H, Mayorga M, and Hamberger A (2008) Neuropathology and pressure in the pig brain resulting from low-impulse noise exposure. *Journal of Neurotrauma*. **25**(12):1397-406.

343.   Petras JM, Bauman RA, and Elsayed NM (1997) Visual system degeneration induced by blast overpressure. *Toxicology*. **121**(1):41-9.

344.   Kaur C, Singh J, Lim MK, Ng BL, Yap EP, and Ling EA (1995) The response of neurons and microglia to blast injury in the rat brain. *Neuropathology and Applied Neurobiology*. **21**(5):369-77.

345.   Saljo A, Bao F, Haglid KG, and Hansson HA (2000) Blast exposure causes redistribution of phosphorylated neurofilament subunits in neurons of the adult rat brain. *Journal of Neurotrauma*. **17**(8):719-26.

346.   Saljo A, Bao F, Hamberger A, Haglid KG, and Hansson HA (2001) Exposure to short-lasting impulse noise causes microglial and astroglial cell activation in the adult rat brain. *Pathophysiology*. **8**(2):105-11.

347.   Saljo A, Bao F, Jingshan S, Hamberger A, Hansson HA, and Haglid KG (2002) Exposure to short-lasting impulse noise causes neuronal c-Jun expression and induction of apoptosis in the adult rat brain. *Journal of Neurotrauma*. **19**(8):985-91.

348.   Saljo A, Bao F, Shi J, Hamberger A, Hansson HA, and Haglid KG (2002) Expression of c-Fos and c-Myc and deposition of beta-APP in neurons in the adult rat brain as a result of exposure to short-lasting impulse noise. *Journal of Neurotrauma*. **19**(3):379-85.

349.   Svetlov SI, Prima V, Kirk DR, Gutierrez H, Curley KC, Hayes RL, and Wang KK (2010) Morphologic and biochemical characterization of brain injury in a model of controlled blast overpressure exposure. *Journal of Trauma*. **69**(4):795-804.

350.   Axelsson H, Hjelmqvist H, Medin A, Persson JK, and Suneson A (2000) Physiological changes in pigs exposed to a blast wave from a detonating high-explosive charge. *Military Medicine*. **165**(2):119-26.

351.   Kato K, Fujimura M, Nakagawa A, Saito A, Ohki T, Takayama K, and Tominaga T (2007) Pressure-dependent effect of shock waves on rat brain: Induction of neuronal apoptosis mediated by a caspase-dependent pathway. *Journal of Neurosurgery*. **106**(4):667-76.

352.   Saljo A, Huang YL, and Hansson HA (2003) Impulse noise transiently increased the permeability of nerve and glial cell membranes, an effect accentuated by a recent brain injury. *Journal of Neurotrauma*. **20**(8):787-94.

353.   Onifer SM, Rabchevsky AG, and Scheff SW (2007) Rat models of traumatic spinal cord injury to assess motor recovery. *ILAR Journal*. **48**(4):385-95.

354.   Fernandez E, Pallini R, Marchese E, and Talamonti G (1991) Experimental studies on spinal cord injuries in the last fifteen years. *Neurological Research*. **13**(3):138-59.

355.   Kwon BK, Oxland TR, and Tetzlaff W (2002) Animal models used in spinal cord regeneration research. *Spine (Phila Pa 1976)*. **27**(14):1504-10.

356.   Liverman CT and Institute of Medicine (U.S.). Committee on Spinal Cord Injury, *Spinal cord injury : Progress, promise, and priorities*. 2005, Washington, DC: National Academies Press. xvi, 343.

357.   Allen AR (1911) Surgery of experimental lesion of spinal cord equivalent to crush injury of fracture dislocation of spinal column. *JAMA*. **Sept 9**:878–80.

358.   Daniell HB, Francis WW, Lee WA, and Ducker TB (1975) A method of quantitating injury inflicted in acute spinal cord studies. *Paraplegia*. **13**(3):137-42.

359.   Ducker TB, Salcman M, and Daniell HB (1978) Experimental spinal cord trauma, III: Therapeutic effect of immobilization and pharmacologic agents. *Surgical Neurology*. **10**(1):71-6.

360.   Kuruvilla A, Theodore DR, and Abraham J (1985) Changes in norepinephrine and histamine in monkey spinal cords traumatized by weight drop and compression. *Central Nervous System Trauma*. **2**(1):61-71.

361.   Crowe MJ, Bresnahan JC, Shuman SL, Masters JN, and Beattie MS (1997) Apoptosis and delayed degeneration after spinal cord injury in rats and monkeys. *Nature Medicine*. **3**(1):73-6.

362.   Fialho SA, Lumb WV, and Scott RJ (1982) Pneumatically powered vertebral displacement device for dogs. *American Journal of Veterinary Research*. **43**(7):1254-7.

363.   Gerber AM and Corrie WS (1979) Effect of impounder contact area on experimental spinal cord injury. *Journal of Neurosurgery*. **51**(4):539-42.

364.   Koozekanani SH, Vise WM, Hashemi RM, and McGhee RB (1976) Possible mechanisms for observed pathophysiological variability in experimental spinal cord injury by the method of Allen. *Journal of Neurosurgery*. **44**(4):429-34.

365.   Kuchner EF, Hansebout RR, and Pappius HM (2000) Effects of dexamethasone and of local hypothermia on early and late tissue electrolyte changes in experimental spinal cord injury. *Journal of Spinal Disorders*. **13**(5):391-8.

366.   Dohrmann GJ, Panjabi MM, and Banks D (1978) Biomechanics of experimental spinal cord trauma. *Journal of Neurosurgery*. **48**(6):993-1001.

367.   Dohrmann GJ and Panjabi MM (1976) "Standardized" Spinal cord trauma: Biomechanical parameters and lesion volume. *Surgical Neurology*. **6**(5):263-7.

368.   Panjabi MM, Dicker DB, and Dohrmann GJ (1977) Biomechanical quantification of experimental spinal cord trauma. *Journal of Biomechanics*. **10**(11/12):681-7.

369.   Hung TK, Lin HS, Albin MS, Bunegin L, and Jannetta PJ (1979) The standardization of experimental impact injury to the spinal cord. *Surgical Neurology*. **11**(6):470-7.

370.   Hitchon PW, McKay TC, Wilkinson TT, Girton RA, 3rd, Hansen T, and Dyste GN (1989) Methylprednisolone in spinal cord compression. *Spine (Phila Pa 1976)*. **14**(1):16-22.

371.   Hitchon PW, Hansen T, McKay T, Girton RA, Dyste GN, and Sokoll MD (1989) Nicardipine after spinal cord compression in the lamb. *Surgical Neurology*. **31**(2):101-10.

372.   Wrathall JR, *Weight-drop models of experimental spinal cord injury*, in *Neurotrauma*, Narayan, R.K., Wilberger, J.E., and Povlischock, J.T., Editors. 1996, McGraw-Hill: New York. 1381-94.

373. Dohrmann GJ (1972) Experimental spinal cord trauma. A historical review. *Archives of Neurology*. **27**(6):468-73.

374. Kwon BK, Hillyer J, and Tetzlaff W (2010) Translational research in spinal cord injury: A survey of opinion from the SCI community. *Journal of Neurotrauma*. **27**(1):21-33.

375. Swindle MM, *Swine in the laboratory: Surgery, anesthesia, imaging and experimental techniques*. 2nd ed. 2007, New York: CRC Press, Taylor and Francis.

376. Duhaime AC (2006) Large animal models of traumatic injury to the immature brain. *Developmental Neuroscience*. **28**(4-5):380-7.

377. Wadouh F, Metzger H, Arndt CF, Hartmann M, Schywalsky M, and Hetzer R (1984) Response of spinal cord oxygen tension to aortic occlusion. *Advances in Experimental Medicine and Biology*. **180**:731-40.

378. Salzano RP, Jr., Ellison LH, Altonji PF, Richter J, and Deckers PJ (1994) Regional deep hypothermia of the spinal cord protects against ischemic injury during thoracic aortic cross-clamping. *Annals of Thoracic Surgery*. **57**(1):65-70; discussion 1.

379. Papakostas JC, Matsagas MI, Toumpoulis IK, Malamou-Mitsi VD, Pappa LS, Gkrepi C, Anagnostopoulos CE, and Kappas AM (2006) Evolution of spinal cord injury in a porcine model of prolonged aortic occlusion. *Journal of Surgical Research*. **133**(2):159-66.

380. Owen JH, Naito M, Bridwell KH, and Oakley DM (1990) Relationship between duration of spinal cord ischemia and postoperative neurologic deficits in animals. *Spine (Phila Pa 1976)*. **15**(7):618-22.

381. Owen JH, Naito M, and Bridwell KH (1990) Relationship among level of distraction, evoked potentials, spinal cord ischemia and integrity, and clinical status in animals. *Spine (Phila Pa 1976)*. **15**(9):852-7.

382. Kuluz J, Samdani A, Benglis D, Gonzalez-Brito M, Solano JP, Ramirez MA, Luqman A, De los Santos R, Hutchinson D, Nares M, Padgett K, He D, Huang T, Levi A, Betz R, and Dietrich D (2010) Pediatric spinal cord injury in infant piglets: Description of a new large animal model and review of the literature. *Journal of Spinal Cord Medicine*. **33**(1):43-57.

383. Bernards CM and Akers T (2006) Effect of postinjury intravenous or intrathecal methylprednisolone on spinal cord excitatory amino-acid release, nitric oxide generation, PGE2 synthesis, and myeloperoxidase content in a pig model of acute spinal cord injury. *Spinal Cord*. **44**(10):594-604.

384. Skinner SA, Transfeldt EE, Mehbod AA, Mullan JC, and Perra JH (2009) Electromyography detects mechanically-induced suprasegmental spinal motor tract injury: Review of decompression at spinal cord level. *Clinical Neurophysiology*. **120**(4):754-64.

385. Zahra M, Samdani A, Piggott K, Gonzalez-Brito M, Solano J, De Los Santo R, Buitrago JC, Alam F, He D, Gaughan JP, Betz R, Dietrich D, and Kuluz J (2010) Acute changes in systemic hemodynamics and serum vasopressin after complete cervical spinal cord injury in piglets. *Neurocritical Care*. **13**(1):132-40.

386. Bozkus H, Crawford NR, Chamberlain RH, Valenzuela TD, Espinoza A, Yuksel Z, and Dickman CA (2005) Comparative anatomy of the porcine and human thoracic spines with reference to thoracoscopic surgical techniques. *Surgical Endoscopy*. **19**(12):1652-65.

387. Yingling VR, Callaghan JP, and McGill SM (1999) The porcine cervical spine as a model of the human lumbar spine: An anatomical, geometric, and functional comparison. *Journal of Spinal Disorders*. **12**(5):415-23.

388. Strauch JT, Lauten A, Zhang N, Wahlers T, and Griepp RB (2007) Anatomy of spinal cord blood supply in the pig. *Annals of Thoracic Surgery*. **83**(6):2130-4.

389. Zurita M, Vaquero J, Bonilla C, Santos M, De Haro J, Oya S, and Aguayo C (2008) Functional recovery of chronic paraplegic pigs after autologous transplantation of bone marrow stromal cells. *Transplantation*. **86**(6):845-53.

390. Ramsey JB, Ramer LM, Inskip JA, Alan N, Ramer MS, and Krassioukov AV (2010) Care of rats with complete high-thoracic spinal cord injury. *Journal of Neurotrauma*. **27**(9):1709-22.

391. Gellad F, Rao KC, Joseph PM, and Vigorito RD (1983) Morphology and dimensions of the thoracic cord by computer-assisted metrizamide myelography. *AJNR: American Journal of Neuroradiology*. **4**(3):614-7.

392. Kameyama T, Hashizume Y, and Sobue G (1996) Morphologic features of the normal human cadaveric spinal cord. *Spine*. **21**(11):1285-90.

393. Ko HY, Park JH, Shin YB, and Baek SY (2004) Gross quantitative measurements of spinal cord segments in human. *Spinal Cord*. **42**(1):35-40.

394. Zaaroor M, Kosa G, Peri-Eran A, Maharil I, Shoham M, and Goldsher D (2006) Morphological study of the spinal canal content for subarachnoid endoscopy. *Minimially Invasive Neurosurgery*. **49**:220-6.

395. Watson C, Paxinos G, Kayalioglu G, and Christopher & Dana Reeve Foundation., *The spinal cord : A Christopher and Dana Reeve Foundation text and atlas*. 1st ed. 2009, Amsterdam; Boston: Elsevier/Academic Press. 387.

396. Blight AR and Decrescito V (1986) Morphometric analysis of experimental spinal cord injury in the cat: The relation of injury intensity to survival of myelinated axons. *Neuroscience*. **19**(1):321-41.

397. Fletcher TF and Kitchell RL (1966) Anatomical studies on the spinal cord segments of the dog. *American Journal of Veterinary Research*. **27**(121):1759-67.

398. Bernards CM (2006) Cerebrospinal fluid and spinal cord distribution of baclofen and bupivacaine during slow intrathecal infusion in pigs. *Anesthesiology*. **105**(1):169-78.

399. Barson AJ and Sands J (1977) Regional and segmental characteristics of the human adult spinal cord. *Journal of Anatomy*. **123**(Pt 3):797-803.

400. Thomas CE and Combs CM (1962) Spinal cord segments. A. Gross structure in the adult cat. *American Journal of Anatomy*. **110**:37-47.

401. Thomas CE and Combs CM (1965) Spinal cord segments. B. Gross structure in the adult monkey. *American Journal of Anatomy*. **116**:205-16.

402. Allen AR (1914) Remarks on the histopathological changes in the spinal cord due to impact. An experimental study. *Journal of Nervous and Mental Disease*. **41**:141-7.

403. Amako T (1936) Surgical treatment of spinal cord injury by blunt forces; experimental study. *Journal of the Japan Surgical Society*. **37**:1843-74.

404. Freeman LW and Wright TW (1953) Experimental observations of concussion and contusion of the spinal cord. *Annals of Surgery*. **137**(4):433-43.

405. Joyner J and Freeman LW (1963) Urea and spinal cord trauma. *Neurology*. **13**:69-72.

406. Panjabi MM and Wrathall JR (1988) Biomechanical analysis of experimental spinal cord injury and functional loss. *Spine (Phila Pa 1976)*. **13**(12):1365-70.

407. Blight A (1988) Mechanical factors in experimental spinal cord injury. *Journal of the American Paraplegia Society*. **11**(2):26-34.

408. Alderman JL, Osterholm JL, D'Amore BR, and Williams HD (1980) Catecholamine alterations attending spinal cord injury: A reanalysis. *Neurosurgery*. **6**(4):412-7.

409. Ducker TB, Kindt GW, and Kemple LG (1971) Pathological findings in acute experimental spinal cord trauma. *Journal of Neurosurgery*. **35**:700-8.

410. Blight AR (1991) Morphometric analysis of a model of spinal cord injury in guinea pigs, with behavioral evidence of delayed secondary pathology. *Journal of the Neurological Sciences*. **103**(2):156-71.

411. Assenmacher DR and Ducker TB (1971) Experimental traumatic paraplegia. The vascular and pathological changes seen in reversible and irreversible spinal-cord lesions. *Journal of Bone and Joint Surgery. American Volume*. **53**(4):671-80.

412. Goldsmith HS, Duckett S, and Chen WF (1975) Spinal cord vascularization by intact omentum. *American Journal of Surgery*. **129**(3):262-5.

413. Gruner JA (1992) A monitored contusion model of spinal cord injury in the rat. *Journal of Neurotrauma*. **9**(2):123-6; discussion 6-8.

414. Bresnahan JC, Beattie MS, Todd FD, 3rd, and Noyes DH (1987) A behavioral and anatomical analysis of spinal cord injury produced by a feedback-controlled impaction device. *Experimental Neurology*. **95**(3):548-70.

415. Noyes DH (1987) Electromechanical impactor for producing experimental spinal cord injury in animals. *Medical and Biological Engineering and Computing*. **25**(3):335-40.

416. Noyes DH (1987) Correlation between parameters of spinal cord impact and resultant injury. *Experimental Neurology*. **95**(3):535-47.

417. Stokes BT, Noyes DH, and Behrmann DL (1992) An electromechanical spinal injury technique with dynamic sensitivity. *Journal of Neurotrauma*. **9**:187-95.

418. Stokes BT (1992) Experimental spinal cord injury: A dynamic and verifiable injury device. *Journal of Neurotrauma*. **9**(2):129-31; discussion 31-4.

419. Scheff SW, Rabchevsky AG, Fugaccia I, Main JA, and Lumpp JE, Jr. (2003) Experimental modeling of spinal cord injury: Characterization of a force-defined injury device. *Journal of Neurotrauma*. **20**(2):179-93.

420. Anderson TE (1982) A controlled pneumatic technique for experimental spinal cord contusion. *Journal of Neuroscience Methods*. **6**(4):327-33.

421. Albin MS, Hung TK, Bunegin L, and Jannetta PJ (1976) Energy attenuation in a new experimental model for closed impact injury of the spinal cord. *The Anatomical Record*. **184**:341.

422. Fiford RJ, Bilston LE, Waite P, and Lu J (2004) A vertebral dislocation model of spinal cord injury in rats. *Journal of Neurotrauma*. **21**(4):451-8.

423. Choo AM, Liu J, Liu Z, Dvorak M, Tetzlaff W, and Oxland TR (2009) Modeling spinal cord contusion, dislocation, and distraction: Characterization of vertebral clamps, injury severities, and node of ranvier deformations. *Journal of Neuroscience Methods*. **181**(1):6-17.

424. Maiman DJ, Coats J, and Myklebust JB (1989) Cord/spine motion in experimental spinal cord injury. *Journal of Spinal Disorders*. **2**(1):14-9.

425. Larson SJ, Walsh PR, Sances A, Jr., Cusick JF, Hemmy DC, and Mahler H (1980) Evoked potentials in experimental myelopathy. *Spine (Phila Pa 1976)*. **5**(4):299-302.

426. Dolan EJ, Transfeldt EE, Tator CH, Simmons EH, and Hughes KF (1980) The effect of spinal distraction on regional spinal cord blood flow in cats. *Journal of Neurosurgery*. **53**(6):756-64.

427. Dabney KW, Ehrenshteyn M, Agresta CA, Twiss JL, Stern G, Tice L, and Salzman SK (2004) A model of experimental spinal cord trauma based on computer-controlled intervertebral distraction: Characterization of graded injury. *Spine (Phila Pa 1976)*. **29**(21):2357-64.

428. Rivlin AS and Tator CH (1978) Effect of duration of acute spinal cord compression in a new acute cord injury model in the rat. *Surgical Neurology*. **10**(1):38-43.

429. Fehlings MG and Tator CH (1995) The relationships among the severity of spinal cord injury, residual neurological function, axon counts, and counts of retrogradely labeled neurons after experimental spinal cord injury. *Experimental Neurology*. **132**(2):220-8.

430. Carlson GD, Minato Y, Okada A, Gorden CD, Warden KE, Barbeau JM, Biro CL, Bahnuik E, Bohlman HH, and Lamanna JC (1997) Early time-dependent decompression for spinal cord injury: Vascular mechanisms of recovery. *Journal of Neurotrauma*. **14**(12):951-62.

431. Carlson GD, Warden KE, Barbeau JM, Bahniuk E, Kutina-Nelson KL, Biro CL, Bohlman HH, and LaManna JC (1997) Viscoelastic relaxation and regional blood flow response to spinal cord compression and decompression. *Spine (Phila Pa 1976)*. **22**(12):1285-91.

432. Hukuda S and Amano K (1980) Spinal cord tissue oxygen in experimental ischemia, compression, and central necrosis. *Spine (Phila Pa 1976)*. **5**(4):303-6.

433. Hukuda S, Matsui K, and Shichikawa K (1980) Effect of hypercarbia and hypertension on spinal cord tissue oxygen in experimental cervical myelopathy. *Spine (Phila Pa 1976)*. **5**(4):307-9.

434. Hukuda S and Wilson CB (1972) Experimental cervical myelopathy: Effects of compression and ischemia on the canine cervical cord. *Journal of Neurosurgery*. **37**(6):631-52.

435. Goto T and Hoshino Y (2001) Electrophysiological, histological, and behavioral studies in a cat with acute compression of the spinal cord. *Journal of Orthopaedic Science*. **6**(1):59-67.

436. Dimar JR, 2nd, Shields CB, Zhang YP, Burke DA, Raque GH, and Glassman SD (2000) The role of directly applied hypothermia in spinal cord injury. *Spine (Phila Pa 1976)*. **25**(18):2294-302.

437. Croft TJ, Brodkey JS, and Nulsen FE (1972) Reversible spinal cord trauma: A model for electrical monitoring of spinal cord function. *Journal of Neurosurgery*. **36**(4):402-6.

438. Brodkey JS, Richards DE, Blasingame JP, and Nulsen FE (1972) Reversible spinal cord trauma in cats. Additive effects of direct pressure and ischemia. *Journal of Neurosurgery*. **37**(5):591-3.

439. Beggs JL and Waggener JD (1975) Vasogenic edema in the injured spinal cord: A method of evaluating the extent of blood-brain barrier alteration to horseradish peroxidase. *Experimental Neurology*. **49**(1 Pt 1):86-96.

440. Braughler JM, Hall ED, Means ED, Waters TR, and Anderson DK (1987) Evaluation of an intensive methylprednisolone sodium succinate dosing regimen in experimental spinal cord injury. *Journal of Neurosurgery*. **67**(1):102-5.

441. Means ED, Anderson DK, Waters TR, and Kalaf L (1981) Effect of methylprednisolone in compression trauma to the feline spinal cord. *Journal of Neurosurgery*. **55**(2):200-8.

442. Eidelberg E, Staten E, Watkins JC, McGraw D, and McFadden C (1976) A model of spinal cord injury. *Surgical Neurology*. **6**(1):35-8.

443. Aki T and Toya S (1984) Experimental study on changes of the spinal-evoked potential and circulatory dynamics following spinal cord compression and decompression. *Spine (Phila Pa 1976)*. **9**(8):800-9.

444. Nystrom B and Berglund JE (1988) Spinal cord restitution following compression injuries in rats. *Acta Neurologica Scandinavica*. **78**(6):467-72.

445. Tarlov IM and Klinger H (1954) Spinal cord compression studies. II. Time limits for recovery after acute compression in dogs. *AMA Arch Neurol Psychiatry*. **71**(3):271-90.

446. Kobrine AI, Evans DE, LeGrys DC, Yaffe LJ, and Bradley ME (1984) Effect of intravenous lidocaine on experimental spinal cord injury. *Journal of Neurosurgery*. **60**(3):595-601.

447.   Griffiths IR, Rowan JO, and Crawford RA (1975) Spinal cord blood flow measured by a hydrogen clearance technique. *Journal of the Neurological Sciences*. **26**(4):529-44.

448.   Kobrine AI, Evans DE, and Rizzoli HV (1979) Experimental acute balloon compression of the spinal cord. Factors affecting disappearance and return of the spinal evoked response. *Journal of Neurosurgery*. **51**(6):841-5.

449.   Sandler AN and Tator CH (1976) Effect of acute spinal cord compression injury on regional spinal cord blood flow in primates. *Journal of Neurosurgery*. **45**(6):660-76.

450.   Evans DE, Kobrine AI, and Rizzoli HV (1980) Cardiac arrhythmias accompanying acute compression of the spinal cord. *Journal of Neurosurgery*. **52**(1):52-9.

451.   Hansebout RR, Kuchner EF, and Romero-Sierra C (1975) Effects of local hypothermia and of steroids upon recovery from experimental spinal cord compression injury. *Surgical Neurology*. **4**(6):531-6.

452.   Kuchner EF and Hansebout RR (1976) Combined steroid and hypothermia treatment of experimental spinal cord injury. *Surgical Neurology*. **6**(6):371-6.

453.   Griffiths IR, Trench JG, and Crawford RA (1979) Spinal cord blood flow and conduction during experimental cord compression in normotensive and hypotensive dogs. *Journal of Neurosurgery*. **50**(3):353-60.

454.   Hansebout RR, van der Jagt RH, Sohal SS, and Little JR (1981) Oxygenated fluorocarbon perfusion as treatment of acute spinal cord compression injury in dogs. *Journal of Neurosurgery*. **55**(5):725-32.

455.   Martin SH and Bloedel JR (1973) Evaluation of experimental spinal cord injury using cortical evoked potentials. *Journal of Neurosurgery*. **39**(1):75-81.

456.   Deecke L and Tator CH (1973) Neurophysiological assessment of afferent and efferent conduction in the injured spinal cord of monkeys. *Journal of Neurosurgery*. **39**(1):65-74.

457.   De La Torre JC, Johnson CM, Goode DJ, and Mullan S (1975) Pharmacologic treatment and evaluation of permanent experimental spinal cord trauma. *Neurology*. **25**(6):508-14.

458.   Kobrine AI, Evans DE, and Rizzoli H (1978) Correlation of spinal cord blood flow and function in experimental compression. *Surgical Neurology*. **10**(1):54-9.

459.   Kobrine AI, Evans DE, and Rizzoli HV (1978) Correlation of spinal cord blood flow, sensory evoked response, and spinal cord function in subacute experimental spinal cord compression. *Advances in Neurology*. **20**:389-94.

460.   Wilcox RK, (2002) A biomechanical investigation of the burst fracture process [PhD. Thesis], *School of Mechanical Engineering*. University of Leeds Leeds, UK.

461.   Wilcox RK, Allen DJ, Hall RM, Limb D, Barton DC, and Dickson RA (2004) A dynamic investigation of the burst fracture process using a combined experimental and finite element approach. *European Spine Journal*. **13**(6):481-8.

462.   Hall RM, Oakland RJ, Wilcox RK, and Barton DC (2006) Spinal cord-fragment interactions following burst fracture: An in vitro model. *Journal of Neurosurgery. Spine*. **5**:243-50.

463.   Ivancic PC, Pearson AM, Tominaga Y, Simpson AK, Yue JJ, and Panjabi MM (2007) Mechanism of cervical spinal cord injury during bilateral facet dislocation. *Spine (Phila Pa 1976)*. **32**(22):2467-73.

464.   Sheng SR, Wang XY, Xu HZ, Zhu GQ, and Zhou YF (2010) Anatomy of large animal spines and its comparison to the human spine: A systematic review. *European Spine Journal*. **19**(1):46-56.

465.   Belytschko T and Privitzer E, (1978) Refinement and validation of the three-dimensional head-spine model, *AMRL-TR-78-7*. Aerospace Medical Research Laboratory, Wright-Patterson Air Force Base, Ohio.

466.   Chang DG, Tencer AF, Ching RP, Treece B, Senft D, and Anderson PA (1994) Geometric changes in the cervical spinal canal during impact. *Spine*. **19**(8):973-80.

467.   Tran NT, Watson NA, Tencer AF, Ching RP, and Anderson PA (1995) Mechanism of the burst fracture in the thoracolumbar spine. The effect of loading rate. *Spine*. **20**(18):1984-8.

468.   Pintar FA, Schlick M, Yoganandan N, and Reinartz J. (1993) Measurement of dynamic spinal cord pressure. In *Proceedings of the 1993 ASME Winter Annual Meeting, Nov 28-Dec 3 1993*.New Orleans, LA, USA: Publ by ASME, New York, NY, USA.

469.   Yoganandan N, Pintar FA, Maiman DJ, Cusick JF, and Sances Jr. A. (1995) Cervical spinal cord injury using biomechanical experimentation. In *39th Annual Proceedings of the Association for the Advancement of Automotive Medicine*.Chicago, Illinois, USA: Association for the Advancement of Automotive Medicine, Des Plaines, Illinois, USA.

470.   Kroeker SG, Morley PL, Jones CF, Bilston LE, and Cripton PA (2009) The development of an improved physical surrogate model of the human spinal cord--tension and transverse compression. *Journal of Biomechanics*. **42**(7):878-83.

471.   Bilston LB, (1996) Biomechanics of cervical spinal cord injury in rollover crashes, Safety, D.O.T.F.O.O.R., Editor. Federal Office of Road Safety: Canberra, ACT, Australia.

472.   Bilston LE and Thibault LE (1997) Biomechanics of cervical spinal cord injury in flexion and extension: A physical model to estimate spinal cord deformations. *International Journal of Crashworthiness*. **2**(2):207-18.

473.   Xie B, Wu M, and Yang J (2001) Pressure changes in spinal canal and evaluation of spinal cord injuries in spinal section subjected to impact. *Chinese Journal of Traumatology*. **4**(3):175-9.

474.   Bilston LE. (1996) Biomechanics of the cervical spinal cord in rollover crashes. In *Proceedings of the Enhanced Safety of Vehicles Conference*.Melbourne, Australia.

475.   Czosnyka M and Pickard JD (2004) Monitoring and interpretation of intracranial pressure. *Journal of Neurology, Neurosurgery and Psychiatry*. **75**(6):813-21.

476.   Allin D, Czosnyka M, and Czosnyka Z (2008) Laboratory testing of the Pressio intracranial pressure monitor. *Neurosurgery*. **62**(5):1158-61; discussion 61.

477.   Czosnyka M, Czosnyka Z, and Pickard JD (1996) Laboratory testing of three intracranial pressure microtransducers: Technical report. *Neurosurgery*. **38**(1):219-24.

478.   Morgalla MH, Cuno M, Mettenleiter H, Will BE, Krasznai L, Skalej M, Bitzer M, and Grote EH (1997) ICP monitoring with a re-usable transducer: Experimental and clinical evaluation of the Gaeltec ict/b pressure probe. *Acta Neurochirurgica*. **139**(6):569-73.

479.   Morgalla MH, Mettenleiter H, and Katzenberger T (1999) ICP measurement accuracy: The effect of temperature drift. Design of a laboratory test for assessment of ICP transducers. *Journal of Medical Engineering and Technology*. **23**(1):10-4.

480.   Morgalla MH, Mettenleiter H, Bitzer M, Fretschner R, and Grote EH (1999) ICP measurement control: Laboratory test of 7 types of intracranial pressure transducers. *Journal of Medical Engineering and Technology*. **23**(4):144-51.

481.   Al-Tamimi YZ, Helmy A, Bavetta S, and Price SJ (2009) Assessment of zero drift in the Codman intracranial pressure monitor: A study from 2 neurointensive care units. *Neurosurgery*. **64**(1):94-8; discussion 8-9.

482.   Piper I, Barnes A, Smith D, and Dunn L (2001) The Camino intracranial pressure sensor: Is it optimal technology? An internal audit with a review of current intracranial pressure monitoring technologies. *Neurosurgery*. **49**(5):1158-64; discussion 64-5.

483.   Huschak G, Hoell T, Hohaus C, Kern C, Minkus Y, and Meisel HJ (2009) Clinical evaluation of a new multiparameter neuromonitoring device: Measurement of brain tissue oxygen, brain temperature, and intracranial pressure. *Journal of Neurosurgical Anesthesiology*. **21**(2):155-60.

484.   Clemedson CJ (1956) Shock wave transmission to the central nervous system. *Acta Physiologica Scandinavica*. **37**(2-3):204-14.

485.   Romba JJ and Martin P, (1961) The propagation of air shock waves on a biophysical model, U.S. Army ordnance: Technical memorandum 17-61, Human Engineering Laboratories, A.P.G., Maryland, Editor.

486.   Nahum AM, Smith R, and Ward CC, (1977) Intracranial pressure dynamics during head impact, *21st Stapp Car Crash Conference*, Sae, Editor. SAE International, Warrendale, Pennsylvania, USA: New Orleans, Louisiana, USA. 339-66.

487.   Örtengren T, Hansson HA, Lövsund P, Svensson MY, Suneson A, and Säljö A (1996) Membrane leakage in spinal ganglion nerve cells induced by experimental whiplash extension motion: A study in pigs. *Journal of Neurotrauma*. **13**(3):171-80.

488.   Suneson A, Hansson HA, and Seeman T (1990) Pressure wave injuries to the nervous system caused by high-energy missile extremity impact: Part I. Local and distant effects on the peripheral nervous system--a light and electron microscopic study on pigs. *Journal of Trauma*. **30**(3):281-94.

489.   Rinder L and Olsson Y (1968) Studies on vascular permeability changes in experimental brain concussion. I. Distribution of circulating fluorescent indicators in brain and cervical cord after sudden mechanical loading of the brain. *Acta Neuropathologica*. **11**(3):183-200.

490.   Suneson A, Hansson HA, and Seeman T (1990) Pressure wave injuries to the nervous system caused by high-energy missile extremity impact: Part II. Distant effects on the central nervous system--a light and electron microscopic study on pigs. *Journal of Trauma*. **30**(3):295-306.

491.   Dietrich WD (2003) Confirming an experimental therapy prior to transfer to humans: What is the ideal? *Journal of Rehabilitation Research and Development*. **40**(4 Suppl 1):63-9.

492.   Lammertse D, Tuszynski MH, Steeves JD, Curt A, Fawcett JW, Rask C, Ditunno JF, Fehlings MG, Guest JD, Ellaway PH, Kleitman N, Blight AR, Dobkin BH, Grossman R, Katoh H, Privat A, and Kalichman M (2007) Guidelines for the conduct of clinical trials for spinal cord injury as developed by the ICCP panel: Clinical trial design. *Spinal Cord*. **45**(3):232-42.

493.   Kwon BK, Okon EB, Tsai E, Beattie MS, Bresnahan JC, Magnuson DK, Reier PJ, McTigue DM, Popovich PG, Blight AR, Oudega M, Guest JD, Weaver LC, Fehlings MG, and Tetzlaff W (2010) A grading system to evaluate objectively the strength of pre-clinical data of acute neuroprotective therapies for clinical translation in spinal cord injury. *Journal of Neurotrauma*. **- Not available-, Epub ahead of print. doi:10.1089/neu.2010.1296.** .

494.   Tator CH (2006) Review of treatment trials in human spinal cord injury: Issues, difficulties, and recommendations. *Neurosurgery*. **59**(5):957-82; discussion 82-7.

495.   Maikos JT, Qian Z, Metaxas D, and Shreiber DI (2008) Finite element analysis of spinal cord injury in the rat. *Journal of Neurotrauma*. **25**(7):795-816.

496.   Kusaka G, Calvert JW, Smelley C, Nanda A, and Zhang JH (2004) New lumbar method for monitoring cerebrospinal fluid pressure in rats. *Journal of Neuroscience Methods*. **135**(1-2):121-7.

497.   Lee SH, Chung YN, Kim YH, Kim YJ, Park JP, Kwon DK, Kwon OS, Heo JH, Ryu S, Kang HJ, Paek SH, Wang KC, Kim SU, and Yoon BW (2009) Effects of human neural stem cell transplantation in canine spinal cord hemisection. *Neurological Research*. **31**(9):996-1002.

498.   Babu RS, Periasamy P, Varadamurthy S, Sethuraman OS, and Namasivayam A (2007) Locomotor behavior of bonnet macaques after spinal cord injury. *Motor Control*. **11**(1):71-85.

499.   Greaves CY, Gadala MS, and Oxland TR (2008) A three-dimensional finite element model of the cervical spine with spinal cord: An investigation of three injury mechanisms. *Annals of Biomedical Engineering*. **36**(3):396-405.

500.   Ducker TB, Salcman M, Perot PL, Jr., and Ballantine D (1978) Experimental spinal cord trauma, I: Correlation of blood flow, tissue oxygen and neurologic status in the dog. *Surgical Neurology*. **10**(1):60-3.

501.   Hillyer JE, Jones CF, Lee JHT, Hildebrandt R, Gray G, Godbey T, and Kwon BK, (2009) Development of a chronic porcine model of spinal cord injury. [program number 542.26], *Neuroscience 2009* Society for Neuroscience: Chicago, IL.

502.   Singer BA, Tresser NJ, Frank JA, McFarland HF, and Biddison WE (2000) Induction of experimental allergic encephalomyelitis in the NIH minipig. *Journal of Neuroimmunology*. **105**(1):7-19.

503.   Broome JR and Dick EJ (1996) Neurological decompression illness in swine. *Aviation Space and Environmental Medicine*. **67**(3):207-13.

504.   Dick EJ, Broome JR, and Hayward IJ (1997) Acute neurologic decompression illness in pigs: Lesions of the spinal cord and brain. *Laboratory Animal Science*. **47**(1):50-7.

505.   Etz CD, Homann TM, Luehr M, Kari FA, Weisz DJ, Kleinman G, Plestis KA, and Griepp RB (2008) Spinal cord blood flow and ischemic injury after experimental sacrifice of thoracic and abdominal segmental arteries. *European Journal of Cardio-Thoracic Surgery*. **33**(6):1030-8.

506.   Dickerson JWT and Dobbing J (1967) Prenatal and postnatal growth and development of the central nervous system of the pig. *Proceedings of the Royal Society of London. Series B, Biological Sciences*. **166**(1005):384-95.

507.   Busscher I, Ploegmakers JJ, Verkerke GJ, and Veldhuizen AG (2010) Comparative anatomical dimensions of the complete human and porcine spine. *European Spine Journal*. **19**(7):1104-14.

508.   Lighthall JW (1988) Controlled cortical impact: A new experimental brain injury model. *Journal of Neurotrauma*. **5**(1):1-15.

509.   Hamberger A, Huang YL, Zhu H, Bao F, Ding M, Blennow K, Olsson A, Hansson HA, Viano D, and Haglid KG (2003) Redistribution of neurofilaments and accumulation of beta-amyloid protein after brain injury by rotational acceleration of the head. *Journal of Neurotrauma*. **20**(2):169-78.

510.   Tator CH (1995) Update on the pathophysiology and pathology of acute spinal cord injury. *Brain Pathology*. **5**(4):407-13.

511.   Courtine G, Bunge MB, Fawcett JW, Grossman RG, Kaas JH, Lemon R, Maier I, Martin J, Nudo RJ, Ramon-Cueto A, Rouiller EM, Schnell L, Wannier T, Schwab ME, and Edgerton VR (2007) Can experiments in nonhuman primates expedite the translation of treatments for spinal cord injury in humans? *Nature Medicine*. **13**(5):561-6.

512.   Jeffery ND, Smith PM, Lakatos A, Ibanez C, Ito D, and Franklin RJ (2006) Clinical canine spinal cord injury provides an opportunity to examine the issues in translating laboratory techniques into practical therapy. *Spinal Cord*. **44**(10):584-93.

513. Rabchevsky AG, Fugaccia I, Sullivan PG, and Scheff SW (2001) Cyclosporin a treatment following spinal cord injury to the rat: Behavioral effects and stereological assessment of tissue sparing. *Journal of Neurotrauma*. **18**(5):513-22.

514. Bouguet J-Y, (2004) Camera calibration toolbox for matlab (software), available at: Http://www.Vision.Caltech.Edu/bouguetj/calib_doc/. California Institute of Technology: Pasadena.

515. Pintar FA, Yoganandan N, Maiman DJ, and Sances AJ. (1995) Cervical spinal bony injury and the potential for cord injury. In *5th Symposium on Injury Prevention Through Biomechanics*. 1995.Detroit.

516. Jones CF, Kwon BK, and Cripton PA. (2009) Cerebrospinal fluid pressures measured during spinal cord injury in a novel pig model [abstract]. In *Neurotrauma 2009: Second Joint Symposium of the International and National Neurotrauma Societies, September 7-11*. August 2009.Santa Barbara, California: Journal of Neurotrauma.

517. Eidlitz-Markus T, Stiebel-Kalish H, Rubin Y, and Shuper A (2005) CSF pressure measurement during anesthesia: An unreliable technique. *Paediatric Anaesthesia*. **15**(12):1078-82.

518. Kodama T, Hamblin MR, and Doukas AG (2000) Cytoplasmic molecular delivery with shock waves: Importance of impulse. *Biophysical Journal*. **79**(4):1821-32.

519. Dall BE and Stauffer ES (1988) Neurologic injury and recovery patterns in burst fractures at the T12 or L1 motion segment. *Clinical Orthopaedics and Related Research*. **233**:171-6.

520. Limb D, Shaw DL, and Dickson RA (1995) Neurological injury in thoracolumbar burst fractures. *Journal of Bone & Joint Surgery (Br)*. **77-B**(5):774-7.

521. Bilston LE, Meaney DF, and Thibault L. (1993) The development of a physical model to measure strain in a surrogate spinal cord during hyperflexion and hyperextension. In *IRCOBI Conference*.Eindhoven, Netherlands.

522. Holsheimer J, den Boer JA, Struijk JJ, and Rozeboom AR (1994) MR assessment of the normal position of the spinal cord in the spinal canal. *AJNR: American Journal of Neuroradiology*. **15**(5):951-9.

523. Yuan Q, Dougherty L, and Margulies SS (1998) In vivo human cervical spinal cord deformation and displacement in flexion. *Spine*. **23**(15):1677-83.

524. Brainerd EL, Baier DB, Gatesy SM, Hedrick TL, Metzger KA, Gilbert SL, and Crisco JJ (2010) X-ray reconstruction of moving morphology (XROMM): Precision, accuracy and applications in comparative biomechanics research. *Journal of Experimental Zoology: Part A, Ecological Genetics and Physiology*. **313**(5):262-79.

525. Candes EL, Demanet DD, and Ying L (2006) Fast discrete curvelet transforms. *Multiscale Modeling and Simulation*. **5**(3):861-99.

526. Leung C, Russell C, Cripton PA, and Jones CF (2011) Dependence of the tensile mechanical properties of porcine dura mater on spinal region, dorsoventral position and orientation. *in preparation*.

527. Fung YC, ed. *Biomechanics: Mechanical properties of living tissues*. 2nd ed. Vol. 1. 1993, Springer-Verlag: New York. 271.

528. Persson C, Summers J, and Hall RM (2011) The importance of fluid-structure interaction in spinal trauma models. *Journal of Neurotrauma*. **28**:113-25.

529. Donovan WH (2007) Donald Munro lecture. Spinal cord injury--past, present, and future. *Journal of Spinal Cord Medicine*. **30**(2):85-100.

530. Lammertse DP (2004) Update on pharmaceutical trials in acute spinal cord injury. *Journal of Spinal Cord Medicine*. **27**(4):319-25.

531. Wada T, Yao H, Miyamoto T, Mukai S, and Yamamura M (2001) Prevention and detection of spinal cord injury during thoracic and thoracoabdominal aortic repairs. *Annals of Thoracic Surgery*. **72**(1):80-4; discussion 5.

532. Carroccio A, Marin ML, Ellozy S, and Hollier LH (2003) Pathophysiology of paraplegia following endovascular thoracic aortic aneurysm repair. *Journal of Cardiac Surgery*. **18**(4):359-66.

533. Estrera AL, Miller CC, 3rd, Chen EP, Meada R, Torres RH, Porat EE, Huynh TT, Azizzadeh A, and Safi HJ (2005) Descending thoracic aortic aneurysm repair: 12-year experience using distal aortic perfusion and cerebrospinal fluid drainage. *Annals of Thoracic Surgery*. **80**(4):1290-6; discussion 6.

534. Coselli JS, Lemaire SA, Koksoy C, Schmittling ZC, and Curling PE (2002) Cerebrospinal fluid drainage reduces paraplegia after thoracoabdominal aortic aneurysm repair: Results of a randomized clinical trial. *Journal of Vascular Surgery*. **35**(4):631-9.

535. Svensson LG, Hess KR, D'Agostino RS, Entrup MH, Hreib K, Kimmel WA, Nadolny E, and Shahian DM (1998) Reduction of neurologic injury after high-risk thoracoabdominal aortic operation. *Annals of Thoracic Surgery*. **66**(1):132-8.

536. Clough C and Pearce JM (1980) Procedures in practice. Lumbar puncture. *British Medical Journal*. **280**(6210):297-9.

537. Di Terlizzi R and Platt S (2006) The function, composition and analysis of cerebrospinal fluid in companion animals: Part I - function and composition. *Veterinary Journal*. **172**(3):422-31.

538. Singer JD and Willett JB, *Applied longitudinal data analysis: Modeling change and event occurrence*. 2003, New York: Oxford University Press.

539. Meyer MJ, Megyesi J, Meythaler J, Murie-Fernandez M, Aubut JA, Foley N, Salter K, Bayley M, Marshall S, and Teasell R (2010) Acute management of acquired brain injury part I: An evidence-based review of non-pharmacological interventions. *Brain Injury*. **24**(5):694-705.

540. Fish RE, Brown MJ, Danneman PJ, and Karas AZ, *Anesthesia and analgesia in laboratory animals*. 2nd ed, ed. Medicine, A.C.O.L.A. 2008, San Diego: Academic Press.

541. Marmarou A, Shulman K, and Rosende RM (1978) A nonlinear analysis of the cerebrospinal fluid system and intracranial pressure dynamics. *Journal of Neurosurgery*. **48**(3):332-44.

542. Redzic ZB and Segal MB (2004) The structure of the choroid plexus and the physiology of the choroid plexus epithelium. *Advanced Drug Delivery Reviews*. **56**(12):1695-716.

543. Potts DG, Gomez DG, and Shaw DD (1985) Cranial and spinal cerebrospinal fluid absorption and the clearance of water-soluble myelographic contrast media. A review. *Investigative Radiology*. **20**(1 Suppl):S51-4.

544. Caversaccio M, Peschel O, and Arnold W (1996) The drainage of cerebrospinal fluid into the lymphatic system of the neck in humans. *ORL; Journal of Oto-Rhino-Laryngology and Its Related Specialties*. **58**(3):164-6.

545. Lowhagen P, Johansson BB, and Nordborg C (1994) The nasal route of cerebrospinal fluid drainage in man. A light-microscope study. *Neuropathology and Applied Neurobiology*. **20**(6):543-50.

546. Szewczykowski J, Sliwka S, Kunicki A, Dytko P, and Korsak-Sliwka J (1977) A fast method of estimating the elastance of the intracranial system. *Journal of Neurosurgery*. **47**(1):19-26.

547.   Avezaat CJ and van Eijndhoven JH (1986) Clinical observations on the relationship between cerebrospinal fluid pulse pressure and intracranial pressure. *Acta Neurochirurgica*. **79**(1):13-29.

548.   Hussey F, Schanzer B, and Katzman R (1970) A simple constant-infusion manometric test for measurement of CSF absorption. II. Clinical studies. *Neurology*. **20**(7):665-80.

549.   Fishman RA, *Cerebrospinal fluid in diseases of the nervous system*. 1980, Philadelphia: Saunders. 384.

550.   Eide PK and Brean A (2010) Cerebrospinal fluid pulse pressure amplitude during lumbar infusion in idiopathic normal pressure hydrocephalus can predict response to shunting. *Cerebrospinal Fluid Res*. **7**(5):11.

551.   Eide PK and Sorteberg W (2006) Intracranial pressure levels and single wave amplitudes, Glasgow coma score and Glasgow outcome score after subarachnoid haemorrhage. *Acta Neurochirurgica*. **148**(12):1267-75; [see discussion 75-6, Czosnyka].

552.   Turgut M, Cullu E, Uysal A, Yurtseven ME, and Alparslan B (2005) Chronic changes in cerebrospinal fluid pathways produced by subarachnoid kaolin injection and experimental spinal cord trauma in the rabbit: Their relationship with the development of spinal deformity. An electron microscopic study and magnetic resonance imaging evaluation. *Neurosurgical Review*. **28**(4):289-97.

553.   Cosan TE, Tel E, Durmaz R, Gulec S, and Baycu C (2000) Non-hindbrain-related syringomyelia. Obstruction of the subarachnoid space and the central canal in rats. An experimental study. *Journal of Neurosurgical Sciences*. **44**(3):123-7.

554.   Guha A, Tator CH, Endrenyi L, and Piper I (1987) Decompression of the spinal cord improves recovery after acute experimental spinal cord compression injury. *Paraplegia*. **25**(4):324-39.

555.   Dolan EJ, Tator CH, and Endrenyi L (1980) The value of decompression for acute experimental spinal cord compression injury. *Journal of Neurosurgery*. **53**(6):749-55.

556.   Konno S, Yabuki S, Sato K, Olmarker K, and Kikuchi S (1995) A model for acute, chronic, and delayed graded compression of the dog cauda equina. Presentation of the gross, microscopic, and vascular anatomy of the dog cauda equina and accuracy in pressure transmission of the compression model. *Spine (Phila Pa 1976)*. **20**(24):2758-64.

557.   Kobrine AI, Doyle TF, and Martins AN (1975) Local spinal cord blood flow in experimental traumatic myelopathy. *Journal of Neurosurgery*. **42**(2):144-9.

558.   Kouyoumdjian P, Lonjon N, Prieto M, Haton H, Privat A, Asencio G, Perrin FE, and Gaviria M (2009) A remotely controlled model of spinal cord compression injury in mice: Toward real-time analysis. *Journal of Neurosurgery. Spine*. **11**(4):461-70.

559.   Papadopoulos SM, Selden NR, Quint DJ, Patel N, Gillespie B, and Grube S (2002) Immediate spinal cord decompression for cervical spinal cord injury: Feasibility and outcome. *Journal of Trauma*. **52**(2):323-32.

560.   Akeson J, Bjorkman S, Messeter K, Rosen I, and Helfer M (1993) Cerebral pharmacodynamics of anaesthetic and subanaesthetic doses of ketamine in the normoventilated pig. *Acta Anaesthesiologica Scandinavica*. **37**(2):211-8.

561.   Pfenninger E, Grunert A, Bowdler I, and Kilian J (1985) The effect of ketamine on intracranial pressure during haemorrhagic shock under the conditions of both spontaneous breathing and controlled ventilation. *Acta Neurochirurgica*. **78**(3-4):113-8.

562.   Bozeman WP and Idris AH (2005) Intracranial pressure changes during rapid sequence intubation: A swine model. *Journal of Trauma*. **58**(2):278-83.

563.   Yasuda N, Targ AG, Eger EI, 2nd, Johnson BH, and Weiskopf RB (1990) Pharmacokinetics of desflurane, sevoflurane, isoflurane, and halothane in pigs. *Anesthesia and Analgesia*. **71**(4):340-8.

564. Roald OK, Forsman M, and Steen PA (1989) The effects of prolonged isoflurane anaesthesia on cerebral blood flow and metabolism in the dog. *Acta Anaesthesiologica Scandinavica*. **33**(3):210-3.

565. Grum DF and Svensson LG (1991) Changes in cerebrospinal fluid pressure and spinal cord perfusion pressure prior to cross-clamping of the thoracic aorta in humans. *Journal of Cardiothoracic and Vascular Anesthesia*. **5**(4):331-6.

566. Fehlings MG (2009) The impact of continued cord compression following traumatic spinal cord injury. *Journal of Neurosurgery. Spine*. **11**(5):568-9; discussion 9.

567. Shields CB, Zhang YP, Shields LB, Han Y, Burke DA, and Mayer NW (2005) The therapeutic window for spinal cord decompression in a rat spinal cord injury model. *Journal of Neurosurgery. Spine*. **3**(4):302-7.

568. Matsuyama Y, Kawakami N, and Mimatsu K (1995) Spinal cord expansion after decompression in cervical myelopathy. Investigation by computed tomography myelography and ultrasonography. *Spine (Phila Pa 1976)*. **20**(15):1657-63.

569. Harada A and Mimatsu K (1992) Postoperative changes in the spinal cord in cervical myelopathy demonstrated by magnetic resonance imaging. *Spine (Phila Pa 1976)*. **17**(11):1275-80.

570. Baba H, Maezawa Y, Uchida K, Furusawa N, Wada M, and Imura S (1997) Plasticity of the spinal cord contributes to neurological improvement after treatment by cervical decompression. A magnetic resonance imaging study. *Journal of Neurology*. **244**(7):455-60.

571. Matsuyama Y, Kawakami N, Yanase M, Yoshihara H, Ishiguro N, Kameyama T, and Hashizume Y (2004) Cervical myelopathy due to OPLL: Clinical evaluation by MRI and intraoperative spinal sonography. *Journal of Spinal Disorders and Techniques*. **17**(5):401-4.

572. Fukushima T, Ikata T, Taoka Y, and Takata S (1991) Magnetic resonance imaging study on spinal cord plasticity in patients with cervical compression myelopathy. *Spine (Phila Pa 1976)*. **16**(10 Suppl):S534-8.

573. Mihara H, Kondo S, Takeguchi H, Kohno M, and Hachiya M (2007) Spinal cord morphology and dynamics during cervical laminoplasty: Evaluation with intraoperative sonography. *Spine (Phila Pa 1976)*. **32**(21):2306-9.

574. Leypold BG, Flanders AE, and Burns AS (2008) The early evolution of spinal cord lesions on MR imaging following traumatic spinal cord injury. *AJNR: American Journal of Neuroradiology*. **29**(5):1012-6.

575. Boldin C, Raith J, Fankhauser F, Haunschmid C, Schwantzer G, and Schweighofer F (2006) Predicting neurologic recovery in cervical spinal cord injury with postoperative MR imaging. *Spine (Phila Pa 1976)*. **31**(5):554-9.

576. Shimada K and Tokioka T (1999) Sequential MR studies of cervical cord injury: Correlation with neurological damage and clinical outcome. *Spinal Cord*. **37**(6):410-5.

577. Miyanji F, Furlan JC, Aarabi B, Arnold PM, and Fehlings MG (2007) Acute cervical traumatic spinal cord injury: MR imaging findings correlated with neurologic outcome--prospective study with 100 consecutive patients. *Radiology*. **243**(3):820-7.

578. Kang JD, Figgie MP, and Bohlman HH (1994) Sagittal measurements of the cervical spine in subaxial fractures and dislocations. An analysis of two hundred and eighty-eight patients with and without neurological deficits. *Journal of Bone and Joint Surgery. American Volume*. **76**(11):1617-28.

579. Bilgen M, Abbe R, Liu SJ, and Narayana PA (2000) Spatial and temporal evolution of hemorrhage in the hyperacute phase of experimental spinal cord injury: In vivo magnetic resonance imaging. *Magnetic Resonance in Medicine*. **43**(4):594-600.

580. Weirich SD, Cotler HB, Narayana PA, Hazle JD, Jackson EF, Coupe KJ, McDonald CL, Langford LA, and Harris JH, Jr. (1990) Histopathologic correlation of magnetic resonance imaging signal patterns in a spinal cord injury model. *Spine*. **15**(7):630-8.

581. Rubin JM and Dohrmann GJ (1985) Intraoperative sonography of the spine and spinal cord. *Seminars in Ultrasound, CT, and MR*. **6**(1):48-66.

582. Mirvis SE and Geisler FH (1990) Intraoperative sonography of cervical spinal cord injury: Results in 30 patients. *AJNR: American Journal of Neuroradiology*. **11**(4):755-61.

583. Finn-Bodner ST, Hudson JA, Coates JR, Sorjonen DC, Simpson ST, Cox NR, Wright JC, Garrett PD, Steiss JE, and Vaughn DM (1995) Ultrasonographic anatomy of the normal canine spinal cord and correlation with histopathology after induced spinal cord trauma. *Veterinary radiology & ultrasound: the official journal of the American College of Veterinary Radiology and the International Veterinary Radiology Association.* **36**(1):39-48.

584. Meyer MJ, Megyesi J, Meythaler J, Murie-Fernandez M, Aubut JA, Foley N, Salter K, Bayley M, Marshall S, and Teasell R (2010) Acute management of acquired brain injury part II: An evidence-based review of pharmacological interventions. *Brain Injury*. **24**(5):706-21.

585. Montalvo BM, Quencer RM, Green BA, Eismont FJ, Brown MJ, and Brost P (1984) Intraoperative sonography in spinal trauma. *Radiology*. **153**(1):125-34.

586. Flanders AE, Spettell CM, Tartaglino LM, Friedman DP, and Herbison GJ (1996) Forecasting motor recovery after cervical spinal cord injury: Value of MR imaging. *Radiology*. **201**(3):649-55.

587. Duhaime AC, Margulies SS, Durham SR, O'Rourke MM, Golden JA, Marwaha S, and Raghupathi R (2000) Maturation-dependent response of the piglet brain to scaled cortical impact. *Journal of Neurosurgery*. **93**(3):455-62.

588. Sherman JL, Nassaux PY, and Citrin CM (1990) Measurements of the normal cervical spinal cord on MR imaging. *AJNR: American Journal of Neuroradiology*. **11**(2):369-72.

589. Inoue H, Ohmori K, Takatsu T, Teramoto T, Ishida Y, and Suzuki K (1996) Morphological analysis of the cervical spinal canal, dural tube and spinal cord in normal individuals using CT myelography. *Neuroradiology*. **38**(2):148-51.

590. Nordqvist L (1964) The sagittal diameter of the spinal cord and subarachnoid space in different age groups. A roentgenographic post-mortem study. *Acta Radiologica (Suppl.)*. **227**.

591. Nahum A and Melvin J, eds. *Accidental injury: Biomechanics and prevention*. 2nd ed. 2002, Springer Science + Business Media: New York.

592. Schmitt K-U, Niederer P, and Walz F, *Trauma biomechanics: Introduction to accidental injury*. 1st ed. 2004, New York: Springer.

593. Bioresources M, The gottingen minipig® growth curve.

594. Pintar FA, Schlick MB, Yoganandan N, and Maiman DJ (1996) Instrumented artificial spinal cord for human cervical pressure measurement. *Bio Medical Materials & Engineering*. **6**(3):219-29.

595. Yang KH, Hu K, White NA, King AI, Chou CC, and Prasad P (2006) Development of numerical models for injury biomechanics research: A review of 50 years of publications in the stapp car crash conference. *Stapp Car Crash Journal*. **50**:429-90.

596. Li XF and Dai LY (2009) Three-dimensional finite element model of the cervical spinal cord: Preliminary results of injury mechanism analysis. *Spine (Phila Pa 1976)*. **34**(11):1140-7.

597. Kwon BK, Casha S, Hurlbert RJ, and Yong VW (2011) Review: Inflammatory and structural biomarkers in acute traumatic spinal cord injury. *Clinical Chemistry and Laboratory Medicine*. **49**(3):425-33.

598. Muir GD and Webb AA (2000) Mini-review: Assessment of behavioural recovery following spinal cord injury in rats. *European Journal of Neuroscience*. **12**(9):3079-86.

599. Eide PK (2006) A new method for processing of continuous intracranial pressure signals. *Medical Engineering and Physics*. **28**(6):579-87.

600. Fehlings MG (2009) Is cerebrospinal fluid drainage safe and of potential therapeutic benefit after acute traumatic spinal cord injury? *Journal of Neurosurgery. Spine*. **10**(3):179-80; discussion 80.

601. Goldberg AL and Kershah SM (2010) Advances in imaging of vertebral and spinal cord injury. *Journal of Spinal Cord Medicine*. **33**(2):105-16.

602. Clarke EC, Choo AM, Liu J, Lam CK, Bilston LE, Tetzlaff W, and Oxland TR (2008) Anterior fracture-dislocation is more severe than lateral: A biomechanical and neuropathological comparison in rat thoracolumbar spine. *Journal of Neurotrauma*. **25**(4):371-83.

603. Burstyn U, Okon EB, Jones CF, Stammers AT, Kooner PS, Wong TO, Lee JHT, Godbey TS, Chua B, Gray G, and Kwon BK, (2010) Histologic and behavioral outcomes in a porcine model of acute spinal cord injury (program no. 468.14), *Neuroscience 2010*: San Diego, CA

604. Wilke HJ, Wenger K, and Claes L (1998) Testing criteria for spinal implants: Recommendations for the standardization of in vitro stability testing of spinal implants. *European Spine Journal*. **7**(2):148-54.

605. Manley GT, Rosenthal G, Lam M, Morabito D, Yan D, Derugin N, Bollen A, Knudson MM, and Panter SS (2006) Controlled cortical impact in swine: Pathophysiology and biomechanics. *Journal of Neurotrauma*. **23**(2):128-39.

606. Gressens P, Dingley J, Plaisant F, Porter H, Schwendimann L, Verney C, Tooley J, and Thoresen M (2008) Analysis of neuronal, glial, endothelial, axonal and apoptotic markers following moderate therapeutic hypothermia and anesthesia in the developing piglet brain. *Brain Pathology*. **18**(1):10-20.

607. Bower TC, Murray MJ, Gloviczki P, Yaksh TL, Hollier LH, and Pairolero PC (1989) Effects of thoracic aortic occlusion and cerebrospinal fluid drainage on regional spinal cord blood flow in dogs: Correlation with neurologic outcome. *Journal of Vascular Surgery*. **9**(1):135-44.

608. Kazama S, Masaki Y, Maruyama S, and Ishihara A (1994) Effect of altering cerebrospinal fluid pressure on spinal cord blood flow. *Annals of Thoracic Surgery*. **58**(1):112-5.

609. Moerman A, Van Herzeele I, Vanpeteghem C, Vermassen F, Francois K, and Wouters P (2011) Near-infrared spectroscopy for monitoring spinal cord ischemia during hybrid thoracoabdominal aortic aneurysm repair. *Journal of Endovascular Therapy*. **18**(1):91-5.
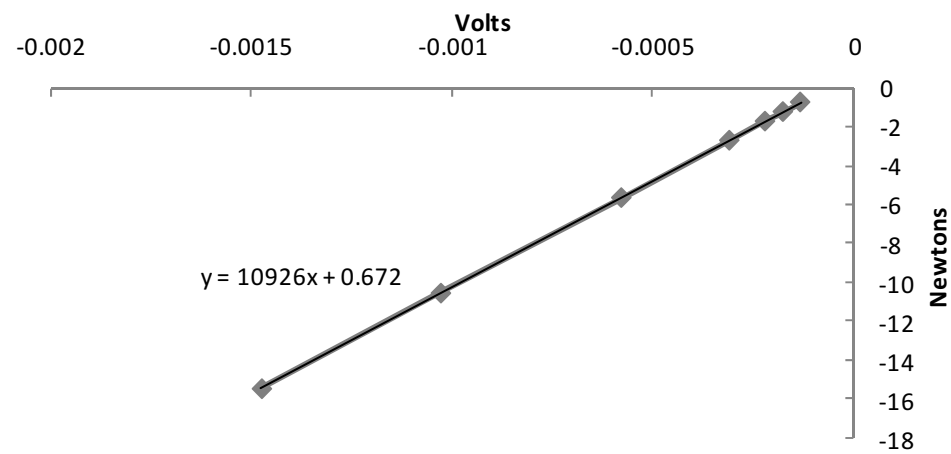
Appendix A: Transducer calibrations

Weight drop load cell calibration curve (compression)

$y = 128913x + 8.0323$
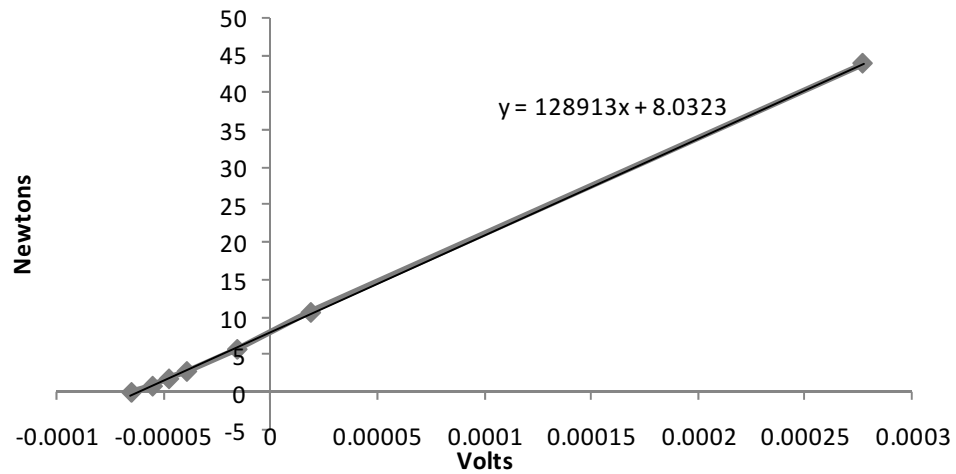
Base load cell calibration curve (compression)

$y = 95012x - 0.0627$
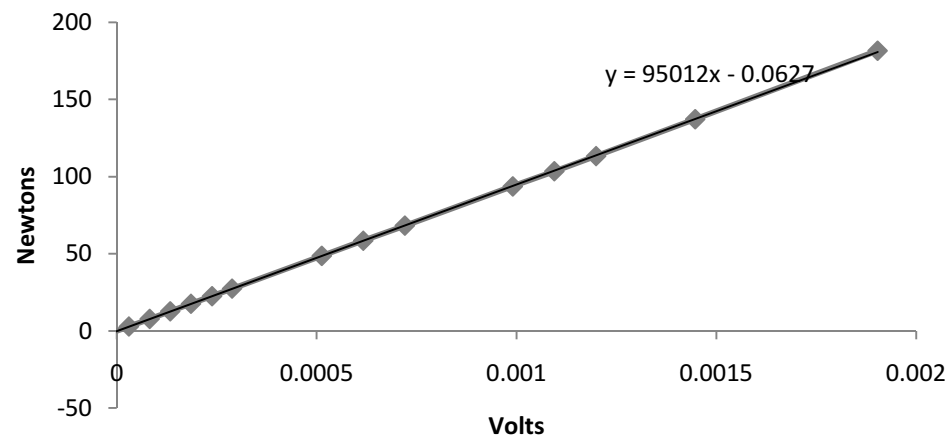
Tether load cell (tension)

$y = 10926x + 0.672$

# Appendix B: High speed x-ray distortion validation

The distance between each pair of dots was determined on the pre-undistorted and post-undistorted images (undistorted images are shown below). The histograms indicate the difference from the mean for the pre- and post-undistorted images. Note that although the distortion was tested across the entire field of view of the image intensifier, only the centre of the field of view was used for the experiments (Chapter 4). The marker carrier used is also depicted below.
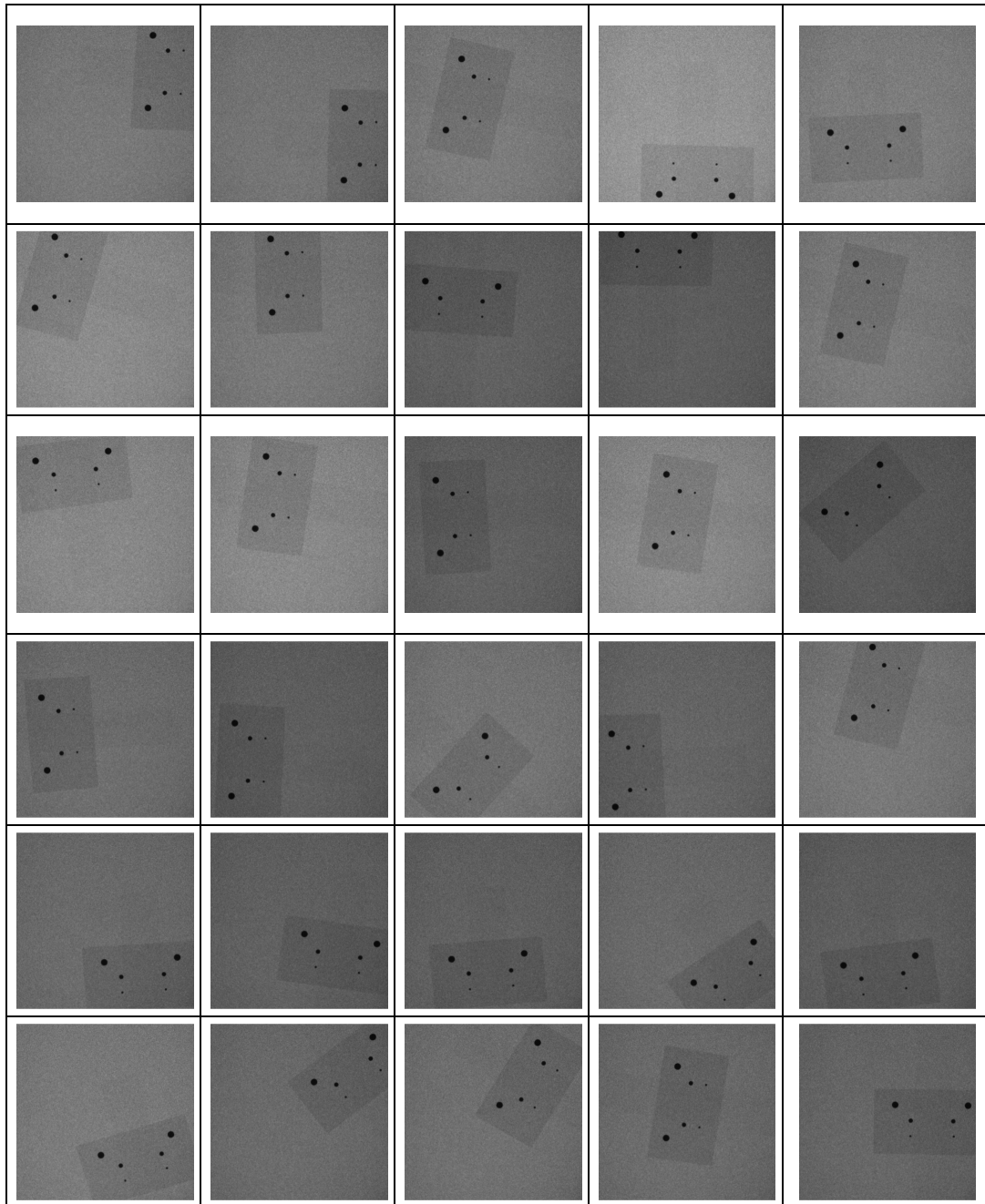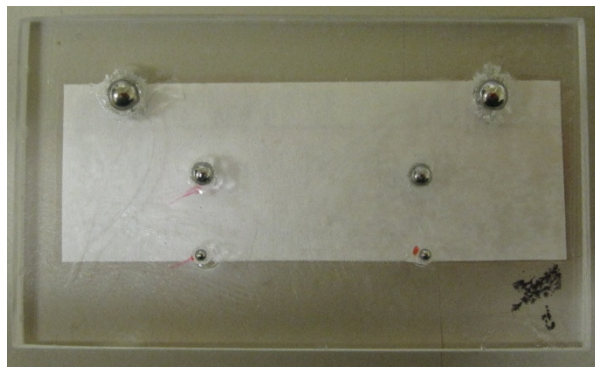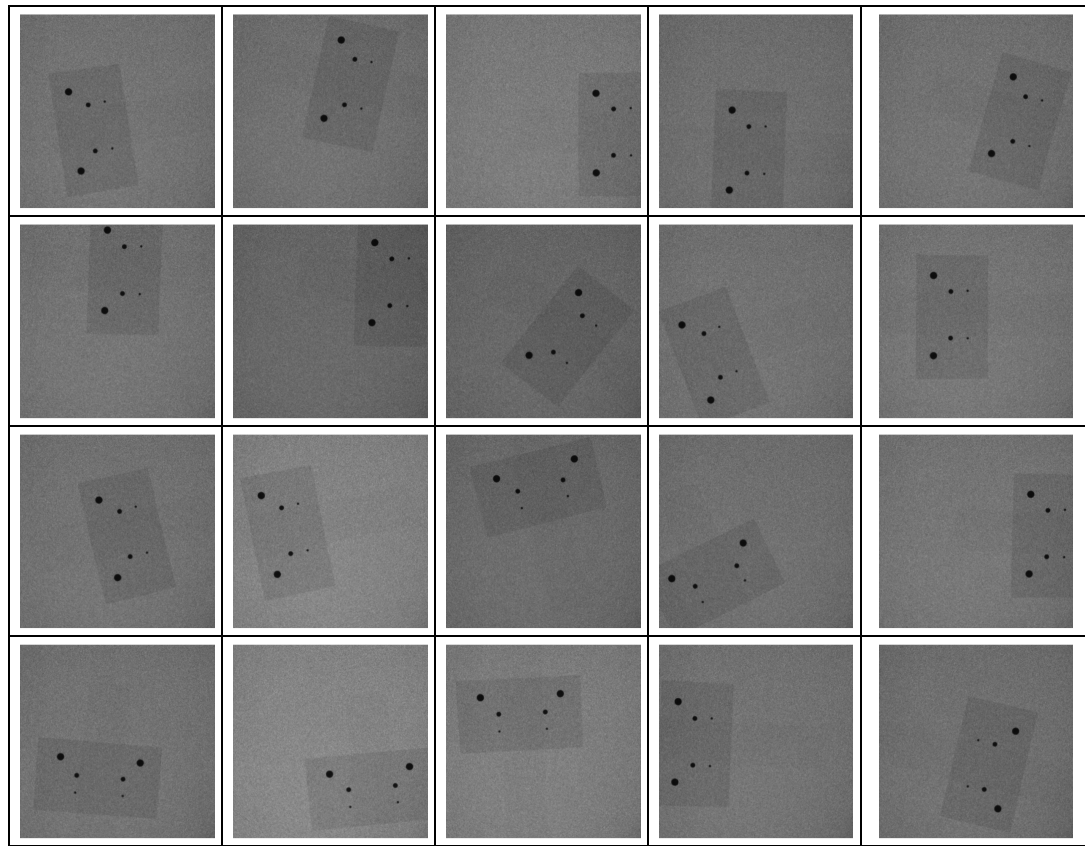
0.1" bead, 32.84 mm centre-to-centre	
2 mm bead, 19.23 mm centre-to-centre	
1 mm bead, 19.46 mm centre-to-centre	

The following histograms demonstrate the spread of the deviation from the mean value (in pixels) for the images shown above. The distances were measured between the two smallest markers, the two central markers and the two largest markers. These are shown on the top, middle and bottom histograms, respectively. The first set of histograms is for the images prior to distortion correction, and the second set is for the images following distortion correction.
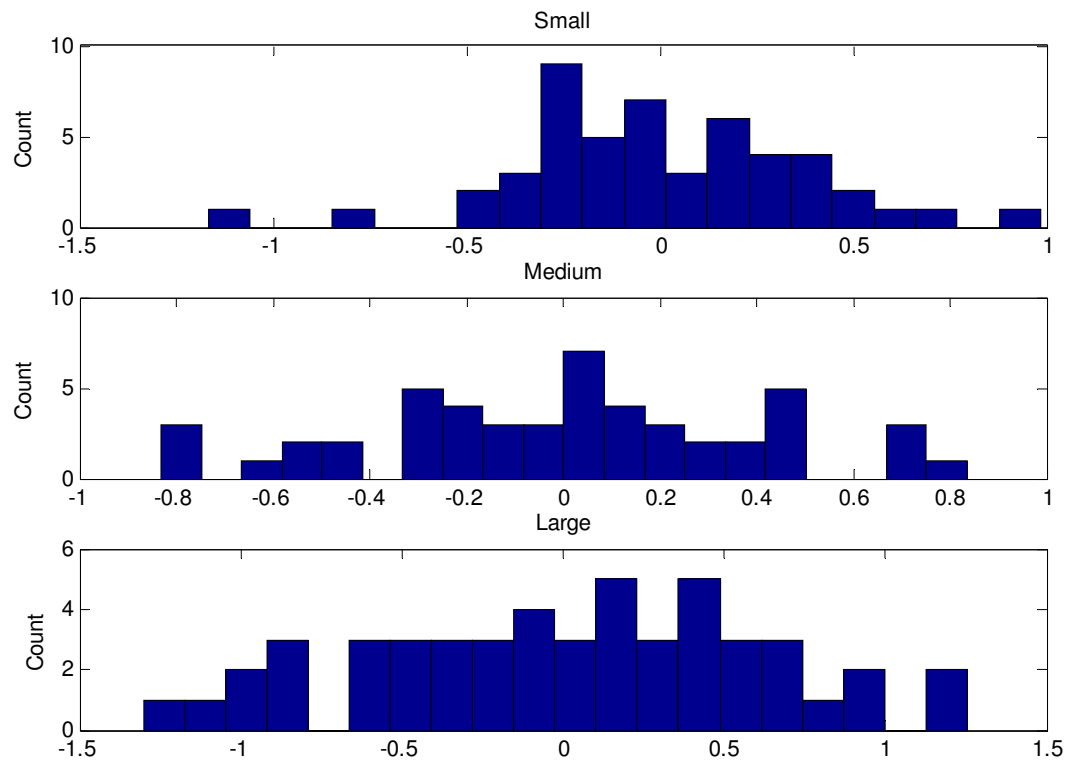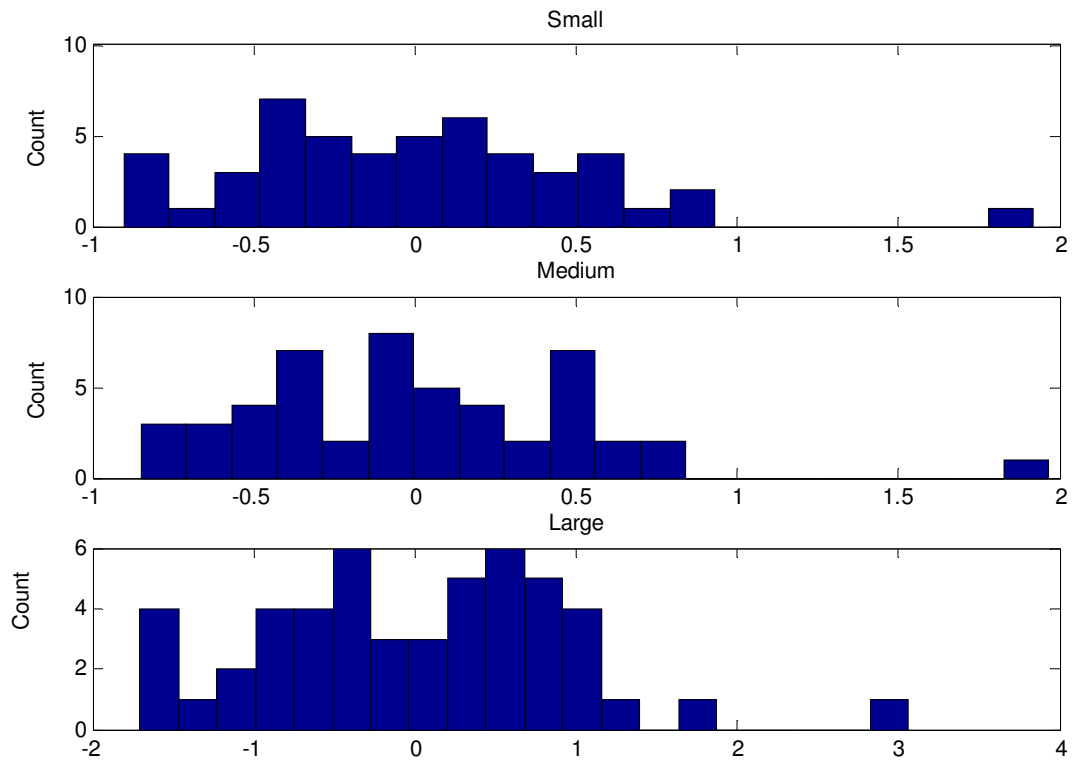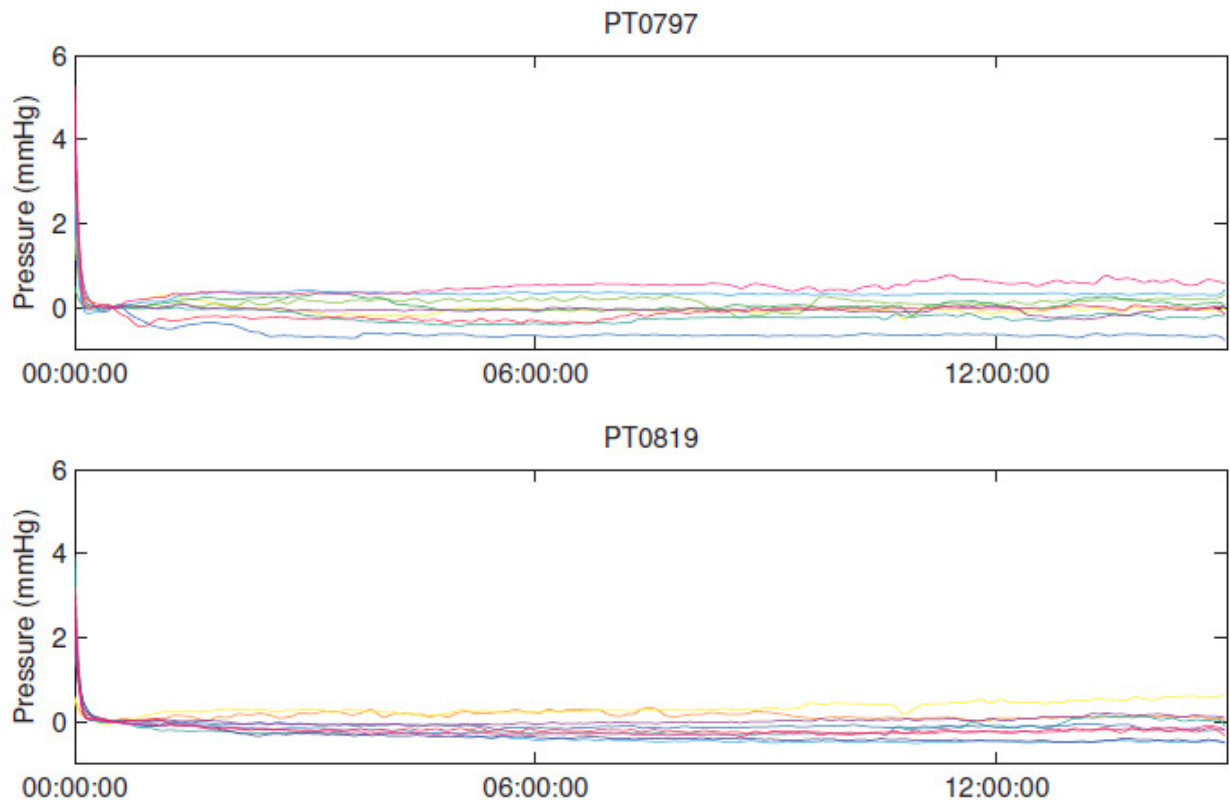
The figure below illustrates the resolution of the high speed x-ray system (2.2 lp/mm), using a standard resolution test tool.
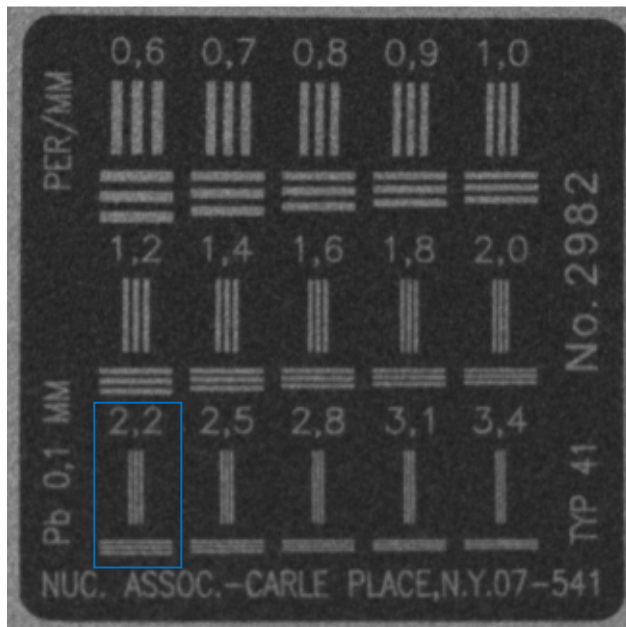
Appendix C: Pressure transducer drift test

Pressure transducers were placed in a temperature and pressure controlled chamber for 15 hours at approximately 10 mmHg to measure drift over time (see Section 5.2.1). In the following plots the pressure data is presented relative to 30 minutes after the start of the test, which was the minimum time allowed for temperature equilibration during the *in vivo* tests.

Cerebrospinal fluid pressure transducers:

Arterial and venous pressure transducers: